CALIFORNIA INSTITUTE OF TECHNOLOGY

EARTHQUAKE ENGINEERING RESEARCH LABORATORY

PARSIMONIOUS MODELING OF INELASTIC STRUCTURES

by

Dar-Yun Chang

Report No. EERL 92-02

Pasadena, California

1992

PARSIMONIOUS MODELING OF INELASTIC SYSTEMS

Thesis by

Dar-Yun Chiang

In Partial Fulfillment of the Requirements

for the Degree of

Doctor of Philosophy

California Institute of Technology

Pasadena, California

1993

(Submitted September 30, 1992)

ACKNOWLEDGEMENTS

I am heartily grateful to my advisor, Professor James L. Beck, for his continued guidance and encouragement throughout the course of my study and research at Caltech. His infectious enthusiasm and continuous availability to advise me with my work are greatly appreciated.

I would like to thank the California Institute of Technology for the generous financial support offered to me, which made my study here possible. I also wish to express my gratitude to the people in Thomas Lab, who created a friendly environment making my stay here a very enjoyable experience. My special thanks are extended to Dr. Jay C. Chen, who was at JPL and is now in the Hong-Kong University of Science and Technology, for his constant help that made my overseas study here so pleasant and memorable.

My deepest thanks are due to my wife, Tsai-Hsiu, not only for her assistance in typing this thesis, but also for her patience, for her love and for her sharing wonderful moments here with me. Finally, I dedicate this thesis to my parents, Kuan and Hsiu-Lien, who always support me in the pursuit of my career goals.

ABSTRACT

Analytical modeling of one-dimensional hysteresis and general multi-axial cyclic plasticity is studied, with particular emphasis on the parsimony of model parameters and the physical consistency of model behavior. General criteria for good models are proposed to provide guidelines to the modeling studies conducted in this research.

Various one-dimensional hysteretic models are examined in detail, including both deteriorating and non-deteriorating models. A general formulation for modeling of degrading systems is presented based on the formulation of the Distributed-Element Model (DEM) and the introduction of a damage index function. A new class of deteriorating Masing models, whose behavior can be completely described by a few simple mathematical rules and the extended Masing rules, is also developed to substitute for a special class of deteriorating DEMs, so that their applicabilty to system identification studies is improved.

The one-dimensional DEMs are extended to the multi-dimensional case for constitutive modeling of cyclic plasticity, while preserving the concept of modeling plasticity by an assemblage of simple ideal elasto-plastic elements. In the generalization, a new invariant-yield-surface theory is proposed, in which no kinematic hardening rule is needed to account for the subsequent yielding and strain hardening behavior. A general theory is also developed to elucidate some important properties of material behavior based on the proposed multi-dimensional DEMs. The establishment of the theory provides instructive insight into the elastic-plastic response mechanisms of real materials under complicated loading conditions. Based on the insight, the Masing rules for one-dimensional hysteresis are extended to the multi-dimensional case by introducing a composition of plane-geometry transformations to a response formula developed for initial loading. This transformation method serves as an efficient way of implementing the classical multi-yield-surface theory with the Mroz kinematic hardening rule. Validity of the new formulations are confirmed by comparison with experimental results from the literature.

TABLE OF CONTENTS

LIST OF TABLES AND FIGURES

CHAPTER 1

INTRODUCTION

Most structures exhibit nearly linearly elastic restoring force behavior under moderately small loading conditions. However, when subjected to severe excitations such as strong earthquake ground motions, structures may respond inelastically and exhibit hysteretic behavior so that the restoring force at a time instant depends not only on the instantaneous state, but also on the past response history. The study of nonlinear, hysteretic behavior of mechanical systems has been of great interest to researchers in many engineering fields, and particularly in earthquake engineering [4, 9, 10, 13, 18-24].

Structures of simple configurations and homogeneous materials may usually be approximated by simplifed analytical models so that their response to complicated external loading can be analyzed more efficiently. For example, normal building structures under seismic excitations can often be modeled as shear buildings (i.e., chain models) so that their response characteristics, such as natural frequencies, maximum displacement response, etc., can be estimated efficiently and with reasonable accuracy. When such simplified models are used, the hysteretic response of structural systems is often described by its overall interstory force-deflection relationship so as to avoid complex stress-strain calculations for which constitutive equations governing material behavior at a point are needed [23].

Although overall planar force-deflection representations in nonlinear structural analysis can reflect behavior of structural members or substructures as a whole, including both material and geometrical effects, they are not suitable for describing local response behavior in the case of complex mechanical systems or complicated loading conditions in which responses in different directions may interact significantly with one another. For that purpose, one needs to introduce appropriate constitutive laws depicting stress-strain relations at different material points, from which local response behavior can then be derived.

As mentioned earlier, linear models for mechanical systems are, in general, sufficient to represent system response resulting from small excitations. The mathematical representations of such linear models are usually simple and of clear physical significance. Thus, modeling of linear systems may be thought of as an easy and straightforward task, if considered solely from the viewpoint of forward analysis. If system identification is under consideration, however, the choice of a suitable class of linear models may become crucial to the success of the model identification from response data. For example, if linear models are to be used in the identification of structures using earthquake data, one should consider identifiable modal models with parameters of modal frequencies, dampings, and mode shape components, not the models in the physical coordinates with parameters of stiffness and damping matrices, as recommended by Beck [3], so that more reliable results can be obtained in the case of a limited number of measurement channels. Once the modal parameters are estimated from the earthquake data, they can be used in a subsequent stage to investigate the generally nonunique inverse problem of going from the incomplete set of modal parameters to structural stiffness parameters.

In contrast to linear models, nonlinear models are usually more mathematically involved, especially when hysteretic behavior is taken into account. For the simplified force-deflection relationship which is a one-dimensional formulation of system behavior, numerous models have been proposed ranging from simple ones such as elasto-perfectly-plastic and bilinear hysteretic models to sophisticated ones like Takeda's and the Bouc-Wen's models [44, 51]. Among these models, the Distributed-Element Model (DEM), developed by Iwan [19], has been successfully applied to structural dynamic analysis because of its physically consistent behavior. The DEM consists of an assemblage of simple ideal elasto-plastic elements that have different yield strengths governed by some distribution function. As shown by Jayakumar [23], the DEM formulation is mathematically equivalent to a general class of Masing models in which Masing's hypothesis is extended for transient behavior of general hysteretic response.

An interesting problem that has not been resolved so far is how the Masing rules can in some way be extended to two or higher dimensions, and how would the general rules compare with the behavior of a general multi-dimensional DEM,

if available. Furthermore, how would the behavior of such general models compare with those based on the classical theory of plasticity? If these questions can be answered clearly, then modeling of general plastic behavior of mechanical systems can be improved and analysis of complex structures can be performed with more success than before.

We remark that not all modeling of structural systems can be done based exclusively on theoretical considerations. In most cases, the mathematical models are so complicated that an empirical approach is needed to identify an appropriate model from within a prescribed class of models using structural response data. Therefore, it is of practical importance to build new models also from the system identification point of view. In general, a good model should be not only mathematically simple, physically consistent, and computationally efficient, but also parsimonious in the number of parameters.

This thesis consists of five independent, yet interrelated chapters in addition to Chapter 1, the introduction, and Chapter 7 in which summary and conclusions of this research are given. In Chapter 2, important issues and practical considerations of system identification are discussed with particular emphasis on the process of model building. Criteria of good models for mechanical systems are also proposed based on considerations of system identification, which provide useful guidelines for the modeling studies conducted in this research.

Chapter 3 gives an extensive review and discussion of various models for modeling of one-dimensional hysteretic behavior, including both the models defined by empirical rules and those by differential equations. In particular, the DEM and Masing models are described in detail, since they form the fundamental starting points of the present research. Hysteretic models including strength and/or stiffness deterioration are also discussed in this chapter. An extension of the hysteretic response rules based on Masing's hypothesis to the case where degradation effects are included is proposed using the distributed-element formulation and the introduction of a "damage" function. Explicit mathematical rules are then derived for a particular class of maximum-displacement-controlled deteriorating DEMs [22]. With these rules, the numerical implementation of this special class of deteriorating

DEMs becomes simpler as compared with the direct computation of model response by keeping track of response behavior of all the elements constituting the model. As a result, identification studies based on such models can then be performed with more efficiency and higher accuracy. Response behavior of this new class of degrading Masing models is compared with those of other well-behaved degrading models. Of particular interest is the response behavior of a class of endochronic models that are described theoretically by integro-differential equations [46, 47]. The flexible, physically consistent behavior of the modified one-dimensional endochronic model motivated the study of the general endochronic models for cyclic plasticity in which complicated multi-axial loading conditions are considered. This is presented in Chapter 4.

Although the behavior of the modified endochronic models is govened by some mathematically involved integro-differential equations, effective procedures for constitutive modeling based on the theory have been established in the past so that numerical implemention of the models is practically feasible. A new way of modeling based on the endochronic theory is proposed in Chapter 4, which was inspired by the modeling technique used in the Masing models. With the introduction of this new modeling technique, the building process of endochronic models is much simpler and identification studies of systems modeled by endochronic theory then become easier in practice. Furthermore, inspired by the study of the endochronic theory for cyclic hardening behavior, the one-dimensional Masing models (or DEMs) are extended, in a very effective way, to account for cyclic hardening behavior.

In Chapter 5, the one-dimensional DEMs are generalized to three dimensions (multi-axial loading case), so that they can be used for constitutive modeling of complex structural systems. Although this work has been pursued by some researchers in the past [20, 56], limited success was achieved. In the present study, a concept of nested yield surfaces that are "invariant" (fixed from moving) in the stress space is proposed for a new class of general multi-dimensional Distributed-Element Models. This concept is different from that of classical plasticity theory, as will be explained later in detail in Chapter 5. With the new formulation of the DEM, constitutive modeling of general structural behavior for cyclic plasticity becomes very simple,

and the associated numerical scheme for implementing the solution algorithm is efficient as well. The new DEM is shown to not only provide more accurate response predictions for experimental results compared with models based on the classical theory of plasticity, but it also serves as a good physical model through which response mechanisms of complicated plastic behavior can be clearly pictured and elucidated. A rather complete mathematical work regarding the properties of the new DEM, such as the existence of equilibrium points and that of a limit surface, will also be covered in Chapter 5.

Though the general multi-dimensional DEM provides a useful and efficient way of constitutive modeling for cyclic plasticity, to implement the theory only a limited number of elements can be introduced due to practical concerns. An interesting question then remaining is whether some mathematical rules can be found which are similar to those used in the one-dimensional Masing models so that even in the general multi-axial loading case, model response can be found without the need of keeping track of each element's behavior. This problem is solved with success in Chapter 6. By introducing a formula good for initial response under multi-axial loading, further unloading and reloading response can then be found by applying a composition of proper transformations to the state variables involved in the formula. This method is theoretically equivalent to that utilizing the classical multi-yield-surface theory with the Mroz kinematic hardening rule [35]. However, it's only with this new approach proposed here that the response behavior of a model with an infinite collection of yield surfaces can be analyzed. Computational efficiency is also preserved in the algorithmic implementation of this new theory, whose validity is confirmed by modeling some biaxial tension-torsion tests [17, 30] under non-proportional cyclic loading conditions. A comparison between the models based on the new approach and the multi-dimensional DEMs is also made at the end of Chapter 6.

A summary of this research and some general conclusions are presented in Chapter 7, in which suggestions for further exploration in related subjects are also given.

CHAPTER 2

SYSTEM IDENTIFICATION AND MODELING

2.1 Introduction

Engineering problems may usually be classified as direct (forward) or inverse according to the nature and purpose of the analysis. Direct problems are those of finding the response of systems to specified input excitations; whereas in inverse problems, the output response to some input is known but either the physical process (the system) or the input excitation is unknown. System identification may be defined as the process of systematically determining a model of a physical system from its observed input and output data , and so it falls obviously into the category of inverse problems. In general, system identification problems can be further divided into two categories: nonparametric identification and parametric identification. If the detailed mathematical description of a system is totally unknown or of little interest, then we have a nonparametric identification problem or a so-called "black box" identification problem, in which a functional relationship between input and output is to be determined. On the other hand, if some knowledge of the mathematical structure of the system is available and the problem is that of determining unknown parameters within the structure, then it is a parametric identification problem. In engineering applications, the main interest is usually in parametric identification problems in which an optimal model out of a certain class of models is to be found for the system under consideration so that prediction of future performance of the system can be improved accordingly. In a parametric identification problem, the introduction of model structure usually reduces statistical variability of the estimated model. Also, the identification problem actually becomes a parameter estimation problem since the mathematical structure of the model is already specified.

In the following sections, practical considerations about system identification will be discussed with particular emphasis on the process of model building to which the chapters that follow are closely related. Criteria of good analytical models for mechanical systems in engineering applications will also be proposed and discussed in detail from the system identification point of view.

2.2 Practical Considerations of System Identification

Identification of structural systems through the use of experimental data is of considerable importance in many areas of engineering studies, particularly in the fields of structural vibration and system control. Identification problems usually are considerably more difficult than forward (response analysis) problems due to the following reasons:

1) The requirement of well-posed analytical models is more critical to identification problems than to forward problems.
2) A characteristic feature of identification problems is that the accuracy of identification results is degraded by a combination of measurement, modeling, and numerical errors.
3) The problem of existence and uniqueness of solution (i.e., identifiability problem) is usually very difficult to be resolved due to practical limitations.

The main purpose of a system identification study is to appropriately represent the physical structure of a system for response prediction, not just to accurately reproduce the observed data. To this end, the parametric identification approach is usually adopted in engineering applications due to its capability of making further predictions. Three important stages are included in a parametric identification problem. The first one is *model selection*, i.e., choosing a mathematical formulation to represent the physical structure of a system. The second stage is *parameter estimation*, which is the determination of the "best" parameters for the specified mathematical structure for the system. The final stage is *model validation*, in which some tests on the identified model are conducted to see if the model adequately represents the system with respect to the desired objectives. Though the nature of the three stages are quite different, they are all important to the success of identification studies. Generally speaking, model selection deals with the application of appropriate physical laws to the systems under consideration. From these laws, some relations involving parameter variables follow, such as equations for constitutive laws in modeling of stress-strain relationships of materials. In a parametric identification problem, the variable parameters of the model are to be estimated based on some systematic approach so that a "best" model whose parameters are optimal in some sense, given the input/output (I/O) data, will be identified from the specified class

of models. Thus far, many systematic approaches have been developed for finding optimal parameters within a class of models. These identification methods almost always involve minimization of some error criterion functions. Three widely-used approaches based on different error criteria are as follows:

1) Equation-error method : The discrepancy between the model equation and the measured I/O data is minimized through a regression analysis technique. This method is simple and computationally effective. However, complete measurements of all the state variables involved in the model equation are required for the method to be effective, which is usually a severe restriction in practical problems.
2) Output-error method: The difference between the output of a system and that of the model in response to some input is minimized by some functional minimization technique. This is probably the most widely-used approach in practical system identification problems due to its great flexibility and moderate mathematical tractability.
3) Combined method: One can take a combined equation-error/output-error approach to perform the identification analysis, such as the Kalman filter method [25, 28] developed for optimal sequential estimates of parameters and states of a system. These kinds of sequential estimation methods are good for modern control problems which require real-time (on-line) analysis capability.

An important aspect of the different identification approaches is that they can be formulated within a unifying statistical framework [6]. For example, the estimate obtained from the classical output-error least-square method used extensively in earthquake engineering can be shown to be equivalent to the classical maximum-likelihood estimate [33], and to that based on Bayesian statistical inference [7], under the assumption that the output error can be modeled as a Gaussian white process.

Probably, the most difficult and important issue of parametric identification is the problem of identifiability of parameters, which refers to the capability of uniquely determining the parameters of a model from the available I/O data. The problem of identifiability can exist even in some of the simplest cases of identification due to the limitation of available measurement data. For example, when linear models are to be

estimated from seismic excitation and response histories, the stiffness and damping matrices of the system may not be determined uniquely in typical situations, as pointed out by Beck [3]. Instead, modal models consisting of dominant modes in the response should be used for the identification purpose, and if estimation of system parameters in the physical coordinates is of interest, a further analysis can always be done in a separate stage utilizing the original data as well as the modal data already obtained.

Recently, Beck and Katafygiotis [7] addressed the issues of *model* identifiability versus *system* identifiability of optimal parameters from a class of models. For a set of parameters to be "model identifiable" (globally or locally), there must exist at most a finite number of sets of parameter values which give "output-equivalent" models under a specified input. In contrast, the parameters that are "system identifiable" determine a finite set of optimal models in which the parameters take the most probable values out of a class of models given a set of I/O data. The problem associated with system identifiability is obviously much more difficult than that of model identifiability due to the additional considerations of modeling error involved in the approximate analytical model and measurement noise contaminated in the response data.

In this thesis work, we are mainly concerned with modeling of general nonlinear mechanical systems. Although there will be no original theory regarding system identification techniques proposed herein, some new modeling theories to be presented later are based on practical considerations of system identification. Moreover, the system identification approach is usually the best way to perform model validation. For this purpose, one could use a set of test data to identify an optimal model out of the class of proposed models, and then make predictions of response behavior observed in another experiment using the identified optimal model. In the next section, some criteria for good analytical models are proposed and discussed mainly from the identification point of view.

2.3 Criteria for Good Modeling

In engineering problems, direct or inverse, a good model is always of crucial importance to the success of investigations. Although models for different problems

depend significantly on the nature of the systems under consideration and may vary considerably from case to case, there are some general rules that may be considered as modeling criteria for most practical mechanical problems. The criteria are proposed as follows:

1) Mathematical Simplicity

A model is a mathematical realization of a physical system which may, in general, have rather complicated behavior. However, considering practical issues such as mathematical tractability, a good model should always be as simple as possible so that it can have greater applicability to widely-spread engineering problems. For example, in system identification problems, parsimony in parameters of a model not only makes numerical computation more easy, but also reduces possible identifiability problems.

2) Physical Reality:

A good model should be able to capture most of the important features observed in the physical system to be modeled. Exhibition of abnormal, nonphysical characteristics can sometimes lead to numerical instability even when the model is used for numerical solution of well-posed physical problems [40]. Following this criterion, parameters selected in a good model should all have clear physical significances.

3) Modeling Versatility:

A class of models should be able, or can be easily extended, to account for various effects exhibited by the physical systems of interest. A versatile mathematical model may also possibly serve different purposes in different engineering applications.

4) Computational Efficiency :

Practical implementation of a good model should be reasonably simple and computationally efficient so that applicability of such a model will not be limited by practical concerns. Computational efficiency for numerical implementation of a model is of particular importance from the identification points of view, since identification processes usually require a large amount of iterations of response calculation.

5) Robustness:

The sensitivity coefficients* of the parameters involved in a model should be neither too high nor too low under practical considerations. This property is referred to as robustness of a model. If the sensitivity of some parameters is too high, the result of a forward response analysis may be significantly degraded by model error; on the other hand, if it is too low, nonunique result of identification may be obtained.

It should be mentioned that in practice it may be difficult to find a model that meets all the criteria listed above. For example, the widely-used Bouc-Wen model [51, 52], which is described solely by a differential equation, can be viewed as both efficient and versatile since it can model various characteristics of hysteresis, and can be easily extended to include the effects of strength and/or stiffness deterioration. Furthermore, the model is applicable to response analysis, including random vibration problems, as well as system identification studies [16, 42]. However, this model may not be simple and realistic enough from some practical points of view. For example, the model may be, in some case, overparameterized such that appropriate choice of the parameter values and identifiability problems can be very tough, as will be discussed later in the chapters that follow. Nevertheless, if a model is always built with the aformentioned criteria in mind, then reliable behavior and practical applicability of the model can always be expected.

2.3.1 An Illustrative Example of Proper Modeling

To make the above ideas clearer, in the following we pose an example to show that a simple, efficient model for forward analysis may lack robustness for identification.

Accurate and efficient algorithms have been developed [5] for computing the response of a single-degree-of-freedom linear oscillator subjected to an arbitrary forcing function, in which any desired response quantity can be computed through the use of a discrete recursive formula based on Duhamel's integral and linear interpolation

* The sensitivity coefficient of a parameter is defined as the change of some response quantity relative to the change of the parameter value.

for the excitation between discrete points sampled uniformly in time. For example, if acceleration response $\ddot{x}(t)$ of a linear oscillator described by

$$\ddot{x} + 2\xi\omega_0\dot{x} + \omega_0^2 x = r(t) \tag{2.1}$$

is of interest, where ξ and ω_0 are damping ratio and natural frequency of the system, one can use the following recursive formula:

$$\ddot{x}_{i+1} = b_1\ddot{x}_i + b_2\ddot{x}_{i-1} + c_1(r_{i-1} + 2r_i + r_{i+1}) \tag{2.2}$$

$$\ddot{x}_1 = b_3 x_0 + b_4\dot{x}_0 + c_2 r_0 + c_3 r_1 \tag{2.3}$$

to compute the acceleration time history, where subscript i denotes the time $t = t_i$, and the expressions for the coefficients can be found in [5]. In particular, the two coefficients b_1 and b_2 are selected such that the transient response due to initial conditions is determined exactly. This yields

$$b_1 = 2e^{-\xi\omega_0}\cos\Omega_d \quad , \quad b_2 = -e^{-2\xi\omega_0}, \tag{2.4}$$

where $\Omega_0 = \omega_0\Delta t$ and $\Omega_d = \sqrt{1-\xi^2}\Omega_0$. Another interpretation of this choice of b_1 and b_2 is that it ensures that the poles of the transfer function of the oscillator are also poles of the transfer function of the algorithm [5]. It may be noted that this model based on the algorithm given by Eqns. (2.2), (2.3) is highly computationally efficient and, in addition, it gives very accurate results. A comparison of a response history obtained using the fast algorithm and that using the 4-th order Runge-Kutta method is shown in Fig. 2.1 for a system with $\omega_0 = 2$ Hz and $\xi = 5\%$ subjected to a scaled El Centro ground motion. The superiority of this algorithm over the Runge-Kutta method is also prominent in other case studies. Suppose now that this model is used for an identification study in which the input/ output data, $\ddot{x}(t)$ and $r(t)$, are given, and the system characteristics ξ and ω_0 are to be identified. According to Eqn. (2.2), the coefficients b_1, b_2, and c_1 can be found easily using regression analysis technique such as the least-square method. Thus, based on Eqn. (2.4) we can solve for ξ and ω_0 from b_1 and b_2 as follows :

$$\xi = \sqrt{\frac{1}{1+\left(\frac{a_2}{a_1}\right)^2}}, \quad \omega_0 = \frac{a_1}{\xi\Delta t}, \tag{2.5}$$

where

$$a_1 = -\frac{1}{2}\log(-b_2), \quad a_2 = \cos^{-1}\left(\frac{b_1}{2}\exp(a_1)\right). \tag{2.6}$$

This method of identification is also computationally efficient, since there is no nonlinear optimization process involved in the parameter identification procedure. However, the identification results using the model based on the foregoing discrete recursive algorithm will be significantly degraded when there is some noise present. This is due to a numerical ill-conditioning inherent with the model. It follows from Eqn. (2.4) that for lightly damped systems, the two coefficients satisfies

$$b_1 \approx 2^-, \quad b_2 \approx -1^+, \tag{2.7}$$

i.e., b_1 is close to but less than 2, and b_2 is close to but greater than -1. If the identified b_1 and b_2 satisfy the relations given in (2.7), then the system parameters ξ and ω_0 can have reasonable values. However, due to the presence of measurement noise or numerical error, it is very possible that the values of b_1 and b_2 identified using the least-square method do not meet (2.7). As a result of this, the parameters ξ and ω_0 computed using (2.5), (2.6) may become totally unrealistic due to the logrithmic function involved in Eqn. (2.6). For example, if we have $b_1 = 2.000$, $b_2 = -1.001$ and $\Delta t = 0.01$ sec, then by Eqns. (2.5), (2.6) we find $\xi \simeq 1\%$ and $\omega_0 \simeq -0.42$ Hz, where the negative frequency does not make any sense in reality. Besides, since ξ and Δt are usually small in practical dynamic analyses, the error of ω_0 computed using Eqn. (2.5) may become quite large even if the error of the identified a_1 is small.

Through the above example we realize that a model which is simple and computationally efficient may lack robustness for identification due to the high sensitivity of its parameter values to "noise." However, we remark that if the output-error method, instead of the equation-error method, is used with the discrete recursive model, i.e., the optimal parameters ξ and ω_0 are obtained directly by minimizing some error function associated with output variables without first finding the coefficients b_1 and b_2, then the lack of robustness of the model vanishes and as demonstrated by Beck [3], the model actually works well in the modal identification of multi-degree-of-freedom linear structural systems.

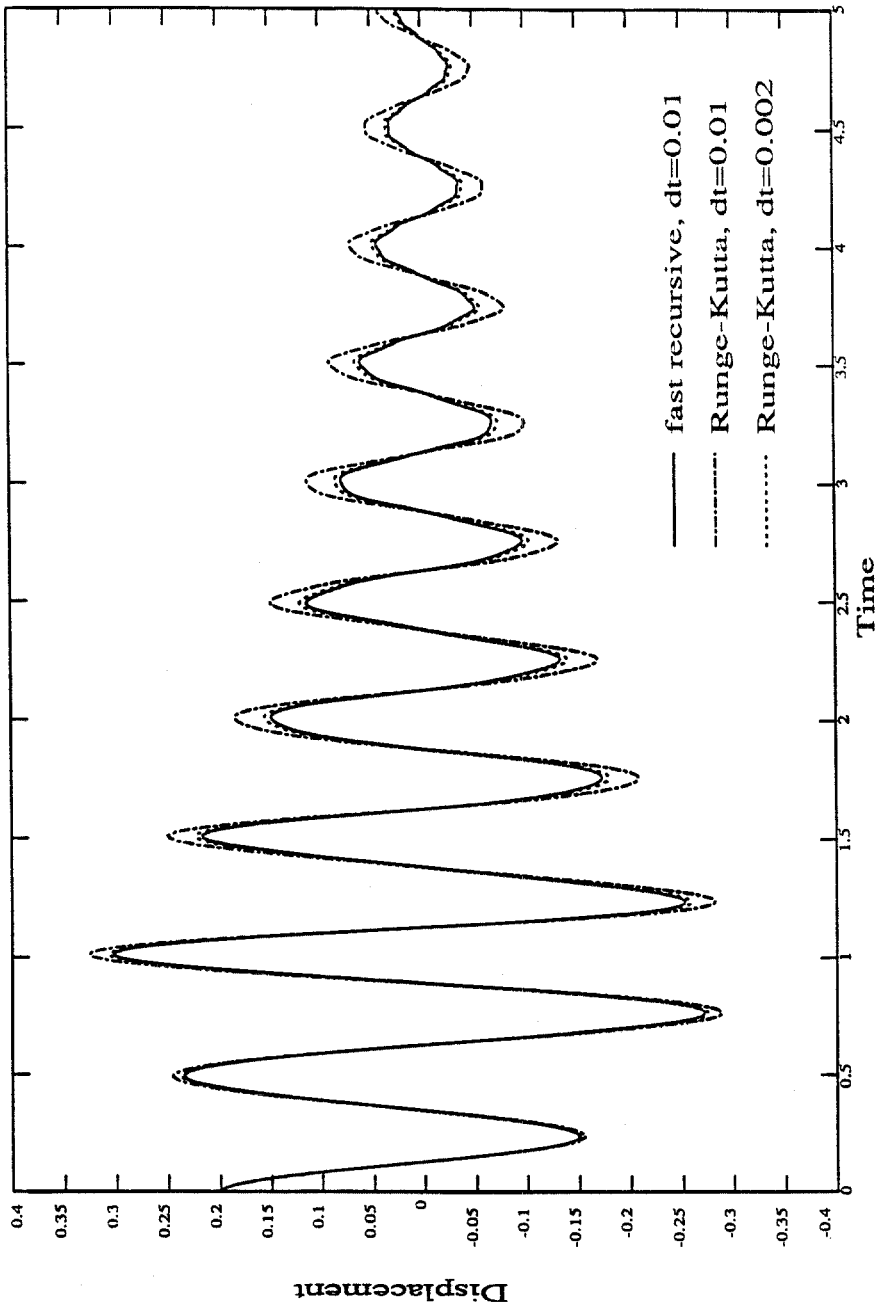

Figure 2.1 Comparison of response histories obtained using the fast algorithm and the 4-th order Runge-Kutta metha

CHAPTER 3

MODELING OF ONE-DIMENSIONAL HYSTERETIC SYSTEMS

3.1 Introduction

Linear models, though mathematically simple, are only good for representing structure response resulting from small loadings. When subjected to severe excitations such as strong seismic ground motions, structures usually respond inelastically so that nonlinear analytical models are required to adequately represent the structural behavior. In most cases, the response of a system that is stressed beyond its "yield point" into the nonlinear regime depends not only on the instantaneous state, but also on its past history. The history-dependence phenomenon is generally referred to as hysteresis. The study of analytical modeling of nonlinear, hysteretic behavior of mechanical systems has thus been a research area of great interest.

In this chapter, we are concerned with one-dimensional hysteretic models that can be used to describe nonlinear restoring force-deflection behavior or uniaxial stress-strain relations of structural systems. The more general modeling of constitutive laws of materials will be discussed later on in the following chapters. The simplest hysteretic models are probably the elasto-perfectly-plastic model and the bilinear model, as sketched in Fig. 3.1(a) and (b), respectively. These models have been used extensively in many engineering applications due to their analytical tractability. However, they are often too simple to yield good approximation to real systems. Previous studies [23, 51] indicated that the deviation from linearity around the yield point of a structural system should have a smooth transition in general as it reflects the effect of the yielding in an assemblage of many structural members. Furthermore, these simple models do not account for the hysteretic energy dissipation at small-amplitude cyclic response after the occurrence of yielding, which can lead to a higher predicted response level than the actual response [39].

Various mathematical models have been proposed for modeling of hysteretic behavior of structural systems. A thorough understanding of these models helps further modeling processes involved in building up new more general models. However, a comprehensive review of existing nonlinear models will not be presented herein,

since many good references on this topic are readily available, for example, [23, 45]. Instead, we will concentrate on those models that can give smooth transition from linear into the nonlinear regime. These models include those described solely by differential equations involving "hidden variables", physically-based Distributed-Element Models [19, 20], and the Masing models which are formulated based on Masing's hypothesis and some extended rules [23].

Since the inelastic response of a structural system is usually accompanied by stiffness and/or strength deterioration, it is important to extend the hysteretic models to account for these effects so that they can be used for modeling of degrading systems. This will also be investigated in this chapter. A new class of deteriorating Masing models will be proposed for identification purposes to substitute for a class of maximum-displacement-controlled deteriorating Distributed-Element Models proposed by Iwan and Cifuentes [22].

3.2 Modeling of Hysteretic Systems without Deterioration

3.2.1 Hysteretic Models Described Solely by Differential Equations

Analytical hysteretic models that are described solely by differential equations in general have the advantage of good mathematical tractability. A well-known model in this category is the Bouc-Wen model which was originally proposed by Bouc and later generalized by Wen [51], who also applied this model to random response analysis of structural systems [52]. The model is completely described by the following first-order, nonlinear ordinary differential equation:

$$\dot{r} = A\dot{x} - (\alpha|\dot{x}||r|^{n-1}r - \beta\dot{x}|r|^n), \tag{3.1}$$

where r is the hysteretic restoring force and x is the displacement of a system. The parameters A, α, β, and n control the slope, amplitude, and shape of the hysteretic loops and the smoothness of yielding. This model can be shown to exhibit an exponential type of curvilinear behavior. A simulated response of the Bouc-Wen model is shown in Fig. 3.2(a), where the model is subjected to a prescribed displacement history of growing sine waves as shown in Fig. 3.2(b). Note that the

Bouc-Wen model is actually a rate-independent model as Eqn. (3.1) can be put into the form

$$\frac{dr}{dx} = A \pm (\alpha \pm \beta)\, r^n, \tag{3.2}$$

depending on the signs of $\dot{x}$ and r.

Some special cases of the Bouc-Wen model are noteworthy, as they form the basis of later investigations on constitutive modeling for the general multi-axial loading cases. One is the Ozdemir's model without "back-stress" [36] which can be described by the differential equation:

$$\frac{\dot{r}}{r_0} = \frac{\dot{x}}{x_0} - \left|\frac{\dot{x}}{x_0}\right| \left(\frac{r}{r_0}\right)^n, \tag{3.3}$$

where r_0 is the yielding force and x_0 the yielding displacement of a system. Another way to write Eqn. (3.3) is

$$\dot{r} = \left(\frac{r_0}{x_0}\right)\left[\dot{x} - |\dot{x}|\left(\frac{r}{r_0}\right)^n\right]. \tag{3.4}$$

Note that r_0/x_0 represents the linear (small-amplitude) stiffness of the system. Another special case of Eqn. (3.1) can be found by putting $A = E$, $\alpha = 1/Z$, $\beta = 0$ and $n = 1$ to yield

$$\dot{r} = E\,\dot{x} - \frac{1}{Z}|\dot{x}|\, r, \tag{3.5}$$

or

$$dr = E\, dx - \frac{1}{Z}|dx|\, r. \tag{3.6}$$

Equation (3.6) describes a simple endochronic model* [46, 47] as shown by Bazant and Bhat [2]. The merit of these models described by differential equations lies in that they are completely defined by a single differential equation so that their applications to various engineering problems can be made more easily. For instance, it is possible to find the closed-form solution of the stochastic equivalent linearization coefficients for the Bouc-Wen model given by Eqn. (3.1) under some mild assumptions of a joint Gaussian distribution on the variables involved [52]. This is the main reason why this model has been widely used in random vibration analysis of hysteretic systems.

---

* A detailed description of the endochronic model will be given in Chapter 4.

Although the foregoing hysteretic models described solely by differential equations have already had many engineering applications, they commonly exhibit some unrealistic characteristics that are inconsistent with the physical behavior of many materials or structural systems. The main problem from a practical point of view is the unstable drift exhibited by these models when subjected to small cyclic excitations. This kind of unrealistic behavior may be attributed to the lack of physical motivation in formulating the models. To examine in detail this unrealistic model behavior, we note that Eqn. (3.6) can be rewritten as

$$\frac{dr}{dx} = E\Big(1 \mp \frac{r}{EZ}\Big) = E\Big(1 \mp \frac{r}{r_0}\Big), \tag{3.7}$$

where the minus sign corresponds to the loading case, while the plus sign corresponds to the unloading case. Also, in Eqn. (3.7), we put $EZ = r_0$, the ultimate strength of the model, since we have $dr/dx \to 0$ as $r \to r_0$. Thus, we may observe from Eqn. (3.7) that the unloading stiffness of the system, given by $E(1 + r/r_0)$, can be much larger than the tangent stiffness of loading, given by $E(1 - r/r_0)$. This property yields artificial drift, and also leads to the violation of Drucker's stability postulates, since under small cyclic loading, the force-deflection loops are wide open, as shown in Fig. 3.3, which means that energy is generated instead of being dissipated through hysteresis. As shown by Sandler [40], such nonphysical behavior will also lead to numerical instability when the models are used for the numerical solution of well-posed mechanical problems.

3.2.2 The Distributed-Element Model

In 1926, Masing [31] proposed the so-called Masing's hypothesis for one-dimensional hysteretic behavior of materials by thinking of a hysteretic system as consisting of a collection of many ideal elasto-plastic elements, all of which have the same elastic stiffness but different yield levels. Later in 1959, Whiteman [54], based on the same idea, derived the uniaxial stress-strain relation of such a model by introducing the concept of the "frequency" distribution function of the yield levels of elements. By postulating a suitable distribution function for the yield levels of elements, he found that the changes in the hysteresis loops are similar to those that occur in reality, and the Bauschinger effect can be appropriately accounted for. It

was Iwan [19] who first referred to such models as the Distributed-Element Models (DEMs) and applied them to structural dynamic analysis. He constructed a model composed of a set of N elements connected in parallel, each of which consists of a linear spring with stiffness k/N in series with a slip element (Coulomb damper) of strength r_i^*/N , as shown in Fig. 3.4. Each element in the assemblage is thus an ideal elasto-plastic element that has a force-deflection behavior as described in Fig. 3.1(a). The DEM has been considered as physically motivated, as many real materials or mechanical systems can be thought of as having a similar structure. For example, real materials may have a crystalline structure that is made up of a distribution of slip-planes or dislocations of different slip strengths. Therefore, the behavior of such a class of models can be expected to be physically consistent, without exhibiting unrealistic characteristics. The restoring force of a DEM consisting of N elements can be found to be given by

$$r = \sum_{i=1}^{n} \frac{r_i^*}{N} + k\,x\,\frac{N-n}{N} \tag{3.8}$$

for initial loading, where n is the number of elements in the yielding state. When the total number of elements N becomes very large, the summation in Eqn. (3.8) may be replaced by an integral so that Eqn. (3.8) becomes

$$r = \int_0^{kx} r^*\phi(r^*)\,dr^* + k\,x\int_{kx}^{\infty} \phi(r^*)\,dr^*, \tag{3.9}$$

where $\phi(r^*)\,dr^*$ denotes the fraction of the total number of elements with strengths in the range $r^* \le r_i^* \le r^* + dr^*$, and the yield-strength distribution function $\phi(r^*)$ satisfies

$$\int_0^{\infty} \phi(r^*)\,dr^* = 1. \tag{3.10}$$

When the loading is reversed after initial loading (i.e., unloading occurs), the force-deflection relation can be found similarly by keeping track of response behavior of elements in different states (yielded or elastic). This procedure can be carried on to trace out the entire history of hysteresis without the need to introduce additional rules for different loading conditions. The adaptability of the DEM to transient loading problems was considered as one of the important advantages of the model. However, evaluation of the integrals involved in the procedure, such as those shown

in Eqn. (3.9), may not be efficient for numerical solutions. Thus, in practical applications using the DEM, such as the system identification study performed by Cifuentes and Iwan [9], one has to introduce a finite number of elements so that their response can be traced with reasonable computation effort. This would, somehow, degrade the results of analysis (e.g., the hysteretic yielding response curves become non-smooth), and, moreover, make the parameter identification more difficult, unless some additional assumptions are made regarding elements' behavior so that the number of parameters involved in the model can be appropriately reduced. It is important to note that the DEMs actually fall within the general class of Masing models whose behavior can be described by the Masing's hypothesis and some extended rules [23]. This will be elucidated in the next section.

3.2.3 The General Class of Masing Models

3.2.3.1 Masing's Hypothsis and Extended Rules

In his original paper titled "Self Stretching and Hardening for Brass" [31], Masing asserted that if the force-displacement curve for a system at the initial loading is described by

$$f(r, x) = 0, \tag{3.11}$$

were r is the restoring force and x the displacement of the system, then the unloading and reloading branches of the steady-state hysteretic response of the system are geometrically similar to the initial loading curve except for a two-fold magnification, and are described by

$$f\left(\frac{r - r_0}{2}, \frac{x - x_0}{2}\right) = 0, \tag{3.12}$$

where (x_0, r_0) is the load reversal point for that particular loading branch. Note that the function f should satisfy

$$f(-r, -x) = f(r, x) \tag{3.13}$$

so that the initial force-deflection curve is symmetric about the origin. The above assertion is usually referred to as Masing's hypothesis for steady-state cyclic hysteretic response. A schematic diagram illustrating Masing's hypothesis is shown in Fig. 3.5. The model behavior obtained using Masing's hypothesis is consistent

with some experimental observations of the Bauschinger effect occurring in some metals, which indicates that an initial plastic deformation in one direction reduces the resistance of the material with respect to a subsequent plastic deformation in the opposite direction. This effect is usually attributed to the residual stresses left in the material due to initial loading or to the anisotropy of the dislocation field generated by loading processes [26]. Some properties of response behavior using Masing's hypothesis were summarized in [23] and are not reiterated here. One major concern associated with the original Masing's hypothesis is that it is useful only for steady-state cyclic response or loading between fixed limits. In the case of transient response, or loading between variable limits, the hypothesis was considered to be of no help. However, Jayakumar [23] proposed an extension of Masing's hypothesis by stipulating two general hysteresis rules so that simple and physical behavior for transient hysteretic response can be obtained accordingly. The two rules are as follows:

Rule 1: Incomplete Loops

The equation of any hysteretic response curve, irrespective of steady-state or transient response, can be obtained simply by applying the original Masing rule to the virgin loading curve using the latest point of loading reversal.

Consider, for example, the hysteretic loops shown in Fig. 3.6. If the virgin loading curve OA is characterized by Eqn. (3.11), then applying Rule 1, the equation for the branch curve CD will be

$$f\left(\frac{r - r_c}{2}, \frac{x - x_c}{2}\right) = 0. \tag{3.14}$$

Based on Eqn. (3.14), it is easy to show that if the reloading curve CD in Fig. 3.6 had been continued, it would have formed a closed hysteresis loop given by $ABCDA$.

Rule 2 : Completed Loops

The ultimate fate of an interior curve under continued loading or unloading is such that once the interior curve crosses a curve described in a previous load cycle, the force-deformation curve follows that of the previous cycle.

Based on Rules 1 and 2, if the transient unloading curve DE in Fig. 3.6 is continued, it will reach point C and then follow the curve ABC.

An effective algorithm for numerical implementation of these extended Masing rules was proposed by Thyagarajan [45], and this algorithm has been adopted in the present study for response simulation of Masing models. In the algorithm, two load reversal points are removed from the memory list each time an interior response curve crosses a curve described in a previous load cycle. One important result regarding the extended Masing rules is that the hysteretic behavior of a DEM can be completely described by these rules without the need of tracing each element's behavior. This has been proven by Jayakumar [23], who then proposed a general class of Masing models based on the extended Masing rules. To specify any particular model in this class, only its initial loading curve need be prescribed. The complete hysteretic behavior of this general class of Masing models is then governed by the extended rules 1 and 2 stated above.

Thus, a DEM can be equivalent to a general Masing model if the yield-strength distribution function $\phi(r^*)$, along with the stiffness constant k, of a DEM is chosen to match identically the initial loading curve for a general Masing model. Considering the equivalence of the two classes of models, one may prefer to use the Masing models in practical applications, since the implementation of the Masing models is much simpler and more efficient than that of the DEMs. In particular, for applications, such as system identification studies, that involve a large number of iterations of model response calculations, numerical efficiency is of vital importance in the choice of models, provided that the models do not exhibit any unrealistic or unstable behavior.

3.2.3.2 A Special Class of Masing Models

Following the general class of Masing models based on the extended Masing rules for transient response, Jayakumar and Beck [24] proposed a special class of Masing models by defining the restoring force-deformation relation for the virgin loading by the differential equation:

$$\frac{dr}{dx} = k\left[1 - \left|\frac{r}{r_u}\right|^n\right], \tag{3.15}$$

where k, r_u and n are three model parameters which provide sufficient flexibility to capture the essential features of hysteretic behavior of most structural systems.

The parameters k and r_u, respectively, represent the small-amplitude stiffness and the ultimate strength of the system to be modeled. The additional parameter n is introduced to model different degrees of smoothness around the yielding point, as shown in Fig. 3.7, where the case $n \to \infty$ corresponds to the elasto-perfectly plastic model.

Based on the extended Masing rules, the force-deformation relation for any loading branch other than the virgin curve is thus defined by the following equation:

$$\frac{dr}{dx} = k\left[1 - \left|\frac{r - r_0}{2r_u}\right|^n\right]. \tag{3.16}$$

It should be noted that the structure of Eqn. (3.15) is similar to those used in many other models, including the Bouc-Wen, Ozdemir, and the simple endochronic models as introduced in Section 3.2. The major difference, though, is that for the special class of Masing models, Eqn. (3.15) is used only for virgin loading, not for the complete response history. The major advantage of introducing the supplementary hysteresis rules is that unrealistic cyclic behavior, such as unstable drift and nonclosure of hysteresis loops, can be eliminated.

This special class of models has been applied to system identification studies using inelastic pseudo-dynamic test data from a full-scale, six-story steel structure [24]. Even though a shear-building approximation was used in the modeling of the pseudo-dynamic test structure, good results obtained confirm the applicability of this class of hysteretic models to real structures. Some other special classes of Masing models can also be proposed by choosing particular yield-strength distribution functions that satisfy Eqn. (3.10) and are characterized by suitable parameters. More will be said about this in the next section when the Masing models are extended to account for the effects of strength and stiffness degradation.

3.3 Modeling of Degrading Hysteretic Systems

The response of mechanical systems to strong excitations can usually be characterized by inelastic behavior through which energy is dissipated due to hysteresis. Frequently, however, the inelastic response of a structural system is accompanied by stiffness and/or strength deterioration due to damage accumulation under cyclic loads. The effects of deterioration of a system usually include:

1) a loss of stiffness, which often results in an increase in the period of vibration,
2) a decrease in energy dissipation capacity,
3) a redistribution of internal forces, and
4) a reduction of ultimate strength.

Iemura and Jennings [18] have observed a stiffness degradation of more than 50%, based on the change of natural frequencies, by analyzing measurements from Millikan Library Building, located on the campus of California Institute of Technology, Pasadena, during the 1971 San Fernando earthquake. Therefore, structures under strong environmental loads are expected to undergo nonlinear and time-dependent degrading behavior. The analysis of such a problem is also important in many other engineering areas, such as damage detection of space structures and adaptive control of mechanical systems. The difficulty of modeling such hysteretic degrading systems often lies in the fact that the exact nature of system degradation depends not only on the structural materials but also on the detailed configurations, and may vary considerably from system to system.

In this section, we will investigate the extension of the three types of one-dimensional hysteretic models described in the previous section to account for the effects of deterioration observed in actual structural systems.

3.3.1 The Degrading Bouc-Wen Model

The versatile nature and simple analytic form of the Bouc-Wen model as described by Eqn. (3.1) has attracted considerable attention from researchers in many related engineering fields. To make it even more general, Wen [52] extended the original model to include the effects of strength and stiffness deterioration. The modeling technique for incorporating system degradation consists of the introduction of more control parameters and the selection of a response index on which the rate of degradation is based. Wen extended Eqn. (3.1) to

$$\dot{r} = \frac{1}{\eta}[A\dot{x} - \nu(\alpha|\dot{x}||r|^{n-1}r - \beta\dot{x}|r|^n)], \tag{3.17}$$

where the two additional parameters η and ν are introduced to control the stiffness and strength degradation, respectively, by assuming that they are functions of a

properly-chosen response index. In his original work, Wen also chose the parameter A that controls the response amplitude to be a function of the response index so that the model thus defined can achieve the maximum flexibility in modeling general hysteretic behavior, including strain hardening or softening effects. The response index on which the degrading parameters depend should be able to reflect the severity and duration of the system response and is usually selected as the maximun displacement experienced by the model or the total energy dissipated through hysteresis, depending on the specific structural system being modeled. Fig. 3.8 illustrates the effects of the degrading parameters on the model behavior, in which the parameters A, η, ν are defined as

$$A(e) = A_0 - \delta_A\, e,$$

$$\eta(e) = 1.0 + \delta_\eta\, e, \quad \nu(e) = 1.0 + \delta_\nu\, e,$$

where e denotes the accumulation of the dissipated hysteretic energy, and the δ's are constants specified for the desired rate of degradation. Although the degrading hysteretic model given by Eqn. (3.17) is general and flexible, and it has closed-form stochastic equivalent linearization coefficients as well, it is in general over-parameterized, which causes difficulties in choosing appropriate parameter values because of lack of identifiability when the model is applied to system identification studies. For example, as reported in the paper by Sues et al. [42], the parameters identified from simulated response can have values very different from those originally used in the simulation of response histories, though the response generated by the identified parameters was found to be almost identical with that generated with the original set of parameters. Another problem with the model is, as stated earlier in this chapter, that it exhibits unrealistic drift behavior when subjected to small cyclic excitations, which leads to a violation of Drucker's postulates of stability.

3.3.2 A Class of Deteriorating Distributed-Element Models

In order to apply the physically-motivated Distributed-Element Model (DEM) to practical structural problems encountered in earthquake engineering, Iwan and Cifuentes [22] presented a class of deteriorating DEMs for the overall restoring force behavior of reinforced concrete structures. This deteriorating model consists of the

same ensemble of linear springs and Coulomb slip elements as shown in Fig. 3.4; however, some of the elements are allowed to "break" if the absolute value of the displacements of an element exceeds some value, say μY_i, $\mu \geq 1$, where Y_i is the slip (yield) displacement of the element. Once the element "fails", it no longer contributes to the overall restoring force. Fig. 3.9 illustrates the restoring force diagram of a typical "breaking" element, and Fig. 3.10 shows an example of the overall response behavior of such a model subjected to a real earthquake excitation. Note that the parameter μ acts as the maximum ductility ratio of an element defined as the ratio of maximum possible displacement response to the yield displacement of an element. It was also assumed for simplicity that all the elements of a model have the same value of μ. This deteriorating model was shown to be capable of describing the major features of the restoring force behavior of concrete structures [22] while still maintaining the inherent simplicity of the original DEM. This model has also been applied to system identification studies of real structures using earthquake data [9] to assess the damage suffered by a structure and to predict its future performance.

Although satisfactory identification results were obtained using this special class of deteriorating DEMs, some additional assumptions were made in [9] pertaining to the relations among parameters and to the number of elements so that the actual number of parameters of the model was low enough for reliable identification. The introduction of these additional assumptions on the class of deteriorating DEMs reduces the generality and physical reality of the otherwise physically-consistent models. This point motivated the extension of the Masing rules described in the previous section to the case where degradation effects are of interest. If we can derive a general class of deteriorating Masing models within which the aforementioned deteriorating DEMs fall, then not only the numerical implementation of the models can be greatly simplified, but also the problem of parameter identifiabilty can be resolved without sacrificing the flexibility and accuracy of the model behavior.

3.3.3 A Class of Deteriorating Masing Models

3.3.3.1 General Formulation

We have mentioned in Section 3.2 the equivalence between the classes of DEMs and Masing models such that a class of DEMs may be replaced by a class of Masing models in system identification applications in which parameter identifiability is of major concern. The extended Masing rules on which the behavior of the general class of nondegrading Masing models are based provide an effective way of implementing numerically the model behavior. In the case where degradation effects are to be taken into account, can we still find some appropriate rules so that the behavior of the DEMs can be found without the need of keeping track of elements' behavior? This question is answered affirmatively in this section for the class of maximum-displacement-controlled DEMs mentioned in the previous section.

To begin with, we propose a general formulation for modeling of degrading systems. Following the integral formulation of the DEM, such as that given by Eqn. (3.9), a *damage index function* $\alpha = \alpha(r^*, x)$ † can be introduced so that at displacement x, the fraction of the total number of elements which are "undamaged" and with yield strengths in the range $[r^*, r^* + dr^*]$ can be denoted as $\alpha(r^*, x)\phi(r^*)\,dr^*$ ‡. Thus, for initial loading, the restoring force can be represented as

$$r(x) = k\,x \int_{kx}^{\infty} \phi(r^*)\,dr^* + \int_0^{kx} r^*\alpha(r^*, x)\phi(r^*)\,dr^*, \tag{3.18}$$

where we assume that $\alpha(r^*, x) = 1$ for $r^* \geq kx$, which means that elements that are unyielded must be undamaged. The second term on the right-hand side of Eqn. (3.18) is the contribution from elements that are yielded at deformation x, and the first term denotes the contribution from elements that are still in the elastic state for which $\alpha(\cdot, \cdot) = 1$.

---

† In general, α can be a function of the history of x, not just $x(t)$.

‡ $(1-\alpha)$ could be viewed as the fraction of elements in the yield range $[r^*, r^*+dr^*]$ which have failed and completely lost their strength, or that $(1-\alpha)$ is the "average" partial loss of strength of each element in the yield range $[r^*, r^* + dr^*]$.

Similarly, for unloading from x_0, we have for $-x_0 \leq x \leq x_0$,

$$r(x) = k\,x \int_{kx_0}^{\infty} \phi(r^*)\,dr^* + \int_{\frac{k(x_0-x)}{2}}^{kx_0} [r^* - k(x_0 - x)]\,\alpha(r^*, x)\,\phi(r^*)\,dr^*$$

$$+ \int_0^{\frac{k(x_0-x)}{2}} -r^*\alpha(r^*, x)\,\phi(r^*)\,dr^*, \tag{3.19}$$

and for $x < -x_0$,

$$r(x) = k\,x \int_{-kx}^{\infty} \phi(r^*)\,dr^* + \int_0^{-kx} -r^*\,\alpha(r^*, x)\,\phi(r^*)\,dr^*. \tag{3.20}$$

Very similar equations can also be derived for reloading. Equations (3.18), (3.19) and (3.20) can be differentiated with respect to x to get equations for the model "stiffness" as follows:

$$\frac{dr}{dx} = k \int_{kx}^{\infty} \phi(r^*)\,dr^* + \int_0^{kx} r^*\,\frac{\partial\alpha(r^*, x)}{\partial x}\,\phi(r^*)\,dr^*, \tag{3.21}$$

for initial loading,

$$\frac{dr}{dx} = k \int_{kx_0}^{\infty} \phi(r^*)\,dr^* + k \int_{\frac{k(x-x_0)}{2}}^{kx_0} \alpha(r^*, x)\,\phi(r^*)\,dr^*$$

$$+ \int_{\frac{k(x_0-x)}{2}}^{kx_0} [r^* - k(x_0 - x)]\,\frac{\partial\alpha(r^*, x)}{\partial x}\,\phi(r^*)\,dr^* - \int_0^{\frac{k(x_0-x)}{2}} r^*\,\frac{\partial\alpha(r*, x)}{\partial x}\,\phi(r^*)\,dr^*, \tag{3.22}$$

for unloading from x_0 with $-x_0 \leq x \leq x_0$, and

$$\frac{dr}{dx} = k \int_{-kx}^{\infty} \phi(r^*)\,dr^* - \int_0^{-kx} r^*\,\frac{\partial\alpha(r^*, x)}{\partial x}\,\phi(r^*)\,dr^*, \tag{3.23}$$

for unloading from x_0 with $x < -x_0$.

We may note that the equations for r and dr/dx in the case of unloading from x_0 with $x < -x_0$ (Eqns. (3.20) and (3.23)) are the same as those for initial loading in the negative direction (cf. Eqns. (3.18) and (3.21)). This is consistent with the extended Masing rule 2 regarding completed loops for transient response, as stated in the previous section. Based on the above general formulation for modeling of degrading systems, we can propose different classes of degrading models by suitably

choosing the damage index functions α. A specific example of choosing α as a Heaviside step function will be given in the next section to illustrate the above formulation.

3.3.3.2 A Special Class of Deteriorating Masing Models

To gain more insight into the above general formulation, we consider the special case where a specific damage index function is chosen for modeling deteriorating behavior of hysteretic systems. If, for example, the maximum-displacement-controlled deteriorating DEM described in the previous section is to be derived from this general formulation, we can choose the following damage index function:

$$\alpha(r^*, x) = 1 - H\left(\frac{kx_m(t)}{\mu} - r^*\right), \tag{3.24}$$

where $H(\cdot)$ is the Heaviside step function, $x_m(t) \equiv \max_{\tau \le t} |x(\tau)|$, which is the maximum displacement magnitude experienced by the model, and μ is the parameter of maximum ductility ratio of the model. Note that the maximum possible displacement of an element with yield strength r^* is given by $\mu r^*/k$. Using Eqns. (3.21), (3.22), and (3.23) with α given by Eqn. (3.24), and defining the "stiffness" function

$$f(x) \equiv k \int_{kx}^{\infty} \phi(r^*)\, dr^*,$$

which is assumed to be differentiable, we can find

$$\frac{dr}{dx} = k \int_{kx}^{\infty} \phi(r^*)\, dr^* - \frac{k^2 x}{\mu^2}\, \phi\left(\frac{kx}{\mu}\right) = f(x) + \frac{x}{\mu^2}\, f'\left(\frac{x}{\mu}\right), \tag{3.25}$$

for initial loading,

$$\frac{dr}{dx} = k \int_{\frac{kx_0}{\mu}}^{\infty} \phi(r^*)\, dr^* = f\left(\frac{x_0}{\mu}\right), \tag{3.26}$$

for unloading from x_0 with $\frac{\mu-2}{\mu} x_0 \le x < x_0$, where we note that $f(x_0/\mu)$ is a constant so that the restoring force r is linear over this portion,

$$\frac{dr}{dx} = k \int_{\frac{k(x_0 - x)}{2}}^{\infty} \phi(r^*)\, dr^* = f\left(\frac{x_0 - x}{2}\right), \tag{3.27}$$

for unloading from x_0 with $-x_0 \leq x < \frac{\mu-2}{\mu} x_0$, and

$$\frac{dr}{dx} = k \int_{-kx}^{\infty} \phi(r^*)\, dr^* + \frac{k^2 x}{\mu^2}\, \phi(\frac{-kx}{\mu}) = f(-x) - \frac{x}{\mu^2}\, f'(\frac{-x}{\mu}) \tag{3.28}$$

for continued loading where $x < -x_0$. Note that in the derivation $\partial\alpha/\partial x$ is zero unless x_m is increasing during the loading branch under consideration. The above results lead to the following remarks pertaining to the behavior of the special class of degrading Masing models:

1) By symmetry of the force-deflection response about the origin, we require that the stiffness function f be even, i.e., $f(-x) = f(x)$, and as a result, $f'(x)$ must be an odd function of x.
2) By comparing with the formulation of the nondegrading case, we can find that the term $\frac{x}{\mu^2} f'(\frac{x}{\mu})$ signifies the effect of stiffness deterioration due to the breaking behavior of elements. One can also find the corresponding term for strength deterioration from equations for the restoring-force function $r(x)$.
3) Eqn. (3.28) is equivalent to Eqn. (3.25) with x replaced by $-x$, which is consistent with the extended Masing rule 2 on completed loops as mentioned earlier.
4) It can be shown that for the case of reloading from $-x_0$, the result will be identical to those derived for unloading from x_0, except for that the term $\frac{x_0 - x}{2}$ is replaced by $\frac{x - x_0}{2}$.
5) The steady-state response behavior of the maximum-displacement-controlled deteriorating DEM can be summarized as follows for the case of cycling between displacement $[-x_0, x_0]$ with previous maximum displacement amplitude x_m:

$$\begin{aligned}
\frac{dr}{dx} &= f(x) + \frac{x}{\mu^2} f'(\frac{x}{\mu}) \quad \text{(for initial loading)}, \\
&= f(\frac{x_m}{\mu}), \quad \text{if} \begin{cases} x_0 > x \geq x_0 - \frac{2x_m}{\mu} & \text{(for unloading)}, \\ -x_0 < x \leq -x_0 + \frac{2x_m}{\mu} & \text{(for reloading)}, \end{cases} \\
&= f(\frac{x_0 - x}{2}), \quad \text{if} \quad x_0 - \frac{2x_m}{\mu} > x \geq -x_m \quad \text{(unloading)}, \\
&= f(\frac{x - x_0}{2}), \quad \text{if} - x_0 + \frac{2x_m}{\mu} < x \leq x_m \quad \text{(reloading)}, \\
&= \text{same as initial loading}, \quad \text{if } |x| = x_m \text{ with } |x| \text{ increasing}.
\end{aligned} \tag{3.29}$$

6) The results given in Eqns. (3.29) can also be obtained by directly keeping track of elements' behavior at different response stages.
7) The behavior for the transient response of the model can be similarly derived and can be shown to be completely consistent with the extended Masing rules 1 and 2 proposed by Jayakumar [23] for the case of no degradation.
8) Typical behavior of the model response for different loading branches is shown in Fig. 3.11, where the effects of strength and stiffness deterioration can be clearly observed. The model is based on a Rayleigh distribution for the yield-strength distribution function $\phi(r)$ (cf. next section) with $k = 20, r_u = 1.2$, and $\mu = 5$.

In summary, we have derived a special class of degrading Masing models, which is equivalent to the maximum-displacement-controlled deteriorating DEMs proposed by Iwan and Cifuentes [22]. This class of degrading Masing models, however, can be completely defined by specifying the stiffness function f (or the initial loading curve) and μ, and the response behavior for other loading branches will follow the rules given in (3.29) and the two extended Masing rules for transient response given in Section 3.2. In this way, we not only simplify the numerical implementation of the special class of DEMs, but also solve the problem of parameter identifiability without introducing additional assumptions regarding model behavior. In other words, the applicability of such models to practical engineering problems is greatly increased.

As a final remark, we note that by choosing other damage index functions (which is equivalent to choosing some particular element behavior of the DEMs) based on theoretical results or physical observations, one can come up with different classes of degrading models that may be suitable for particular structural systems. An important feature of this modeling approach is that the models thus derived are all based on the behavior of distributed elements, which is supposed to be physically consistent, i.e., will not exhibit any unrealistic characteristics or introduce any physical or numerical instabilities.

3.3.3.3 Yield-Strength Distribution Function

Similar to the general class of nondegrading Masing models, a class of degrading Masing models can be completely defined by specifying the initial loading curves with some appropriate functions. This can, in general, be accomplished in two ways. One way is to specify the "stiffness" function $f(x)$ as shown in (3.29) directly in terms of x, or in the form of a differential equation, such as the special class of Masing models proposed by Jayakumar [24]. This special class of Masing models is described by the following differential equation for initial loading:

$$\frac{dr}{dx} = k\Big(1 - \Big|\frac{r}{r_u}\Big|^n\Big), \tag{3.30}$$

where only three parameters k, r_u and n are needed for modeling general yielding behavior. However, the function $f(x)$ cannot, in general, be found explicitly from Eqn. (3.30) except for the cases where $n = 1$ and $n = 2$, which results in the following relationships:

$$r = r_u\Big[1 - \exp\Big(\frac{-kx}{r_u}\Big)\Big] \tag{3.31a}$$

for $n = 1$, and

$$r = r_u \tanh\Big(\frac{kx}{r_u}\Big) \tag{3.31b}$$

for $n = 2$.

Another way of specifying the initial loading curve can be done by choosing appropriately the yield-strength distribution function $\phi(r^*)$. One may have noted that the distribution function $\phi(r^*)$ behaves the same as a probability density function does, as suggested by Eqn. (3.10). In this study, we propose the use of Rayleigh distribution described by

$$\phi(r) = \frac{\pi}{2}\frac{r}{r_u^2}\exp\Big(\frac{-\pi}{4}\frac{r^2}{r_u^2}\Big), \quad 0 \le r < \infty. \tag{3.32}$$

And by definition we can find the corresponding "stiffness" function given by

$$f(x) = k\int_{kx}^{\infty}\phi(r^*)\,dr^* = k\exp\Big[\frac{-\pi}{4}\big(\frac{kx}{r_u}\big)^2\Big], \tag{3.33}$$

which is expressed explicitly in terms of x. Also, we can find that the corresponding restoring force is given by

$$r(x) = \int_0^x f(\xi)\, d\xi = r_u \operatorname{erf}\Big(\frac{\sqrt{\pi}}{2}\frac{kx}{r_u}\Big), \tag{3.34}$$

where the error function $\operatorname{erf}(\cdot)$ is defined as

$$\operatorname{erf}(\eta) \equiv \sqrt{\frac{2}{\pi}} \int_0^\eta \exp(-\eta^2)\, d\eta.$$

We remark that the parameter r_u represents the ultimate strength of the model, since by Eqn. (3.34), $r(x) \to r_u$ as $x \to \infty$ (since $\operatorname{erf}(\infty) = 1$). The choice of the Rayleigh distribution is thought to be a natural one, since it distributes within [0, ∞) and has only one single parameter, as r_u in Eqn. (3.32). From Eqn. (3.34), we note that the Masing model derived using the Rayleigh distribution involves only two parameters k and r_u, which is similar to Eqns. (3.30) and (3.31) corresponding to fixed values of n. It can be shown, by numerical calculation, that the model using the Rayleigh distribution is very close to Jayakumar's special class of Masing models with $n = 2.5$, as illustrated in Fig. 3.12, where initial loading curves of the two models with the same values of k and r_u are compared.

A more general distribution function can be proposed, based on the Rayleigh distribution, as follows:

$$\phi(r) = \frac{2n\, r^{2n-1}}{\big(\frac{4}{\pi} r_u^2\big)^n} \exp\Big[-\Big(\frac{\pi r^2}{4 r_u^2}\Big)^n\Big], \quad 0 \le r < \infty, \quad n > 0, \tag{3.35}$$

which may be referred to as the *generalized Rayleigh distribution.* The additional parameter n is introduced to control the smoothness of transition from elastic to plastic state. When $n = 1$, Eqn. (3.35) reduces to the Rayleigh distribution given by Eqn. (3.32). A plot of the distribution curves described by the generalized Rayleigh distribution function for different values of n is shown in Fig. 3.13. We find from Eqn. (3.35) that

$$f(x) = k \exp\Big[-\Big(\frac{\pi}{4}\frac{k^2 x^2}{r_u^2}\Big)^n\Big], \tag{3.36}$$

and the restoring force can also be found in closed form as

$$r(x) = \frac{2}{\sqrt{\pi}}\, r_u\, \Gamma\Big(\nu x^{2n}, \frac{2n+1}{2n}\Big) + k\, x\, e^{-\nu x^{2n}}, \tag{3.37}$$

where we defined $\nu \equiv (\frac{\pi k^2}{4r_u^2})^n$ and

$$\Gamma(x, \alpha) \equiv \int_0^x e^{-t}\, t^{\alpha-1}\, dt, \tag{3.38}$$

which is the Incomplete Gamma function with parameter α.

Thus, we have defined a general class of degrading Masing models based on the generalized Rayleigh distribution function. Some major advantages of this class of models are as follows:

1) There are only 3 parameters k, r_u and n needed for modeling general one-dimensional non-degrading, hysteretic behavior. For modeling of degrading systems governed by maximum displacement response, only one additional parameter μ is needed. The parsimony and clear physical significance of parameters make this class of models excellent for identification purposes.
2) Explicit closed-form representations in terms of x can be obtained for the stiffness function f and the restoring force r. This feature makes the numerical implementation of this class of models computationally efficient, especially when the displacement history $x(t)$ is prescribed.
3) The mathematically tractable form of the stiffness function $f(x)$, given by Eqn. (3.36) in terms of the exponential function, allows this formulation to be handled more easily in the case of system deterioration, since the extended hysteretic rules for degrading behavior, described by (3.29), involve $f'(x)$ in addition to $f(x)$.
4) The specification of the yield-strength distribution function $\phi(r^*)$ facilitates the computation of some response quantities of the model based on statistical results. For example, if the drift (plastic deformation) response $d(t)$ of a non-degrading DEM based on the Rayleigh distribution is of interest, then we can simply find the mean (expected) value of the drifts of all the distributed elements constituting the model. Thus, for initial loading with $\dot{x} > 0$,

$$\begin{aligned} d(t) &= \int_0^{kx} \left(x - \frac{r}{k}\right) \phi(r)\, dr \\ &= \int_0^{kx} \left(x - \frac{r}{k}\right) \frac{\pi r}{2r_u^2} \exp\left(-\frac{\pi r^2}{4r_u^2}\right) dr \end{aligned}$$

$$= x - \frac{r_u}{k} \operatorname{erf}\left(\frac{\sqrt{\pi} k x}{2 r_u}\right)$$
$$= x - \frac{r(x)}{k}. \tag{3.39}$$

This "statistical" interpretation of plastic deformation is thus equivalent to the conventional formulation of the total-deformation theory, as illustrated in Fig. 3.14. Also, for unloading or reloading from x_0,

$$\begin{aligned} d(t) &= d_0 \pm \int_0^{\frac{k|x-x_0|}{2}} \left(|x - x_0| - \frac{2r}{k}\right) \phi(r)\, dr \\ &= d_0 \pm \left[|x - x_0| - \frac{2r_u}{k} \operatorname{erf}\left(\frac{\sqrt{\pi}}{4} \frac{k|x - x_0|}{r_u}\right)\right] \\ &= d_0 \pm 2\left[\bar{x} - \frac{r_u}{k} \operatorname{erf}\left(\frac{\sqrt{\pi} k \bar{x}}{2 r_u}\right)\right] \quad \left(\bar{x} \equiv \frac{|x - x_o|}{2}\right) \\ &= d_0 \pm 2\left[\bar{x} - \frac{r(\bar{x})}{k}\right], \end{aligned} \tag{3.40}$$

where "+" and "−" correspond to the cases where $\dot{x} > 0$ and $\dot{x} < 0$, respectively, and d_o denotes the drift response corresponding to x_0. From Eqn. (3.40), we can derive

$$\bar{d} = \bar{x} - \frac{r(\bar{x})}{k} \quad \left(\bar{d} \equiv \frac{|d - d_o|}{2}\right). \tag{3.41}$$

Comparing (3.41) with (3.39), one can realize that with the statistical formulation of the Masing models (or the DEMs), the Masing rules for restoring force response also apply to the drift response or possibly other response quantities.

Thus, with the formulas given in Eqns. (3.39) to (3.41), we can compute effectively the drift response history, in addition to other response quantities, of a hysteretic system modeled by the special class of Masing models. A numerical simulation using these formulas* is performed for a DEM and the result is shown in

* The numerical implementation of the error function is done by using the Hasting's formula [15]:

$$\operatorname{erf}(x) \simeq 1 - (a_1 t + a_2 t^2 + a_3 t^3 + a_4 t^4 + a_5 t^5)\, e^{-x^2},$$

where

$$t = \frac{1}{1 + 0.3275911x}, a_1 = 0.254829592, a_2 = -0.284496736,$$

Fig. 3.15, where the comparison has been made to a one-dimensional endochronic model which will be investigated in detail later in Chapter 4. The good agreement of the drift response histories between the models again indicates the validity of the "statistical" formulation based on the "probabilistic" distribution function $\phi(r)$ of the yield strengths of distributed elements.

Based on the previous experience with identification of structural systems using the general class of Masing models [23], it should be noted that, in practice, more reliable results of identification can be obtained by fixing the value of the parameter n in the general model so that the interactions among parameters can be greatly reduced, which implies that model identifiability is much improved. This is particularly important for the identification studies in which the system response is not driven far into the strongly inelastic regime. Therefore, although there is some loss in the flexibility of the model, it is proposed in later identification studies to fix the value of n based on appropriate engineering judgement.

3.3.4 Other Models for Degrading Systems

There have been many other models than those described above for modeling of degrading systems. For earthquake motions, building structures made of reinforced concrete often exihibit stiffness deteriorating behavior. Iwan [21] presented a hysteretic model for stiffness degrading systems which may be thought of as a subclass of the distributed-element model. This model consists of three types of basic elements, including the E-type (elastic elements), the Y-type (elasto-perfectly plastic elements), and the C-type (elements exhibiting cracking and crushing like behavior), as shown in Fig. 3.16. Gates [13] applied this model to earthquake response analysis of deteriorating systems by using only one element from each of the three basic types. The model configuration and its response behavior are shown in Fig. 3.17, where the contributions from each type of element are also included. Although this model is capable of modeling a wide range of deteriorating structures, the model characteristics and its response behavior are considered to be too complicated as far as system identification is concerned. An attempt at deriving the

---

$$a_3 = 1.421413741, a_4 = -1.453152027, a_5 = 1.061405429.$$

This formula is accurate over $[0, \infty)$ to within $\pm 1.5 \times 10^{-7}$.

corresponding response rules for the model as was done earlier for the maximum-displacement-controlled DEM was made. However, the result was too complicated for practical applications, as a complete description of the model behavior required too many mathematical rules for different response branches.

Clough [10] proposed a stiffness-degrading hysteretic model based on the bilinear hysteretic model. The model behavior is shown schematically in Fig. 3.18. In this model, stiffness degradation is introduced only as "load reversal" occurs (i.e., when the restoring force r changes its sign). This is not completely consistent with experimental observations which show that stiffness degradation occurs also during unloading behavior. Takeda et al. [44] presented a rather complicated degrading model based on their experimental results regarding reinforced concrete behavior. The model behavior is based on a trilinear primary curve which represents the three stages of uncracked, cracked, and post-yielding response of concrete structural members. The general behavior of the model is sketched in Fig. 3.19. However, a complete description of the model behavior requires more than a dozen rules governing different response branches. In contrast to Clough's model, Takeda's model takes account of stiffness degradation at both unloading and load reversals. The slope of an unloading curve after yielding occurs is given by the empirical equation

$$k_{unloading} = k' \left(\frac{x_y}{x_m} \right)^{0.4}, \tag{3.42}$$

where k' is the slope of a line joining the yield point in one direction to the cracking point in the opposite direction (cf. Fig. 3.19), and x_y and x_m denote, respectively, the yield deformation and maximum deformation experienced by the system in the direction of current loading. Although the model was built based on observations made in many experimental studies on reinforced concrete members, it is, in general, too complicated for practical applications, especially for identification studies.

A simplified version of Takeda's model was developed by Saiidi and Sozen [38] in which the trilinear primary curve is replaced by a bilinear curve as shown in Fig. 3.20. To simplify the model behavior, the largest excursion point in both directions is viewed as the largest excursion point in either direction. This model takes into account hysteretic energy dissipation during low-amplitude deformation if the model has yielded in at least one direction . This is true also for Takeda's and

Clough's model, but not for the elasto-perfectly plastic or bilinear models. This characteristic is important as reported in [39] for accurate prediction of response peaks and frequency content of hysteretic systems subject to earthquake excitations.

The unloading slope in the inelastic region of the Saiidi and Sozen's model is similar to that given by Eqn. (3.42) except that k' is replaced by the initial elastic slope of the response. It was shown in [39] that Saiidi and Sozen's hysteretic model incorporates the principal features of hysteresis presented in Takeda's model, including:

1) dependence of unloading stiffness on the maximum deformation experienced by the system,
2) stiffness degradation during load reversals, and
3) hysteretic energy dissipation for small-amplitude deformation after yielding.

But the model is considerably simpler than Takeda's, which makes this model more suitable in practice for determining hysteretic response, or for identifying system characteristics of reinforced concrete structures.

The investigation of the preceding degrading models is to gain better insight into the behavior of degrading hysteretic systems and to provide some justification for the aforementioned degrading Masing models. The maximum-displacement-controlled degrading Masing model possesses all the three response features stated above without the need to introduce any additional empirical approximations regarding its hysteretic behavior. This indicates that the proposed Masing model has a physically consistent behavior and is good for modeling of reinforced concrete structural systems. Another interesting hysteretic model based on endochronic theory will be presented in the next chapter. This generally-formulated model for multi-axial cyclic plasticity also serves as a comparison basis for the Masing models or the DEMs, as we did in Fig. 3.15 for the drift response of a Masing model. Besides, the general, consistent behavior of the endochronic model also motivates the generalization of the DEMs into multi-dimensional representations for constitutive modeling of stress-strain relations of materials. This will be covered in the next two chapters.

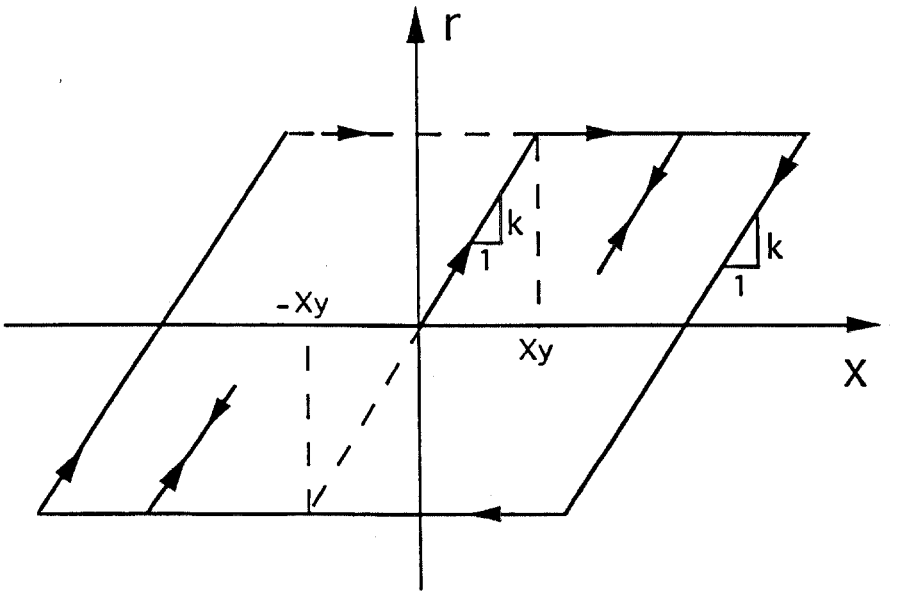

(a)

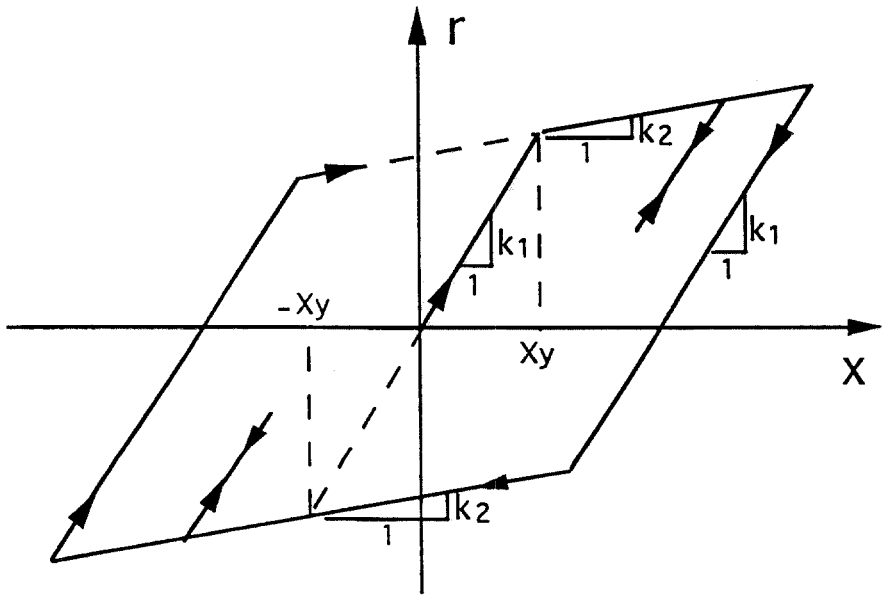

(b)

Figure 3.1 Hysteretic restoring force behavior of (a) the elasto-perfectly plastic model (b) the bilinear model

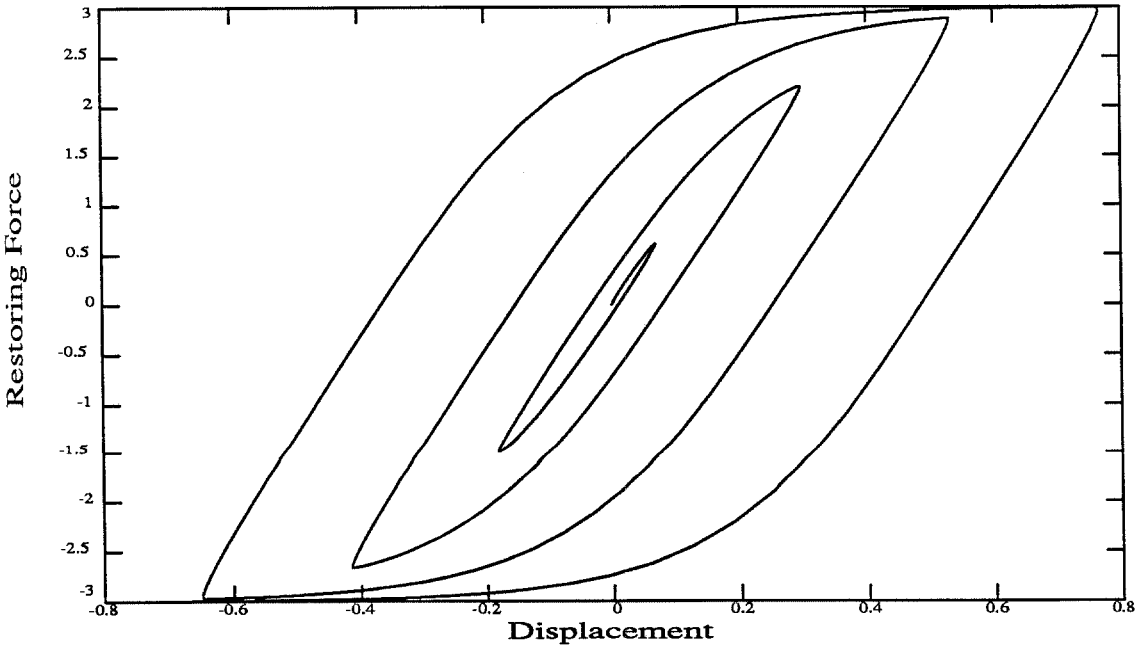

(a) restoring force diagram

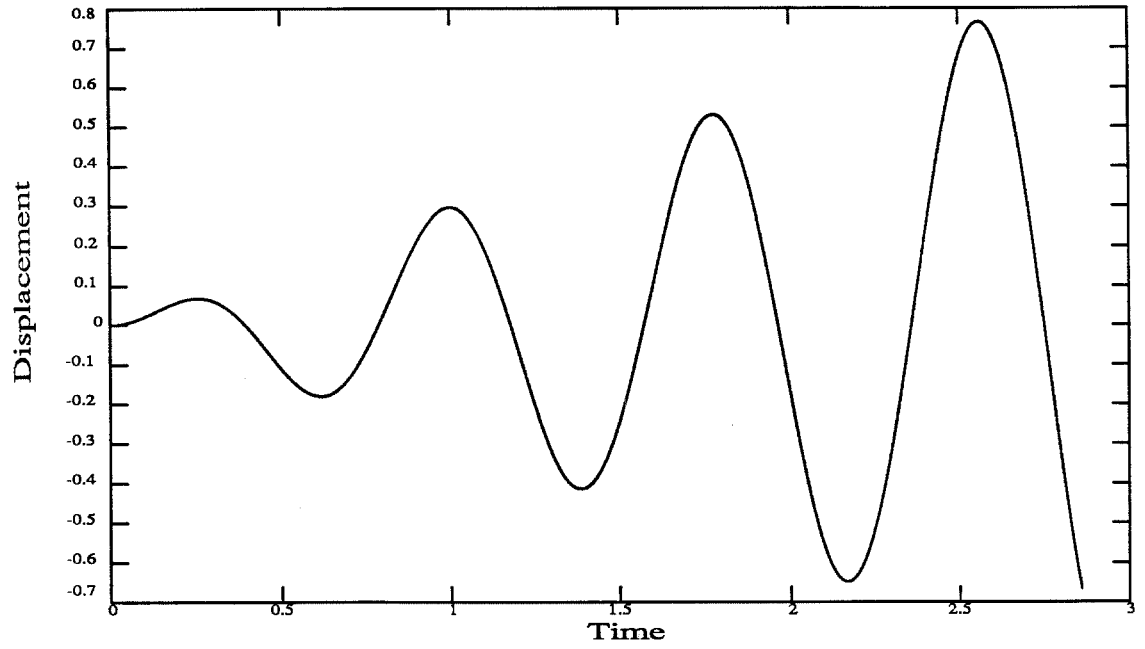

(b) prescribed displacement history

Figure 3.2 Response behavior of the Bouc-Wen model

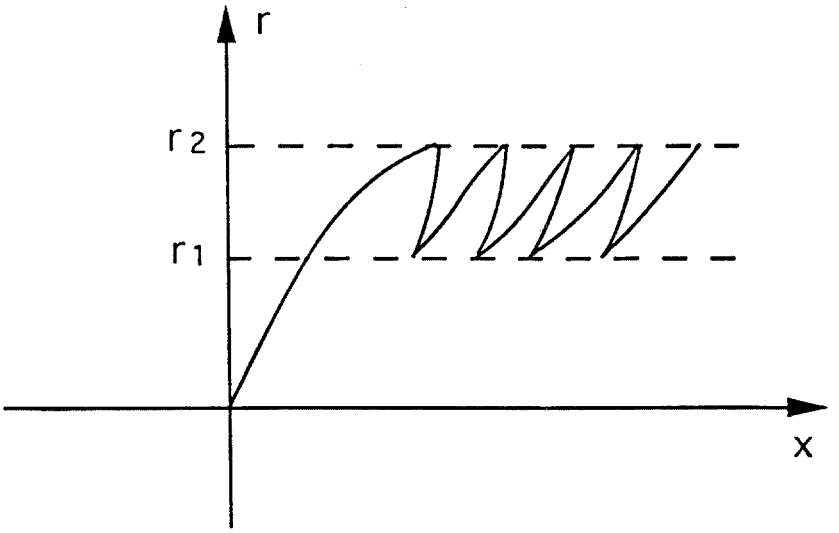

Figure 3.3 The unstable drift exhibited by the Bouc-Wen model

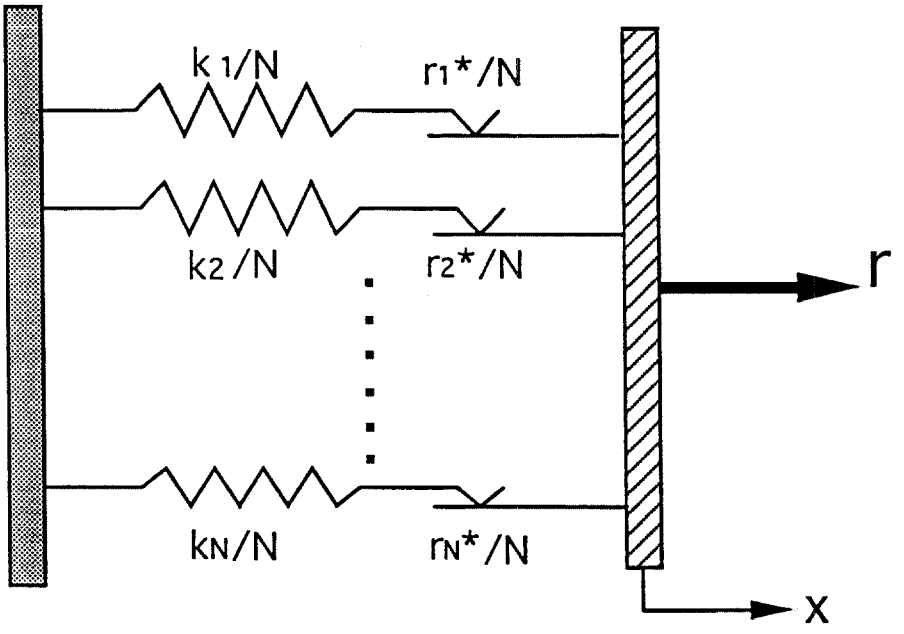

Figure 3.4 The Distributed-Element Model for one-dimensional hysteresis

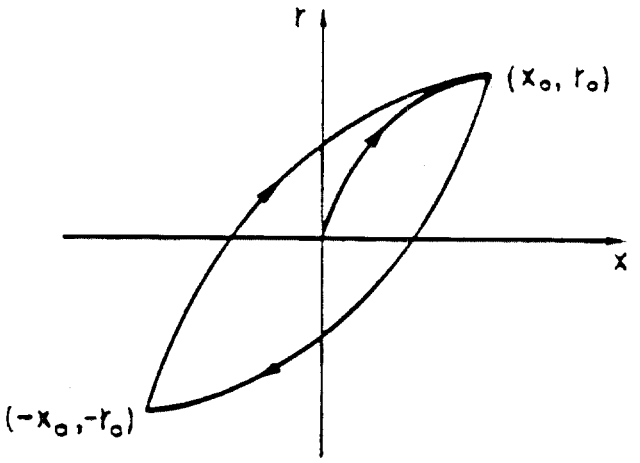

Figure 3.5 Masing's hypothesis for cyclic hysteretic loops

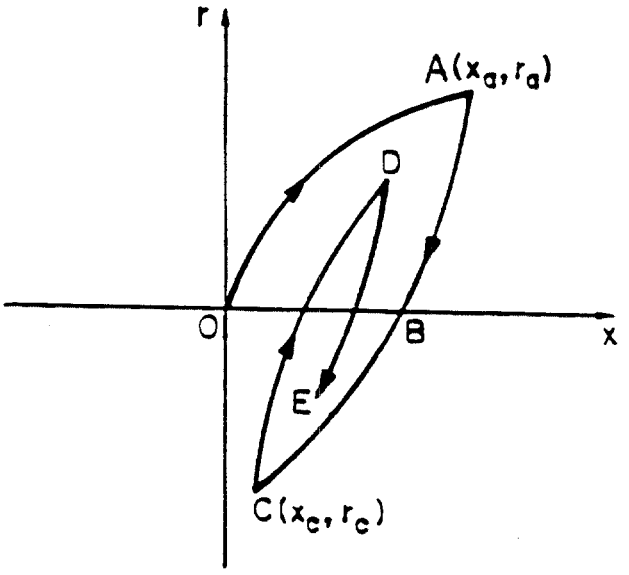

Figure 3.6 Hysteretic loops for transient response

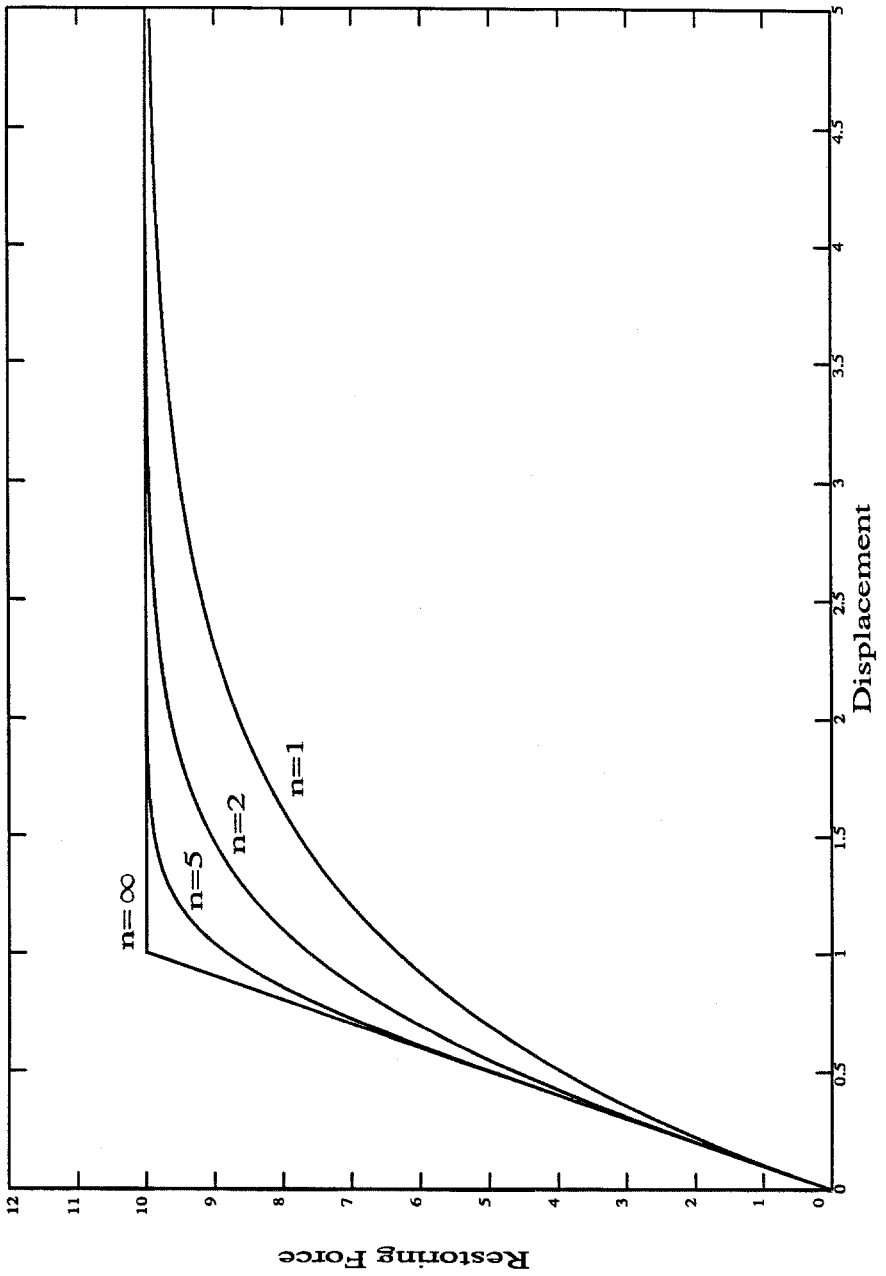

Figure 3.7 Effect of the parameter n of a special class of Masing models [24] on the smoothness of yielding curves

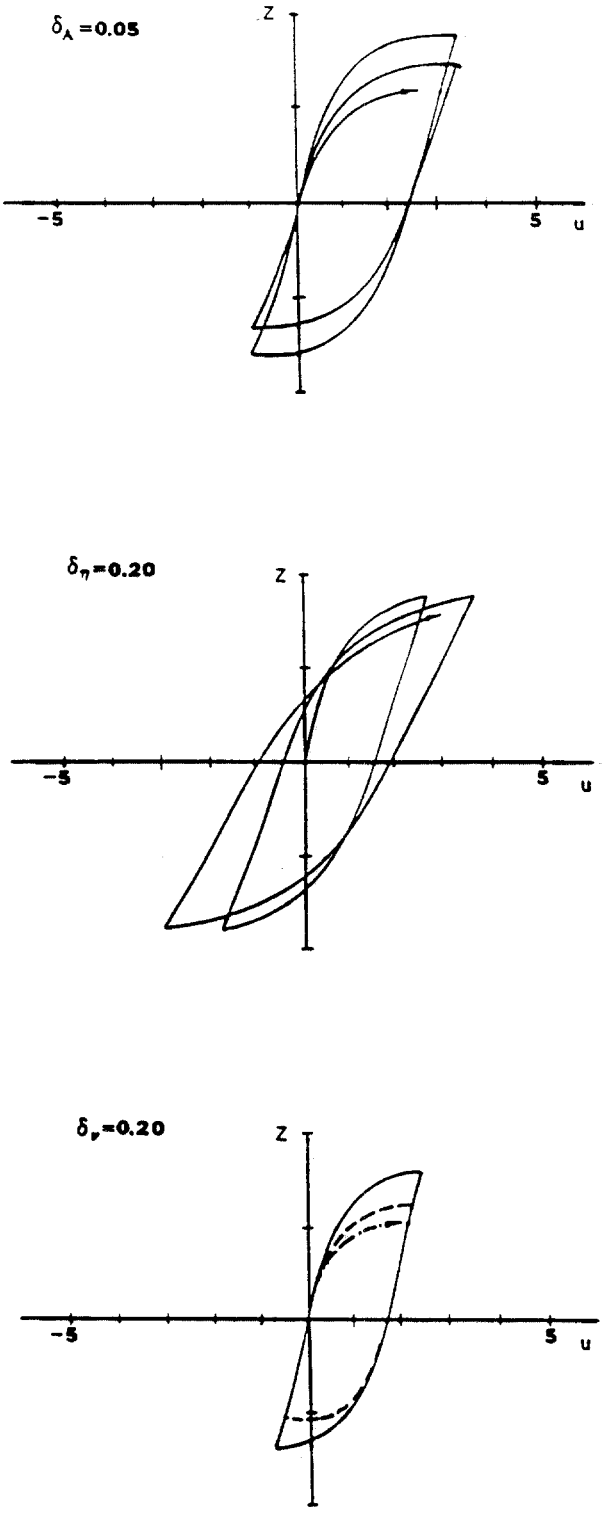

Figure 3.8 Effects of the degrading parameters on the behavior of the deteriorating Bouc-Wen model (from [52])

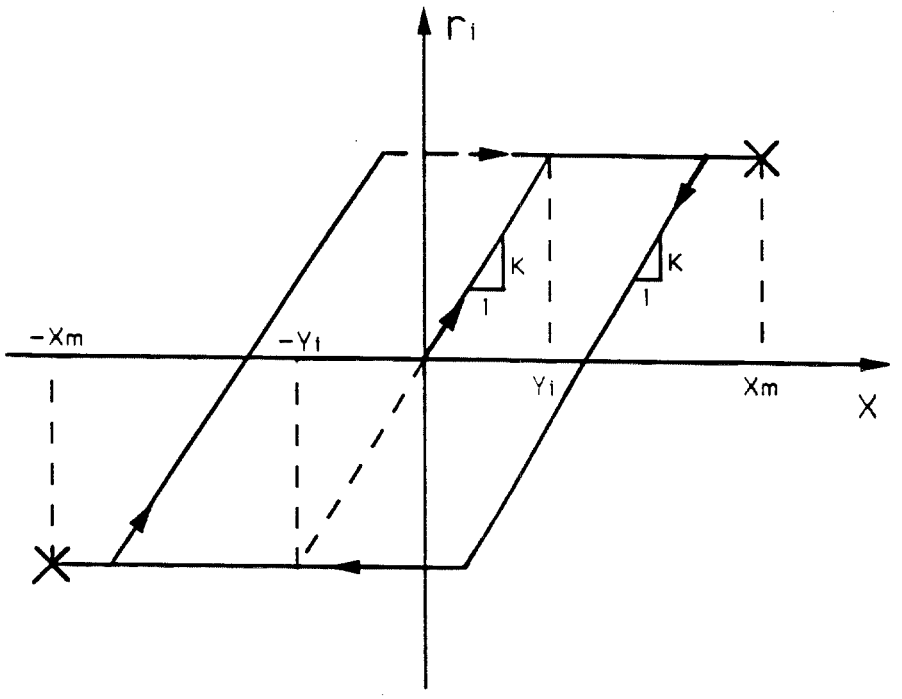

Figure 3.9 Restoring force diagram of a typical breaking element in the maximum-displacement-controlled deteriorating DEM

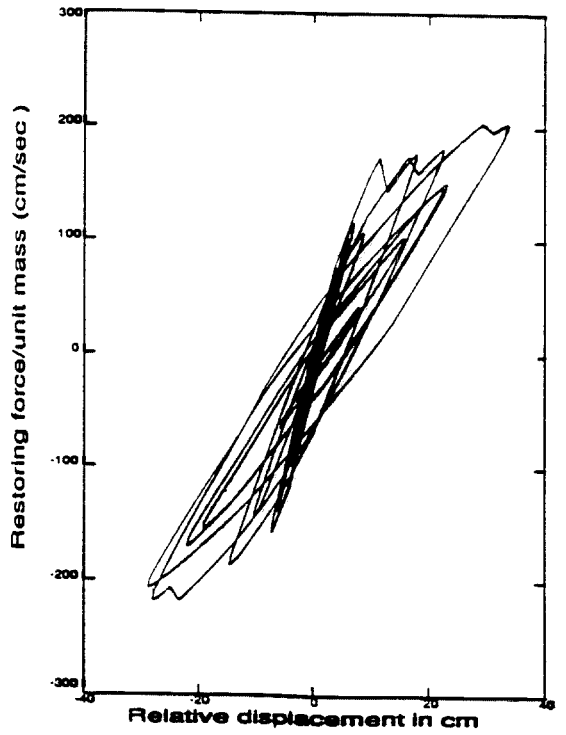

Figure 3.10 Restoring force behavior of the maximum-displacement-controlled deteriorating DEM subject to an earthquake excitation (from [22])

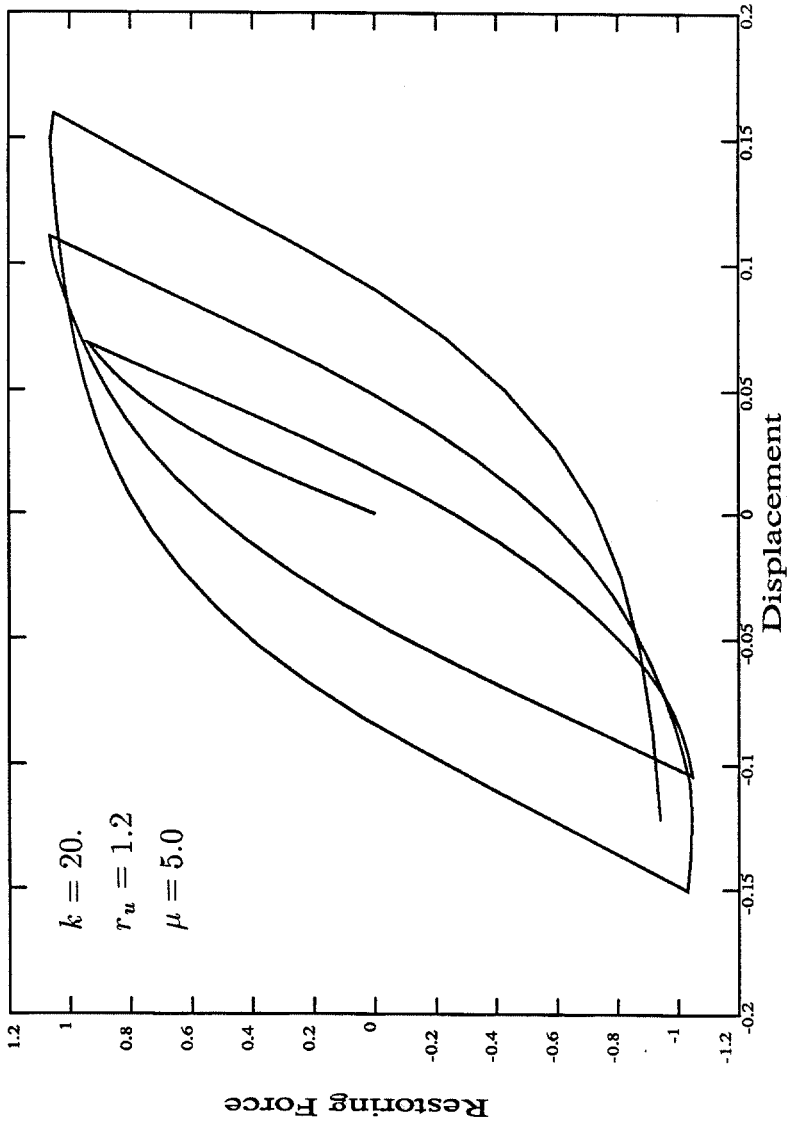

Figure 3.11 Simulated restoring force behavior of the proposed deteriorating Masing model based on a Rayleigh distribution function

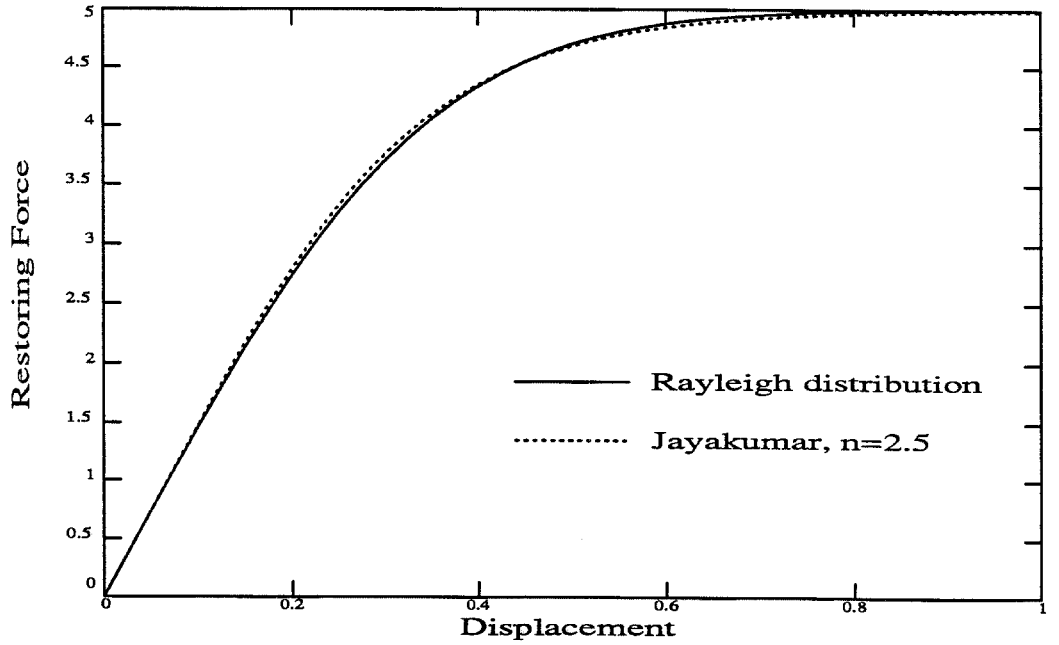

Figure 3.12 Comparison of the behavior of two matching Masing models

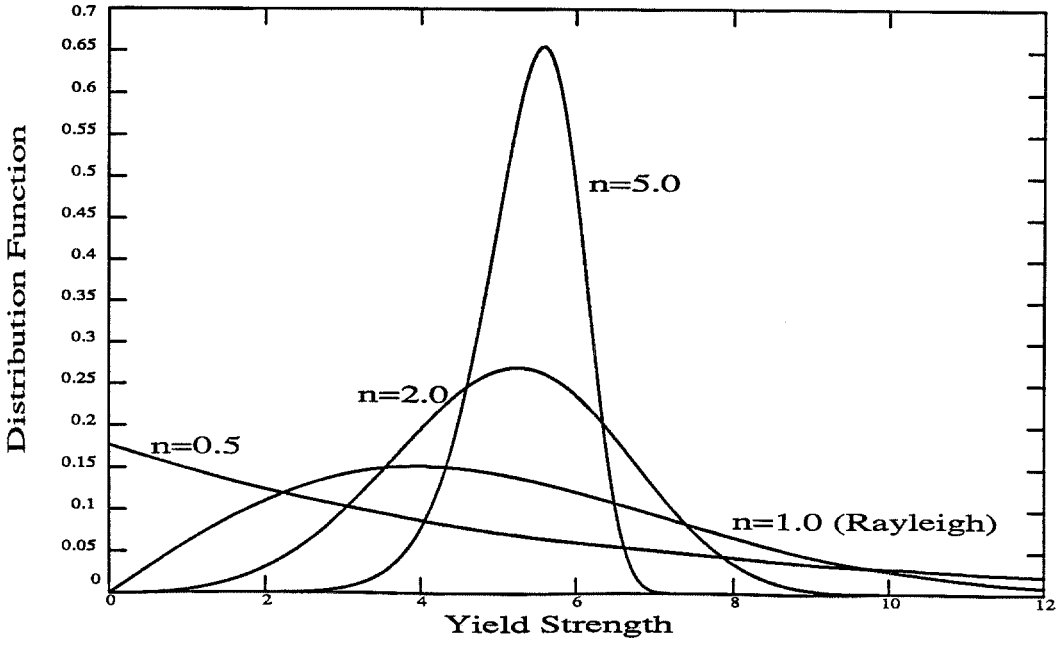

Figure 3.13 Distribution curves described by the generalized Rayleigh distribution function with different values of n

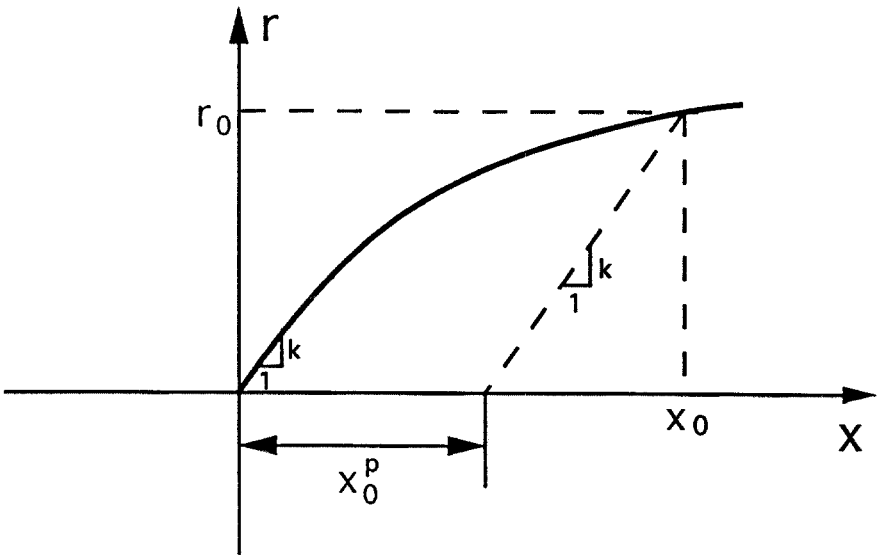

Figure 3.14 Plastic deformation of the Masing model based on a statistical interpretation of the Rayleigh yield-strength distribution function

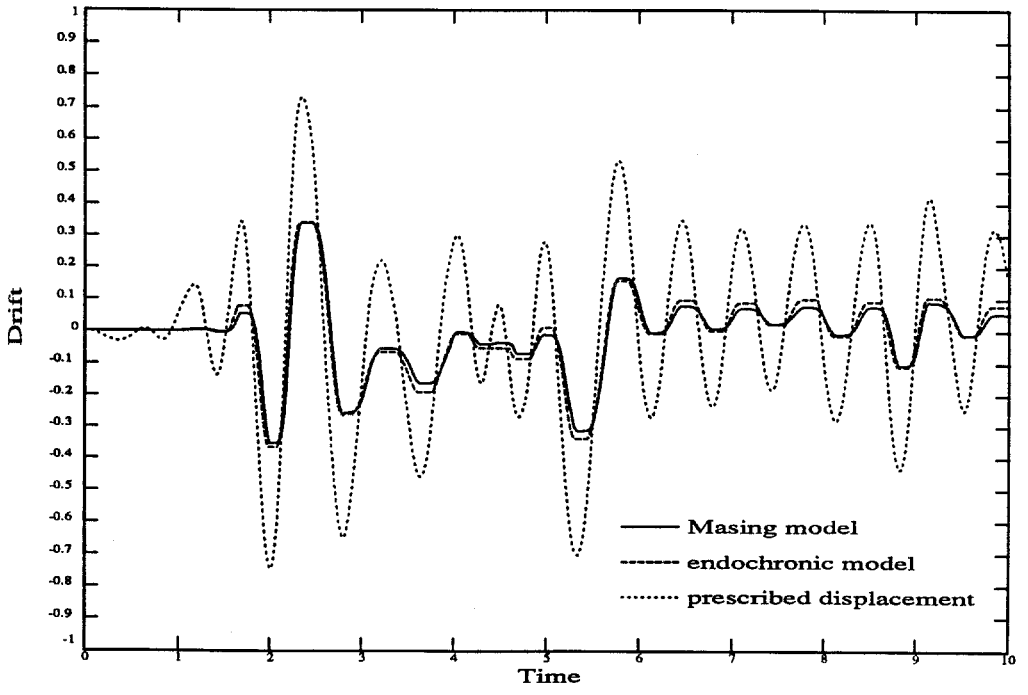

Figure 3.15 Drift response of a Masing model based on the Rayleigh distribution function as compared with an endochronic model

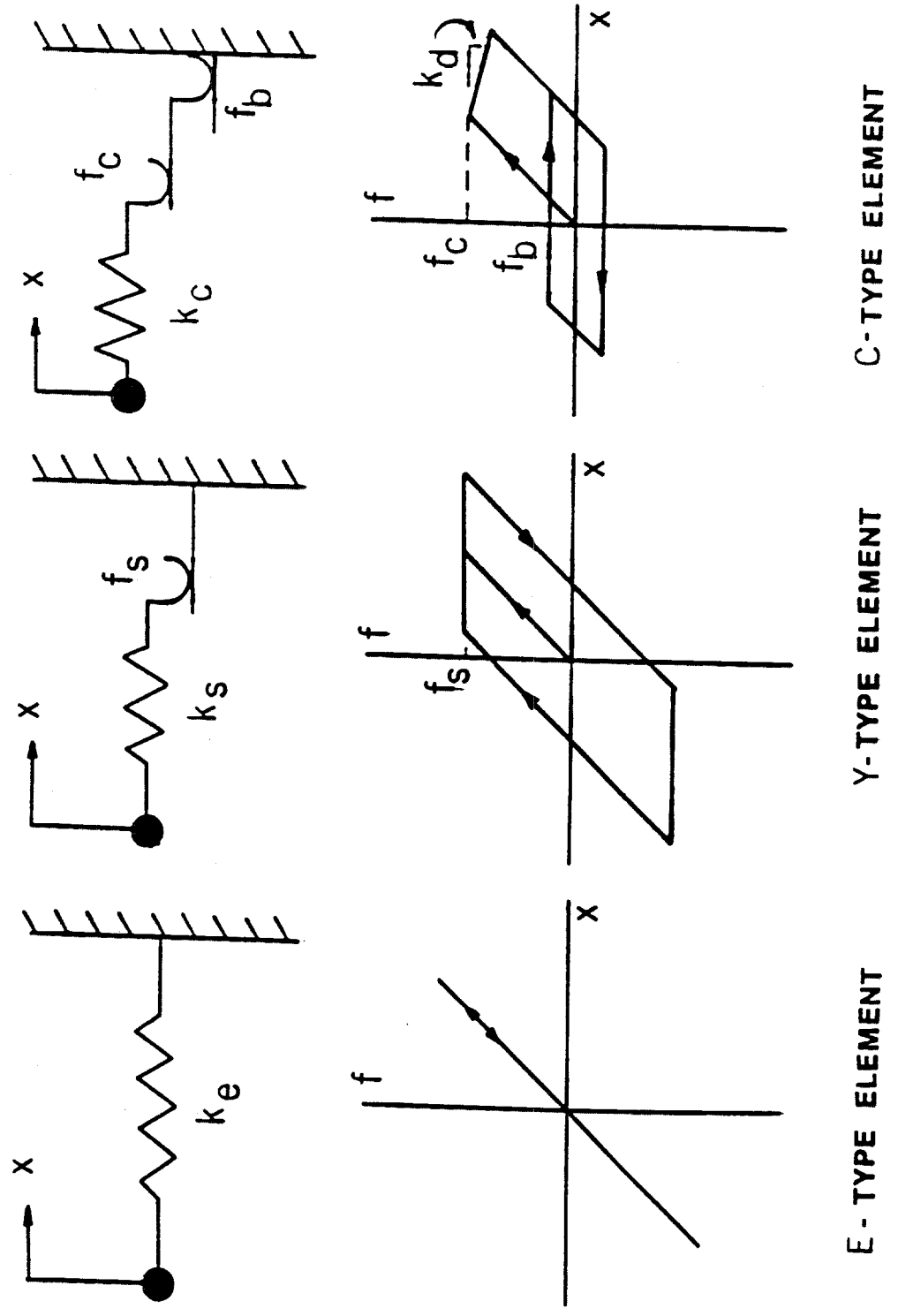

Figure 3.16 Different types of elements used in a model for hysteretic systems with stiffness degradation (from [13])

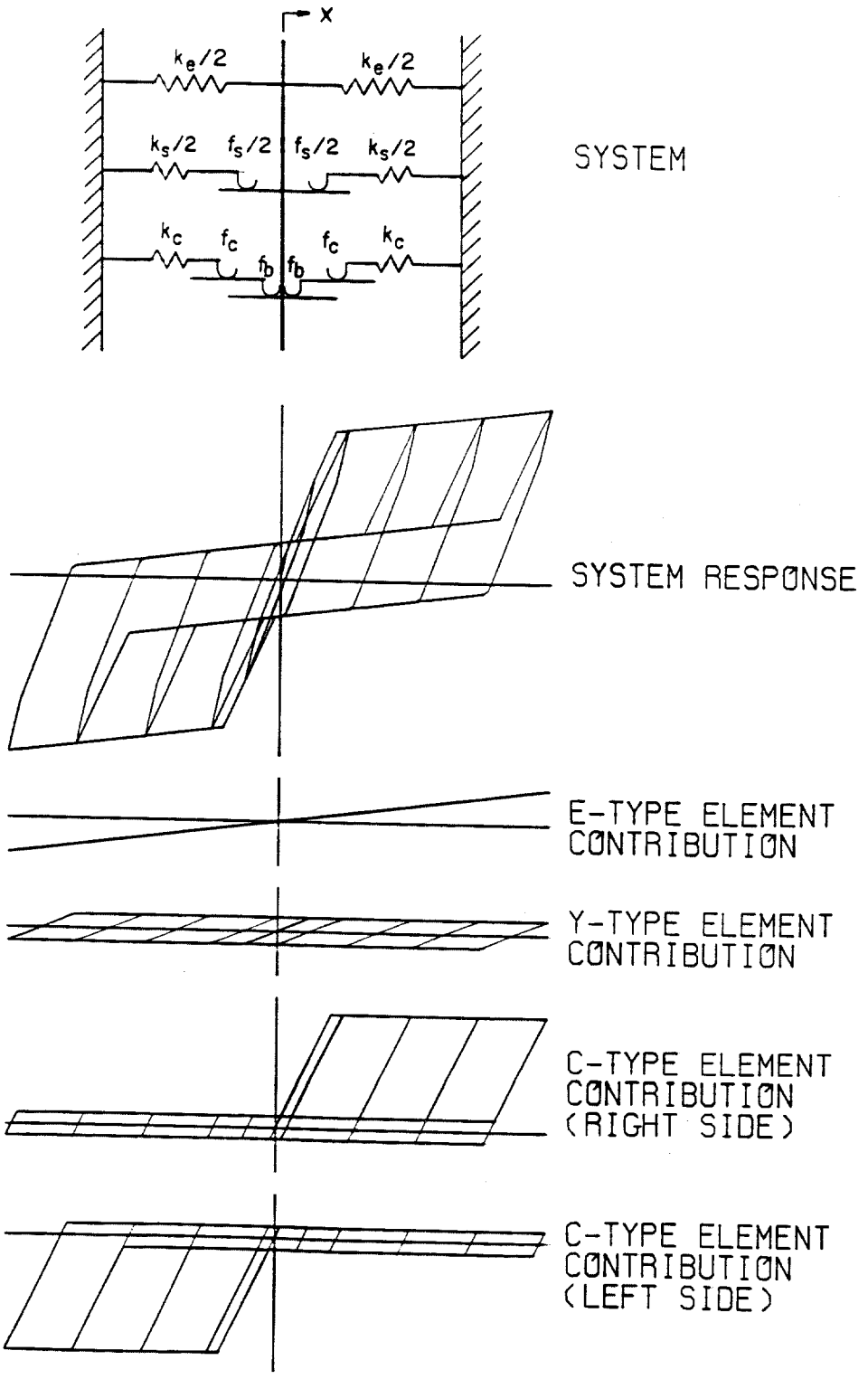

Figure 3.17 Configuration and behavior of Gates' degrading model (from [13])

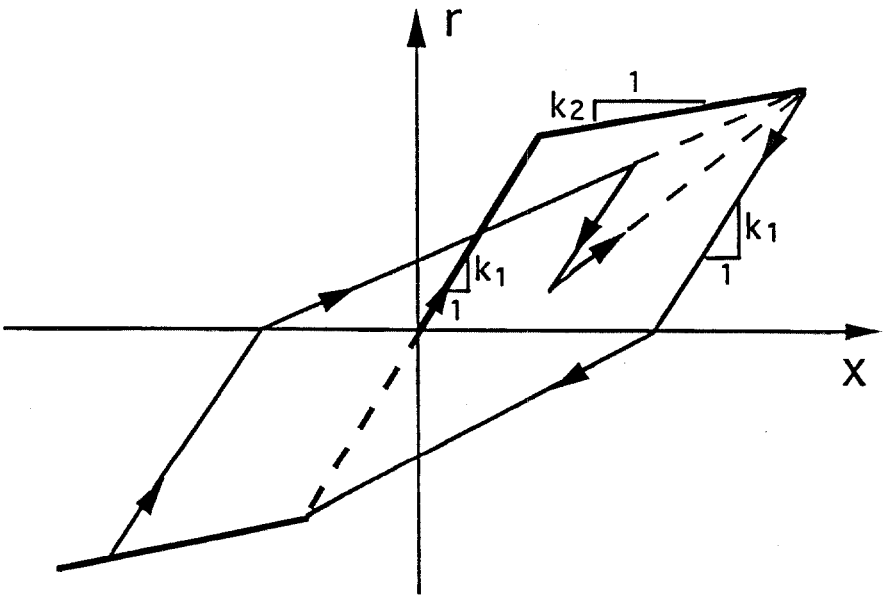

Figure 3.18 Clough's hysteretic model for stiffness-degrading behavior

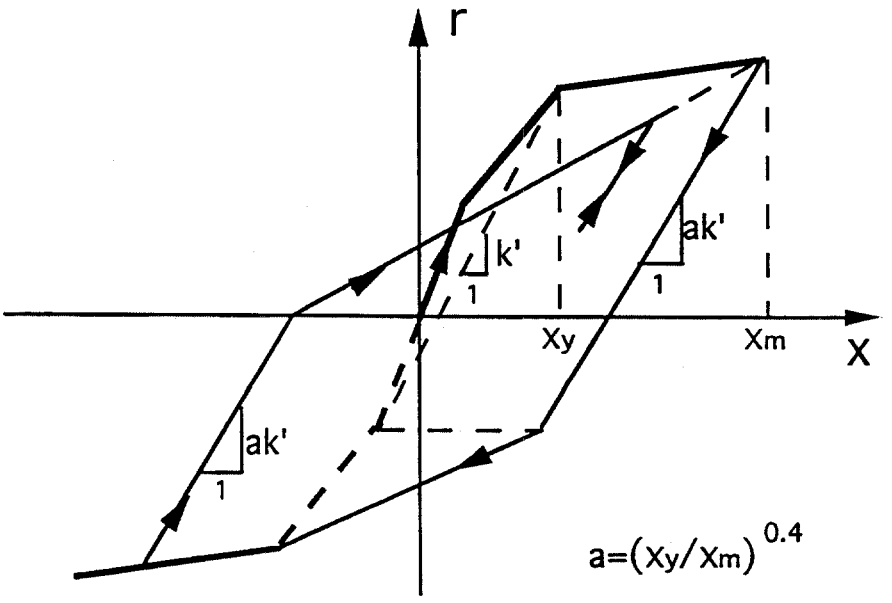

Figure 3.19 Takeda's hysteretic model for reinforced concrete structural systems

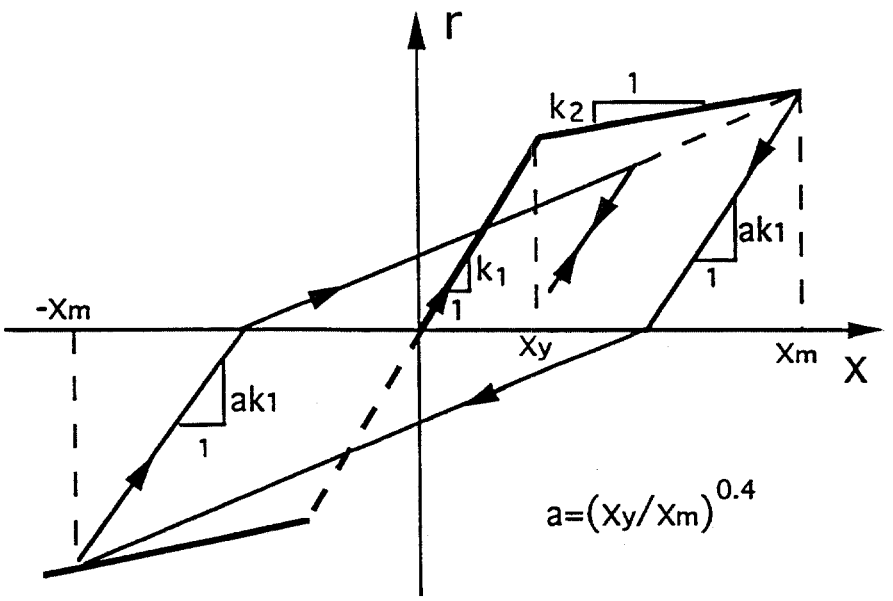

Figure 3.20 Saiidi and Sozen's hysteretic model for stiffness-degrading behavior

CHAPTER 4

MODELING BASED ON ENDOCHRONIC THEORY

4.1 Introduction

A simple endochronic model described by a differential equation has been introduced in Chapter 3 (cf. Eqn. (3.5)) as a special case of the Bouc-Wen model. The original endochronic theory was proposed and developed by Valanis in 1971 [46], and modified later in 1980 [47] for constitutive modeling in cyclic plasticity. The endochronic theory can be viewed as a generalization of the theory of viscoelasticity in which the real time variable is replaced by an auxiliary variable, called the intrinsic time, which is a monotonically increasing measure of deformation history of a material. The constitutive law developed based on the endochronic theory can adequately characterize hysteresis, and strain hardening behavior of some metals, without resorting to the definition of yield conditions, flow rules, or any hardening rules. The original endochronic theory, of which the model described by Eqn. (3.5) serves as a special case of a one-dimensional formulation, was shown to violate Drucker's postulates of stability, as discovered by Sandler [40]. This discovery led to a major modification of the theory in which the intrinsic time was defined in the plastic-strain space, instead of the total-strain space [47]. This makes the stiffness at the onset of unloading identical to the "small-amplitude" stiffness of the initial loading, and the resulting endochronic formulation shows proper hysteresis-loop closure and hence more realistic response behavior. Although the endochronic theory was originally developed for modeling material behavior of some metals, extensions of the theory have been made for modeling of some other materials, such as concrete [2] and soils [48].

The major contribution of the endochronic theory is that the theory provides a unifying approach of describing the elasto-plastic behavior of materials without the requirement of introducing a yield surface and a loading function which distinguishes between loading and unloading. In the next section, the basic formulation of the modified endochronic theory and an effective algorithmic implementation of the theory will be described. Moreover, some inherent properties and difficulties associated with the endochronic model will also be mentioned from some practical points of

view. In Section 4.3, a very effective modeling technique for models based on the endochronic theory will be proposed to simplify the otherwise complicated modeling process. Comparison of simulated responses between the endochronic models and the Masing models will also be made for the uniaxial loading case to examine further the model behavior. Finally, cyclic hardening behavior exhibited by real materials and issues pertaining to the modeling of such behavior will be discussed.

4.2 Endochronic Theory And Its Implementation

The endochronic theory was originally derived based on the internal variable theory of irreversible thermodynamics and the concept of intrinsic time which acts as a proper measure of material memory of its past deformation history. As mentioned earlier, the endochronic theory can be viewed as a generalization of the theory of viscoelasticity. To demonstrate this, let us consider the one-dimensional Maxwell model in viscoelasticity [11], given by

$$d\epsilon = \frac{1}{E}\, d\sigma + \frac{\sigma}{EZ}\, dt, \tag{4.1}$$

or equivalently,

$$\sigma = \int_0^t E\, e^{\frac{-(t-\tau)}{Z}} \frac{\partial \epsilon}{\partial \tau}\, d\tau, \tag{4.2}$$

where E is Young's modulus and Z is the relaxation time of the material being modeled. If we replace the time differential dt by a differential of the intrinsic time $d\zeta$, which is defined by

$$d\zeta = |d\epsilon|, \tag{4.3}$$

then we get the simple endochronic model given by Eqn. (3.5), or equivalently by

$$\sigma = \int_0^\zeta \rho(\zeta - \zeta') \frac{\partial \epsilon}{\partial \zeta'}\, d\zeta', \tag{4.4}$$

where

$$\rho(\zeta) = E\, e^{\frac{-\zeta}{Z}}. \tag{4.5}$$

The integro-differential form of Eqn. (4.4), in which $\rho(\zeta)$ represents a material function, is typical for general endochronic models.

A complete set of constitutive equations for plastically incompressible, rate independent materials based on the modified endochronic theory [47] can be summarized as follows:

$$\sigma_{ij} = C_{ijkl}\,\epsilon^e_{kl}, \tag{4.6}$$

$$\epsilon_{ij} = \epsilon^e_{ij} + \epsilon^p_{ij}, \tag{4.7}$$

and

$$s_{ij} = \int_0^z \rho(z - z')\,\frac{d\epsilon^p_{ij}}{dz'}\,dz', \tag{4.8}$$

where ϵ^e_{ij} and ϵ^p_{ij} are, respectively, the elastic and plastic components of the total strain tensor ϵ_{ij}, and s_{ij} is the deviatoric stress tensor defined as

$$s_{ij} = \sigma_{ij} - \frac{1}{3}\sigma_{kk}\delta_{ij}, \tag{4.9}$$

and

$$dz = \frac{d\eta}{f(\eta)}, \qquad f(\eta) > 0, \tag{4.10}$$

$$d\eta = (d\epsilon^p_{ij}\,d\epsilon^p_{ij})^{1/2}, \tag{4.11}$$

where $\rho(z)$ and $f(\eta)$ are material functions called the kernel (or memory) function and the (cyclic) hardening function, respectively. The differential quantity $d\eta$ represents the distance between two consecutive plastic-strain states, so that η defines a memory path in the plastic-strain space through which history-dependent effects of a material are introduced into the endochronic model. Note the resemblance of Eqn. (4.8) to Eqn. (4.4), where the total-strain increment is replaced by the plastic-strain increment so as to make the model behavior more physically consistent [47]. In the case of isotropic materials, Eqn. (4.6) becomes

$$\sigma_{ij} = \frac{E\nu}{(1+\nu)(1-2\nu)}\,\epsilon^e_{kk}\,\delta_{ij} + 2G\,\epsilon^e_{ij}, \tag{4.12}$$

where E is Young's modulus, ν Poisson's ratio, $G = E/2(1+\nu)$, the shear modulus, and δ_{ij} denotes the Kronecker delta function, i.e., $\delta_{ij} = 1$, if $i = j$, and $\delta_{ij} = 0$, otherwise.

By introducing different forms for the two material functions $\rho(z)$ and $f(\eta)$, various types of elasto-plastic behavior of materials can be adequately modeled. An

important feature of the kernel function $\rho(z)$ in Eqn.(4.8) is that the function must be singular at the origin, that is

$$\rho(0) = \infty, \tag{4.13}$$

so that the model can account appropriately for the elastic behavior at the onset of initial loading and unloading response. There are basically two major types of endochronic models based on the assumed form of the kernel function $\rho(z)$, which are now described.

The first one utilizing the Dirac delta function $\delta(z)$ is given by

$$\rho(z) = s_y^0\,\delta(z) + \rho_1(z), \tag{4.14}$$

where $\rho_1(z)$ is a regular function and s_y^0 is a material constant that has the physical significance of the initial yield stress in simple tension. This formulation leads from Eqn. (4.8) to

$$s_{ij}(z) = s_y^0\,\frac{d\epsilon_{ij}^p}{dz} + r_{ij}(z), \tag{4.15}$$

where

$$r_{ij}(z) = \int_0^z \rho_1(z - z')\,\frac{d\epsilon_{ij}^p}{dz'}\,dz'. \tag{4.16}$$

Note that Eqns. (4.10), (4.11) and (4.15) imply

$$\|\mathbf{s}(z) - \mathbf{r}(z)\| = s_y^0\,f(\eta), \tag{4.17}$$

where $\mathbf{s}$ and $\mathbf{r}$ denote respectively the two tensors s_{ij} and r_{ij}, and $\|\mathbf{s}\| \equiv (s_{ij}\,s_{ij})^{1/2}$. Note, however, that when $z = 0$, i.e., in the process of initial loading and $\|\mathbf{s}\| < s_y^0$, the model response is governed by purely elastic behavior, such as that given by Eqn. (4.12) in the case of isotropic materials. From Eqn. (4.17), it can be deduced that this formulation results in a generalization of the classical theory of plasticity in such a way that the hardening function $f(\eta)$ signifies isotropic hardening behavior (yield-surface expansion), while the tensor $r_{ij}(z)$ denotes kinematic hardening behavior (yield-surface translation). Furthermore, it can be shown [50] that by a suitable choice of $\rho_1(z)$ as a sum of exponential functions, the theory becomes similar to the classical multiple-yield-surface theory in which nested yield surfaces translate in the stress space according to some kinematic hardening rule.

Although the above formulation that uses the Dirac delta function in $\rho(z)$ led to a generalization of the classical plasticity theory, the original idea of avoiding the concept of yield surfaces and hardening rules was not completely preserved. Thus, another type of formulation of the endochronic theory has been developed [49] by assuming the kernel function as

$$\rho(z) = \sum_{k=1}^{\infty} c_k \, e^{-\alpha_k z}, \tag{4.18}$$

where the non-negative constants c_k and α_k satisfy

$$\sum_{k=1}^{\infty} c_k = \infty, \qquad \sum_{k=1}^{\infty} \frac{c_k}{\alpha_k} < \infty, \tag{4.19}$$

so that Eqn. (4.13) is satisfied and the integrability of $\rho(z)$ can also be guaranteed.

An effective numerical algorithm for implementing the endochronic theory can be derived based on the assumption of Eqn. (4.18) for the kernel function [17]. Suppose that the loading process is divided into many small steps and in each step no load reversal occurs, then Eqn. (4.8) can be written as

$$\begin{aligned} s_{ij}(z) &= \int_0^{z_1} \rho(z-z') \frac{d\epsilon_{ij}^p}{dz'} \, dz' + \int_{z_1}^{z_2} \rho(z-z') \frac{d\epsilon_{ij}^p}{dz'} \, dz' + \ldots \\ &\approx \left. \frac{d\epsilon_{ij}^p}{dz} \right|_{z=0} \int_0^{z_1} \rho(z-z') \, dz' + \left. \frac{d\epsilon_{ij}^p}{dz} \right|_{z=z_1} \int_{z_1}^{z_2} \rho(z-z') \, dz' + \ldots, \end{aligned} \tag{4.20}$$

where an approximation has been made by assuming that $d\epsilon_{ij}^p/dz$ is constant within each loading step. With the kernel function defined by Eqn. (4.18), (4.20) can be manipulated further to obtain

$$s_{ij}(z_m) \approx \sum_{k=1}^{n} \frac{c_k}{\alpha_k} \Big[\sum_{i-1}^{m} \left. \frac{\Delta\epsilon_{ij}^p}{\Delta z} \right|_{z_{i-1}} e^{-\alpha_k (z_m - z_{i-1})} \left(e^{\alpha_k \Delta z_i} - 1 \right) \Big], \tag{4.21}$$

where $\Delta z_i \equiv z_i - z_{i-1}$ and the subscript m denotes the m-th loading step. Note that in Eqn. (4.21), the infinite sum over k has been approximated by a finite sum of n terms as a practical consideration. In order to avoid the numerical difficulty of

small numbers involved in the term $e^{-\alpha_k(z_m - z_{i-1})}$, one can, based on mathematical induction, convert (4.21) into a recursive formula:

$$s_{ij}(z_m) = \sum_{k=1}^{n} s_{ij}^k(z_m), \tag{4.22}$$

and

$$s_{ij}^k(z_m) \approx e^{-\alpha_k \Delta z_m} s_{ij}^k(z_{m-1}) + \frac{c_k}{\alpha_k}\left(1 - e^{-\alpha_k \Delta z_m}\right) \frac{\Delta \epsilon_{ij}^p}{\Delta z}\Big|_{z_{m-1}}. \tag{4.23}$$

It should be noted that the aforementioned approximate numerical scheme will result in an exact solution to the constitutive equations based on the endochronic theory if the material being modeled does not exhibit cyclic hardening behavior (i.e., $f(\eta) \equiv 1$), and the deformation history follows a piecewise linear path in the plastic-strain space, such as the uni-axial loading case. Equations (4.6) to (4.11), with (4.8) replaced by (4.22) and (4.23), provide a set of recursive formulas for computation of the response of models based on endochronic theory. The advantage of using this numerical scheme is that only the values of the response states at the end of the previous loading step need be stored. Once the loading increment $(\Delta \epsilon_{ij}^p)_m$ (or $(\Delta s_{ij})_m$) is given, $(s_{ij}^k)_m$ can then be determined by referring to $(s_{ij}^k)_{m-1}$. Hsu, et al. [17] proposed two efficient schemes following the above algorithm for either stress-controlled or strain-controlled response simulations, by making a few more algebraic manipulations on the foregoing formulas.

In the following, we address some important points regarding the general behavior and properties of the endochronic model. With the kernel function defined by Eqn. (4.14), Watanbe and Atluri [50] introduced the concept of "limit surfaces" associated with the endochronic models. When the hardening function $f(\eta)$ saturates to a limit value, a limit surface exists which can move around in the stress space, as can be deduced from Eqn. (4.17). As indicated by experimental observations [30], however, materials such as metals, which have been cyclically stabilized, in general exhibit response behavior with "fixed" limit surfaces, beyond which the stress state never goes. Thus, we reject Eqn. (4.14) and it is interesting to see whether the endochronic model based on the alternative formulation of the kernel function given by Eqn. (4.18) can exhibit such a physical behavior.

Note that Eqn. (4.23) may be rewritten as

$$(\Delta s_{ij}^k)_m = \Big[\frac{c_k}{\alpha_k} \frac{\Delta \epsilon_{ij}^p}{\Delta z}\Big|_m - s_{ij}^k(z_{m-1}) \Big](1 - e^{-\alpha_k \Delta z_m}). \tag{4.24}$$

If the stress state reaches an "equilibrium state", at which the stress increments approach zero for appreciable *unidirectional* strain increments [30], i.e.,

$$(\Delta s_{ij}^k)_{eq} = 0 \quad \forall\ k = 1, 2, \ldots, n, \tag{4.25}$$

then by Eqn. (4.24) we have

$$(s_{ij}^k)_{eq} = \frac{c_k}{\alpha_k} \frac{\Delta \epsilon_{ij}^p}{\Delta z}\Big|_{eq}, \tag{4.26}$$

or

$$(s_{ij})_{eq} = \Big(\sum_{k=1}^{\infty} \frac{c_k}{\alpha_k} \Big) \frac{\Delta \epsilon_{ij}^p}{\Delta z}\Big|_{eq}. \tag{4.27}$$

From Eqn. (4.27), we see that the stress state will remain at the equilibrium state until the plastic-strain path changes its direction. Noting that in the case of no cyclic hardening, $(\Delta z)^2 = \Delta \epsilon_{ij}^p \Delta \epsilon_{ij}^p$, we get, from Eqn. (4.27),

$$(s_{ij})_{eq}\,(s_{ij})_{eq} = \Big(\sum_{k=1}^{\infty} \frac{c_k}{\alpha_k} \Big)^2 \equiv k_u^2, \tag{4.28}$$

where k_u is a finite model constant (see Eqn. (4.19)) that can be related to some material constant, as will be done later. Equation (4.28) signifies that all the equilibrium states $(s_{ij})_{eq}$ form a hypersurface in the six-dimensional stress space (considering the symmetry of a stress tensor). This hypersurface is actually a limit surface associated with an endochronic model based on the kernel function given by Eqn. (4.18). This can be shown as follows: Considering the cyclically stabilized behavior (i.e., $f(\eta) \equiv 1$), from Eqns. (4.10) and (4.11) we can put

$$\frac{d\epsilon_{ij}^p(z)}{dz} = n_{ij}(z), \tag{4.29}$$

where $n_{ij}(z) \leq 1$ and satisfies

$$\|n_{ij}(z)\| = (n_{ij}(z)\, n_{ij}(z))^{1/2} = 1. \tag{4.30}$$

Thus, it follows from Eqn. (4.8) that

$$s_{ij}(z) = \int_0^z \rho(z - z')\, n_{ij}(z')\, dz'. \tag{4.31}$$

Using the tensorial product, we get

$$\begin{aligned} s_{ij}(z)\, s_{ij}(z) &= \int_0^z \rho(z - z')\, n_{ij}(z')\, dz' \int_0^z \rho(z - z'')\, n_{ij}(z'')\, dz'' \\ &= \int_0^z \int_0^z \rho(z - z')\rho(z - z'')\, n_{ij}(z')\, n_{ij}(z'')\, dz' dz'' \\ &\leq \int_0^z \int_0^z \rho(z - z')\rho(z - z'')\, \|n_{ij}(z')\|\, \|n_{ij}(z'')\|\, dz' dz'' \\ &= \Big[\int_0^z \rho(z - z')\, dz' \Big]^2. \end{aligned} \tag{4.32}$$

Now if the kernel function $\rho(z)$ is given by Eqn. (4.18), then

$$\begin{aligned} \Big[\int_0^z \rho(z - z')\, dz' \Big]^2 &= \Big[\int_0^z \sum_{k=1}^{\infty} c_k\, e^{-\alpha_k (z - z')} dz' \Big]^2 \\ &= \Big[\sum_{k=1}^{\infty} \frac{-c_k}{\alpha_k}\, e^{-\alpha_k (z - z')} \Big|_0^z \Big]^2 \\ &\leq \Big[\sum_{k=1}^{\infty} \frac{c_k}{\alpha_k} \Big]^2 \;=\; k_u^2. \end{aligned} \tag{4.33}$$

Thus, from (4.32), (4.33) we obtain

$$s_{ij}(z)\, s_{ij}(z) \;\leq\; k_u^2. \tag{4.34}$$

This proves that Eqn. (4.28) represents a limit surface associated with an endochronic model so that no stress state of the model can lie outside the limit surface. In other words, the set of the stress points associated with different equilibrium states of an endochronic model represents the limit surface of that model. The issues of existence and uniqueness of equilibrium states and the associated limit surface will be addressed in detail in the next chapter where the Distributed-Element Model is generalized to a multi-dimensional representation.

Another interesting point about the endochronic model is the resemblance of Eqn. (4.28) to the von Mises yield criterion in the classical theory of plasticity, given by

$$s_{ij}\, s_{ij} = \frac{2}{3}\sigma_0^2, \tag{4.35}$$

where σ_0 is the yield stress of a material in the uniaxial tension test. Actually, considering the uniaxial tension case where $s_{11} = 2\sigma_{11}/3 = -2s_{22} = -2s_{33}$, and $s_{ij} = 0, i \neq j$, Eqn. (4.28) implies

$$(s_{ij})_{eq}\,(s_{ij})_{eq} = \frac{2}{3}\sigma_0 = k_u^2,$$

since we have $(\sigma_{11})_{eq} = \sigma_0$. Thus, we obtain the relation:

$$\sum_{k=1}^{\infty} \frac{c_k}{\alpha_k} \;=\; k_u \;=\; \sqrt{\frac{2}{3}}\,\sigma_0, \tag{4.36}$$

which relates the model constants to the material constant σ_0. Equation (4.36) provides a guideline for choosing the model constants c_k and α_k, in addition to the constraints given in (4.19). This relation motivates a new effective modeling technique for endochronic models based on the formulation of the kernel function given by Eqn. (4.18), as will be presented in the next section.

4.3 A Modeling Technique for the Endochronic Models

So far we have formulated a complete set of constitutive equations based on the endochronic theory which is ready for numerical calculation of model response under general cyclic loading conditions. To apply an endochronic model to simulation studies, however, one needs to choose proper values for those model constants involved in the definition of the kernel function in the model, as given by Eqn. (4.18). According to the previous experience with modeling of the kernel function [17, 49], at least three exponential terms in the series representation of $\rho(z)$ are required to adequately represent the smooth yielding behavior of hysteretic systems. The response behavior of a one-dimensional endochronic model based on Eqn. (4.18) is illustrated in Figure 4.1, where hysteresis loops of model response using one, two, or three exponential terms are plotted together for comparison. It can be observed that the one-term

formulation of the kernel function leads to elasto-perfectly-plastic behavior, and the three-term model gives a smooth yielding behavior as desired. In previous studies, for example [17, 49], the model constants involved in the three-term kernel function were chosen exclusively based on a trial-and-error procedure, which may be very difficult and inefficient in practical situations. Furthermore, from a system identification point of view, such a model involving at least eight model parameters (c_k and α_k, $k = 1, 2, 3$, in addition to at least two other parameters of elasticity, E and ν say) would definitely violate the criteria of simplicity, physicality and robustness for a good model, as stated in Chapter 2. Thus, it is very desirable that the modeling procedure for the kernel function of an endochronic model be simplified. In the following, an efficient modeling technique is proposed to define the kernel function of an endochronic model based on Eqn. (4.18) so that the number of parameters involved can be reduced.

As mentioned above, in practice, a three-term representation for the kernel function $\rho(z)$ is sufficient to yield a smooth yielding curve for general hysteretic response. Thus, consistent with Eqn. (4.36), we may introduce the following additional conditions regarding the model constants:

$$\frac{c_k}{\alpha_k} = \frac{k_u}{3} \quad \forall\, k = 1, 2, 3. \tag{4.37}$$

The generality of the model behavior is not lost by introducing these conditions because it is the α_k that primarily control the shape of the hysteresis loops. In order to satisfy approximately the first condition in (4.19), we can always choose α_1 to be a very large number, say

$$\alpha_1 \;\equiv\; 1.0 \times 10^{16}. \tag{4.38}$$

Moreover, as suggested by results of numerical simulations, we may fix the ratio of α_2 to α_3 so that a smooth yielding curve can always be attained, regardless of the shape of the hysteresis loops. For this, we can set

$$\alpha_2 = 3\,\alpha_3, \tag{4.39}$$

as suggested by numerical simulations. Equations (4.37) to (4.39) provide five equations for the six constants c_k and $\alpha_k, k = 1, 2, 3$, in which only one model parameter k_u is required.

To completely define the six constants, we need one more equation to determine the absolute magnitude of the constant α_3 (or α_2). We note that since we defined $\alpha_1 > \alpha_2 > \alpha_3$ in our modeling based on Eqn. (4.18), α_3 controls the final portion of the yielding curve near the ultimate stress, as illustrated by the portion ABC in Fig. 4.2. Thus, we can choose the value of α_3 to match appropriately that portion in a uniaxial initial loading curve so that it is related to other model parameters. In the one-dimensional case, using the three-term representation for the kernel function based on Eqn. (4.18), we can derive the following equation for the n-th branch of the response curve:

$$\sigma(z) = \sqrt{\frac{3}{2}} \sum_{k=1}^{3} \frac{c_k}{\alpha_k} \left[(-1)^n - e^{-\alpha_k z} + 2 \sum_{i=1}^{n} (-1)^{i-1} e^{-\alpha_k (z - z_i)} \right] \tag{4.40}$$

for $z > z_n$, where z_n corresponds to the n-th load reversal point. Thus, for initial loading curve ($n = 0$), we have

$$\sigma(z) = \sqrt{\frac{3}{2}} \sum_{k=1}^{3} \frac{c_k}{\alpha_k} \left[1 - e^{-\alpha_k z} \right] = \sigma_0 - \sqrt{\frac{3}{2}} \sum_{k=1}^{3} \frac{c_k}{\alpha_k} e^{-\alpha_k z}, \tag{4.41}$$

where we made use of Eqn. (4.36). For the final portion of the initial loading curve, i.e., $\sigma \to \sigma_0$, the variable z, which is a measure of accumulated plastic deformation, will not be small and hence, by Eqn. (4.37),

$$\sum_{k=1}^{3} \frac{c_k}{\alpha_k} e^{-\alpha_k z} \approx \frac{c_3}{\alpha_3} e^{-\alpha_3 z} = \frac{k_u}{3} e^{-\alpha_3 z} = \sqrt{\frac{2}{27}} \sigma_0 e^{-\alpha_3 z}, \tag{4.42}$$

where we assumed that $e^{-\alpha_1 z}$, $e^{-\alpha_2 z} \ll e^{-\alpha_3 z}$, since α_1 and α_2 are considerably larger than α_3. Thus, by (4.41) and (4.42), we can derive

$$\sigma(z) \approx \sigma_0 \left(1 - \frac{1}{3} e^{-\alpha_3 z} \right) = \sigma_0 \left(1 - \frac{1}{3} e^{-\sqrt{\frac{3}{2}} \alpha_3 \epsilon^p} \right), \tag{4.43}$$

where we use the fact that $dz = \sqrt{3/2}\, d\epsilon^p$ for the initial loading in the positive direction of the uniaxial case. Thus, for a given yielding curve, we can find the value of α_3 by matching some point, say B in Figure 4.2, in the final portion of the curve.

For example, if at point B, $\sigma_B = 0.95\sigma_0$ and $\epsilon_B^p = \gamma\,\sigma_0/E$ where $\gamma > 0$, as shown in Fig. 4.2, then by (4.43) we have

$$0.95\sigma_0 \approx \sigma_0(1 - \frac{1}{3}\,e^{-\sqrt{\frac{3}{2}}\alpha_3\gamma\frac{\sigma_0}{E}}),$$

which yields

$$\alpha_3 \;\approx\; \frac{1.549}{\gamma}\,\frac{E}{\sigma_0}$$

For yielding curves of different shapes (but with the same E and σ_0), we may thus define

$$\alpha_3 = \frac{1.549}{\gamma}\,\frac{E}{\sigma_0} \equiv (2.0)^p\,\frac{E}{\sigma_0}, \tag{4.45}$$

where p is an alternative parameter to γ for controlling the degree of smoothness of yielding. This is demonstrated in Figure 4.3, where we note that as $p \to \infty$, a yielding curve corresponding to the elasto-perfectly-plastic behavior is obtained.

To summarize, we have the following result for modeling of the kernel function using three exponential terms:

$$\rho(z) = \sum_{k=1}^{3} c_k\,e^{-\alpha_k z}, \tag{4.46}$$

$$\frac{c_1}{\alpha_1} = \frac{c_2}{\alpha_2} = \frac{c_3}{\alpha_3} = \sqrt{\frac{2}{27}}\,\sigma_0, \tag{4.47}$$

$$\alpha_1 = 1.0 \times 10^{16}, \quad \alpha_2 = 3\alpha_3, \quad \alpha_3 = 2^p\frac{E}{\sigma_0}. \tag{4.48}$$

Thus, only three parameters, E, σ_0, and p, are needed in the modeling process for general uniaxial hysteretic behavior, as before when the generalized Rayleigh distribution function was used for the one-dimensional Masing models. In the case where multi-axial response behavior of *isotropic* materials is of interest, only one additional parameter, the Poisson's ratio ν, is needed for the endochronic models based on the preceding formulation. This makes the modeling of endochronic models much easier so that they become widely applicable to general multi-axial response problems of cyclic plasticity, especially in the case where system identification is of interest.

Note that the parameter σ_0 should have been defined as the ultimate stress (or force) in the uniaxial (or one-dimensional) case where only cyclically stablized behavior is to be accounted for. This definition of σ_0 may be viewed as an extension of defining σ_0 as the yield stress of simple tension, since for engineering applications, structural systems do not, in general, exhibit hysteretic behavior with prominent yielding point [23]. Another point to remark regarding the identifiability of parameters of this class of endochronic models is that under the circumstance where the model response is not driven into a strong nonlinear regime, the two parameters σ_0 and p may not be identified accurately due to their interactive effects on the system response. As a consequence, in practical identification studies, we tend to fix the value of the parameter p (or σ_0) so that more reliable identification result can be achieved. For most structural systems, the value of p can be set to be around 1.0 (which yields an endochronic model having uniaxial response behavior close to that of a distributed-element model based on the Rayleigh distribution for the yield-strength distribution function, as will be shown later in Fig. 4.4), so that only two parameters E, σ_0 are left in the one-dimensional models based on the endochronic theory. These two parameters, E and σ_0, have clear physical significance since they represent the initial stiffness and ultimate strength of a system in the context of the generalized one-dimensional force-deflection behavior, or the Young's modulus and the simple-tension yield stress in the context of general plasticity. The two-parameter endochronic model (excluding Poisson's ratio) based on the three-term kernel function formulation can thus be summarized as follows:

$$\begin{aligned} \alpha_1 &= 1.0 \times 10^{16}, \qquad c_1 = \sqrt{\frac{2}{27}}\,\sigma_0\alpha_1, \\ \alpha_2 &= 6.0\,\frac{E}{\sigma_0}, \qquad c_2 = \sqrt{\frac{2}{27}}\,\sigma_0\alpha_2, \\ \alpha_3 &= 2.0\,\frac{E}{\sigma_0}, \qquad c_3 = \sqrt{\frac{2}{27}}\,\sigma_0\alpha_3. \end{aligned} \tag{4.49}$$

It should be noted, however, that the numerical values defined in (4.49) for α_2 and α_3 may vary slightly for particular applications in practice so as to reach the best results.

The main idea presented here is that Eqns. (4.46) to (4.48) set up a simple class of models based on the endochronic theory that is generally applicable to plasticity problems. Even in the general multi-axial loading case, modeling of isotropic materials based on such a class of endochronic models can be based only on the uniaxial initial loading curve of the material being modeled, as long as the Poisson's ratio is given. As a special case of the above general formulation, the one-dimensional hysteretic behavior can be modeled with the tensorial quantities replaced by scalar quantites. Thus, the uniaxial plastic strain response (or, equivalently, the drift response) using the endochronic model is readily obtained through the recursive solution procedure introduced above. A comparison of the drift response of an endochronic model to that of a Masing model has already been shown in Figure 3.15. A simulated restoring-force response of a one-dimensional endochronic model based on (4.49) (i.e., $p = 1$) and that of a matching Masing model subject to a prescribed cyclic displacement history are also compared, as shown in Fig. 4.4, where excellent agreement of response behavior between the two models is observed. In the example, the two models were chosen to have the same E and σ_0, and the Masing model was based on a Rayleigh yield-strength distribution function. It can be noted, however, that the endochronic model exhibits slightly different response characteristics from those of the Masing model. The main differences are that for the endochronic model, the small cyclic loops of transient response may not be "strictly" closed (i.e., the loops may not go through the associated unloading points even though they are closed), and the geometrical shape of the unloading or reloading branches is not the same as that of the virgin loading curve in contrast to the Masing model. Nevertheless, the behavior of the two differently-formulated models is essentially consistent as far as the overall response is concerned.

4.4 Investigation of Cyclic Hardening Behavior

In the previous section, modeling based on the endochronic theory was mainly conducted for cyclically stablized behavior of materials, for which the hardening function in the formulation was taken as unity, i.e., $f(\eta) \equiv 1$. To model material behavior including cyclic hardening (or softening) based on the endochronic theory, one must appropriately define the hardening function $f(\eta)$, which should be positive,

and a monotonically increasing function in the case of hardening, or a monotonically decreasing function in the case of softening. The effect of the hardening function $f(\eta)$ is to stretch or compress the memory path defined through η in the plastic-strain space, as can be deduced from Eqn. (4.10). Also, from Eqn. (4.17), we see that if $f(\eta)$ is a monotonically increasing function of η, the corresponding yield surface will expand accordingly, which signifies the hardening behavior of materials.

Some particular forms for the hardening function of an endochronic model have been previously proposed. Valanis and Fan [49] proposed a form described by :

$$f(\eta) = 1 + \beta_1 \eta^{\beta_2}, \qquad \beta_1, \beta_2 \geq 0. \tag{4.50}$$

But the harding behavior of such a model in relation to the two parameters β_1 and β_2 is not very clear. Another form of the hardening function has been proposed [43], which is described by :

$$f(\eta) = \beta_1 + (1 - \beta_1)\, e^{-\beta_2 \eta}, \qquad \beta_1 \geq 1,\ \beta_2 \geq 0. \tag{4.51}$$

This function form involves only two parameters and exhibits appropriate and general hardening behavior with $f(0) = 1$ and $f(\infty) = \beta_1$. Physically, the parameter β_1 denotes the ratio of the two ultimate strengths of the model after and before hardening occurs, and β_2 accounts for the rate of hardening.

An important property of the cyclic hardening behavior, as observed from the experimental result shown in Fig. 4.5(b), is that only the ultimate stress σ_u is changed during the cyclic process, while the Young's modulus E which governs the initial unloading or reloading slope of the response curves almost stays invariant. Based on this idea, we can extend the Masing models (or DEMs) to account for the cyclic hardening behavior in a very effective way by utilizing the hardening function given in (4.51). For example, if the special class of Masing models based on the Rayleigh distribution function (cf. Sec. 3.3.3.3), which involves only two parameters E and σ_u, is to be extended to model cyclic hardening behavior, we need only make the parameter σ_u an appropriate function of some response quantity, such as the accumulated plastic deformation, so that the ultimate strength σ_u of the model changes with cyclic response. Fig. 4.5(a) shows a simulated cyclic hardening behavior of a

Masing model based on a Rayleigh yield-strength distribution function, in which the parameter σ_u is modeled as

$$\sigma_u(\eta) = \sigma_o\, f(\eta), \tag{4.52}$$

where σ_0 is the initial strength of the model and $f(\eta)$ is given by Eqn. (4.51). Note that in Eqn. (4.52), η is defined as the accumulation of plastic deformation, i.e.,

$$\eta \equiv \int |d\epsilon^p|. \tag{4.53}$$

Recall that the plastic deformation of a Masing model based on a Rayleigh yield-strength distribution function can be found through Eqns. (3.39) and (3.40). In the example, the material constants used for the model are $E = 16,700\ ksi$, $\sigma_0 = 5\ ksi$, and $\beta_1 = 4.4$, $\beta_2 = 14.0$. It is clearly demonstrated in Fig. 4.5 that the behavior of the Masing model based on Eqn. (4.51) for cyclic hardening effect is almost identical to the experimental result.

Another issue in modeling for cyclic hardening behavior is the effect of non-proportional (or "out-of-phase") hardening exhibited by real materials. According to experimental observations, the peak normal stress resulting from nonproportional hardening is about 40 percent higher than that after uniaxial cycling [30, 43]. This phenomenon is physically complicated and, as a consequence, modeling of this behavior is much more difficult considering the very limited experimental results currently available. Sugiura, et al. [43] proposed a modified model based on the endochronic theory that can adequately predict the nonproportional hardening behavior of materials by introduing a nonproportionality function, which depends in some empirical way on the nonproportional plastic-strain response path. However, further exploration on this topic is beyond the scope of the current study.

The purpose of this work is not to investigate extensive material behavior in depth, but to get some physical insight regarding mathematical modeling of general plasticity behavior of materials. Based on these insights, one can possibly extend the Distributed-Element Models or the Masing models to account for various hardening effects, as we did above for cyclic hardening behavior. Also motivated by the close similarity between the behavior of the one-dimensional endochronic models and that of the Masing models, generalization of the Distributed-Element Models and Masing models to a multi-dimensional representation becomes of great interest. These are to be investigated in the next two chapters.

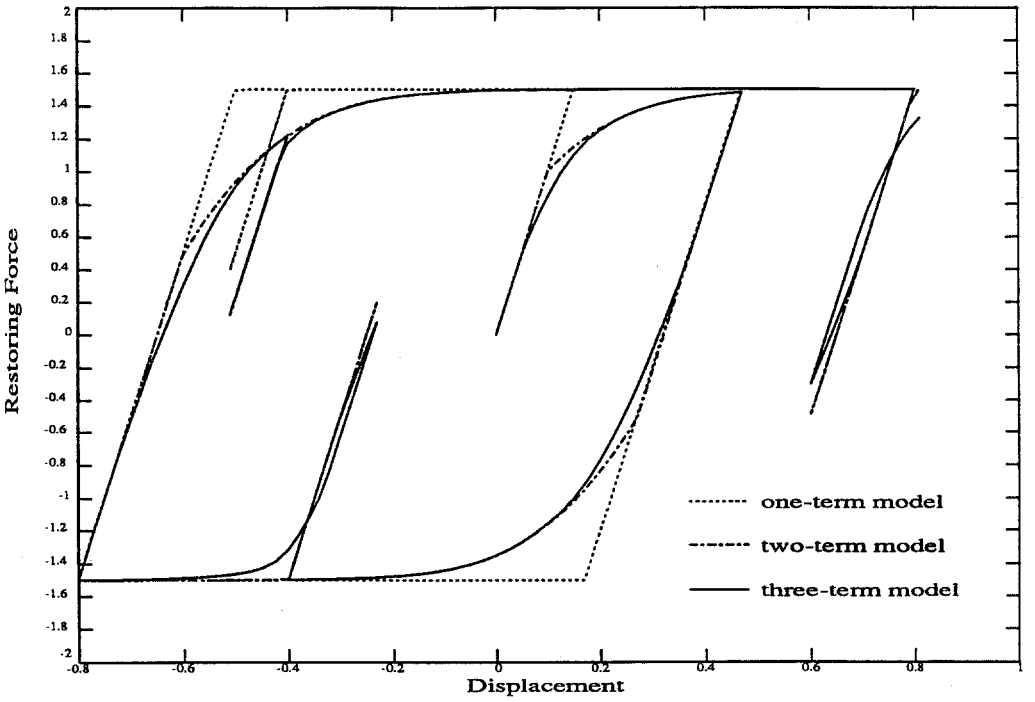

Figure 4.1 Behavior of the endochronic model using the kernel function defined by Eqn. (4.18)

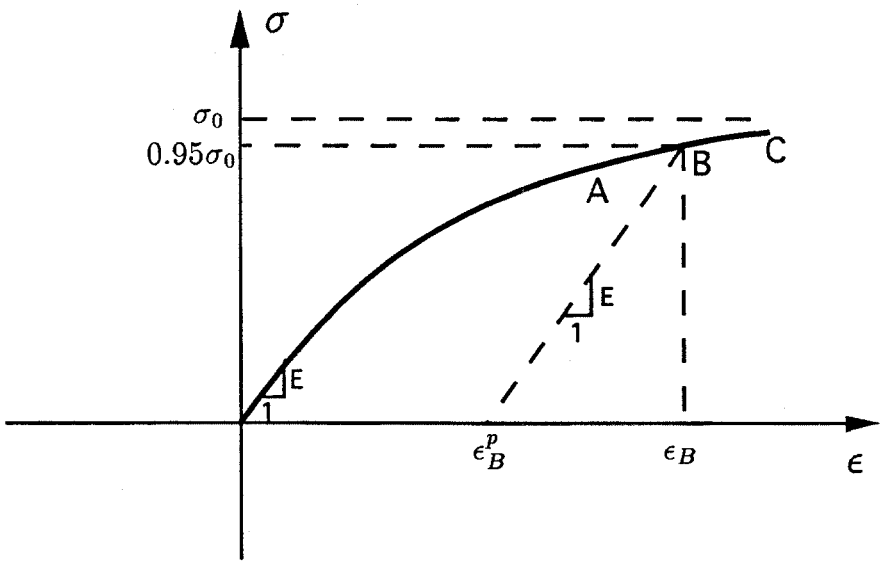

Figure 4.2 A typical yielding curve for illustration of the proposed modeling technique based on the endochronic theory

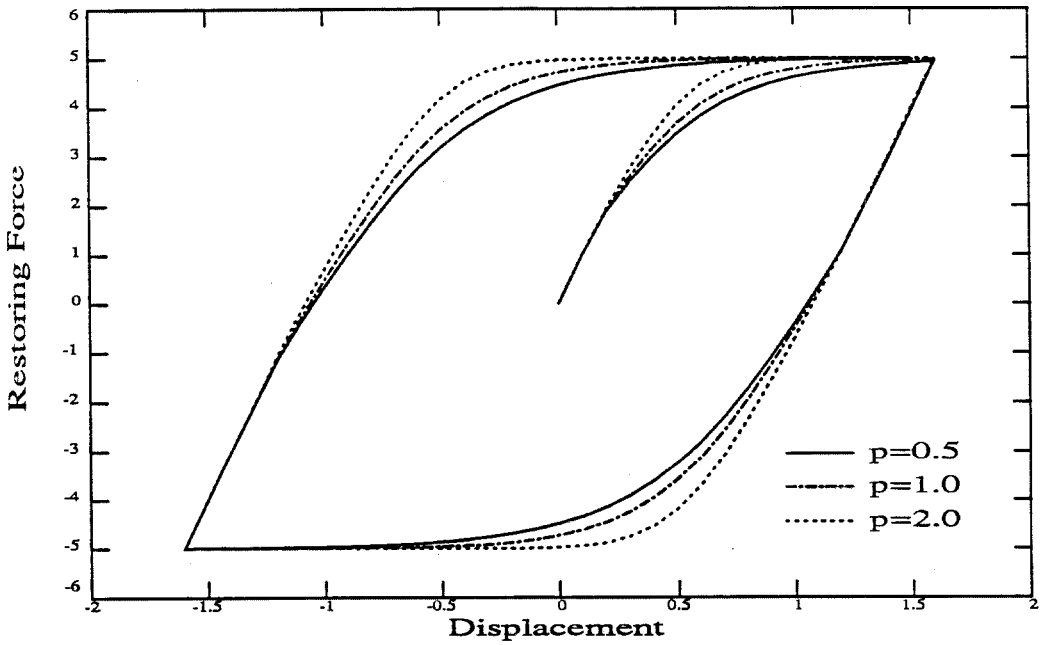

Figure 4.3 Effect of the parameter p of the proposed endochronic model on yielding behavior

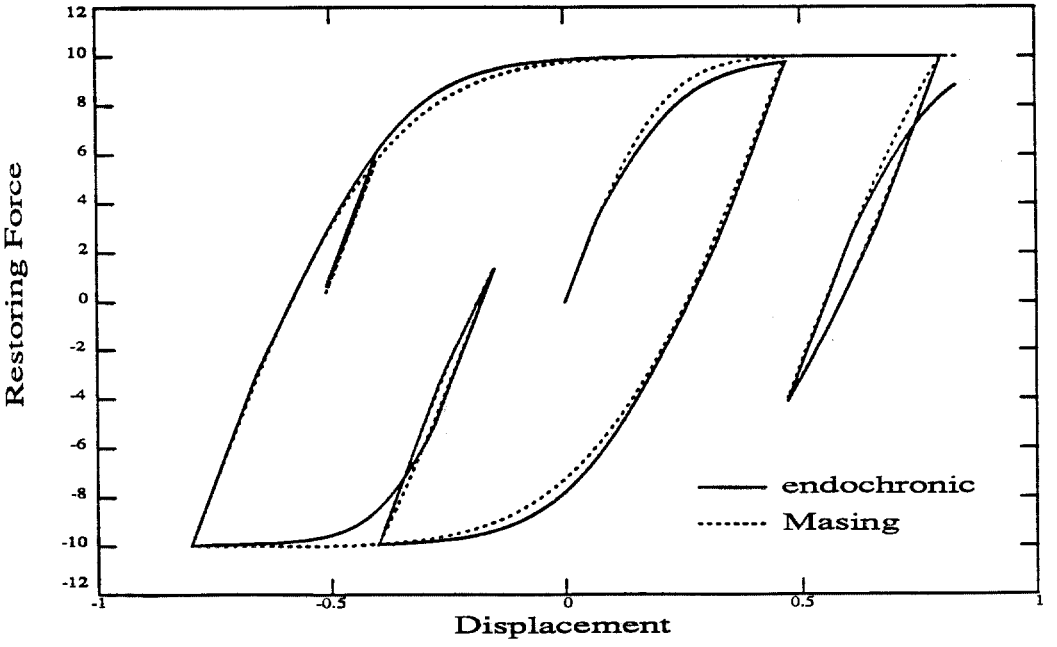

Figure 4.4 Response behavior of a one-dimensional endochronic model and a matching Masing model

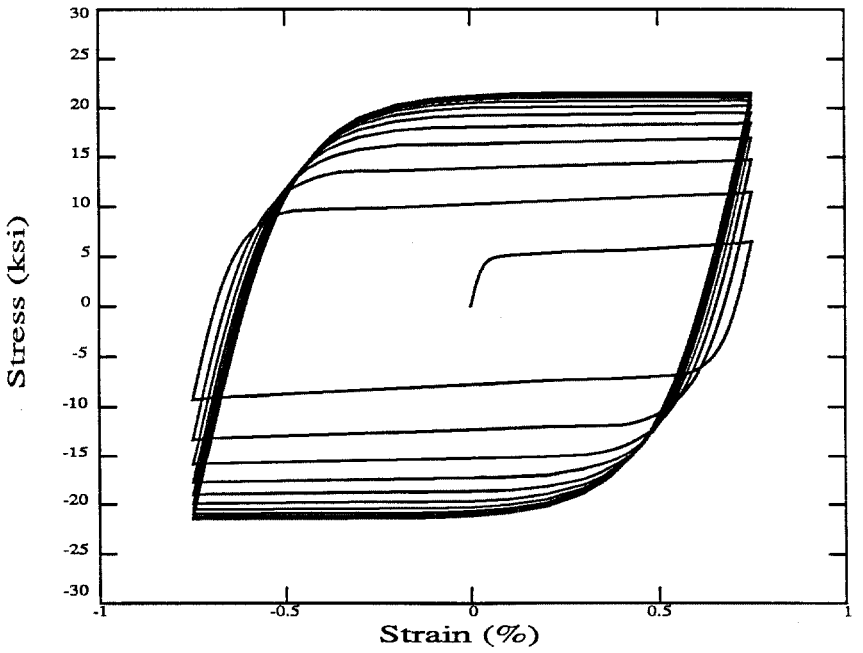

(a)

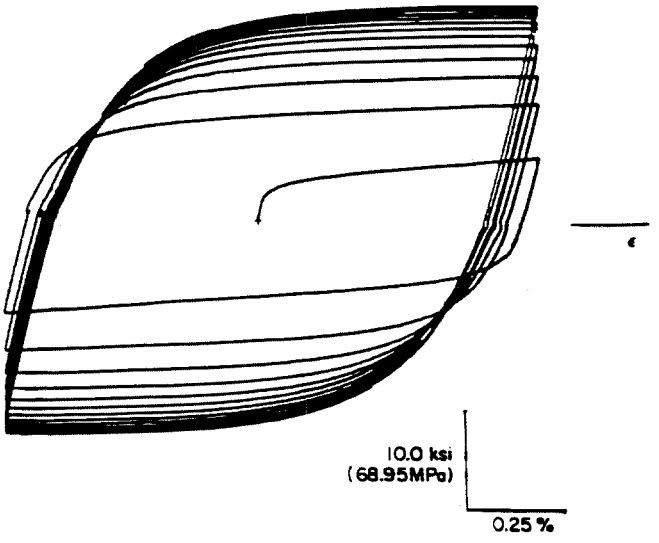

Fig. 2 Recording of axial cyclic hardening (previously undeformed)

(b)

Figure 4.5 Uniaxial cyclic hardening behavior of (a) a Masing model (b) a real material (from [30])

CHAPTER 5

GENERALIZATION OF DISTRIBUTED-ELEMENT MODEL TO MULTIPLE DIMENSIONS

5.1 Introduction

The one-dimensional Distributed-Element Models (DEMs), introduced by Iwan [19] for structural dynamic analysis, have been investigated in detail in Chapter 3 for both deteriorating and non-deteriorating hysteretic behavior. In order to extend the one-dimensional DEMs to multiple dimensions for constitutive modeling of general plasticity, Iwan [20] introduced the concept of a collection of nested yield surfaces associated with a DEM, which move around in the stress space according to some kinematic rules so that the Bauschinger effect could be accounted for in a more realistic way. This class of multi-dimensional models for plasticity based on the distributed-element formulation provided a conceptual generalization of the customary formulation of the incremental theory of classical plasticity. However, the numerical implementation of such a class of multi-dimensional models involves tracing subsequent yield surfaces and hence is quite difficult and computationally inefficient. Yoder [56] proposed an alternative version of plasticity theory formulated in the strain space. That theory, based on a different class of DEMs from that used by Iwan, is closely parallel to the traditional theory of plasticity, but interchanges the roles of stress and strain. In contrast to Iwan's multi-dimensional model, the model proposed by Yoder consists of a collection of yield surfaces formulated in the *strain* space. However, the same problem pertaining to the numerical implementation of the model behavior arises.

In the following sections, a new class of plasticity models, also based on the distributed-element behavior, will be proposed, in which yield surfaces of different yield levels are introduced for the elements involved in a model. The main idea behind this new class of DEMs is that the yield surfaces are defined in the "element" stress space and are "invariant", i.e., fixed from moving in that space, no matter how the model response varies. Due to the invariant characteristics of the yield surfaces thus defined, the theoretical formulation of such models is so simple that there is

no need for any kinematic hardening rules for subsequent yielding behavior. Furthermore, the numerical implementation of the new model is straightforward and highly efficient, even though quite a few elements are needed for the model to yield good results in applications. What might be more interesting is that the behavior of this new class of DEMs provides us with a physical model for understanding complicated response mechanisms in cyclic plasticity. Some experimentally-observed material behavior can be adequately elucidated by the model through the establishment of some relevant properties of the model behavior. The validity of this new class of Distributed-Element Models is confirmed by comparison with experimental results from the literature. Excellent response predictions using the new models have been obtained under complicated multi-axial loading conditions.

5.2 A New Class of Distributed-Element Models for Plasticity

5.2.1 Concept and Theoretical Background

Before looking into the generalization of the one-dimensional (1-D) DEMs to higher dimensions, let us examine two different classes of 1-D DEMs that have been used before. The two classes of models are composed of collections of elasto-perfectly-plastic elements in either a parallel-series (P-S) or a series-parallel (S-P) combination, as shown in Fig. 5.1(a) and (b), respectively. It can be shown [20] that when the number of elements become very large so that the element strengths σ_i^* are described in terms of some distributed function $\phi(\sigma^*)$, where $\phi(\sigma^*)d\sigma^*$ denotes the fraction of the total number of elements that have a slip stress between σ^* and $\sigma^* + d\sigma^*$, then the model behavior can be described by

$$\sigma = \int_0^\infty \sigma(\sigma^*)\,\phi(\sigma^*)\,d\sigma^* \tag{5.1}$$

for the P-S model, or

$$\epsilon = \int_0^\infty \epsilon(\sigma^*)\,\phi(\sigma^*)\,d\sigma^* \tag{5.2}$$

for the S-P model. It should be noted, however, that for the S-P model to be physically consistent, the distribution function has to be singular at the origin, i.e., $\phi(0) \to \infty$, so that $d\epsilon/d\sigma|_{\epsilon=0} \neq 0$; otherwise we will have $d\sigma/d\epsilon|_{\epsilon=0} = \infty$, which means that the initial slope of the stress-strain curve is infinitely large. Thus, from both physical and

mathematical points of view, the S-P model is considered to be not so good as the P-S model for which the distribution function $\phi(\sigma^*)$ can be any function that satisfies

$$\int_0^\infty \phi(\sigma^*)\, d\sigma^* = 1, \tag{5.3}$$

even though both models can be shown to exhibit Masing type of behavior [45].

In the following, we will extend the 1-D P-S model to the general multi-dimensional case so that they can be used for constitutive modeling in cyclic plasticity problems. The generalization of the S-P model will not be done here, though it can be treated in a similar way. More will be said about this later.

To account for the general multi-axial response behavior, we need to first define the basic kinematic behavior of the distributed elements constituting the model. In this study, we postulate the following rules for the new multi-dimensional DEM :

1) Each element in the model is subject to the same total-strain response as experienced by the model itself.
2) Each element has the response behavior of ideal plasticity so that its associated yield surface remains "invariant" in the stress space. In other words, the yield surface associated with an element is described by a function that depends only on the element stress.
3) All the elements have the same elastic properties and the associated yield functions have the same mathematical form, but they have different yield constants which are governed by some distribution function.
4) The stress state of the model is defined as the average of the stress states of all the elements.

Following these rules, the overall stress of the model can be expressed in terms of the element stress states as follows :

$$\tilde{\sigma}(t) \equiv \int_0^\infty \tilde{\sigma}(k,t)\, \phi(k)\, dk, \tag{5.4}$$

where $\tilde{\sigma}$ denotes the tensor σ_{ij}, and $\tilde{\sigma}(k,t)$ is the corresponding stress state of the elements having yielding constant k governed by a distribution function $\phi(k)$. Note the resemblance of Eqn. (5.4) to Eqn. (5.1). The constant k is related to the yield function associated with each element in the model so that the equation

$$F(\tilde{\sigma}(k), k) = 0 \tag{5.5}$$

represents a yield surface associated with an element of yield constant k in the element stress space. Note that without loss of generality, we can choose

$$k \equiv \sigma_0(k), \tag{5.6}$$

where $\sigma_0(k)$ is the uniaxial yield stress of the associated element. The definition of the yield function defined in Eqn. (5.5) is conceptually the same as that used in the classical theory of plasticity so as to characterize the general behavior of materials under multi-axial loading conditions. However, in this new formulation, the yield surfaces are defined in the element-stress space, not in the model-stress space as in the classical theory of plasticity. Moreover, since each element in the model has the behavior of ideal plasticity, the yield surfaces associated with the elements will remain "invariant" in their space of definition, no matter how the model behaves. Also, the stress response of each element remains linearly elastic until yielding occurs, after which the element stress state will move on the associated yield surface during plastic flow and will never go beyond it. An important remark regarding the overall model behavior is that the stress state of the model may possibly lie outside some of the yield surfaces associated with the elements, which makes the new model distinctive from those based on classical multi-yield-surface theory. It is also this formulation in the "invariant-yield-surface" space that makes this new model mathematically simple, physically realistic, and computationally effective, in contrast to the aforementioned multi-dimensional DEMs proposed by Iwan and Yoder [20, 56].

The theoretical background of this new formulation lies in the deduction that corresponding to a yield surface in the stress space, there should be a yield surface in the strain space regardless of what model is being considered. Consider, for example, the case of ideal plasticity where a yield surface formulated in the stress space always stays invariant throughout the deformation history. However, the corresponding yield surface formulated in the strain space has to move around, along with the current strain state of the model, so as to account adequately for the Bauschinger effect exhibited by real materials under cyclic plastic deformations. This space-dependent yielding behavior is illustrated in Fig. 5.2 for the one-dimensional (uniaxial) case. With this concept in mind, the formulation of plasticity in either stress or strain space can be made equivalent to that in the other space, as long as appropriate

kinematic behavior of the yield surfaces is taken into consideration. However, it is obvious that the formulation without the need of kinematic hardening rules (such as the stress-space formulation in the foregoing example) would be much easier than the other, especially in the case where multiple yield surfaces are needed in obtaining model response, as for the models based on distributed elements.

5.2.2 Mathematical Formulation

As mentioned above, the behavior of the new class of multi-dimensional DEMs for plasticity is based on the element behavior formulated in stress space, instead of in strain space, so that complicated kinematic hardening rules can be avoided for response after initial yielding. Thus, the yield surfaces associated with the elements stay invariant in the stress space under the assumption of ideal plasticity, and they are nested within one another in the element stress space due to the different yield strengths of the elements. This is illustrated in Fig. 5.3, where concentric circles of different radii represent yield surfaces of different yield strengths in the two-dimensional (biaxial) case.

If the yield surface associated with an element with yield constant k is described by Eqn. (5.5), then under the assumption of ideal plasticity, we have that when $F(\tilde{\sigma}(k), k) = 0$, the plastic flow takes place without limit, and therefore,

$$dF = \frac{\partial F}{\partial \sigma_{ij}(k)} \, d\sigma_{ij}(k) = 0 \tag{5.7}$$

for plastic flow. Then, from the normality rule of plastic flow given by the classical theory of plasticity, which specifies that the direction of a plastic strain increment is normal to the yield surface at the current stress point, we have the flow rule for an element of yield strength k:

$$d\epsilon^p_{ij}(k) = \frac{\partial F}{\partial \sigma_{ij}(k)} \, d\lambda_k, \tag{5.8}$$

where $d\lambda_k$ is a coefficient of proportionality, whose value can be determined as follows. Firstly, we introduce the general stress-strain relation in incremental form as

$$d\sigma_{ij}(k) = C_{ijmn}(d\epsilon_{mn} - d\epsilon^p_{mn}(k)), \tag{5.9}$$

where C_{ijmn} denotes the tensor of elasticity constants and it has been assumed that all elements in the model have the same elasticity constants and identical total-strain response so that the dependence of C_{ijmn} and $d\epsilon_{mn}$ on k can be dropped. Based on Eqns. (5.7), (5.8) and (5.9), we can find the expression for the coefficient of proportionality as:

$$d\lambda_k = \frac{\partial F/\partial \sigma_{ij}(k)\; C_{ijmn}\, d\epsilon_{mn}}{\partial F/\partial \sigma_{pq}(k)\; C_{pqrs}\; \partial F/\partial \sigma_{rs}(k)}. \tag{5.10}$$

Summarizing from the above, we arrive at the following set of constitutive equations for the new Distributed-Element Model for general plasticity formulated in the "invariant-yield-surface" space:

$$\tilde{\sigma} = \int_0^\infty \tilde{\sigma}(k)\, \phi(k)\, dk, \tag{5.11a}$$

and $$F(\tilde{\sigma}(k), k) \leq 0 \qquad \text{always.} \tag{5.11b}$$

If $$F(\tilde{\sigma}(k), k) = 0, \tag{5.11c}$$

and $$dF = \frac{\partial F}{\partial \sigma_{ij}(k)}\, d\sigma_{ij}(k) = 0, \quad (\text{never} > 0) \tag{5.11d}$$

then $$d\sigma_{ij}(k) = C_{ijmn}\big(d\epsilon_{mn} - \frac{\partial F}{\partial \sigma_{mn}(k)}\, d\lambda_k\big), \tag{5.11e}$$

where $d\lambda_k$ is given by Equation (5.10).

If Equation (5.11c) or (5.11d) is violated, then

$$d\sigma_{ij}(k) = C_{ijmn} d\epsilon_{mn}. \tag{5.11f}$$

Throughout the above, all the derivatives involving F are to be evaluated at the current value of $\tilde{\sigma}(k)$. Eqn. (5.11f) signifies that the instantaneous element response will be linearly elastic if the element is not yielded ($F(\tilde{\sigma}(k), k) < 0$) , or it is subject to a condition of unloading ($dF < 0$).

Through the equations in (5.11), the model behavior is completely defined as long as the mathematical forms of the two material functions, the yield-strength distribution function $\phi(k)$ and the element yield function $F(\tilde{\sigma}(k), k)$, are specified. The way to define the distribution function $\phi(k)$ is similar to that used for the one-dimensional DEMs, or Masing models, since the general multi-dimensional model

should reduce to the one-dimensional case as the loading is restricted to be uniaxial. Thus, similar to Eqn. (5.3), the distribution function satisfies

$$\int_0^\infty \phi(k)\, dk = 1. \tag{5.12}$$

Also, by Eqn. (5.11a), using $\forall\ k\ \ \sigma_{11}(k) = k$ and $\sigma_{ij}(k) = 0$ if $i \neq 1$ or $j \neq 1$ (which signifies that every element is in yielding state under the uniaxial loading condition), we have

$$\sigma_u = \int_0^\infty k\, \phi(k)\, dk, \tag{5.13}$$

where σ_u denotes the ultimate uniaxial stress of the model. Eqns. (5.12) and (5.13) provide two conditions for the yield-strength distribution function $\phi(k)$ to satisfy. As a consequence, $\phi(k)$ can be chosen as any probability density function that has the mean value σ_u as a parameter. To this end, the Rayleigh distribution, defined as

$$\phi(k) = \frac{\pi}{2}\frac{k}{\sigma_u^2} \exp\left(\frac{-\pi}{4}\frac{k^2}{\sigma_u^2}\right), \tag{5.14}$$

serves as a good candidate for $\phi(k)$, as already demonstrated in Chapter 3. Additional parameters may be incorporated in the definition of $\phi(k)$ so that more general response behavior can be modeled. For example, if the degree of smoothness of yielding behavior is to be modeled accurately, then the generalized Rayleigh distribution, as given by Eqn. (3.35), can be used with the introduction of one additional parameter n.

As mentioned earlier, the definition of the yield function associated with each element is the same as that used in classical theory of plasticity. There have been many yield criteria proposed in plasticity theory for various materials. Among them, the von Mises yield criterion described by

$$F(\tilde{\sigma}(k), k) \equiv \frac{1}{2} s_{ij}(k)\, s_{ij}(k) - \frac{1}{3}\sigma_0^2(k) = 0 \tag{5.15}$$

is probably the most widely recognized criterion for modeling yielding behavior of materials due to its physical consistency and mathematical tractability. In Eqn. (5.15), s_{ij} denotes the deviatoric stress tensor defined as

$$s_{ij} = \sigma_{ij} - \frac{1}{3}\sigma_{mm}\, \delta_{ij},$$

where δ_{ij} is the Kronecker delta function. In the present study of constitutive modeling, however, the yield function can be chosen appropriately for the material under consideration based on any criterion used in plasticity theory or any empirical condition observed experimentally.

In addition to the two material functions discussed above, one needs to specify the elastic constants C_{ijmn} involved in the constitutive equations of the model. It is noted that these constants, assumed to be identical for all elements, are essentially the same as those of the model itself. This can be proven as follows. When the system response is very small, the model and all its elements can be assumed to be in purely elastic states, then, from (5.11a), we have

$$\begin{aligned}\sigma_{ij} &= \int_0^\infty \sigma_{ij}(k)\,\phi(k)\,dk \\ &= \int_0^\infty C_{ijmn}\,\epsilon_{mn}(k)\,\phi(k)\,dk \\ &= C_{ijmn}\,\epsilon_{mn}\int_0^\infty \phi(k)\,dk \\ &= C_{ijmn}\,\epsilon_{mn},\end{aligned}$$

where we used Eqn. (5.11) and $\epsilon_{mn}(k) \equiv \epsilon_{mn}\ \forall\ k$. This property makes the modeling of this class of multi-dimensional DEMs very straightforward, since the elastic constants associated with various materials have been well documented, or can be found through simple experiments.

It should be pointed out that although we assume that all the elements in the DEM are subject to the same total strain increment as experienced by the model itself, i.e., $d\epsilon_{ij}(k) = d\epsilon_{ij}\ \forall\ k$, the plastic strain response of the model is given by

$$d\epsilon^p_{ij} = \int_0^\infty d\epsilon^p_{ij}(k)\,\phi(k)\,dk,$$

as can be derived using Eqns. (5.4) and (5.9), where $d\epsilon^p_{ij}(k)$ is to be found from Eqns. (5.8) and (5.10).

In summary, this class of DEMs formulated in the "invariant-yield-surface" space for cyclic plasticity involves only very few parameters that have clear physical significance. In the case where isotropic materials are of interest, only four parameters are sufficient to represent general multi-axial elastic-plastic response behavior: two

parameters (σ_u and n) are used for describing various shapes of hysteresis loops; and another two (E and ν) are for elastic behavior. As discussed in Chapter 3, the Rayleigh distribution serves as a good model for the yield-strength distribution function $\phi(k)$ in many engineering applications. In this case, only three parameters (n is fixed to be 1) need be specified (or identified, in identification studies), which makes the modeling process or the identification procedure even simpler and more efficient.

5.2.3 Numerical Implementation of the New Distributed-Element Model

The theoretical background and mathematical formulation of the new class of multi-dimensional DEMs formulated in the invariant-yield-surface space have been presented in the previous sections. In theory, the model may consist of an infinite number of elements whose yield strengths distribute according to the specified distribution function $\phi(k)$, and the model response is found by keeping track of all the element behavior (cf. (5.11)). However, to numerically implement the formulation, one has to introduce a finite number of elements so that the solution algorithm is practically feasible. In order to preserve the advantages of this simple, physical model, it is proposed that the introduction of the finite number of elements be made according to the specified yield-strength distribution function $\phi(k)$, so that the number of parameters involved in the model does not increase with the number of elements introduced. In the case where the Distributed-Element Model consists of a finite number of, say N, elements, the integral operation in Eqn. (5.11a) is replaced by the summation operation as follows

$$\tilde{\sigma} = \sum_{i=1}^{N} \tilde{\sigma}(k_i)\, \psi(k_i), \tag{5.16}$$

where the "weighting function" $\psi(k_i)$ satisfies

$$\sum_{i=1}^{N} \psi(k_i) = 1, \tag{5.17}$$

in place of Eqn. (5.12). Also, Eqn. (5.13) becomes

$$\sum_{i=1}^{N} k_i\, \psi(k_i) = \sigma_u. \tag{5.18}$$

In order to obtain smooth response curves, one can choose, without loss of generality,

$$\psi(k_i) = \frac{1}{N} \quad \forall \ \ i = 1, \ldots, N, \tag{5.19}$$

and the yield constants k_i, $i = 1, \ldots, N$ are selected based on the specified distribution function $\phi(k)$, $k \in [0, \infty)$, so that each time a new element yields, the model loses $1/N$ of its initial stiffness. This can be done by dividing the region below the curve described by the distribution function into N equal-area portions, and selecting k_i as a representative value for the i-th portion, so that Eqns. (5.18) and (5.19) are satisfied, that is

$$\sum_{i=1}^{N} k_i = N \, \sigma_u. \tag{5.20}$$

The aforementioned modeling procedure is illustrated schematically in Fig. 5.4. For most applications, it suffices to use ten elements or so in representing the new model in order to get a reasonably smooth hysteresis curve. For example, the yield constants for the ten elements corresponding to a Rayleigh distribution can be defined as:

$$\begin{aligned} &\bar{k}_1 = 0.2638, \quad \bar{k}_2 = 0.4601, \quad \bar{k}_3 = 0.6097, \quad \bar{k}_4 = 0.7448, \quad \bar{k}_5 = 0.8767, \\ &\bar{k}_6 = 1.0128, \quad \bar{k}_7 = 1.1612, \quad \bar{k}_8 = 1.3347, \quad \bar{k}_9 = 1.5630, \quad \bar{k}_{10} = 1.9732, \end{aligned} \tag{5.21}$$

where we define $\bar{k}_i \equiv k_i / \sigma_u$.

The numerical procedure for obtaining the stress response of an N-element model based on the invariant-yield-surface formulation, subject to some prescribed strain path, can be best described by a flow diagram as shown in Fig. 5.5, where we assume that the strain increment in each loading step is small; otherwise, some subdivision of $\Delta\epsilon$ is needed to assure that Eqn. (5.11*b*) is satisfied appropriately. As can be seen from the flow diagram in Fig. 5.5, the numerical implementation of this new multi-dimensional class of DEMs is surprisingly simple and computationally efficient, due to the formulation in the invariant-yield-surface space, which avoids the usually complicated kinematic hardening rule required for accounting for the Bauschinger effect in cyclic plasticity.

5.2.4 An Application to Biaxial Loading

A series of simulation studies on the response of the new model to some prescribed strain paths are conducted to examine the model behavior in the biaxial tension-torsion case, for which published work is readily available for comparison. Lamba and Sidebottom [30] conducted a series of biaxial tension-torsion tests on copper in which cyclic, nonproportional axial-torsional strain paths were applied to examine material response behavior. The test samples used were thin-walled hollow cylindrical shafts and were loaded with combined axial force and torsion. In the experimental studies, the state of axial stress and shear stress resulting from the applied axial force and torsion respectively was considered to be uniform in the test region at every time instant. We have the following tensors of stress and strain in the biaxial loading case:

$$\sigma_{ij} = \begin{pmatrix} \sigma_{11} & \sigma_{12} & 0 \\ \sigma_{12} & 0 & 0 \\ 0 & 0 & 0 \end{pmatrix}, \qquad \epsilon_{ij} = \begin{pmatrix} \epsilon_{11} & \epsilon_{12} & 0 \\ \epsilon_{12} & -\gamma\epsilon_{11} & 0 \\ 0 & 0 & -\gamma\epsilon_{11} \end{pmatrix} \tag{5.22}$$

where the coefficient γ represents the Poisson effect which is a variable when inelastic deformations are involved in the response. It can be shown [14] that if we assume incompressibility of plastic deformation, then we have the following expression for γ:

$$\gamma = \frac{1}{2} - \frac{1}{E}(\frac{1}{2} - \nu)\frac{d\sigma_{11}}{d\epsilon_{11}}, \tag{5.23}$$

where ν is the Poisson's ratio for linear elasticity.

In the simulation studies, the model used consists of ten distributed elements, and the Rayleigh distribution is used for describing the yield-strength distribution in the formulation, so that Eqn. (5.21) defines the yield constants of the elements. The model parameters used are $E = 16,700\ ksi, \nu = 0.33$, and $\sigma_0 = 30\ ksi$. The prescribed strain loading paths are shown in Fig. 5.6, for which the corresponding experimentally-observed stress responses are available [30], as shown in Figures 5.7 and 5.8. Note that the loading path sequence in Fig. 5.6(a) is 0-1-0-2-0-3-0-..., so as to study the property of erasure-of-memory. Also, the stress path resulting from the repetition of path 0 each time is not plotted in Fig. 5.7(a) for clarity.

The stress responses predicted using the DEMs are shown respectively in Figures 5.9 and 5.10, where both von Mises' and Tresca's yield criteria were used in the simulations for comparison purposes. In general, the results obtained in all cases are both

qualitatively and quantitatively consistent with those observed experimentally, and Tresca's yield condition gives slightly better results than von Mises' does considering the value of the ultimate shear stress predicted. Note that Fig. 5.9(a) contains the full stress path whereas Fig. 5.7(a) does not. It can be clearly seen in Figures 5.7 and 5.8, that there exists equilibrium points corresponding to those uni-directional strain paths, at which the stress increments approach zero for appreciable strain increments that remain uni-directional. In addition, it can be deduced that there exists a limit surface in the stress space in each of the two loading cases so that stress states can never go beyond it. Moreover, the property of erasure-of-memory is clearly demonstrated by the DEM, as one can see that the model is always brought back to the same state every time the path 0 in Fig. 5.6(a) is traced.

Other important response features in cyclic plasticity, such as smooth yielding, nonlinear strain hardening and multi-axial Bauschinger effect are also well demonstrated by the new DEMs. The computational effort involved in obtaining the response based on the new model is low, since no kinematic hardening rule is required to account for the subsequent yielding behavior of materials. We remark that models based on the classical theory of plasticity in general do not predict response behavior so well as the DEMs do, as we can see in Fig. 5.11, where different yield conditions together with different kinematic hardening rules were employed to predict the response to the strain loading path given in Fig. 5.6(b) [30]. The dashed curve in each plot of Fig. 5.11 represents the locus of the center of the yield surface, which is irrelevant to the discussion made here. A clear deficiency of the first two models, which use respectively the von Mises yield condition with the Prager hardening rule and the Tresca yield condition with the Ziegler hardening rule,† is that the axial stress predicted does not return to zero. In more specific terms, these two models fail to demonstrate the behavior of equilibrium points and a limit surface exhibited by real materials. In Fig. 5.11(c), a much more elaborated model is used, which employs a Tresca yield surface, a Tresca limit surface, the Mroz kinematic hardening rule, and

† The Prager hardening rule specifies that the yield surface translates in the direction of the outward normal at the current stress point, while the Ziegler hardening rule specifies that the yield surface moves in the same direction as the line joining the center of the yield surface to the current stress point [30].

an empirical nonlinear strain hardening assumption [30], so as to give the plasticity model a maximum chance of success. Although the result shown in Fig. 5.11(c) is much better than those shown in Fig. 5.11(a) and (b), it is still not so good in accuracy as that predicted by the DEM, as justified by the experimental result shown in Fig. 5.8(a).

It should be noted that in the preceding examples, we did not use any system identification technique to choose optimally the model parameters. Instead, the values of the three parameters E, ν, σ_0 were specified directly from the corresponding experimental results [30]. This advantage is obviously due to the physical consistency and the parsimony in parameters of the proposed DEM for cyclic plasticity. In the case where complex structural systems are of interest, the parameters may be optimally identified using structural response data. Furthermore, we can treat some constants in the yield condition required for the model as parameters to be identified, so that the "best" result may be achieved in practice.

In the next section, we will address some important properties associated with the new class of DEMs for general plasticity. Thorough understanding of these properties helps to explain some material properties and complicated material behavior under cyclic loading conditions. As a final remark, we note that the new Distributed-Element Model for multi-dimensional plasticity can be viewed as a statistical mechanical model which is a generalization of the classical formulation of plasticity theory. In the new theory, the yield condition for elasto-plastic response characterization and the flow rule for prescribing plastic strain increment are treated in a statistical sense, so that the model response is the statistical average of the element response, each of which follows from the classical theory of plasticity.

5.3 Important Properties of the New Multi-dimensional DEMs

In the foregoing simulation studies, we have seen the existence of equilibrium points and a limit surface associated with a new multi-dimensional DEM. Furthermore, the property of erasure-of-memory exhibited by real materials is also demonstrated by the new model so that excellent results of response prediction have been obtained when compared to experimental observations. It is of great interest to further investigate these general properties of material behavior from a theoretical point

of view, which will surely help the study of complicated response behavior of cyclic plasticity. A thorough understanding of these properties may also provide useful insight and guidelines for validating analytical models and for performing analytical/experimental studies in the related areas of plasticity.

5.3.1 General Behavior of Ideal Plasticity of a Single Element

In view of the physically consistent behavior of the multi-dimensional DEM, we would like to further study some relevant properties of the new model, which consists of a collection of distributed elements of different yield strengths. Before doing this, let us examine in detail the response characteristics of a single element. Each element in the model exhibits the behavior of ideal plasticity, and so is governed by the constitutive equations given in (5.11*b*) to (5.11*f*). If we rewrite the incremental stress-strain relation (5.9) as

$$d\sigma_{ij} = C^e_{ijkl}(d\epsilon_{kl} - d\epsilon^p_{kl}), \tag{5.24}$$

then based upon the normality principle of plastic strain increment, we can derive for a yielding state from (5.8) and (5.10):

$$d\epsilon^p_{kl} = \frac{\partial F}{\partial \sigma_{kl}}\, d\lambda = \frac{\frac{\partial F}{\partial \sigma_{kl}} \frac{\partial F}{\partial \sigma_{ij}} C^e_{ijmn}\, d\epsilon_{mn}}{\frac{\partial F}{\partial \sigma_{pq}} C^e_{pqrs} \frac{\partial F}{\partial \sigma_{rs}}}, \tag{5.25}$$

where $d\lambda \geq 0$ is a constant of proportionality and F is the yield function.

In order to characterize the complicated elasto-plastic behavior more easily, we consider the biaxial tension-torsion loading case and employ the well-recognized von Mises yield criterion. If we denote the axial stress and strain components as σ and ϵ, and the shear stress and strain components as τ and γ, respectively, then we can derive the following set of equations from the general formulation:

$$F(\sigma, \tau, k) = \sigma^2 + 3\tau^2 - k^2 = 0, \tag{5.26}$$

$$\frac{\partial F}{\partial \sigma} = 2\sigma, \quad \frac{\partial F}{\partial \tau} = 6\tau, \tag{5.27}$$

$$d\sigma = E(d\epsilon - d\epsilon^p), \quad d\tau = G(d\gamma - d\gamma^p), \tag{5.28}$$

$$d\epsilon^p = 2\sigma d\lambda, \quad d\gamma^p = 6\tau d\lambda, \tag{5.29}$$

where $d\lambda = 0$ in the elastic state ($F < 0$), while in the yielding state ($F = 0$):

$$d\lambda = \frac{(2\sigma)Ed\epsilon + (6\tau)Gd\gamma}{E(2\sigma)^2 + G(6\tau)^2}. \tag{5.30}$$

An important remark regarding the biaxial formulation is that in the above we have defined $\epsilon \equiv \epsilon_{11}, \sigma \equiv \sigma_{11}, \gamma \equiv 2\epsilon_{12} \equiv 2\epsilon_{21}$, whereas $\tau \equiv \sigma_{12} \equiv \sigma_{21}$. It is more convenient and consistent to adopt these definitions due to the fact that in the general flow rule given in Eqn. (5.25), the yield function F is considered as a function of nine stress components, counting σ_{12} and σ_{21} as separate variables. Note that the above definitions imply that

$$\frac{\partial F}{\partial \sigma} = \frac{\partial F}{\partial \sigma_{11}} \quad \text{and} \quad \frac{\partial F}{\partial \tau} = \frac{\partial F}{\partial \sigma_{12}} + \frac{\partial F}{\partial \sigma_{21}} = 2\frac{\partial F}{\partial \sigma_{12}}, \tag{5.31}$$

so that $d\epsilon^p = (\partial F/\partial \sigma)\, d\lambda$ and $d\gamma^p = (\partial F/\partial \tau)\, d\lambda$.

In order to understand the detailed behavior of an element after yielding occurs, we first consider a simple case where a proportional strain loading path is prescribed, as the path $0 - 1$ shown in Fig. 5.12(a). The response of an element having perfect plastic behavior to such a loading path can be depicted in a correponding stress space as shown in Fig. 5.12(b). If the element yields at point P on path $0 - 1$, then the corresponding stress state will just reach the yield surface at, say, P' in the stress space. As the loading is continued, the stress state will move around on the yield surface without going beyond it. But then an interesting question arises concerning which direction the point P' will move under further loading. To answer this, we have to look back at the constitutive equations which govern the response behavior. Combining (5.28), (5.29) and (5.30) we get

$$\begin{aligned} d\sigma &= \frac{12EG\tau}{E(2\sigma)^2 + G(6\tau)^2}(3\tau d\epsilon - \sigma d\gamma), \\ d\tau &= \frac{-4EG\sigma}{E(2\sigma)^2 + G(6\tau)^2}(3\tau d\epsilon - \sigma d\gamma). \end{aligned} \tag{5.32}$$

Thus, given strain increments $d\epsilon$ and $d\gamma$, we are able to determine the direction of stress increments at a yield state by using (5.32), which leads to the following rules for response behavior:

(I) If $3\tau d\epsilon > \sigma d\gamma$:

$$d\sigma \sim \tau, \qquad d\tau \sim -\sigma, \tag{5.33}$$

(II) If $3\tau d\epsilon = \sigma d\gamma$:

$$d\sigma = d\tau = 0, \tag{5.34}$$

(III) If $3\tau d\epsilon < \sigma d\gamma$:

$$d\sigma \sim -\tau, \qquad d\tau \sim \sigma, \tag{5.35}$$

where "$\sim$" means "proportional to". In Rule (II) we have the situation that if the ratio of $d\epsilon$ to $d\gamma$ is kept fixed (e.g., in the case of proportional loading) and the stress state satisfies $\sigma/3\tau = d\epsilon/d\gamma$, then the stress state will remain invariant unless the strain path changes its direction. In this case, we say that the response state reaches an "equilibrium state"* associated with that particular uni-directional strain path. Mathematically, it can be shown that if the current state is governed by (I) or (III), then it will approach a state described by (II). Thus, physically, the above rules signify that a response state of a yielded element moves on the yield surface in a direction toward an equilibuium state corresponding to the prescribed strain path.

Following the rules we can find that in Fig. 5.12(b), the response state at P' will move in the direction of $P'Q'$ and will finally stop at the equilibrium state at Q', as shown schematically in the figure. Similarly, we can determine the directions of stress increments corresponding to the strain paths in different quadrants as shown in Fig. 5.12(b), provided that the initial strain loading path remains uni-directional in each of the cases. It should be noted, however, that the direction of a stress increment corresponding to a stress state on the yield surface may be different from those given in Fig. 5.12(b) in case of a strain loading path that is not virgin loading or uni-directional. Nevertheless, the direction of a stress increment at a given yield state can always be determined based on the foregoing rules.

An important property regarding the element behavior is the existence of equilibrium states associated with different uni-directional strain paths. The equilibrium states can be defined as the states at which the stress increments approach zero for appreciable strain increments that remain uni-directional. This property of response in cyclic plasticity has actually been observed in experimental studies of some

* A more rigorous definition for equilibrium states will be given later in this chapter.

materials [30]. Each equilibrium state thus defined is associated with a particular uni-directional strain path. The mathematical aspects of the existence and uniqueness of an equilibrium state will be treated later on within a general formulation of plasticity. However, we remark here that the existence and uniqueness of equilibrium states leads to another important material property called the property of erasure-of-memory. The property of erasure-of-memory is also deduced from experimental observations [30] and can be stated as follows: If a material has been stabilized by "out-of-phase" cycling (i.e., loading with non-proportional strain cycles) and if the subsequent strain paths remain in the region enclosed by the out-of-phase cycling, then one "big" strain cycle, which is sufficiently smooth and long so that there exists at least one equilibrium state associated with it, will always bring the material back to the particular equilibrium state that is unique to that big strain cycle. This property is very useful in conducting experiments on cyclic plasticity, since a single specimen can always be brought back to the same reference state, and so can be used repeatedly in charactizing material response to various loading paths. This ensures that more reliable results can be obtained with considerably less labor and cost.

We remark that for the existence of erasure-of-memory, the out-of-phase stabilization is a prerequisite condition† since experimental results have shown that the peak stress (or yield stress) resulting from out-of-phase hardening is about 40% higher than that from uniaxial cycling, as already discussed in Chapter 4. Hence, if a material has not yet been out-of-phase stabilized, its yield condition becomes variant and depends on the non-proportionality of the loading path. This phenomenon cannot be characterized by conventional plasticity models‡ unless special treatment is made [43].

---

† As shown later, the property of erasure-of-memory is closely related to the existence and uniqueness of equilibrium states, which in turn depends upon the associated yield condition.

‡ Most constitutive theories of cyclic plasticity are concerned with cyclically stabilized behavior. One reason for this is that crack initiation predictions are generally based on cyclically stabilized states [8].

5.3.2 General Treatment of the Theory of Plasticity

In the following, a general treatment of the classical incremental theory of plasticity is presented and some properties of the formulation are summarized. The general formulation will then be used to derive important properties associated with the new class of multi-dimensional DEMs

Let $\tilde{\sigma} \equiv (\sigma_{ij})$ be the total stress tensor and $\tilde{\epsilon} \equiv (\epsilon_{ij})$ the total strain tensor. Define the *elastic* component and the *plastic-relaxation* component of the stress increment tensor, $d\tilde{\sigma}^e$ and $d\tilde{\sigma}^p$, respectively by:

$$d\sigma^e_{ij} \equiv C^e_{ijkl}\, d\epsilon_{kl}, \tag{5.36}$$

$$d\sigma^p_{ij} \equiv d\sigma^e_{ij} - d\sigma_{ij}, \tag{5.37}$$

where C^e_{ijkl} is an elastic modulus tensor which is independent of response states. The above definitions can be better understood through the schematic diagram shown in Figure 5.13, where the uniaxial stress-strain relation is considered.

Introduce a *plastic modulus reduction tensor* Λ_{ijkl} so that

$$d\sigma^p_{ij} \equiv C^e_{ijmn}\, \Lambda_{mnkl}(\tilde{\sigma}, \tilde{\epsilon}, d\tilde{\sigma}, d\tilde{\epsilon}) d\epsilon_{kl}, \tag{5.38}$$

then following from the incremental stress-strain relation:

$$d\sigma_{ij} = C^e_{ijkl}\, d\epsilon^e_{kl} = C^e_{ijkl}(d\epsilon_{kl} - d\epsilon^p_{kl}), \tag{5.39}$$

we can derive that

$$d\sigma^p_{ij} = C^e_{ijkl}\, d\epsilon^p_{kl}$$

and

$$d\epsilon^p_{ij} = \Lambda_{ijkl}(\tilde{\sigma}, \tilde{\epsilon}, d\tilde{\sigma}, d\tilde{\epsilon})\, d\epsilon_{kl}. \tag{5.40}$$

Note that the plastic modulus reduction tensor is, in general, a function of not only the current state, but also the load increment.

The above equations can be put in a vector form as follows. Since σ_{ij} and ϵ_{ij} are symmetric second-order tensors, they can be written as vectors $\underline{\sigma}, \underline{\epsilon} \in \Re^6$ defined by

$$\underline{\sigma} = < \sigma_{11}, \sigma_{22}, \sigma_{33}, \sigma_{12}, \sigma_{23}, \sigma_{13} >^T, \tag{5.41}$$

$$\underline{\epsilon} =< \epsilon_{11}, \epsilon_{22}, \epsilon_{33}, 2\,\epsilon_{12}, 2\,\epsilon_{23}, 2\,\epsilon_{13} >^T, \tag{5.42}$$

so that the values of the inner products between tensors and between vectors are preserved, and where the superscript T denotes matrix transpose, i.e.,

$$\begin{aligned}\tilde{\sigma} \cdot \tilde{\epsilon} &\equiv \sigma_{ij}\epsilon_{ij} \\ &= \sigma_{11}\epsilon_{11} + \sigma_{22}\epsilon_{22} + \sigma_{33}\epsilon_{33} + 2\sigma_{12}\epsilon_{12} + 2\sigma_{23}\epsilon_{23} + 2\sigma_{13}\epsilon_{13}\,. \\ &= \underline{\sigma} \cdot \underline{\epsilon}\end{aligned}$$

Thus, Eqn. (5.40) becomes

$$d\underline{\epsilon}^p = \mathbf{\Lambda}(\underline{\sigma}, \underline{\epsilon}, d\underline{\sigma}, d\underline{\epsilon})\, d\underline{\epsilon}, \tag{5.43}$$

and Eqn. (5.39) can be rewritten as

$$d\underline{\sigma} = \mathbf{C}^e[\mathbf{I} - \mathbf{\Lambda}(\underline{\sigma}, \underline{\epsilon}, d\underline{\sigma}, d\underline{\epsilon})]\, d\underline{\epsilon}, \tag{5.44}$$

where $\mathbf{\Lambda}$ and $\mathbf{C}^e$ are the matrices corresponding to the fourth-order tensors Λ_{ijkl} and C^e_{ijkl} so that the equations defined accordingly are consistent, and $\mathbf{I}$ is the 6×6 identity matrix. The elastic modulus matrix $\mathbf{C}^e$ is symmetric because of the symmetries associated with the tensor C^e_{ijkl} for elastic behavior. Also, it is a constant matrix under the assumption that the elastic behavior of the material is linear. It is positive definite if the material is stable to small strain perturbations (or if a Drucker's postulate holds), which we assume is the case. Equation (5.44) can be reformulated as

$$d\underline{\sigma} = [\mathbf{C}^e - \mathbf{C}^p(\underline{\sigma}, \underline{\epsilon}, d\underline{\sigma}, d\underline{\epsilon})]\, d\underline{\epsilon}, \tag{5.45}$$

where $\mathbf{C}^p \equiv \mathbf{C}^e\mathbf{\Lambda}$ can be referred to as the *plastic modulus matrix.*

Equation (5.44) (or (5.45)) gives the general formulation of the basic constitutive law that we will use in the following, where we establish some theorems pertaining to the properties of the formulation. With these theorems, some important properties associated with the new class of multi-dimensional DEMs can then be derived and presented in a more efficient way.

[Theorem 1]: Within the classical formulation of plasticity*, the plastic modulus reduction matrix $\mathbf{\Lambda}$ and the plastic modulus matrix $\mathbf{C}^p$ are both of rank one or zero, corresponding to yielding and elastic behavior respectively.

[Proof]: If the classical theory of plasticity is considered, the yield function can be assumed to be of the form :

$$F(\underline{\sigma}, \underline{\alpha}(\underline{\epsilon}^p), k(\underline{\epsilon}^p)) \equiv \hat{F}(\underline{\sigma} - \underline{\alpha}(\underline{\epsilon}^p)) - k(\underline{\epsilon}^p) = 0, \tag{5.46}$$

where both isotropic and kinematic hardening are taken into account. In the case of ideal plasticity, $\underline{\alpha} \equiv \underline{0}$ and $k \equiv$ *constant* throughout the response history. Based on the "associated flow rule," which states that the yield function is the same as the plastic potential function which defines the directions of the plastic strain increments, we have

$$d\epsilon_{ij}^p = d\lambda \frac{\partial F}{\partial \sigma_{ij}}, \qquad d\lambda \geq 0. \tag{5.47}$$

During plastic deformation we require $F = 0$, and so $dF = 0$, i.e.,

$$\frac{\partial F}{\partial \sigma_{ij}} d\sigma_{ij} + \frac{\partial F}{\partial \epsilon_{ij}^p} d\epsilon^p = 0. \tag{5.48}$$

Define

$$\underline{a} \equiv \nabla_{\underline{\sigma}} F(\underline{\sigma}, \underline{\epsilon}^p) \in \Re^6, \qquad \underline{d} \equiv -\nabla_{\underline{\epsilon}^p} F(\underline{\sigma}, \underline{\epsilon}^p) \in \Re^6, \tag{5.49}$$

where the vector gradient of a scalar function is defined by

$$\nabla_{\underline{u}} F(\underline{u}, \underline{v}, \ldots) \equiv \langle \frac{\partial F}{\partial u_1}, \frac{\partial F}{\partial u_2}, \ldots, \frac{\partial F}{\partial u_n} \rangle^T \tag{5.50}$$

if $\underline{u} \equiv < u_1, u_2, \ldots, u_n >^T$. From Eqns. (5.47), (5.48) and (5.49), and the incremental stress-strain relation

$$d\underline{\sigma} = \mathbf{C}^e (d\underline{\epsilon} - d\underline{\epsilon}^p), \tag{5.51}$$

---

* By classical formulation of plasticity we mean that the elastic-plastic response behavior is characterized by a yield condition, a flow rule, and a strain hardening rule. The flow rule relates the increment of plastic strain to the current state and the stress increment. The strain hardening rule specifies how the yield surface is changed during plastic flow.

it follows that

$$d\lambda = \begin{cases} \alpha\, \underline{b}^T d\underline{\epsilon} & \text{if } \underline{b}^T d\underline{\epsilon} > 0; \\ 0 & \text{if } \underline{b}^T d\underline{\epsilon} \leq 0, \end{cases} \tag{5.52}$$

where $\underline{b} \equiv \mathbf{C}^e \underline{a}$ and $\alpha \equiv 1/(\underline{d}^T \underline{a} + \underline{b}^T \underline{a})$, which is just a scalar, and hence

$$d\underline{\sigma} = \begin{cases} \mathbf{C}^e(\mathbf{I} - \alpha\, \underline{a}\, \underline{b}^T)\, d\underline{\epsilon} & \text{if } \underline{b}^T d\underline{\epsilon} > 0; \\ \mathbf{C}^e\, d\underline{\epsilon} & \text{if } \underline{b}^T d\underline{\epsilon} \leq 0. \end{cases} \tag{5.53}$$

Therefore, by comparing (5.53) with (5.44), and using the fact that $\mathbf{C}^e$ is invertible, we find

$$\mathbf{\Lambda} = \begin{cases} \alpha\, \underline{a}\, \underline{b}^T & \text{if } \underline{b}^T d\underline{\epsilon} > 0; \\ 0 & \text{if } \underline{b}^T d\underline{\epsilon} \leq 0. \end{cases} \tag{5.54}$$

Thus, we may conclude that $\mathbf{\Lambda}$ is a 6×6 matrix of rank one (only one independent row or column) or zero. Also since

$$\mathbf{C}^p \equiv \mathbf{C}^e \mathbf{\Lambda}, \tag{5.55}$$

$\mathbf{C}^p$ is of rank one or zero, too. Since yielding is equivalent to a non-zero plastic strain increment $d\underline{\epsilon}^p$, from Eqn.(5.43) we see that $\mathbf{\Lambda}$ and $\mathbf{C}^p$ are both of rank one during yielding and are both zero during elastic behavior. We remark that even if a non-associated flow rule is used, the same conclusion can still be made.

The practical significance of Theorem 1 in the theory of plasticity may be stated as another theorem as follows.

[Theorem 2]: Within the context of classical plasticity, the incremental plastic deformation, if it exists, only occurs in a one-dimensional subspace (which changes with the current yielding stress state) of the six-dimensional space of the total strain increment.

[Proof]: We know from Theorem 1 that the plastic modulus reduction matrix $\mathbf{\Lambda}$ is a 6×6 matrix of rank 1 during plastic flow. Thus, there exists $\{\underline{x}_i : i = 1, 2, \ldots, 5\}$ forming a basis for the 5-dimensional null space of $\mathbf{\Lambda}$, i.e.,

$$\mathbf{\Lambda}\, \underline{x}_i = 0, \qquad \forall\, i = 1, 2, \ldots, 5. \tag{5.56}$$

Equations (5.43), (5.44) and (5.56) imply that there always exists five linearly-independent strain increment vectors $d\underline{\epsilon}_i = d\mu_i \underline{x}_i, d\mu_i > 0, i = 1, \ldots, 5$, such that

$$d\underline{\sigma}_i = \mathbf{C}^e d\underline{\epsilon}_i \quad \text{and} \quad d\underline{\epsilon}_i^p = \mathbf{\Lambda}\, d\underline{\epsilon}_i = 0, \quad \forall\, i = 1, 2, \ldots, 5, \tag{5.57}$$

and the corresponding plastic-relaxation stress increment satisfies

$$d\underline{\sigma}_i^p = \mathbf{C}^p d\underline{\epsilon}_i = \mathbf{C}^e \mathbf{\Lambda}\, d\underline{\epsilon}_i = 0. \tag{5.58}$$

Thus, purely elastic behavior always occurs in, at least, a 5-dimensional subspace of the six-dimensional space of the total strain increment, and then the conclusion of Theorem 2 follows.

We remark that in the case of ideal plasticity, the plastic modulus reduction matrix takes the form (cf. Eqn. (5.54) with $\underline{d} = \underline{0}$ in α)

$$\mathbf{\Lambda}(\underline{\sigma}, \underline{\epsilon}, d\underline{\sigma}, d\underline{\epsilon}) = \frac{\underline{a}\ \underline{b}^T}{\underline{b}^T \underline{a}} \qquad \text{if } \underline{b}^T d\underline{\epsilon} > 0. \tag{5.59}$$

during plastic deformation, where $\underline{a}$, $\underline{b}$ are defined as before. Thus, as a result of Theorem 1, the eigenvalues $\lambda_i, i = 1, \ldots, 5$, of $\mathbf{\Lambda}$ are zero, and the remaining eigenvalue λ_6 must be 1, since

$$\lambda_6 = \sum_{i=1}^{6} \lambda_i = Tr(\mathbf{\Lambda}) = \frac{\sum_{i=1}^{6} a_i b_i}{\underline{b}^T \underline{a}} = 1, \tag{5.60}$$

where $Tr(\cdot)$ denotes the trace of a square matrix. Let the corresponding eigenvectors be $d\underline{\epsilon}_i$, $i = 1, \ldots, 6$, where $d\underline{\epsilon}_i$, $i = 1, \ldots, 5$, give purely elastic behavior, as in the proof of Theorem 2, then,

$$\mathbf{\Lambda}\, d\underline{\epsilon}_6 = 1 \cdot d\underline{\epsilon}_6 = d\underline{\epsilon}_6$$

which implies

$$d\underline{\epsilon}_6 = d\underline{\epsilon}_6^p, \quad \text{or} \quad d\underline{\epsilon}_6^e = \underline{0}. \tag{5.61}$$

Thus, we get *purely* plastic strain increment in a one-dimensional subspace. In the case where strain hardening is taken into account, however, $d\underline{\epsilon}_6$ will not, in general, be fully plastic, since λ_6 may be less than one, as can be deduced from Eqn. (5.54) and Theorem 1.

[Theorem 3]: If an associated flow rule is used in the formulation based on the classical theory of plasticity, the plastic modulus matrix $\mathbf{C}^p$ is symmetric. Also, in general, Drucker's postulates of stability imply that $\mathbf{C}^p$ is positive semi-definite.

[Proof]: From Eqns. (5.54) and (5.55) we get

$$\mathbf{C}^p = \alpha \mathbf{C}^e \underline{a}\, \underline{b}^T = \alpha (\mathbf{C}^e \underline{a})(\mathbf{C}^e \underline{a})^T,$$

since $\underline{b} \equiv \mathbf{C}^e \underline{a}$. Thus, we have

$$(\mathbf{C}^p)^T = \mathbf{C}^p,$$

i.e., $\mathbf{C}^p$ is a symmetric matrix. Drucker's postulate requires that

$$d\underline{\sigma}^T\, d\underline{\epsilon}^p \geq 0, \tag{5.62}$$

so by Eqns. (5.43) and (5.44), we have

$$\begin{aligned}
& [\mathbf{C}^e(\mathbf{I} - \mathbf{\Lambda})\, d\underline{\epsilon}]^T \mathbf{\Lambda}\, d\underline{\epsilon} \geq 0 \\
\Longrightarrow \quad & d\underline{\epsilon}^T (\mathbf{I} - \mathbf{\Lambda}) \mathbf{C}^e \mathbf{\Lambda}\, d\underline{\epsilon} \geq 0 \\
\Longrightarrow \quad & d\underline{\epsilon}^T (\mathbf{C}^p - \mathbf{\Lambda}^T \mathbf{C}^e \mathbf{\Lambda})\, d\underline{\epsilon} \geq 0 \\
\Longrightarrow \quad & d\underline{\epsilon}^T \mathbf{C}^p d\underline{\epsilon} - d\underline{\epsilon}^T \mathbf{\Lambda}^T \mathbf{C}^e \mathbf{\Lambda}\, d\underline{\epsilon} \geq 0.
\end{aligned}$$

Since $\mathbf{C}^e$ is positive definite, we may conclude that

$$d\underline{\epsilon}^T \mathbf{C}^p d\underline{\epsilon} \geq 0, \tag{5.63}$$

i.e., $\mathbf{C}^p$ is positive semi-definite. Note that actually (5.63) does *not* hold for all $d\underline{\epsilon}$, only $\underline{b}^T d\underline{\epsilon} > 0$, but $\mathbf{C}^p$ is itself zero otherwise.

[Theorem 4]: The plastic modulus reduction matrix $\mathbf{\Lambda}$, formulated based on an associated flow rule, has, at most, one nonzero positive eigenvalue whose value is never greater than one.

[Proof]: Define $\mathbf{S} \equiv (\mathbf{C}^e)^{-1/2}$, which is a symmetric, positive-definite matrix, since $\mathbf{C}^e$ is symmetric and positive definite. Now consider the eigenvalue problem:

$$\mathbf{S}\mathbf{C}^p\mathbf{S}\, \underline{x} = \lambda\, \underline{x}.$$

Following from Theorem 3 which claims that $\mathbf{C}^p$ is symmetric, positive semi-definite if an associated flow rule is used, we have $\lambda \geq 0$. Let $\underline{y} \equiv \mathbf{S}\,\underline{x}$ then

$$\mathbf{S}\mathbf{C}^p\mathbf{S}\,\underline{x} = \lambda\,\underline{x}$$

$$\iff \qquad \mathbf{S}\mathbf{C}^p\underline{y} = \lambda\mathbf{S}^{-1}\underline{y}$$

$$\iff \qquad (\mathbf{C}^e)^{-1}\mathbf{C}^p\underline{y} = \lambda\,\underline{y} \quad (\text{since } \mathbf{S}^2 = (\mathbf{C}^e)^{-1}),$$

i.e.,

$$\iff \qquad \mathbf{\Lambda}\,\underline{y} = \lambda\,\underline{y} \qquad (\text{since } \mathbf{C}^p = \mathbf{C}^e\mathbf{\Lambda}).$$

Hence, the eigenvalues of $\mathbf{\Lambda}$ are non-negative. Furthermore, by Drucker's postulate:

$$d\underline{\epsilon}^T\,d\underline{\sigma} = d\underline{\sigma}^T\,d\underline{\epsilon} \geq 0,$$

we can derive

$$d\underline{\epsilon}^T[\mathbf{C}^e(\mathbf{I} - \mathbf{\Lambda})\,d\underline{\epsilon}] \geq 0,$$

$$\implies \qquad d\underline{\epsilon}^T(\mathbf{C}^e - \mathbf{C}^p)d\underline{\epsilon} \geq 0,$$

which implies that the symmetric matrix $\mathbf{C}^e - \mathbf{C}^p$ is positive semi-definite. Thus,

$$det(\mathbf{I} - \mathbf{\Lambda}) \geq 0,$$

where $det(\cdot)$ designates the determinant of a matrix. Since the determinant is a product of all the eigenvalues of the matrix and Theorem 1 implies that $\mathbf{\Lambda}$ must have 5 zero eigenvalues, it follows from the above results that there is at most one nonzero eigenvalue λ_6 such that

$$0 \leq \lambda_6 \leq 1.$$

We remark that as in the proof leading to Eqn. (5.61), the case $\lambda_6 = 1$ corresponds to the behavior of ideal plasticity.

With the general formulation introduced above, we are now in a position to derive some important properties of the multi-dimensional DEMs. To begin with, we introduce the following theorem regarding the plastic behavior of the DEMs.

[**Theorem 5**]: For a DEM, the plastic modulus matrix $\mathbf{C}^p$ is symmetric and positive semi-definite, and the eigenvalues of the plastic modulus reduction matrix $\mathbf{\Lambda}$ are all non-negative. Besides,

$$0 \leq Tr(\mathbf{\Lambda}) \leq 1. \tag{5.64}$$

[Proof]: In the formulation of the DEM with a finite number of elements, the plastic strain increment of the model is given by

$$d\underline{\epsilon}^p = \sum_{i=1}^{N} \psi_i \, d\underline{\epsilon}_i^p, \tag{5.65}$$

which can be easily derived from the basic assumptions of the kinematic behavior of the DEM and the incremental stress-strain relation. By Eqn. (5.43) and the definition of the plastic modulus matrix, we have

$$\mathbf{\Lambda}(\underline{\sigma}, d\underline{\epsilon}) = \sum_{i=1}^{N} \psi_i \, \mathbf{\Lambda}_i(\underline{\sigma}_i, d\underline{\epsilon}) \tag{5.66a}$$

and

$$\mathbf{C}^p(\underline{\sigma}, d\underline{\epsilon}) \equiv \mathbf{C}^e \mathbf{\Lambda}(\underline{\sigma}, d\underline{\epsilon}) = \sum_{i=1}^{N} \psi_i \, \mathbf{C}_i^p(\underline{\sigma}_i, d\underline{\epsilon}), \tag{5.66b}$$

where $\mathbf{\Lambda}_i$ and $\mathbf{C}_i^p$ are matrices associated with each of the elements in the DEM. From the result of Theorem 3, it follows that $\mathbf{C}_i^p, \forall\ i = 1, \ldots, N$, are symmetric and positive semi-definite, and so therefore is $\mathbf{C}^p$. Also, as in the proof of Theorem 4, we can show that all the eigenvalues of $\mathbf{\Lambda}$ are non-negative. In addition, since each element in the DEM has the behavior of ideal plasticity, we have $Tr(\mathbf{\Lambda}_i) = 0$ or 1, depending on whether the element state is elastic or yielded, and then by Eqn. (5.66a)

$$0 \ \leq \ Tr(\mathbf{\Lambda}) \ = \ \sum_{i=1}^{N} \psi_i \, Tr(\mathbf{\Lambda}_i) \ \leq \ \sum_{i=1}^{N} \psi_i \ = \ 1.$$

In order to develop a mathematically rigorous theory on the properties of the DEM, we make the following definition regarding the "state of equilibrium":

[Definition 1]: An "equilibrium point (state)" is a response state associated with a uni-directional strain path $d\underline{\epsilon} = \underline{c}\, dt$, with $\underline{c} \neq 0$ and $dt > 0$, at which

$$d\underline{\sigma} = \mathbf{C}^e[\mathbf{I} - \mathbf{\Lambda}(\underline{\sigma}, \underline{\epsilon}, d\underline{\sigma}, d\underline{\epsilon})]\, d\underline{\epsilon} = \underline{0}, \tag{5.67}$$

i.e.,

$$[\mathbf{I} - \mathbf{\Lambda}(\underline{\sigma}, \underline{\epsilon}, \underline{0}, \underline{c})]\, \underline{c} = 0, \tag{5.68}$$

where the dependence of $\mathbf{\Lambda}$ on dt is dropped since we are mainly concerned with rate-independent plasticity in this research.

The uni-directional strain path that defines an equilibrium point is referred to as the *reference path* associated with that equilibrium point. From (5.68), the reference path is an eigenvector with eigenvalue unity corresponding to Λ evaluated at the equilibrium state. The term "equilibrium point (state)" was used because if we consider the following system

$$\frac{d\underline{\sigma}}{dt} = \mathbf{C}^e[\mathbf{I} - \mathbf{\Lambda}(\underline{\sigma}, \underline{\epsilon}, \underline{0}, \underline{c})]\, \underline{c} \equiv \underline{f}(\underline{\sigma}, \underline{\epsilon}, \underline{c}) \tag{5.69}$$

with $d\underline{\epsilon} = \underline{c}\, dt \neq 0$, we get that the state $(\underline{\sigma}^{\underline{c}}_{\underline{eq}}, \underline{\epsilon}^{\underline{c}}_{\underline{eq}})$, at which

$$\frac{d\underline{\sigma}^{\underline{c}}_{\underline{eq}}}{dt} = \underline{f}(\underline{\sigma}^{\underline{c}}_{\underline{eq}}, \underline{\epsilon}^{\underline{c}}_{\underline{eq}}, \underline{c}) = \underline{0}, \tag{5.70}$$

is an equilibrium point of the system described by the ordinary differential equation (5.69).

One important property associated with equilibrium states follows from the definition and can be stated as follows.

[Theorem 6]: At an equilibrium state for a DEM (or a classical plasticity model), the plastic modulus reduction matrix $\mathbf{\Lambda}$ is of rank one, and the only nonzero eigenvalue of $\mathbf{\Lambda}$ has a value of one.

[Proof]: By Eqn. (5.68), we know that the matrix $\mathbf{I} - \mathbf{\Lambda}(\underline{\sigma}, \underline{\epsilon}, \underline{0}, \underline{c})$ must be singular at an equilibrium state associated with the reference path $\underline{c}$, so that $\mathbf{\Lambda}$ has an eigenvalue of 1. As a consequence, we may conclude that the matrix $\mathbf{\Lambda}(\underline{\sigma}^{\underline{c}}_{\underline{eq}}, \underline{\epsilon}^{\underline{c}}_{\underline{eq}}, \underline{0}, \underline{c})$ must have 5 zero eigenvalues and an eigenvalue of 1 (Theorem 5), regardless of what $\underline{c}$ might be. This concludes the proof.

The physical significance of this property is that strain hardening effect must vanish as an equilibrium state is approached. This can be deduced from the result of Theorem 4. Furthermore, Theorem 6 implies the following corollary.

[Corollary]: Purely plastic deformation at a state of a DEM occurs only in a one-dimensional subspace of the 6-dimensional strain-increment space if and only if the state is an equilibrium point.

This property of the DEM is different from those of the models based on the classical theory of plasticity, by which purely plastic deformation always occurs in a one-dimensional subspace due to the use of the principle of normality.

We remark that at an equilibrium state (for any plasticity model) corresponding to some reference path $\underline{c}$, the work done over any strain loading increment $d\underline{\epsilon} = \underline{c}\,dt$ must be zero, since $d\underline{\sigma}$ is identically zero. This remark, which seems trivial, turns out to be useful later in deriving the properties associated with the DEMs.

It should be noted that although an equilibrium point is defined to be associated with a uni-directional strain path, a strain cycle which is sufficient smooth and long may also have particular equilibrium points associated with itself, as mentioned earlier in the description of the property of erasure-of-memory. This situation is illustrated in Figures 5.14(a) and (b), where the ellipse in the $\epsilon - \gamma$ strain space denotes the prescribed strain cycle with discrete increments, and the corresponding stress response calculated for a DEM shows two equilibrium points on the ellipse in the $\sigma - \tau$ stress space with the densest stress increments around them. A big smooth strain cycle is needed to get the stress response on the limit surface, then whenever a strain increment matches the direction of the normal to the limit surface at the current stress point, an equilibrium state is reached.

Two important issues pertaining to the equilibrium points are the existence and uniqueness of an equilibrium point given a specified reference path. Mathematically, it is difficult to show directly the existence of an equilibrium state considering the rather complicated formulation of plasticity involved. Instead, we use some simple energy arguments to solve the problem, as presented in the following theorem.

[Theorem 7]: For stable materials which have bounded elastic strain energy, given a specified uni-directional strain path, a corresponding equilibrium point always exists.

[Proof]: Define the elastic strain energy of a system as

$$W^e \equiv \frac{1}{2}\epsilon^e_{ij}\, C^e_{ijkl}\, \epsilon^e_{kl} = \frac{1}{2}(\underline{\epsilon}^e)^T \mathbf{C}^e \underline{\epsilon}^e.$$

By assumption, W^e is bounded so that the elastic strain response ϵ^e_{ij} is also bounded. Along a uni-directional strain loading path $\underline{\epsilon} = \underline{c}\, t \neq \underline{0}$, where, by definition t is monotonically increasing ($dt > 0$), the elastic strain energy would never decrease after a certain state at, say, $t = t_i$. Thus, it requires for all $t > t_i$

$$dW^e \approx \epsilon^e_{ij}\, C^e_{ijkl}\, d\epsilon^e_{kl} = (\underline{\epsilon}^e)^T \mathbf{C}^e d\underline{\epsilon}^e \geq 0. \tag{5.71}$$

For bounded elastic strain energy we must have $dW^e(t) \to 0$, as $t \to t_0$, where t_0 corresponds to some state at which $dW^e(t) = 0$, possibly $t_0 = \infty$. By (5.71), we must have*

$$d\epsilon^e_{kl}(t_0) = 0,$$

i.e.,

$$d\sigma_{ij}(t_0) = C^e_{ijkl}\, d\epsilon^e_{kl}(t_0) = 0, \quad \forall\ i, j.$$

Thus, following from the definition of an equilibrium point, as in Eqn. (5.67), existence of the equilibrium state associated with a reference path $\underline{\epsilon} = \underline{c}\, dt \neq \underline{0}$ is always guaranteed.

The issue of uniqueness of an equilibrium point associated with a reference path will be discussed later after we have introduced the concept of the limit surface and its associated properties.

5.3.3 Geometrical Considerations of Yield Surfaces for the New DEM

In defining the kinematics of an element in the DEM, we introduced a yield condition for characterizing the general multi-axial elasto-plastic behavior of the

* We can rule out the possibilty that $d\underline{\epsilon}^e$ becomes orthogonal to $\mathbf{C}^e\underline{\epsilon}^e$, since in (5.71), we have neglected the high-order terms, which never vanish unless $d\underline{\epsilon}^e = 0$.

element. The yield condition has been defined in the same sense as done in the classical theory of plasticity. In other words, the yield condition for a given material is essentially the extension of a single yield point in the uniaxial (or one-dimensional) case to a hypersurface in the six-dimensional stress space (considering the symmetry of stress tensors). Since the DEM consists only of ideal plasticity elements, we may concentrate on the corresponding formulation, so that a yield condition is simply described by

$$F(\sigma_{ij}(k), k) = 0, \tag{5.72}$$

where k represents a yield constant corresponding to some particular element. For isotropic materials, since rotating the axes does not affect the yielding behavior, we can choose the principal stress axes for defining the coordinate system so that Eqn. (5.72) may be rewritten as

$$F(\sigma_1(k), \sigma_2(k), \sigma_3(k), k) = 0. \tag{5.73}$$

In the $(\sigma_1, \sigma_2, \sigma_3)$ coordinate system, which represents a stress space sometimes referred to as the Haigh-Westergaard stress space, Eqn. (5.73) specifies a normal three-dimensional surface that one can easily picture. As discussed in many textbooks of plasticity, e.g., [26, 34], the yield locus that a yield surface intersects with the π plane, a plane passing through the origin and perpendicular to the hydrostatic axis for which $\sigma_1 = \sigma_2 = \sigma_3$, must be symmetric in the principal stresses. If one further assumes equal yielding in tension and compression, then the yield locus can be divided into twelve symmetric sectors, each of 30 degrees. In the following, we will formulate some important properties related to the yield surfaces of a DEM based on some basic principles in operator theory.

Recall that we defined a DEM as consisting of a collection of elasto-perfectly-plastic elements whose yield surfaces are nested within one another and are governed by yield functions of the same mathematical form so that the yield surfaces may have similar shapes. To make it clearer, we introduce the following definition.

[**Definition 2**]: Two hypersurfaces $S_1 : F(\underline{\sigma}, k_1) = 0$ and $S_2 : F(\underline{\sigma}, k_2) = 0$ are said to be *similar* (in shape) with dimension ratio k_1/k_2, if any ray from the origin that passes through S_1 at $\underline{\sigma}_1$ intersects S_2 at $\underline{\sigma}_2$ such that

$$k_2\, \underline{\sigma}_1 = k_1\, \underline{\sigma}_2.$$

Mathematically, if the dimension ratio of two similar surfaces S_2 and S_1 is $c > 0$, then by definition we have

$$F(\underline{\sigma}_0, k_0) = 0 \iff F(c\underline{\sigma}_0, ck_0) = 0. \tag{5.74}$$

Thus, we have the following theorem regarding the condition for similar surfaces.

[Theorem 8]: A set of yield surfaces S defined by $S = \{\underline{\sigma} : F(\underline{\sigma}, ck_0) = 0, c > 0\}$ are all similar with dimensions proportional to c, if the yield function $F(\cdot, \cdot)$ is homogeneous (of any order).

[Proof]: If $F(\cdot, \cdot)$ is homogeneous of some order, say m, and

$$F(\underline{\sigma}_0, k_0) = 0, \tag{i}$$

then

$$F(c\underline{\sigma}_0, ck_0) = c^m F(\underline{\sigma}_0, k_0) = 0 \quad \forall c > 0. \tag{ii}$$

By (5.74) we may conclude that all surfaces are similar with dimensions proportional to c.

Based on the above result we now assume that the yield function used to define the yield surfaces of a DEM is homogeneous so that the nested yield surfaces are all similar in shape with dimensions proportional to the yield constants k's. Thus, the domain of elasticity, Ω_i, in the element stress space for an element with yield constant k_i, defined by

$$\Omega_i = \{\underline{\sigma}_i : F(\underline{\sigma}_i, k_i) < 0\}, \tag{5.75}$$

can be expressed as

$$\Omega_i = k_i \, \Omega_0, \qquad k_0 = 1, \tag{5.76}$$

or

$$\Omega_i = \{k_i \, \underline{\sigma}_0^{(i)} : \underline{\sigma}_0^{(i)} \in \Omega_0\}, \tag{5.77}$$

where Ω_0 is the domain of elasticity of some element with yield constant $k_0 = 1$, and it is assumed to be a bounded, convex set. The boundedness follows from the fact that any real material has finite ultimate strength (peak stress), and the convexity

follows from the well-known result that a yield surface is convex if Drucker's postulates hold [12, 34]. Since the model response of a DEM can be written as (using the formulation of a finite number of elements):

$$\underline{\sigma} = \sum_{i=1}^{N} \psi_i \, \underline{\sigma}_i, \tag{5.78}$$

where N is the total number of elements and

$$\sum_{i=1}^{N} \psi_i = 1, \quad \psi_i \geq 0, \tag{5.79}$$

by operator theory on convex sets [27], the set of all model stress points, denoted as the domain Ω, is given by

$$\Omega = \sum_{i=1}^{N} (\psi_i \, \Omega_i) = \sum_{i=1}^{N} (\psi_i \, k_i \, \Omega_0) = \Big(\sum_{i=1}^{N} \psi_i \, k_i \Big) \Omega_0 \quad \text{(since } \Omega_0 \text{ is convex and } k_i \, \psi_i > 0\text{)}$$

$$= k_u \, \Omega_0 \qquad (k_u \equiv \sum_{i=1}^{N} \psi_i \, k_i). \tag{5.80}$$

In the derivation we used some fundamental theorems in operator theory on convex sets. The relevant theory is summarized in Appendix A. By (5.80), the existence of Ω is guaranteed as long as $k_u < \infty$ in the case where $N \to \infty$, which may again be thought of as a condition of finite ultimate strength for any real materials. Furthermore, we may conclude that Ω is similar in shape to Ω_0. Thus, the boundary of Ω, $\partial\Omega$, defines a limit surface of a DEM, which can be described by

$$F(\underline{\sigma}, k_u) = 0, \tag{5.81}$$

such that a model stress state can never go beyond the limit surface associated with the model. This proves the following theorem specifying an important property of the DEM:

[**Theorem 9**]: There exists a limit surface associated with a DEM, described by

$$F(\underline{\sigma}, k_u) = 0,$$

where $k_u \equiv \sum_{i=1}^{N} \psi_i \, k_i$, and $k_i, i = 1, \ldots, N$, are the yield constants of the N elements constituting the model. The limit surface is similar in shape to the yield surfaces associated with each of the distributed elements.

In the following, we will derive some important properties related to the equilibrium points and the limit surface associated with a DEM. First of all, we note that, from Definition 1 and Theorem 6, at an equilibrium state corresponding to a reference path $d\underline{\epsilon} = \underline{c}\, dt$, the plastic-strain response increment will be the same as the prescribed strain increment, i.e.,

$$d\underline{\epsilon}^p(\underline{\sigma}^{\underline{c}}_{eq}) = \mathbf{\Lambda}(\underline{\sigma}^{\underline{c}}_{eq}, d\underline{\epsilon})\, d\underline{\epsilon} = d\underline{\epsilon} = \underline{c}\, dt.$$

Thus, we have the following theorem pertaining to the equilibrium states of a DEM.

[Theorem 10]: At an equilibrium state of a DEM, all elements in the model are in corresponding equilibrium states, which lie on the associated yield surfaces at points having the same outward normal direction as the reference strain path, and conversely (all elements in equilibrium states implies DEM in equilibrium state).

[Proof]: Converse is trivial since if each element is in an equilibrium state, we have $\forall\ i \quad d\underline{\sigma}_i = 0$ for $d\underline{\epsilon} = \underline{c}\, dt$, then $d\underline{\sigma} = \sum_{i=1}^{N} \psi_i \, d\underline{\sigma}_i = 0$.

Now, if a DEM is in an equilibrium state corresponding to a reference path $\underline{c}$, then the work done over any strain loading increment $d\underline{\epsilon} = \underline{c}\, dt$ must be zero, as we remarked earlier. Since the DEM actually consists of an assemblage of ideal plasticity elements that are subject to the same total strain increment, the sum of the work done by all the elements must also vanish. Thus, since the incremental work done by each individual element is non-negative (Drucker's postulate), we may conclude that

$$d\underline{\sigma}_i^T \, d\underline{\epsilon} = 0 \quad \forall\ i = 1, ..., N. \tag{5.82}$$

Also, by the assumption of ideal plasticity for each element, we have [34]

$$d\underline{\sigma}_i^T \, d\underline{\epsilon}_i^p = 0 \quad \forall\ i = 1, ..., N. \tag{5.83}$$

It follows from (5.82) and (5.83) that

$$d\underline{\sigma}_i^T \, d\underline{\epsilon}_i^e = (d\underline{\epsilon}_i^e)^T \, \mathbf{C}^e \, d\underline{\epsilon}_i^e = 0 \quad \forall\ i = 1, ..., N.$$

Since $\mathbf{C}^e$ is positive definite, we must have $d\underline{\epsilon}_i^e = \underline{0}\ \forall\ i$, and hence $d\underline{\sigma}_i = \underline{0}\ \forall\ i$, which shows that each element is in an equilibrium state corresponding to reference path $\underline{c}$. Furthermore, each $d\underline{\epsilon}_i^p = \underline{c}\,dt$, so by the principle of normality for each element, the outward normal at each element's equilibrium point is in the direction of $\underline{c}$.

[Theorem 11]: If all the element stress states of a DEM lie on the associated yield surfaces and line up in the stress space on a ray from the origin, then the stress state of the DEM is on the associated limit surface.

[Proof]: Firstly, we note that each yield surface associated with an element is the boundary, $\partial\Omega_i$, of the domain of elasticity Ω_i of that element, i.e.,

$$\partial\Omega_i = \{\underline{\sigma}_i : F(\underline{\sigma}_i, k_i) = 0\}. \tag{5.84}$$

From Eqn. (5.76), we have

$$\partial\Omega_i = k_i(\partial\Omega_0), \tag{5.85}$$

that is, each yield surface is described by

$$\partial\Omega_i = \{k_i\,\underline{\sigma}_0 : \underline{\sigma}_0 \in \partial\Omega_0\}. \tag{5.86}$$

Also, from Theorem 9, the limit surface is the set given by

$$\partial\Omega = \{k_u\,\underline{\sigma}_0 : \underline{\sigma}_0 \in \partial\Omega_0\}. \tag{5.87}$$

Thus, if all the element stress states of a DEM lie on the associated yield surfaces and line up in the stress space on a ray from the origin, then the element stress states must be proportional to one another with proportionality constants of yield strengths, i.e.,

$$\underline{\sigma}_i = k_i\underline{\sigma}_0, \qquad (\text{for some } \underline{\sigma}_0 \in \partial\Omega_0)$$

and hence we have

$$\begin{aligned}\underline{\sigma} \equiv \sum_{i=1}^{N} \psi_i\,\underline{\sigma}_i &= \sum_{i=1}^{N} \psi_i(k_i\,\underline{\sigma}_0) \\ &= \Big(\sum_{i=1}^{N} k_i\,\psi_i\Big)\underline{\sigma}_0 = k_u\,\underline{\sigma}_0.\end{aligned}$$

From Eqn. (5.87), the conclusion of the theorem follows.

It is of great importance to note that the limit surface to a DEM is like the yield surface to a model of ideal plasticity as far as the plastic behavior is concerned. This can be deduced from the following important theorem which relates the equilibrium points to the limit surface of a DEM.

[Theorem 12]: If the admissible stress region bounded by the limit surface is convex†, then the limit surface associated with a DEM is the set of all the equilibrium points corresponding to all possible reference paths.

[Proof]: It is equivalent to showing that a stress state of a DEM is an equilibrium state if and only if it lies on the limit surface, which is convex, of the model.
Sufficiency: If $\underline{\sigma}$ is a stress state of a DEM on the limit surface, then from Eqn. (5.87)

$$\underline{\sigma} = k_u \, \underline{\sigma}_0 \quad (\text{for some } \underline{\sigma}_0 \in \partial\Omega_0). \tag{i}$$

Also, by definition, we have

$$\underline{\sigma} = \sum_{i=1}^{N} \psi_i \, \underline{\sigma}_i = \sum_{i=1}^{N} \psi_i \, k_i \, \underline{\sigma}_0^{(i)} \qquad (\underline{\sigma}_0^{(i)} \in \Omega_0 \;\; \forall \; i = 1, ..., N). \tag{ii}$$

If we rotate the coordinate axes so that the x_1 axis in the stress space is perpendicular to the tangent plane to the yield surface $\partial\Omega_0$ at the point $\underline{\sigma}_0$, as shown in Fig. 5.15, and define the x_1 coordinate of $\underline{\sigma}_0$, $(\underline{\sigma}_0)_1$, to be $\alpha, \alpha > 0$, then from (i)

$$(\underline{\sigma})_1 = k_u \, (\underline{\sigma}_0)_1 = \alpha \, k_u = \alpha \sum_{i=1}^{N} k_i \, \psi_i. \tag{iii}$$

Since each yield surface is convex and so the region Ω_0 lies completely on one side of any tangent plane of $\partial\Omega_0$, we can deduce

$$(\underline{\sigma}_0^{(i)})_1 \leq \alpha. \tag{iv}$$

† This is equivalent to the earlier assumption that Ω_0 is convex, which is actually a consequence of Drucker's postulates.

It follows from $(ii), (iii), (iv)$ that

$$(\underline{\sigma}_0^{(i)})_1 = \alpha = (\underline{\sigma}_0)_1, \quad \forall\ i = 1, ..., N,$$

i.e., $\underline{\sigma}_0^{(i)}, \forall\ i = 1, ..., N$, lie on the tangent plane $x_1 = \alpha$. Thus, it follows from the shape similarity of the yield surfaces that all the element stress states are on the associated yield surfaces at the points having the same outward normal direction (perpendicular to the tangent plane). By the principle of normality for each element, the corresponding plastic strain increments of elements are all in the same direction, say $\underline{c}$, and so is the plastic strain increment of the DEM at $\underline{\sigma}$ (following from Eqn. (5.65)). This shows that the principle of normality holds for a state of the DEM on the limit surface. Now if the total strain increment prescribed is in the direction of $\underline{c}$, then the elastic strain increment at $\underline{\sigma}$ must be zero under loading condition (otherwise, the stress increment will point outward so that the stress state goes beyond the limit surface), and so therefore is the stress increment. Thus, by definition, the state $\underline{\sigma}$ must be an equilibrium point associated with the reference path $\underline{c}$.

Necessity: If $\underline{\sigma}$ is an equilibrium point corresponding to a reference path $\underline{c}$, then according to Theorem 10, every element state must lie on its associated yield surface at the point corresponding to the outward normal direction $\underline{c}$. Note that, however, without the assumption of *strict convexity*‡ of the yield surfaces, we cannot conclude that all element stress states are on a line from the origin (so that by Theorem 11, the model stress state is on the limit surface). Nevertheless, we can still argue as follows. Let R_i denote the subset on a yield surface of contant k_i, in which all points correspond to the same outward normal direction, i.e., R_i lies on a hyperplane in the stress space, which may be described by a linear function in $\underline{\sigma}_i$, so

$$R_i = \{\underline{\sigma}_i : \hat{F}(\underline{\sigma}_i) \equiv \sum_{j=1}^{6} a_j (\underline{\sigma}_i)_j = k_i \text{ and } F(\underline{\sigma}_i, k_i) = 0\}, \tag{5.88}$$

‡ A region Ω and its boundary $\partial\Omega$ are said to be strictly convex, if $\partial\Omega$ is convex and there are no two points on $\partial\Omega$ that have the same outward normal direction.

where j denotes the j-th component of a vector, so that the vector gradient $\nabla_{\underline{\sigma}}\hat{F}$ is a constant vector throughout the region R_i. Thus, it follows from Theorem 9 that the subset R on the limit surface, corresponding to R_i, can be described by

$$R = \{\underline{\sigma} : \hat{F}(\underline{\sigma}) = \sum_{j=1}^{6} a_j(\underline{\sigma})_j = k_u \text{ and } F(\underline{\sigma}, k_u) = 0\}. \tag{5.89}$$

From Eqn. (5.78), it follows that

$$\sum_{j=1}^{6} a_j(\underline{\sigma})_j = \sum_{j=1}^{6} a_j[\sum_{i=1}^{N} \psi_i(\underline{\sigma}_i)_j] = \sum_{i=1}^{N} \psi_i[\sum_{j=1}^{6} a_j(\underline{\sigma}_i)_j]. \tag{5.90}$$

Now if $\underline{\sigma}_i \in R_i$, then by Eqns. (5.88) and (5.90)

$$\sum_{j=1}^{6} a_j(\underline{\sigma})_j = \sum_{i=1}^{N} \psi_i \, k_i = k_u.$$

Following from (5.89), we conclude that $\underline{\sigma}$ lies in R, which is on the limit surface.

[Corollary]: The principle of normality holds for any state of a DEM on the limit surface.

The existence of equilibrium points has been assured by employing the concept of bounded elastic strain energy. Now we are in a position to address the problem of uniqueness of an equilibrium point associated with a reference strain path. This is given as the following theorem.

[Theorem 13]: An equilibrium point assocated with a reference strain path is uniquely defined (regardless of past response history) if and only if the admissible stress region bounded by the limit surface is *strictly* convex

The proof of Theorem 13 can be done simply by considering the schematic diagram shown in Figure 5.16, where the yield surfaces (and the associated limit surface) are not strictly convex. Given a uni-directional strain path following different previous histories, we may end up with different equilibrium points as points 1 and 2 shown in the figure. If, instead, the admissible stress region is strictly convex, then corresponding to a reference strain path, there is only one point on the limit surface that

has the outward normal in that direction. Thus, following the flow rule based on the principle of normality, the equilibrium point is uniquely defined.

With the theorems presented above, we may now investigate in detail the property of erasure-of-memory that is exhibited by real materials [30]. It may be deduced that the existence and uniqueness of equilibrium points associated with different reference paths are the necessary and sufficient conditions for a DEM to exhibit the property of erasure-of-memory, since then every time a "big" smooth strain cycle is prescribed, the system will be brought back to the particular equilibrium states associated with that strain cycle, regardless of what the previous history is. This leads to the following important theorem.

[**Theorem 14**]: A DEM possesses the property of erasure-of-memory if and only if its admissible stress region bounded by the associated limit surface is bounded and strictly convex, from which the existence and uniqueness of equilibrium points follow.

In summary, if the yield functions used in the definition of a DEM is homogeneous and *strictly quasi-convex** so that the limit surface exists and forms a strictly convex region, then the DEM can exhibit the property of erasure-of-memory. Actually, as can be deduced, the conditions stated in Theorem 14 serve as the general criteria for any plasticity model to demonstate the property of erasure-of-memory that real materials have. Furthermore, establishment of the above theorems provides us with clear insight into the elastic-plastic response mechanisms of real materials under complicated cyclic loading conditions, which surely helps further studies on the related subjects of general plasticity.

---

* Mathematically, it can be shown [12] that if a yield function is strictly quasi-convex, then the associated yield surface forms a strictly convex region. A scalar function $F(\underline{\sigma})$ is strictly quasi-convex at $\underline{\sigma}_1$ if

$$F(\underline{\sigma}_2) < F(\underline{\sigma}_1) \implies F(\underline{\sigma}) < F(\underline{\sigma}_1)$$

$$\forall\, \underline{\sigma} = \alpha\, \underline{\sigma}_1 + (1-\alpha)\, \underline{\sigma}_2, \quad 0 < \alpha < 1.$$

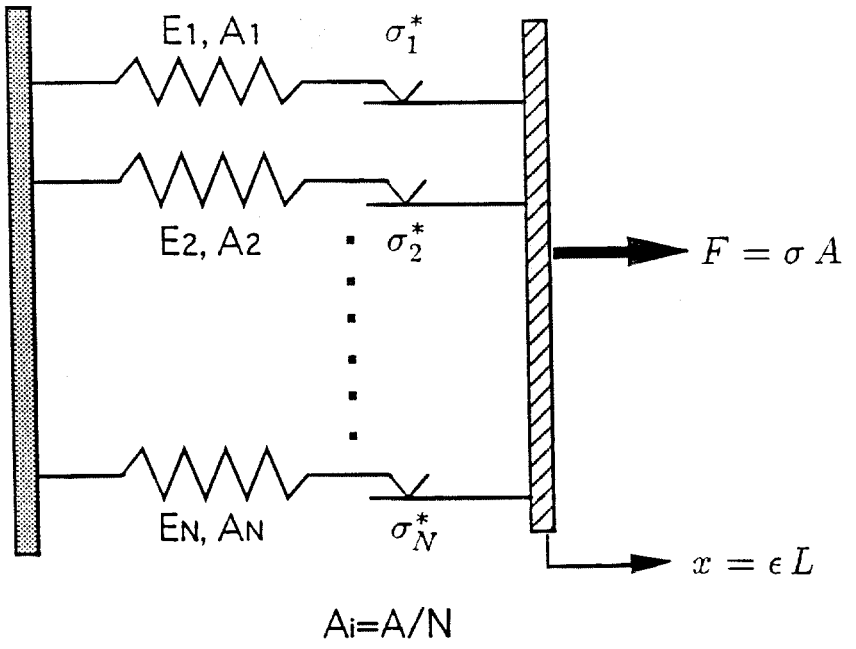

(a) Parallel-Series Model

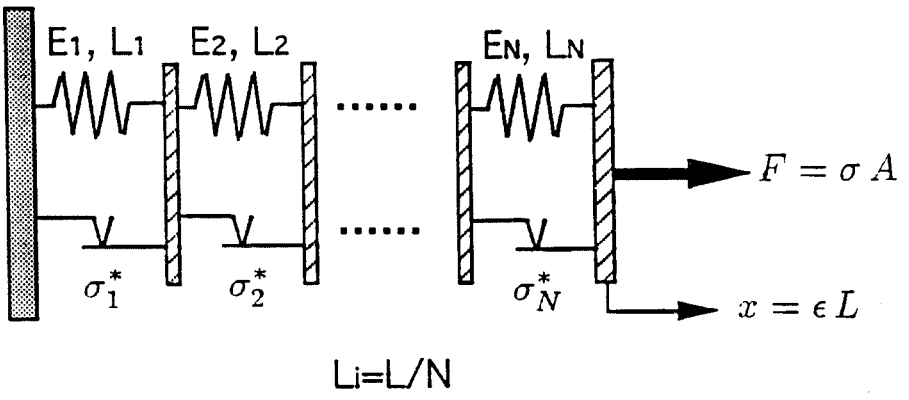

(b) Series-Parallel Model

Figure 5.1 Two different one-dimensional Distributed-Element Models

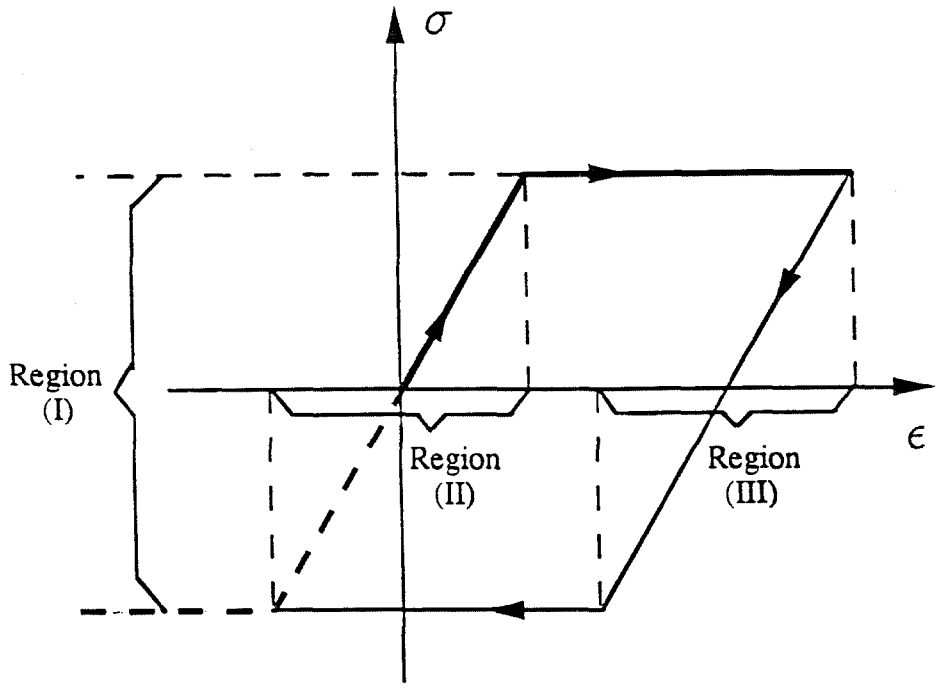

(I) Region enclosed by the invariant yield surface in the stress space

(II) Region enclosed by the initial yield surface in the strain space

(III) Region enclosed by the subsequent yield surface in the strain space

Figure 5.2 Illustration of the space-dependent yielding behavior of ideal plasticity

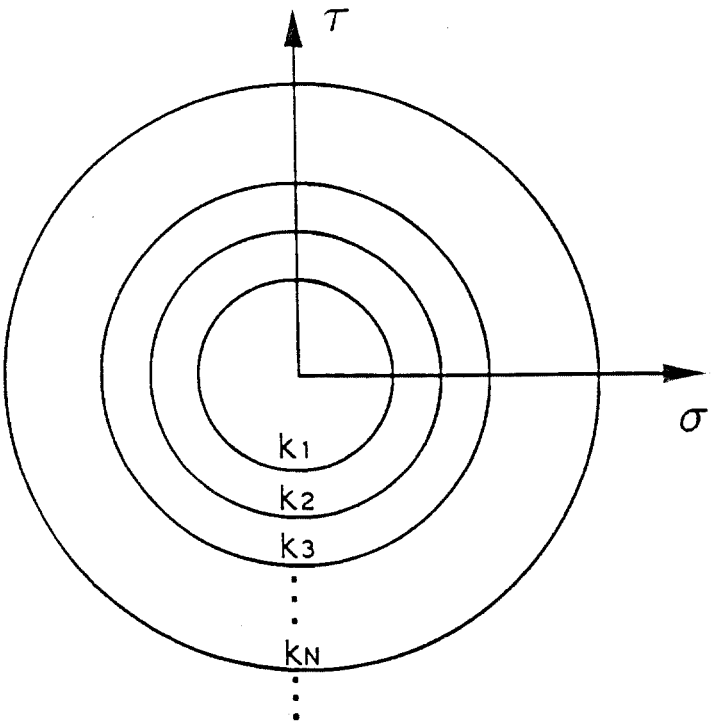

Figure 5.3 Invariant yield surfaces nested in the element stress space

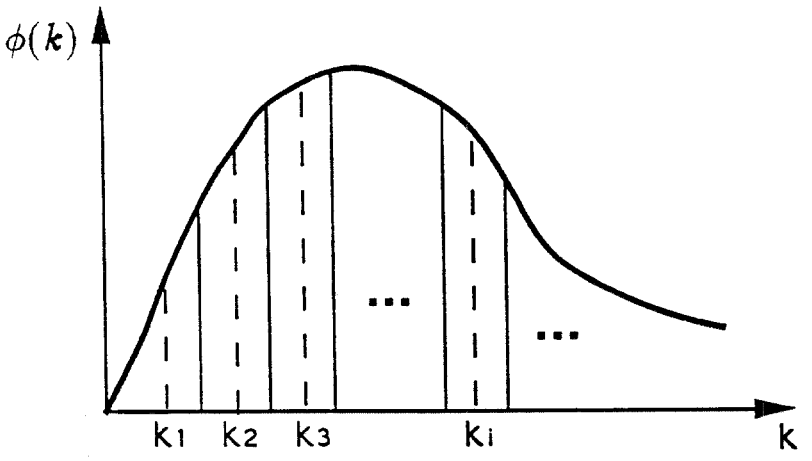

Figure 5.4 Selection of yield constants for a finite number of elements according to the specified strength distribution function

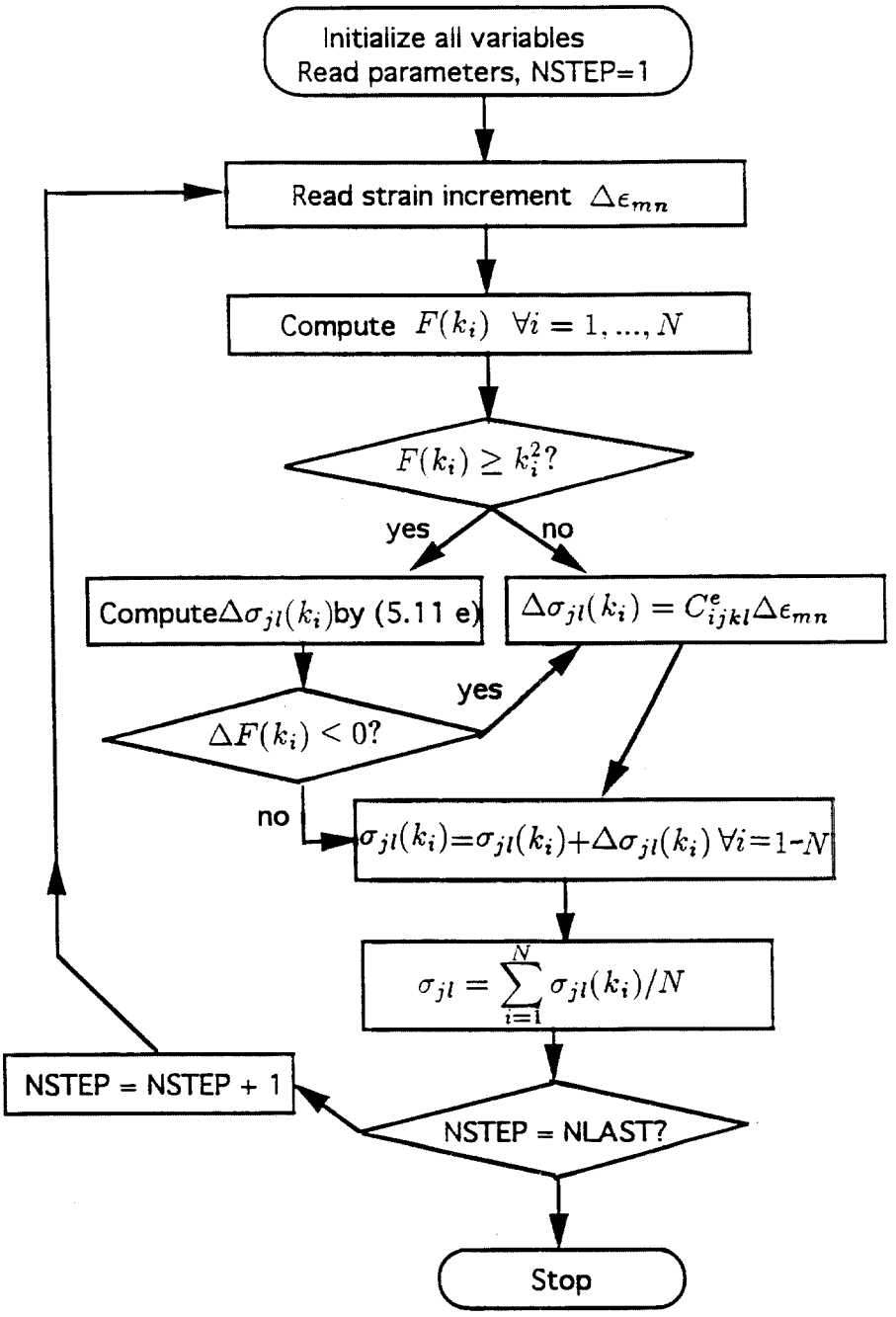

Figure 5.5 A flow diagram showing numerical procedure for obtaining stress response of an N-element DEM

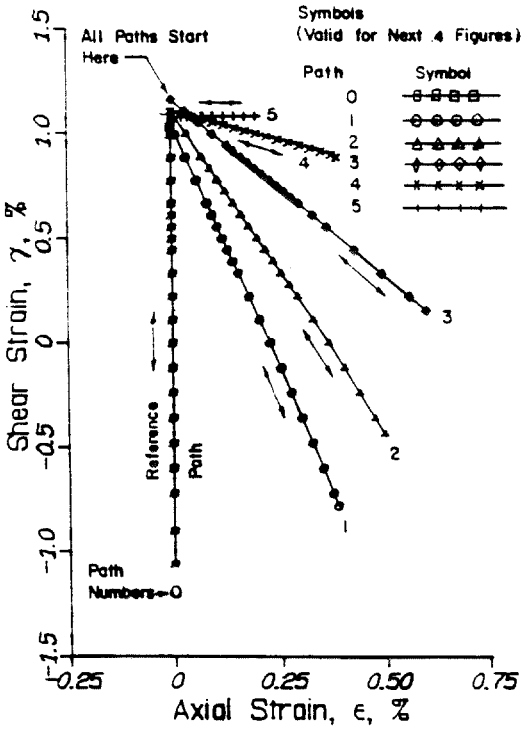

(a)

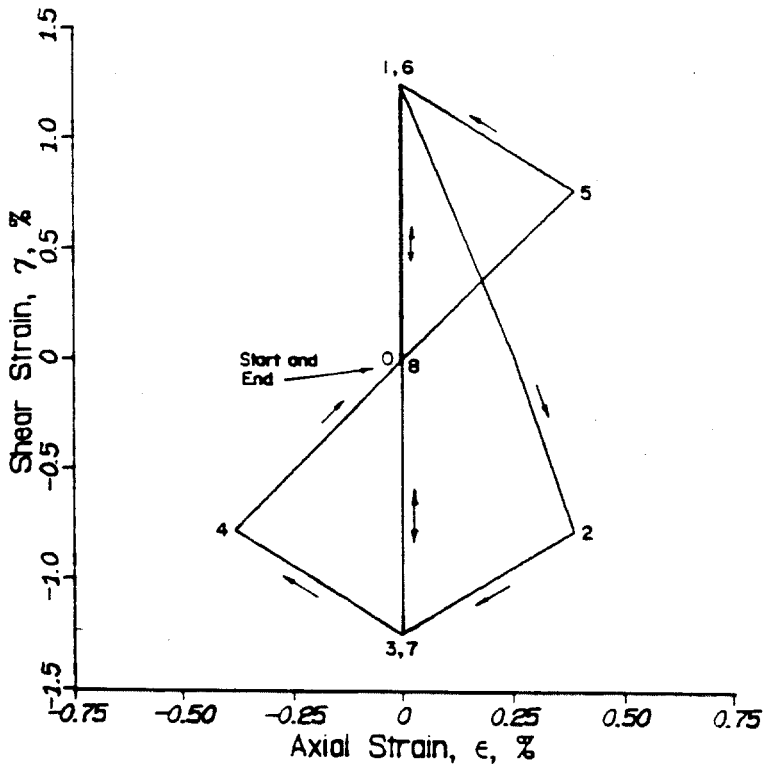

(b)

Figure 5.6 Prescribed strain loading paths for response studies of the proposed multi-dimensional DEMs (from [30])

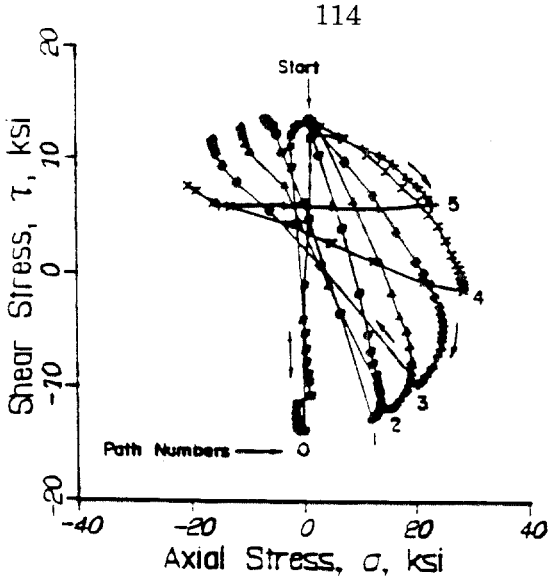

(a) biaxial stress space

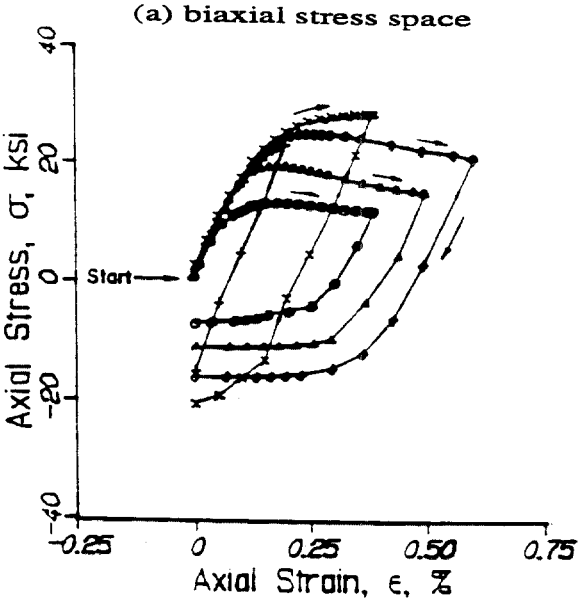

(b) axial stress-strain space

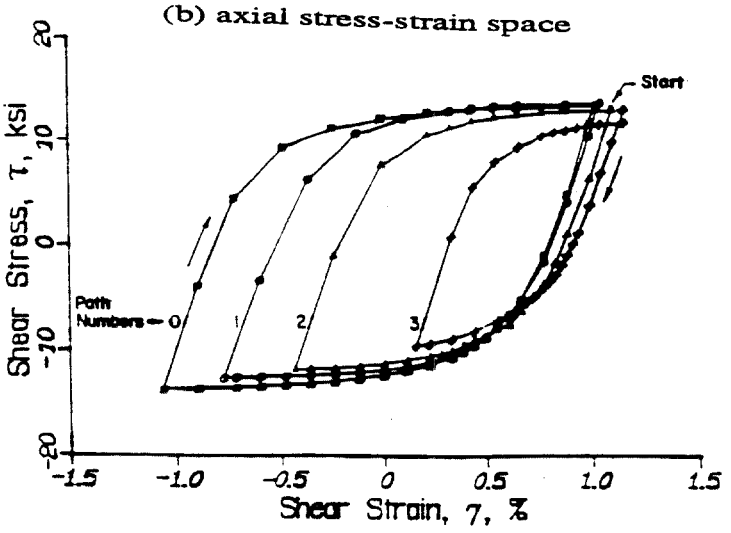

(c) shear stress-strain space

Figure 5.7 Experimentally-observed stress response of copper to the prescribed strain path given in Figure 5.6(a) (from [30])

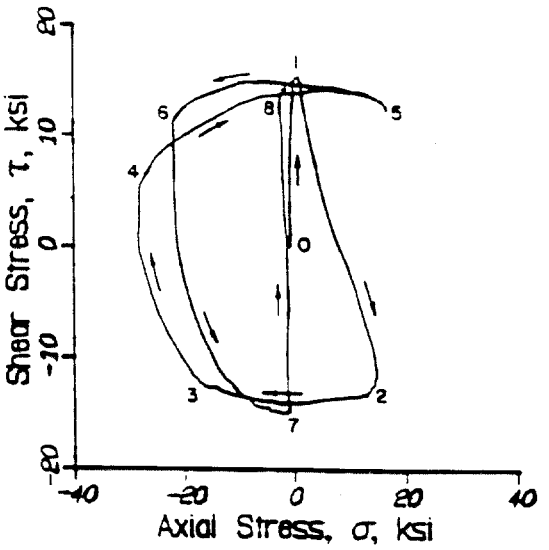

(a) biaxial stress space

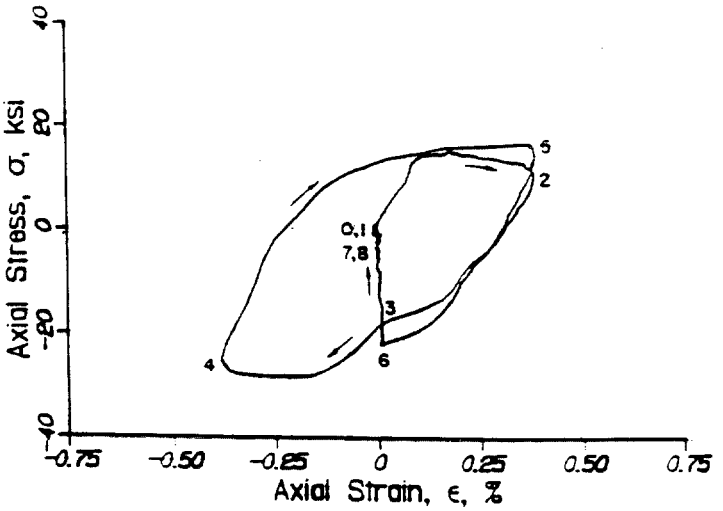

(b) axial stress-strain space

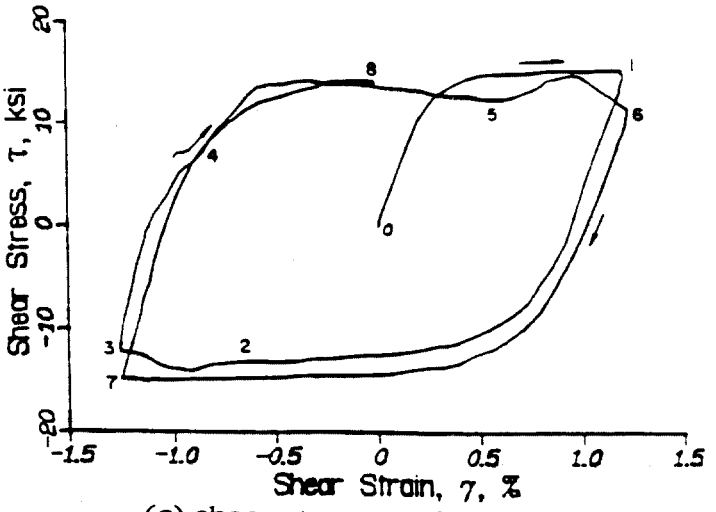

(c) shear stress-strain space

Figure 5.8 Experimentally-observed stress response of copper to the prescribed strain path given in Figure 5.6(b) (from [30])

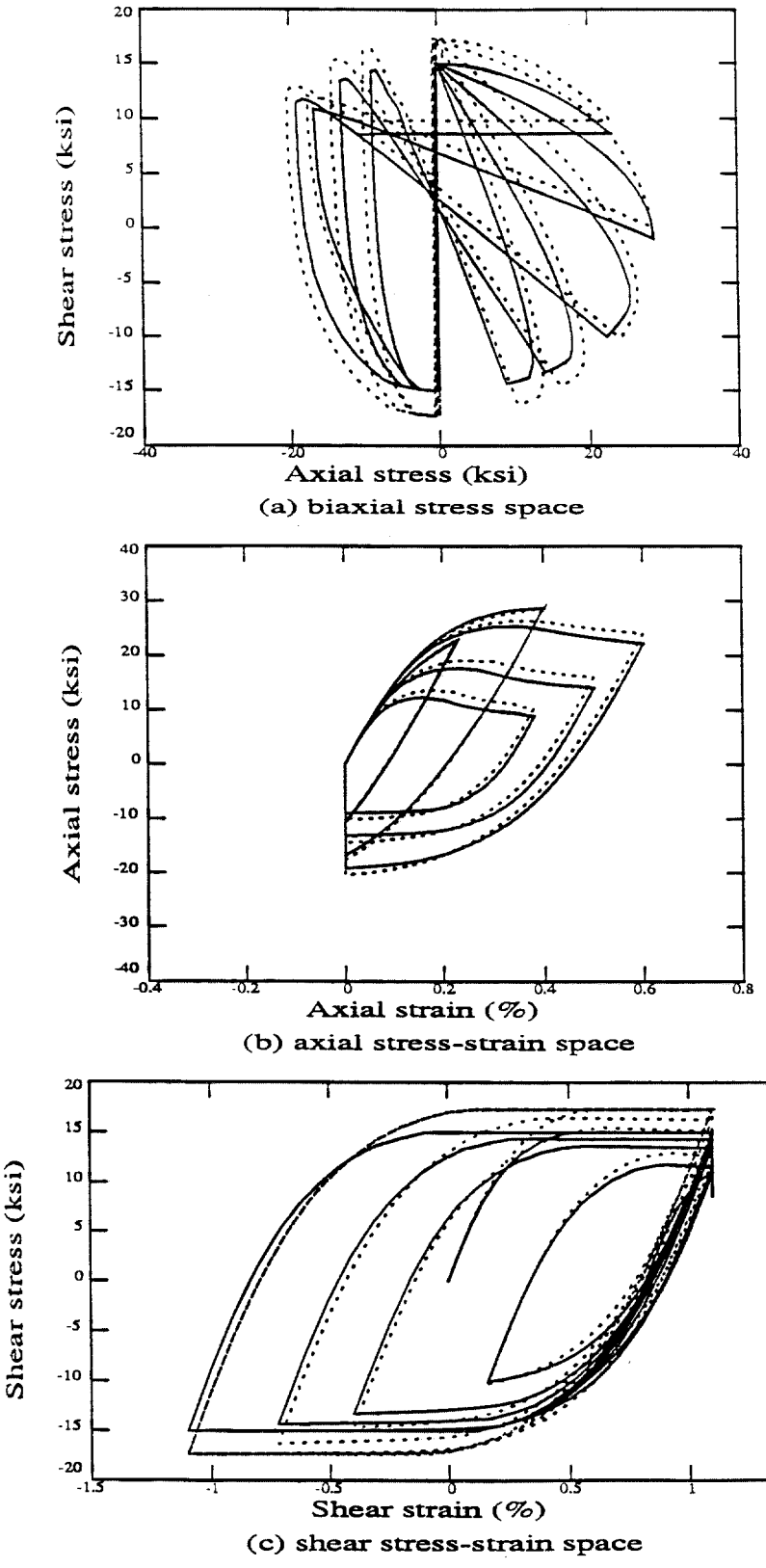

Figure 5.9 Stress response predicted by a new DEM subject to the prescribed strain path given in Figure 5.6(a) (Tresca ——— , von Mises - - - -)

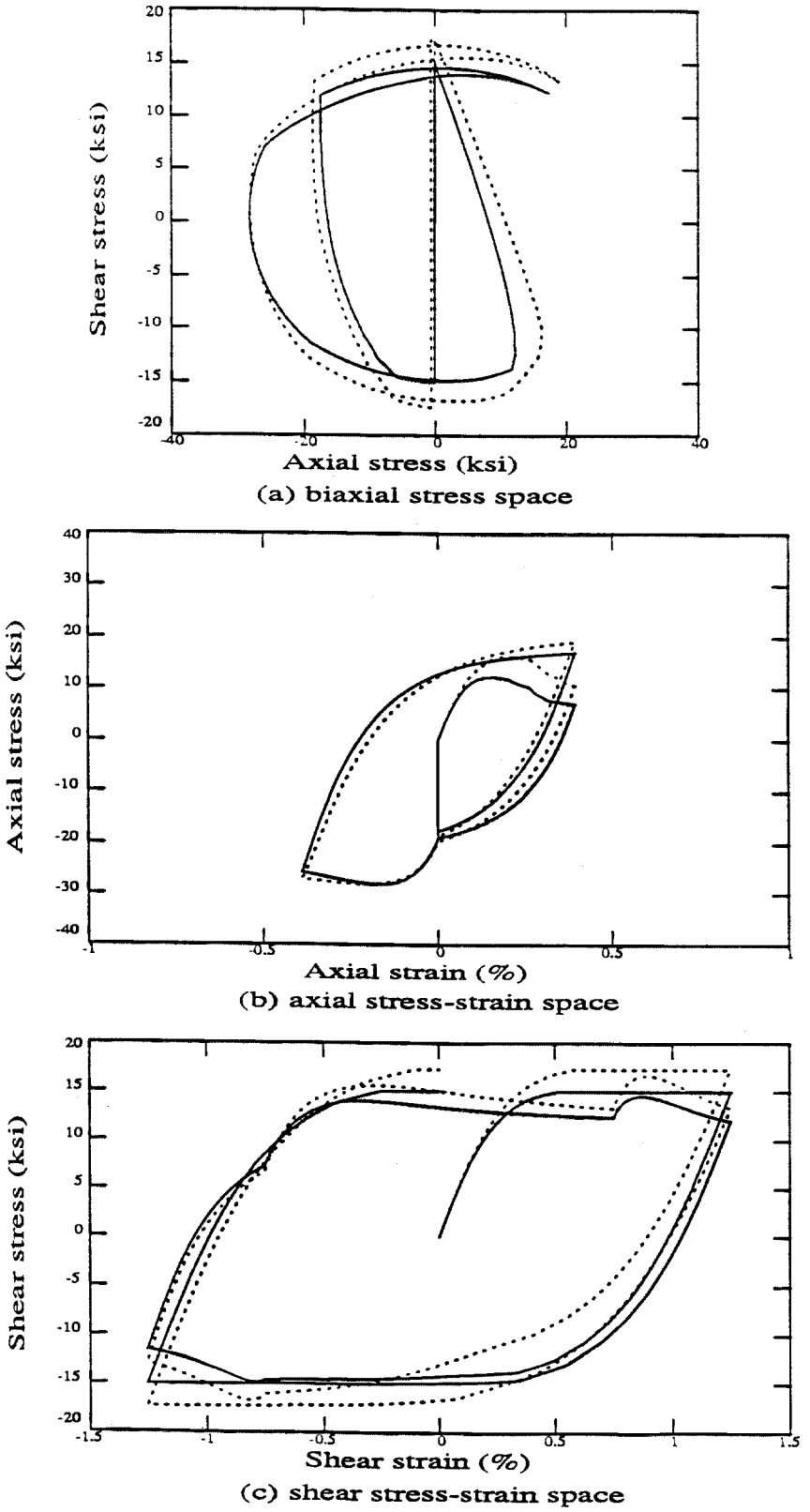

Figure 5.10 Stress response predicted by a new DEM subject to the prescribed strain path given in Figure 5.6(b) (Tresca ——— , von Mises - - - -)

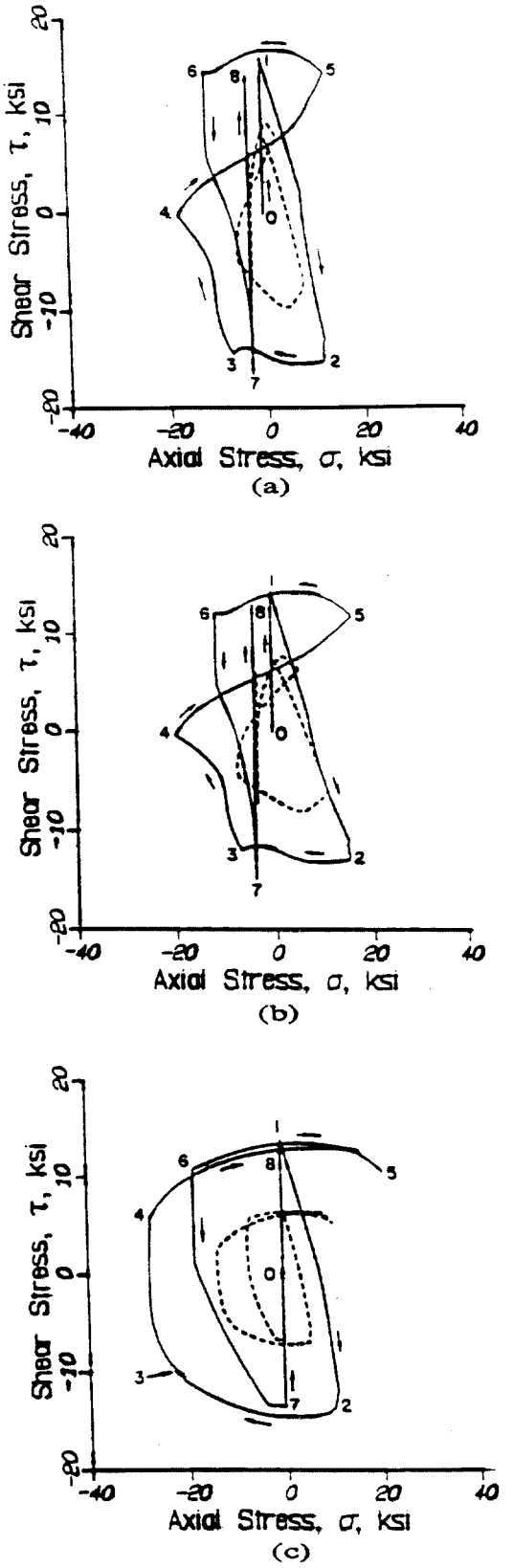

Figure 5.11 Response predicted by different models of plasticity to the strain path given in Figure 5.6(b): (a) von Mises' yield surface with Prager's hardening rule (b) Tresca's yield surface with Ziegler's hardening rule (c) Tresca's yield surface and limit surface with Mroz' hardening rule (from [30])

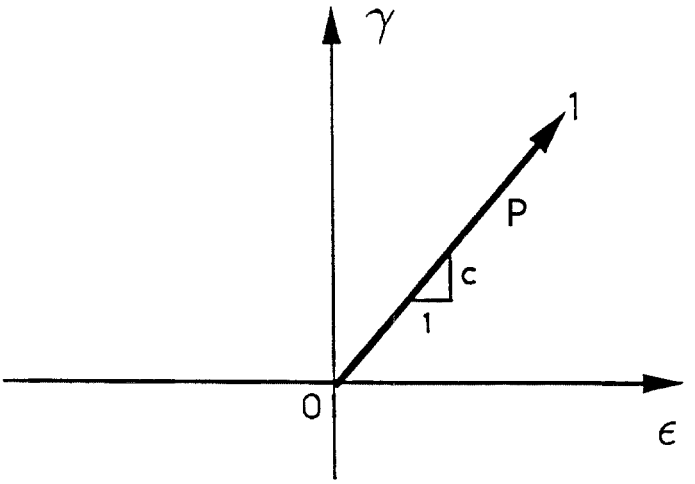

(a) proportional strain path

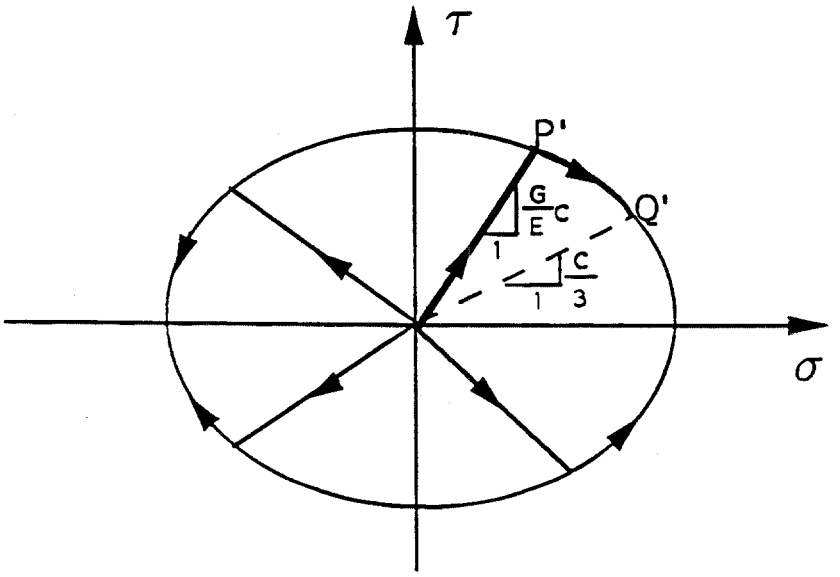

(b) stress response behavior

Figure 5.12 Response behavior of ideal plasticity under proportional strain loading path

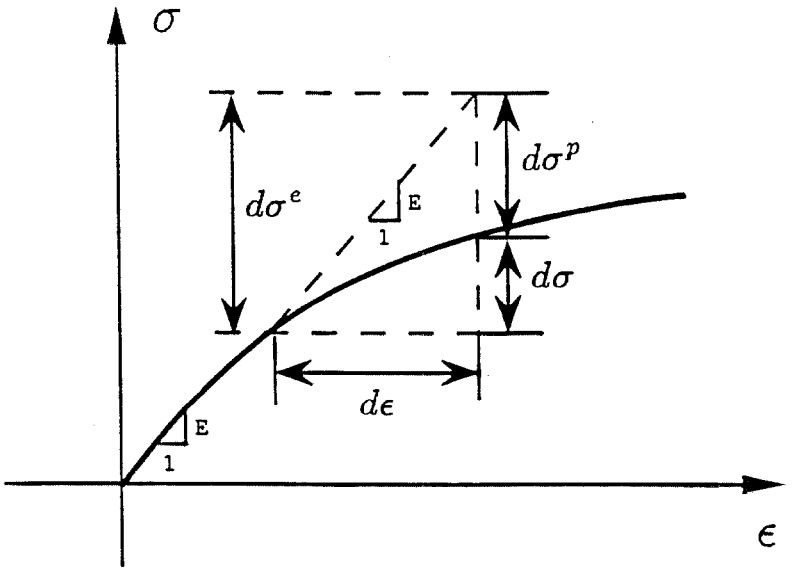

Figure 5.13 Definition of the plastic-relaxation stress increment in the uniaxial case

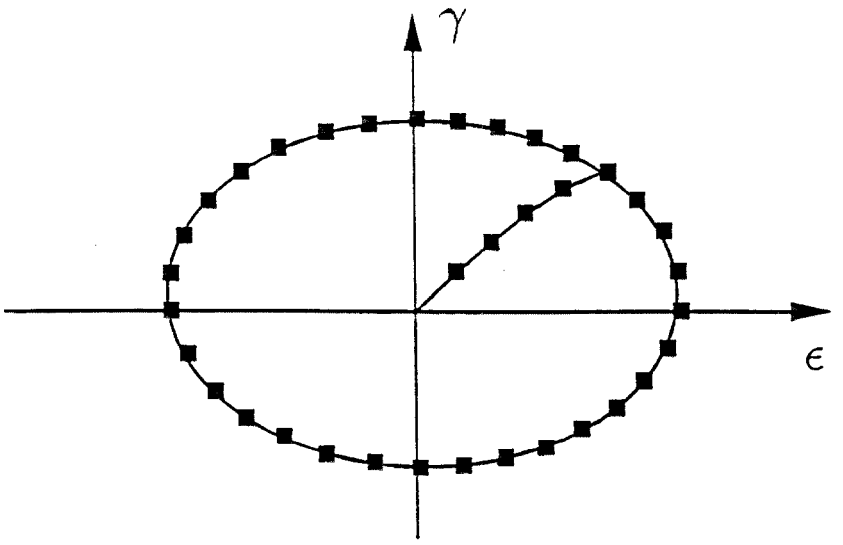

(a) a big strain cycle

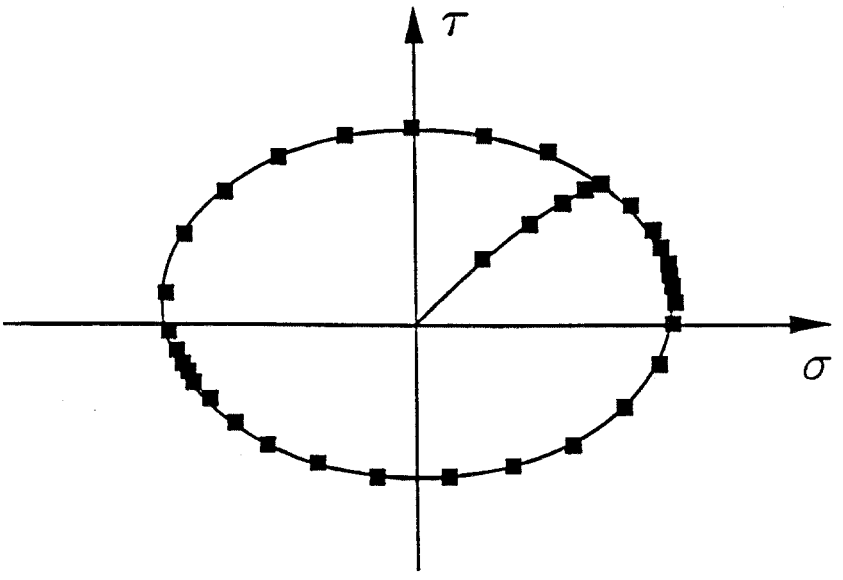

(b) the corresponding stress response

Figure 5.14 Illustration of existence of the equilibrium points associated with a big strain cycle

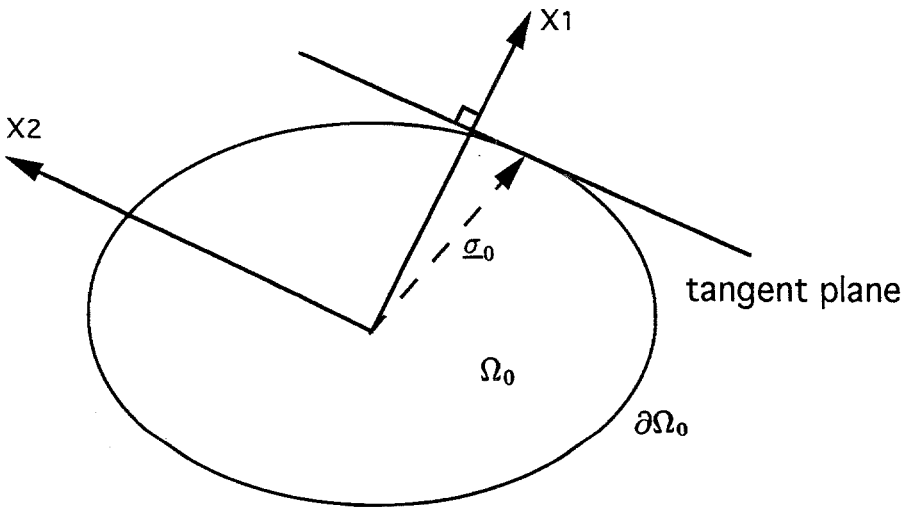

Figure 5.15 A diagram showing the rotation of coordinate axes which makes the x1 axis perpendicular to the tangent plane to the yield surface $\partial\Omega_0$ at $\underline{\sigma}_0$

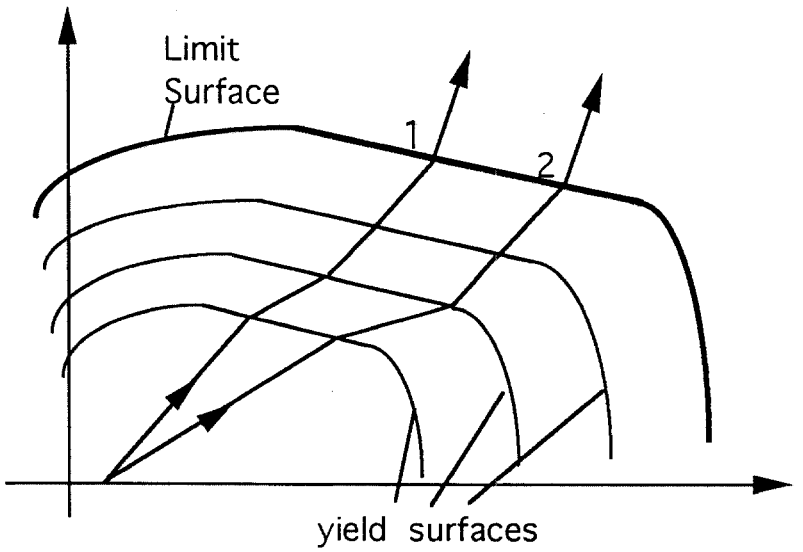

Figure 5.16 An illustrative diagram showing non-strict convexity of yield surfaces

CHAPTER 6

GENERALIZED MASING RULES FOR CYCLIC PLASTICITY

6.1 Introduction

In the previous chapter, we have extended the one-dimensional Distributed-Element Models (DEMs) to a multi-dimensional representation, so that they can be used for constitutive modeling within the context of general plasticity. While the formulation of the multi-dimensional DEMs provides a useful and realistic way for analysis of general multi-axial cyclic response behavior, efficient numerical implementation of the theoretical formulation requires that only a limited number of elements be introduced. Furthermore, the model response has to be found by keeping track of each element's behavior throughout the response history. Recall that in Chapters 3 and 4, we gave the extended Masing rules for response of one-dimensional DEMs with or without deterioration. As a result, the response of a DEM can be found without the need to trace each element's behavior. An interesting question can then be raised: can we possibly find some mathematical rules similar to those previously used in the one-dimensional Masing models so that general multi-axial response of the models based on the distributed-element formulation can be obtained without keeping track of each element's behavior. If such mathematical rules governing multi-axial cyclic response exist, then based on these rules we may be able to come up with numerical schemes that are more efficient and more accurate than those based on a finite number of distributed elements.

In the following sections, it will be shown that by introducing a response formula good for initial loading, further unloading and reloading response to a general loading can then be found by applying a composition of proper transformations to the state variables involved in the initial loading formula. This method can be shown to be conceptually equivalent to the classical multi-yield-surface theory using the Mroz kinematic hardening rule. However, the idea proposed here can actually work out the response of a model with a collection of an (uncountably) infinite number of yield surfaces and with proper kinematic hardening rules taken into account. Even though the proposed formulation based on the transformation rules is not exactly mathematically equivalent to that of the generalized three-dimensional DEM presented in the previous chapter, it still provides us with an alternative way of

obtaining complicated cyclic response in general plasticity. Furthermore, the transformation rules that govern the response behavior corresponding to different loading branches also give instructive insight into the physics of material behavior in cyclic plasticity.

6.2 Extension of 1-D Response Formulas to Higher Dimensions

In the one-dimensional case, there have been many response formulas or mathematical models proposed for describing nonlinear, hysteretic response behavior of structural or material systems, such as those presented in Chapters 3 and 4. The problem of extending such one-dimensional models to the much more involved multi-dimensional case has been a task of great challenge among researchers in the related fields, and very little success has been attained on this subject.

6.2.1 Two-Dimensional Bouc-Wen Model

The theory of plasticity provides the theoretical background for analyzing general multi-axial hysteretic response of mechanical and structural systems. However, such an entirely theoretical approach would be usually computationally impractical for studying structural systems. Park, Wen, and Ang [37] proposed a two-dimensional hysteretic model for random vibrations of structures subject to biaxial excitations, which is an extension to the well-known Bouc-Wen model introduced in Chapter 3. The one-dimensional non-deteriorating Bouc-Wen model, described by

$$\dot{r} = A\dot{u} - (\alpha|\dot{u}||r|^{n-1}r - \beta\dot{u}|r|^n), \tag{6.1}$$

was extended to the biaxial case so as to account for the interaction of the restoring forces in two different directions. It was proposed [37] that for structural systems with "isotropic" restoring force behavior, the forces r_x and r_y in the two directions are described by the following coupled differential equations:

$$\dot{r}_x = A\dot{x} - \alpha|\dot{x}r_x|r_x - \beta\dot{x}r_x^2 - \alpha|\dot{y}r_y|r_x - \beta\dot{y}r_xr_y, \tag{6.2}$$

$$\dot{r}_y = A\dot{y} - \alpha|\dot{y}r_y|r_y - \beta\dot{y}r_y^2 - \alpha|\dot{x}r_x|r_y - \beta\dot{x}r_xr_y, \tag{6.3}$$

where $\dot{x}$ and $\dot{y}$ are the velocities in the x and y directions respectively. The hysteretic behavior given by Eqns. (6.2) and (6.3) can be illustrated by considering a simple uni-directional displacement path for which it is assumed that

$$r_x = r\cos\theta, \quad r_y = r\sin\theta, \quad x = u\cos\theta, \quad y = u\sin\theta, \tag{6.4}$$

where r and u are, respectively, the uni-directional force and displacement, and θ is held constant on loading or unloading. Substituting (6.4) into Eqns. (6.2) and (6.3) we can show that each of (6.2) and (6.3) reduces to Eqn. (6.1) with $n = 2$. This illustrative situation is sketched in Fig. 6.1 for easier understanding. Note that the ultimate strength r_u of the one-dimensional model with $n = 2$ can be found to be

$$r_u = \sqrt{\frac{A}{\alpha+\beta}}, \tag{6.5}$$

which may serve as a guideline for choosing the model parameters.

For an orthotropic system, whose stiffness and strength in two orthogonal directions are different (A_x vs. A_y, $(r_x)_u$ vs. $(r_y)_u$), Eqns. (6.2) and (6.3) can be replaced by

$$\dot{r}_x = A_x\dot{x} - \alpha\frac{A_x}{(r_x)_u^2}|\dot{x}r_x|r_x - \beta\frac{A_x}{(r_x)_u^2}\dot{x}r_x^2 - \alpha\frac{A_y}{(r_y)_u^2}|\dot{y}r_y|r_x - \beta\frac{A_y}{(r_y)_u^2}\dot{y}r_xr_y, \tag{6.6}$$

$$\dot{r}_y = A_y\dot{y} - \alpha\frac{A_y}{(r_y)_u^2}|\dot{y}r_y|r_y - \beta\frac{A_y}{(r_y)_u^2}\dot{y}r_y^2 - \alpha\frac{A_x}{(r_x)_u^2}|\dot{x}r_x|r_y - \beta\frac{A_x}{(r_x)_u^2}\dot{x}r_xr_y, \tag{6.7}$$

where we require $\alpha + \beta = 1$. For example, in the biaxial tension-torsion loading case, Eqns. (6.6), (6.7) can be written in terms of stress and strain components as:

$$\dot{\sigma} = E\dot{\epsilon} - \alpha\Big(\frac{E}{\sigma_u^2}|\dot{\epsilon}\sigma|\sigma + \frac{G}{\tau_u^2}|\dot{\gamma}\tau|\sigma\Big) - \beta\Big(\frac{E}{\sigma_u^2}\dot{\epsilon}\sigma^2 + \frac{G}{\tau_u^2}\dot{\gamma}\sigma\tau\Big),$$

$$\dot{\tau} = G\dot{\gamma} - \alpha\Big(\frac{E}{\sigma_u^2}|\dot{\epsilon}\sigma|\tau + \frac{G}{\tau_u^2}|\dot{\gamma}\tau|\tau\Big) - \beta\Big(\frac{E}{\sigma_u^2}\dot{\epsilon}\sigma\tau + \frac{G}{\tau_u^2}\dot{\gamma}\tau^2\Big),$$

where σ_u and τ_u represent respectively the ultimate axial stress and the ultimate shear stress of the system being modeled. An important feature of Eqns. (6.6) and (6.7) is that under the transformation

$$\hat{r}_y \equiv \frac{(r_x)_u}{(r_y)_u}r_y, \quad \hat{y} \equiv \frac{A_y(r_x)_u}{A_x(r_y)_u}y, \tag{6.8}$$

Eqns. (6.6), (6.7) will reduce to Eqns. (6.2), (6.3) of the isotropic case.

The foregoing formulation of the two-dimensional Bouc-Wen model is phenomenological in nature; however, the new models exhibit reasonable biaxial hysteretic behavior as justified by some experimental results [37, 53]. This may be attributed to an implicit assumption of the model behavior on the "yield" condition. From Eqns. (6.4) (using $\hat{r}_y = r\sin\theta$ and treating r and θ as general polar coordinates) and (6.8) , it follows that

$$\frac{r_x^2}{(r_x)_u^2} + \frac{r_y^2}{(r_y)_u^2} = \hat{r}^2 \qquad (\hat{r} \equiv \frac{r}{(r_x)_u}). \tag{6.9}$$

Thus, since $r_x \leq (r_x)_u$ and $r_y \leq (r_y)_u$ we may conclude that the two-dimensional Bouc-Wen model actually employs the concept of a *limit* surface of elliptic shape in the biaxial "stress" space.

An important advantage of the two-dimensional Bouc-Wen model is that it is versatile and amenable to analytical treatment, and thus can be applied to systems of considerable complexity and under random excitation. However, the biaxial model inherits the disadvantage of the one-dimensional model in that it exhibits unstable drift under small cyclic excitations, as explained in Chapter 3. Moreover, there is another unrealistic response feature inherent in the model due to the "empirical" formulation given above. That is, under proportional (displacement) loading, the biaxial restoring force response is also proportional at all times, even if the response is in plastic state. This can be easily deduced by noting that when $\dot{x} = c\dot{y}$ in Eqns. (6.2) and (6.3), we obtain $r_x = cr_y$. This behavior is not consistent with the theory of plasticity or experimental observations. Another major disadvantage of the model is that it is difficult to extend it to higher dimensions, due to a lack of sound theoretical basis, to allow for a general analysis of cyclic plasticity.

6.2.2 A Recent Procedure for Generalizing 1-D Hysteretic Models

Recently, Graesser and Cozzarelli [14] presented a systematic procedure for extending a one-dimensional model of hysteresis to a multi-dimensional tensorial representation provided that the model behavior is governed by some simple power laws. In particular, they considered the generalization of the one-dimensional Ozdemir model which was proposed originally for hysteretic behavior of yielding structures [36]. However, due to some unrealistic characteristics associated with the original

one-dimensional Ozdemir model, as discussed in Chapter 3, the extended multi-dimensional model will inherently exhibit some nonphysical behavior, which may lead to violation of Drucker's postulates of stability. The inconsistency of these generalized models (Bouc-Wen and Ozdemir models) with real behavior can be attributed to their simplified mathematical formulation and lack of physical motivation. Nevertheless, the approach used in the derivation of the generalized Ozdemir model still provides useful guidelines to the generalization of one-dimensional hysteretic models to the general multi-dimensional case, and is discussed in the following.

The one-dimensional Ozdemir model with zero backstress can be described by [36]

$$d\sigma = E(d\epsilon - d\epsilon^p) \tag{6.10}$$

and

$$d\epsilon^p = |d\epsilon| \left|\frac{\sigma}{\sigma_Y}\right|^{n-1} \frac{\sigma}{\sigma_Y}, \tag{6.11}$$

where E denotes Young's modulus (i.e., initial stiffness), and σ_Y represents the simple-tension yield stress of the model. The corresponding multi-dimensional model can be found to be [14]:

$$d\sigma_{ij} = C^e_{ijkl}(d\epsilon_{kl} - d\epsilon^p_{kl}) \tag{6.12}$$

and

$$d\epsilon^p_{kl} = (3K_2)^{\frac{1}{2}} \left(\frac{3J_2}{\sigma_Y^2}\right)^{\frac{n-1}{2}} \left(\frac{s_{kl}}{\sigma_Y}\right), \tag{6.13}$$

where we define

$$K_2 \equiv \frac{1}{2} d\epsilon_{mn} d\epsilon_{mn}, \quad J_2 \equiv \frac{1}{2} s_{mn}\, s_{mn},$$

and s_{ij} denotes the deviatoric stress components. We may observe the close relationship between the sets of Eqns. (6.10), (6.11) and (6.12), (6.13), and note that (6.12) and (6.13) reduce to (6.10) and (6.11) in the uniaxial (one-dimensional) loading case. In the derivation of Eqns. (6.12) and (6.13), incompressibility of plastic deformations has been assumed and the term $3J_2/\sigma_Y^2$ can be seen to be analogous to the von Mises yield criterion in the theory of plasticity.

Our aim here is to find multi-dimensional response formulas that can adequately predict general, physically consistent elastic-plastic response behavior. In the one-dimensional case, Masing's hypothesis and the extended rules given by Jayakumar [23] provide the theoretical basis for the Masing models, which have been shown

to be equivalent to the associated Distributed-Element Models (DEMs). A special class of Masing models, proposed by Jayakumar [24] for modeling hysteretic behavior of structures, uses the following one-dimensional response formulas in addition to Eqn. (6.10):

$$d\epsilon^p = \left|\frac{\sigma}{\sigma_u}\right|^n d\epsilon \tag{6.14}$$

for initial loading, and

$$d\epsilon^p = \left|\frac{\sigma - \sigma_0}{2\sigma_u}\right|^n d\epsilon \tag{6.15}$$

for other response branches, where n is a parameter that controls the smoothness of transition from elastic to plastic state, σ_0 the stress state corresponding to the latest unloading point, and σ_u is the ultimate stress (strength) of the model. Based on the generalization rules used in Eqns. (6.10) to (6.13), one can find the following general formula corresponding to Eqn. (6.14) for initial loading:

$$d\epsilon^p_{kl} = \left(\frac{3J_2}{k_u^2}\right)^{\frac{n}{2}} d\epsilon_{kl}. \tag{6.16}$$

We remark that Eqns. (6.11) and (6.14) are identical for initial loading, yet their generalizations to multiple dimensions (Eqns. (6.13) and (6.16)) are quite different, even in the case of initial loading. This is because that when applying those generalization rules, which were developed for general response of plasticity, we treated Eqns. (6.11) and (6.14) as general formulas valid for all response branches. The formula given by Eqn. (6.16) is mathematically simple; however, it predicts that the plastic strain increment is always proportional to the total strain increment at a given stress state, which is obviously incorrect, as suggested by the behavior of the multi-dimensional DEMs, or demonstrated by the classical theory of plasticity. Fig. 6.2 shows a comparison example where biaxial stress responses under proportional strain loading were simulated using both a multi-dimensional DEM and Eqns. (6.12), (6.16). A deficiency of the model behavior based on Eqns. (6.12) and (6.16) is that the stress response never decreases in each of the two components under the prescribed proportional strain path. This is inconsistent with the result using the DEM or models based on the classical theory of plasticity. In addition to the aforementioned problem, there are some other difficulties with the generalization of Masing rules based on Eqns. (6.14) and (6.15), which are stated as follows:

1) In the general multi-axial case, it is very difficult to specify appropriately the virgin loading curve (or the "skeleton" curve) due to the path-dependent charateristic of hysteretic response. We may note that the path-dependent property actually invalidates the use of a scalar quantity $(3J_2/k_u^2)^{n/2}$ in Eqn. (6.16), since otherwise two response histories with identical histories of $(3J_2/k_u^2)^{n/2}$ will have the same stress response according to the formula (6.16).
2) To extend the Masing rules given in Eqns. (6.14), (6.15) to higher dimensions, one has to characterize the response history into different branches including initial loading, unloading and reloading cases. Based on the classical theory of plasticity, characterization of different loading cases can be done by introducing a loading function F, such as the "yield" function $F(\underline{\sigma}) = 3J_2 - k_u^2$ implicitly used in Eqn. (6.16). Thus, in the case of neutral loading ($F = 0$ and $dF = 0$) where $3J_2/k_u^2$ stays invariantly at the value of one, the stress state should still vary with the change of the prescribed strain path. But this is again not true if Eqn. (6.16) is used for describing the response to initial loading, which may possibly include the neutral loading case.

Considering the response behavior of the multi-dimensional DEM proposed in the previous chapter and the difficulties mentioned above, one can see that the task of finding simple mathematical formulas for describing general multi-axial hysteretic response is formidably challenging. Before we present an innovative idea of generalizing response formulas for multi-axial plasticity, let us compare two similar formulations based on different concepts of multiple yield surfaces. The first one is associated with the new class of multi-dimensional DEMs in which a collection of yield surfaces is defined in the *element* stress space so that the yield surfaces stay invariant in the space regardless of the change of the model response. Another formulation with multiple yield surfaces is based on the classical theory of plasticity using the Mroz kinematic hardening rule [35]. In the second formulation, the yield surfaces are defined in the *model* stress space and they move around with the model response so that the current stress state of the model never lies outside any of the yield surfaces. The Mroz kinematic hardening rule specifies that the "active" yield surfaces on which the current stress state lies will translate in the same direction as the line joining the current stress point to the point on the outer yield surface corresponding to the same direction of outward normal [35]. This rule is sketched schematically in Fig. 6.3, where the point P is the current stress state on the active

yield surface F_m and Q is the point on the outer surface F_{m+1} corresponding to the same direction of outward normal. The translation of the surface Fm (as well as the inner surfaces, such as F_{m-1}) will follow the direction given by the line PQ. The Mroz hardening rule ensures that the inscribed yield surfaces have a common tangent at the current stress point. Based on the theorems given in Chapter 5, it can be shown that models based on the Mroz hardening rule exhibit correct response behavior in the sense that the properties associated with equilibrium points and a limit surface can be adequately demonstrated. Other often-used kinematic hardening rules, such as the Prager and the Ziegler kinematic hardening rules, fail to exhibit such physical properties of response behavior shown by real materials [30]. While the Mroz rule leads to good response predictions, its numerical implementation has been thought to be too involved and inefficient for complicated structural analysis [30, 32].

It is noted that the response of a multi-dimensional DEM is governed by the response of its elements, while response behavior of a model based on the classical formulation of plasticity is determined mainly by translation of yield surfaces. A comparison of the detailed response behavior between the two multi-yield-surface models reveals that mathematically it is easier to deal with the classical model than with the DEM in generalizing 1-D response formulas for general plasticity. Effective response formulas for plasticity based on the classical multi-yield-surface theory will be proposed in the following sections. It will be shown that these well-proposed response formulas provide a very efficient way of implementing the classical multi-yield-surface theory using the Mroz kinematic hardening rule.

6.3 A Class of Generalized Masing Models for Multi-axial Plasticity

6.3.1 A Response Formula for Initial Loading

To find mathematical rules similar to Masing's hypothesis for govening response behavior in cyclic plasticity, one has to first define a formula good for response of initial loading, and then find corresponding formulas for describing subsequent response behavior. By initial loading here, we mean that no unloading defined according to the classical theory of plasticity* has ever occurred.

* In the classical theory of plasticity, the characterization of different loading cases for strain hardening materials is done by introducing a loading function (which is

As noted above, the initial loading formula (6.16), derived from extending a special class of 1-D Masing models, or the formulas (6.14) and (6.15) based on Ozdemir's model (which was proposed for complete history of response) do not yield proper response behavior for cyclic plasticity. This kind of deficiency may be attributed to lack of physical insight in formulating the general response behavior, so that the formulas may lead to unrealistic or even unstable response behavior.

A new response formula for initial loading is proposed here based on the response behavior of ideal plasticity and the introduction of a "damage" function. The theory of classical plasticity is formulated mainly based on experimental observations, and hence a model showing the behavior of ideal plasticity can be thought of as physically motivated. Based on the insight obtained in developing the multi-axial DEM which consists of a collection of elements of ideal plasticity, we extend the "ideal plasticity" model to account for strain hardening behavior as follows.

Recall that by Eqn. (5.43), the plastic strain increment in a yielding state of perfectly plastic behavior with a corresponding yield function F can be expressed in a vector form as

$$\begin{aligned} d\underline{\epsilon}^p &= \mathbf{\Lambda}(\underline{\sigma}, d\underline{\epsilon})\, d\underline{\epsilon}, \\ &= \begin{cases} \mathbf{\Lambda}_0(\underline{\sigma})\, d\underline{\epsilon} & \text{if } dF = 0; \\ 0 & \text{if } dF < 0, \end{cases} \end{aligned}$$

---

usually the same as the yield function) defined by $F(\sigma_{ij}) = k$ so that when

$$(1) \quad F = k, \quad dF = \frac{\partial F}{\partial \sigma_{ij}}\, d\sigma_{ij} > 0,$$

it is called *loading*. When

$$(2) \quad F = k, \quad dF = \frac{\partial F}{\partial \sigma_{ij}}\, d\sigma_{ij} = 0,$$

it is called *neutral loading*. When

$$(3) \quad F = k, \quad dF = \frac{\partial F}{\partial \sigma_{ij}}\, d\sigma_{ij} < 0,$$

it is called *unloading*.

where dF is a function of both the current state and the load increment, and $\mathbf{\Lambda}$ is the plastic modulus reduction matrix and

$$\mathbf{\Lambda}_0(\underline{\sigma}) = \frac{\underline{a}\,\underline{a}^T\mathbf{C}^e}{\underline{a}^T\mathbf{C}^e\underline{a}}, \tag{6.17}$$

where $\underline{a}$ is defined in (5.49). Note that in the above, dF is never greater than zero and $\mathbf{\Lambda} = \mathbf{0}$ corresponds to the case where response is purely elastic.

For our purpose of developing a general response formula for initial loading, a *modulus-reduction* function which signifies the "degree of yielding" can be introduced as

$$D(\underline{\sigma}) = \left(\frac{3J_2}{k_u^2}\right)^{\frac{n}{2}}, \tag{6.18}$$

where $J_2 = \frac{1}{2}s_{mn}\,s_{mn}$ is the second invariant of the deviatoric stress tensor and the parameter n is introduced to control the smoothness of yielding. The response formula (6.17) for ideal plasticity in the case of initial loading is then modified by including the modulus-reduction function D as

$$d\underline{\epsilon}^p = D(\underline{\sigma})\,\mathbf{\Lambda}_0(\underline{\sigma})\,d\underline{\epsilon}. \tag{6.19}$$

By Eqn. (6.19), when the response is small, $3J_2 \ll k_u^2$, and we have $d\underline{\epsilon}^p \approx \underline{0}$; when $3J_2 = k_u^2$, the response state reaches the limit surface associated with the model and the response behavior becomes perfectly plastic as loading is continued. In the biaxial tension-torsion case where von Mises yield criterion is used, Eqn. (6.19) gives

$$\begin{aligned} d\epsilon_{11}^p &= C\left[Es_{11}^2 d\epsilon_{11} + 4Gs_{11}s_{12}d\epsilon_{12}\right] \\ d\epsilon_{12}^p &= C\left[Es_{11}s_{12}d\epsilon_{11} + 4Gs_{12}^2 d\epsilon_{12}\right] \end{aligned}, \tag{6.20}$$

where $C \equiv \frac{(3J_2/k_u)^{n/2}}{Es_{11}^2+4Gs_{12}^2}$ and s_{ij} is the deviatoric stress tensor.

A simulation study of the response behavior based on the formulas (6.19) and (6.13), respectively, was conducted to get an idea of how the formulas perform in complicated loading conditions. The prescribed loading path under consideration is the strain loop 0-1-2-...-8 as shown in Fig. 6.4. In the simulation, the strain loop was traced twice, while only the response corresponding to the second loop is considered in order for comparison with the experimental result shown in Fig. 6.5, where only cyclically stablized behavior is demonstrated. The corresponding response curves

are presented in Figures 6.6 and 6.7, where we can see the superiority of Eqn. (6.19) in response prediction of initial loading to Eqn. (6.13), as justified by the experimental result and the response predicted by a DEM. The response predicted by Eqn. (6.19) shows correct behavior in terms of the positions of equilibrium points and the associated limit surface. We remark that all the loading branches in the above example are treated as initial loading so that only Eqn. (6.19) (together with Eqn. (6.12)), which is derived for response of initial loading only, is used throughout the response history.

In summary, we note that there are three important features of the response formula (6.19) derived for initial loading:

(i) The model based on Eqn. (6.19) preserves all the equilibrium points of a perfectly plastic model so that it always leads to stable and physically consistent response behavior.

(ii) Analogous to the multi-dimensional DEM, there is no special restriction on the yield condition (or modulus-reduction function) needed in the formula for initial loading. In general, we should replace Eqn. (6.18) by

$$D(\underline{\sigma}) = \left(\frac{F(\underline{\sigma})}{k_u}\right)^n, \tag{6.21}$$

where $F(\underline{\sigma}) = k_u$ is the equation of the *limit* surface associated with the model and can assume any appropriate form. Note that $F(\underline{\sigma})$ is also the "loading" function controlling the cases of loading or unloading. Furthermore, the power law employed in Eqn. (6.21) may be replaced by some other function forms so as to provide more general, flexible response behavior.

(iii) The key point in the new formula for initial loading is that the modulus-reduction function $D(\underline{\sigma})$ replaces a conventional yield condition and subsequent hardening rules, so that continuous yielding behavior on initial loading is adequately modeled.

6.3.2 Response Formulas for Unloading and Reloading Branches

With the initial loading formula defined in Eqn. (6.19), we then want to find corresponding mathematical rules that can govern appropriately the response behavior of unloading and reloading branches, so that complete response history to

any multi-axial loading path can be calculated accordingly. Recall that loading and unloading correspond to $dF \geq 0$ and $dF < 0$ respectively, where $F(\underline{\sigma})$ is the loading function as employed in Eqn. (6.21).

It can be recognized that Masing's hypothesis implies mathematically that the behavior of unloading response can be found from that of virgin response by introducing a proper transformation on the state variables describing the response. Motivated by this concept and the behavior of the classical multi-yield-surface model using Mroz' kinematic hardening rule (cf. Fig. 6.3), we propose the idea of introducing a composition of transformations on the state variables involved in the initial loading formula (6.19), so that unloading response can be found based on the same formula as for the response of initial loading. Based on this idea, we have the following formula, corresponding to Eqn. (6.19), for unloading and reloading branches:

$$d\underline{\epsilon}^p = D(\underline{\sigma}')\, \mathbf{\Lambda}_0(\underline{\sigma}')\, d\underline{\epsilon}, \tag{6.22}$$

where $\underline{\sigma}'$ denotes the vector of transformed stress state, which is a function of not only the current response state, but also the past history.

To determine the effective transformation required for our purpose, we remark that for the classical multi-yield-surface model, the yield surfaces reached by the current stress state must be carried along with the response state instead of staying invariant, so that they all have the current stress point as a common tangent point. The movement of the yield surfaces along with the current state is illustrated schematically in Fig. 6.8, where the circles represent yield "surfaces" in a two-dimensional stress space and points A, B denote two instantaneous stress states. Thus, the response behavior corresponding to the unloading branch from a point B can be found by transforming the geometrical configuration in Fig. 6.8(c) back into that in 6.8(a), so that Eqn. (6.22) can be used effectively for response calulation of any unloading (or reloading) branches. Care must be taken in performing the transformations so that not only the transformation of geometrical configurations is appropriately done, but also the normality rule for determining increments of plastic strain is preserved (cf. Appendix B). In the following, we will be concerned only with the two-dimensional loading case so that we need only deal with transformations of planar configurations. An effective transformation formula for "steady-state" cyclic

response (i.e., loading between points symmetric to the origin) that is derived from a composition of a series of proper transformations can be found as follows:

$$\sigma' + i\tau' = \frac{-r_1}{2\sin\theta_2}\, e^{-i\theta_4}, \tag{6.23}$$

where (σ', τ') denotes the transformed stress state, and

$$\begin{gathered} r_1 = \sqrt{(\sigma-\sigma_0)^2 + (\tau-\tau_0)^2}, \quad \theta_2 = \theta_1 - \theta_0 + \frac{\pi}{2}, \\ \theta_1 = \tan^{-1}\left(\frac{\tau-\tau_0}{\sigma-\sigma_0}\right), \quad \theta_0 = \tan^{-1}\left(\frac{\tau_0}{\sigma_0}\right), \\ -\theta_4 = 2\theta_2 + \theta_0 = 2\theta_1 - \theta_0 + \pi. \end{gathered} \tag{6.24}$$

In (6.24), (σ, τ) is the current actual stress state and (σ_0, τ_0) is the actual stress state corresponding to the latest unloading point. The detailed derivation of the transformation rules (6.23), (6.24) is given in Appendix B. Note that in the derivation of the transformation rules we assumed that the yield surfaces in the 2-D space can be represented by circles which are initially concentric. This, however, does not put any limitation on applications using the above idea, since according to the well-known Riemann's Mapping Theorem [55], a simply-connected region of arbitrary shape can always be mapped onto a circle through a conformal mapping.* Therefore, the yield surfaces in the 2-D space can be of any shape and the transformation rules (6.23), (6.24) will still work, as long as we can find the transformation whose existence is guaranteed by Riemann's theorem so that the yield surfaces of arbitrary shape can be transformed into circles.

The transformation approach mentioned above works, in principle, only for the 2-D case. However, it is also applicable to the general multi-axial plasticity provided that isotropic materials are considered and the plastic deformation can be treated as independent, or as some simple function, of the hydrostatic stress state. Many real materials exhibit approximately these kinds of behavior, such as metals and soils. In this case, we can always convert a stress state (which is a symmetric two

* The Riemann Mapping Theorem has also been extended to the case where a region bounded by two simple closed curves, one inside the other, is mapped into a region bounded by two concentric circles [41].

tensor) into a corresponding principal stress state (a diagonal two tensor) for which the shear stress components vanish, and apply the 2-D transformations to the stress state projected on a shifted π plane which is perpendicular to the hydrostatic axis $\sigma_1 = \sigma_2 = \sigma_3$ in the principal stress space. This is shown in Fig. 6.9(a), and 6.9(b), in which the circular cylinder and cone represent the yield surfaces corresponding to the von Mises and Drucker-Prager yield conditions [1], respectively. A schematic diagram illustrating this idea of transformation on the π plane is shown in Fig. 6.10.

6.3.3 Rules for Transient Response

With the initial response formula (6.19) and the transformation rules (6.22) to (6.24) for other response branches, we are able to determine the steady-state cyclic response of a system characterized by multiple yield surfaces without the need to calculate the response of elements or to trace the motions of yield surfaces. However, in the general cyclic loading case, we still need to extend the foregoing formulas to account for transient behavior of cyclic response, as Jayakumar [23] did in the one-dimensional case for extending the Masing's hypothesis for hysteresis.

Recall that in the one-dimensional case, we had the rules for incomplete loops and completed loops of transient response (cf. Sec. 3.2.3). In the multi-dimensional case, however, the cyclic loops between fixed strain points may not be "strictly closed" in general. Here, by "strictly closed" we mean that a stress-strain loop is closed at a load reversal point so that this point is both the starting and the ending point of the loop. Based on geometrical considerations of multiple yield surfaces and the Mroz hardening rule, we can modify the definitions for incomplete and completed loops and deduce corresponding rules for them in the general multi-axial case.

Firstly, we define a *completed loop* as a "loop" along which the outermost yield surface that contains the latest point of load reversal is reached again during the loading process. Otherwise, the loop is said to be *incomplete*. For example, in Fig. 6.11, the stress response "loop" ABC is incomplete, while the "loop" BCE is a completed one since the outermost yield surface (level curve 2) containing the latest point of load reversal C is reached at E. With these definitions we can propose the following two rules for transient response of cyclic plasticity:

Rule 1: Incomplete loops

The equation of any response curve can be obtained simply be using Eqn. (6.19) and applying the $\underline{\sigma} - \underline{\sigma}'$ transformation, as given by Eqns. (6.23), (6.24) to the latest point of load reversal (σ_0, τ_0) and the outermost yield surface on which (σ_0, τ_0) lies. For example, the response curve CE in Fig. 6.11 can be found by applying the transformation rule to point C and "level curve" 2.

Rule 2: Completed loops

Once the stress state reaches the outermost yield surface on which the latest load reversal occcurs, the transformation rule is applied to the previous point of load reversal and the corresponding outermost yield surface.

For example, in Fig. 6.11, as the loop BCE is completed at E, the transformation rule is then applied to point B and level curve 4 for the response that follows. Note that Rule 2 for completed loops is different from that in the one-dimensional case where two points of load reversal are erased at a time when an interior curve crosses a curve from a previous load cycle. This rule for one-dimensional hysteresis can be shown to be actually a special case of the two-dimensional rule, in which only proportional loading is taken into account.

We remark that in the case of transient response, the geometrical configuration of yield surfaces is different from that of a steady-state case, not only in the position of the active point of load reversal, but also in that θ_0 in (6.24) is measured by reference to a new center point, which may be different from the origin of the stress space. Therefore, the θ_0 in (6.24) should be replaced by the more general formula

$$\theta_0 = \tan^{-1}\left(\frac{\tau_0 - \tau_C}{\sigma_0 - \sigma_C}\right), \tag{6.25}$$

where (σ_C, τ_C) represents the coordinates of the center of the current reference circle (the outermost yield surface that the latest unloading point is on). This situation is illustrated in Fig. 6.12. Fig. 6.12(a) shows the process of initial loading from the origin O to point A and then unloading from there. Fig. 6.12(b) shows the geometrical configuration corresponding to the transient response of unloading from point B , where point C represents the center of the current reference circle. The coordinates of the new center point C can be generally found as

$$(\sigma_C, \tau_C) = (\sigma_A, \tau_A) - \frac{r_B}{r_A}(\sigma_A - \sigma_{C'}, \tau_A - \tau_{C'}), \tag{6.26}$$

where r_A and r_B denote the radii of the outermost "active" circles on which points A and B lie respectively, and $(\sigma_{C'}, \tau_{C'})$ represents the coordinates of the center of the previous reference circle (C' coincides with the origin O for the case in Fig. 6.12). Based on the preceding rules, numerical implementation of the foregoing algorithm requires for each point of load reversal to store in a list both the strength constant (radius) and the coordinates of the center point of the outermost yield surface on which the reversal point lies. Every time the yield surface with the smallest strength on the memory list is reached, its corresponding point of load reversal and center of reference is erased from memory. This phenomenon may be viewed as an additional attribute of the property of erasure-of-memory, and is the counterpart to the property of unraveling of interior loops in the one-dimensional case.

While the mathematical manipulation involved in the above approach based on transformation formulas is simple and effective, a major problem of implementing the above rules for multi-axial transient response exists. This problem is associated with the numerical ill-conditioning which occurs when the response formulas are applied to states near the points of load reversal, which are singular points of the corresponding transformations as can be deduced from the derivation of the transformation formulas. To illustrate this, we consider the following example. When unloading occurs from a point, say the point B or C in Fig. 6.11, the "yielding value," $3J_2(\underline{\sigma}')$, at any point on curve BC or CE is computed by reference to the corresponding unloading point B or C. After a transient loop is completed, such as the loop BCD or BCE in Fig. 6.11, the yielding value at D or E should be calculated by reference to the previous unloading point B, according to the Rule 2 stated above. However, when the point at which a transient loop is completed is very close to the previous unloading point (such as point D in Fig. 6.11 which is close to point B), due to the singular behavior at an unloading point ,the yielding value cannot be found accurately (as we can see in Fig. 6.11, all the level curves signifying different yielding values pass through point B). In other words, the calculation of $\underline{\sigma}'$ from the transformation formulas is numerically ill-conditioned. In the one-dimensional case, we can get around this problem by always erasing two points of load reversal whenever a loop is completed; but in the more general case, special care must be taken in doing so in order not to introduce significant error. A remedy for dealing with the problem is that two latest points of load reversal, instead of just one (Rule 2), will be

erased every time a loop is completed if the current yielding value with reference to the previous point of load reversal is found to be considerably less than the yielding constant of the active yield surface on which the latest point of load reversal lies. For example, in Fig. 6.11, the points D and E, which both lie on the level curve 2, should always have the same yielding value, say 2, no matter which unloading point is referenced. But due to the singular behavior around the unloading point B, the yielding value at D may be found numerically as much less than 2, e.g., if point D coincides with (or very close to) the unloading point B, the yielding value will be found zero there. In this case, we may erase two latest points of load reversal, i.e., B and C in Fig. 6.11, so that the active reversal point becomes A and then the yielding value at D with reference to A will be found to be about 4 (corresponding to the level curve 4), which is correct for continued response from D. On the other hand, if the response curve goes from C to E at which the yielding value with reference to point B is close to the yield constant of the active yield surface (level curve 2), then only one point of load reversal (point C) will be removed from the memory.

6.3.4 Simulation Studies

Thus far, based on the classsical formulation of ideal plasticity and multi-yield-surface theory, we have derived a class of "generalized Masing models" based on the response formula (6.19) for initial loading, together with the transformation formulas, (6.22) to (6.24), and the rules governing the rest of a response history for general multi-axial cyclic loading. It is of interest to examine the performance of such a model that is actually composed of an infinite number of yield surfaces moving in the stress space according to the Mroz kinematic hardening rule. In the following, the model performance will be evaluated under the same biaxial tension-torsion loading conditions as before.

The results of response predictions using a generalized Masing model for different prescribed strain paths, given in Figures 5.6(a) and (b), are shown in Figures 6.13 and 6.14 respectively, where the response predicted by a DEM is also included for comparison. Recall that the loading sequence in Fig. 5.6(a) is 0-1-0-2-0-3-0-..., so as to demonstrate the property of erasure-of-memory exhibited by real materials. In the simulations, Tresca's yield criterion has been adopted for the

modulus-reduction function defined in Eqn. (6.21), and the model parameters used are $E = 16,700\ ksi, \nu = 0.33,\ \sigma_0 = 30\ ksi$, and $n = 2.5$. A comparison between the model predictions and the experimentally-observed results, given in Figures 5.7 and 5.8, leads to the following remarks. It is immediately recognized that the response behavior described by the initial loading formula (6.19) (or (6.20) for the biaxial case) and the transformation rules (6.22) to (6.24) is in good agreement with the experimental results in almost every aspect. Transition from elastic to plastic regime is smooth and well-behaved, while the complicated biaxial Bauschinger effect is also well accounted for. Moreover, the model behavior clearly shows the existence of equilibrium points and a limit surface, as well as the property of erasure-of memory. One may thus conclude that the behavior of the generalized Masing model is physically consistent. In addition, the computational effort in making response prediction based on the above response-formula approach is even less than that using a ten-element multi-dimensional DEM, which is already computationally efficient compared with models based on the classical theory of plasticity. The excellent accuracy of the model in response prediction may be attributed to the formulation based on a collection of an uncountably infinite number of yield surfaces and the well-formulated Mroz kinematic hardening rule.* The numerical efficiency of the model is due to the proposed transformation method which avoids costly bookkeeping of the movement of multiple yield surfaces involved in the model.

6.4 Comparison of the Generalized Masing models with the DEMs

In the above, we have proposed two constitutive models for plasticity based on different multi-yield-surface theories. As shown in the simulation studies, both models are physically consistent and parsimonious in parameters. It is thus of interest to see whether these two models can become equivalent under general situations.

The generalized Masing models utilize yield surfaces defined in the *model* stress space, together with the Mroz hardening rule to account for the Bauschinger effect in cyclic plasticity, yet the DEMs use *invariant* yield surfaces defined in the *element*

* Response behavior based on the Mroz kinematic hardening rule has been shown to be consistent with those observed from real metals [30]. Besides, it has been shown mathematically that the rule never results in intersection of two yield surfaces [32].

stress space. Even though it may be possible to choose the distribution of the yield surfaces in a generalized Masing model to match that in a DEM so that they exhibit the same kinematic hardening behavior, for the two models to be completely equivalent, we need also take into account the flow rules adopted.

The flow rule used in the formulation of the multi-dimensional DEMs specifies that the current plastic strain increment of the model is given by the average of the corresponding plastic strain increments of the elements, and is not a simple function of the model state itself. As for the generalized Masing models, the current plastic strain increment is solely determined by the corresponding model stress state (using the principle of normality). Thus, we may conclude that in general, the two models with different formulations cannot be made exactly equivalent. Also, we remark that for response analysis based on the proposed multi-dimensional DEMs, we need not distinguish *model* response into different loading cases, such as loading or unloading; however, for the generalized Masing models based on the proposed plane-geometry transformation method, we have to keep track of all the unloading points throughout reponse histories.

As a final remark, we mention that although the numerical implementation of the generalized Masing models avoids costly bookkeeping of the movement of multiple yield surfaces or the response behavior of distributed elements, it requires in practice smaller load increments than those needed for the implementation of the proposed DEMs, in order to achieve satisfactory accuracy.

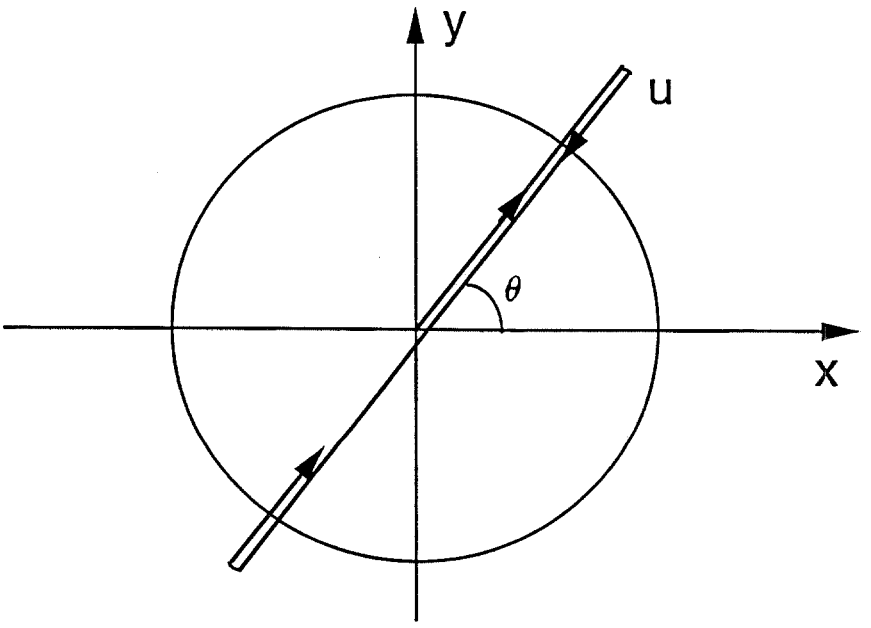

(a) proportional displacement path

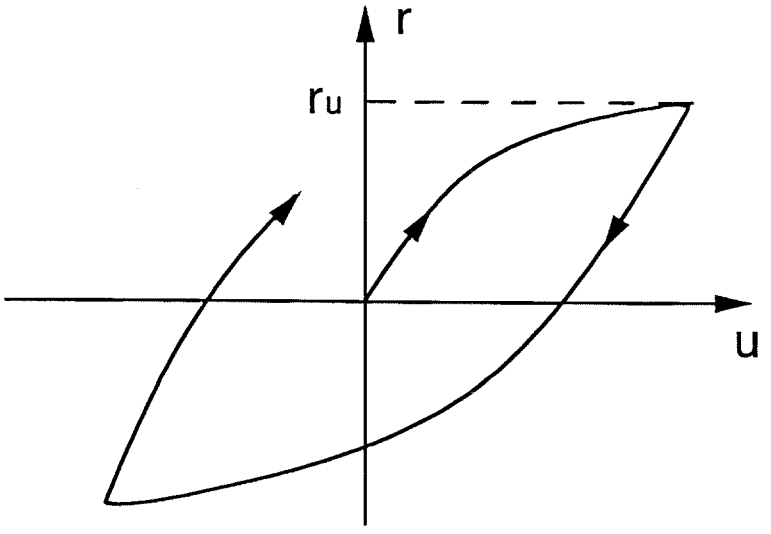

(b) hysteretic restoring force behavior

Figure 6.1 Hysteretic behavior of the two-dimensional Bouc-Wen model

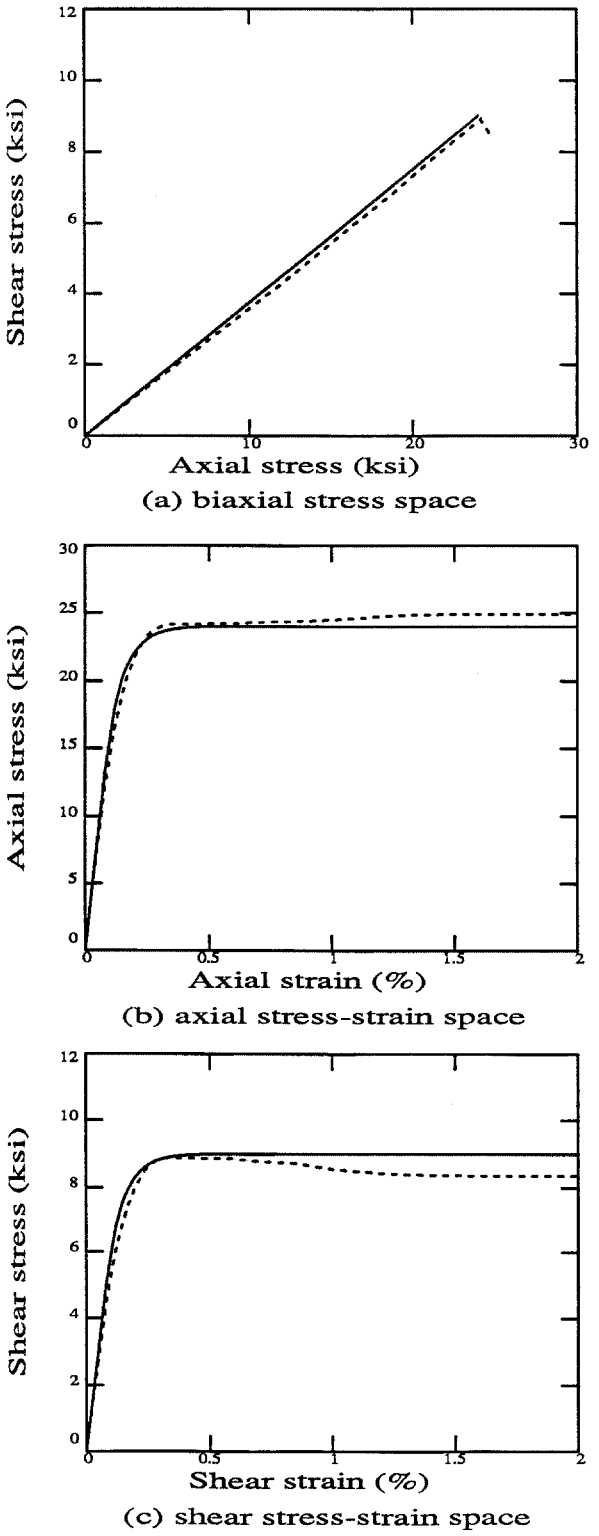

Figure 6.2 Comparison of the initial response predicted by Eqn. (6.16) and by a DEM (Eqn. (6.16) ——— , DEM - - - -)

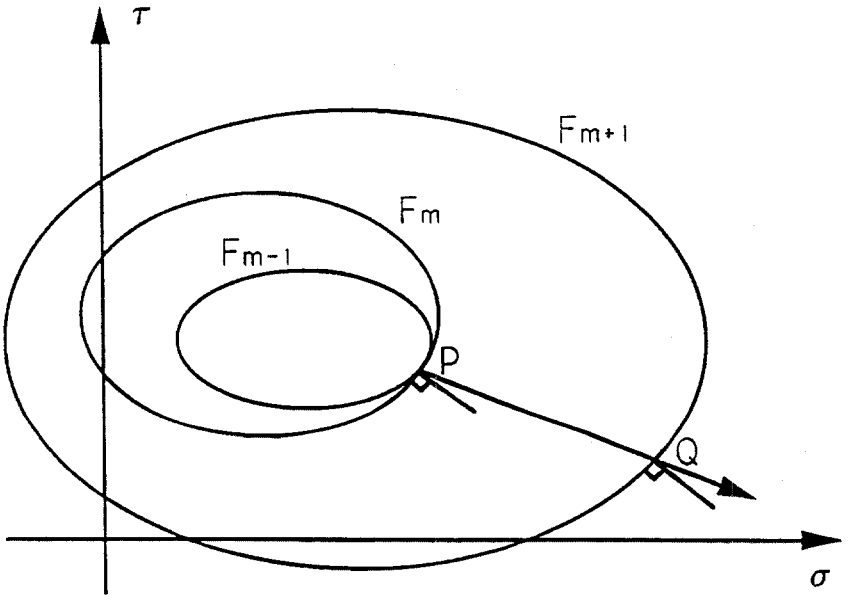

Figure 6.3 The Mroz kinematic hardening rule

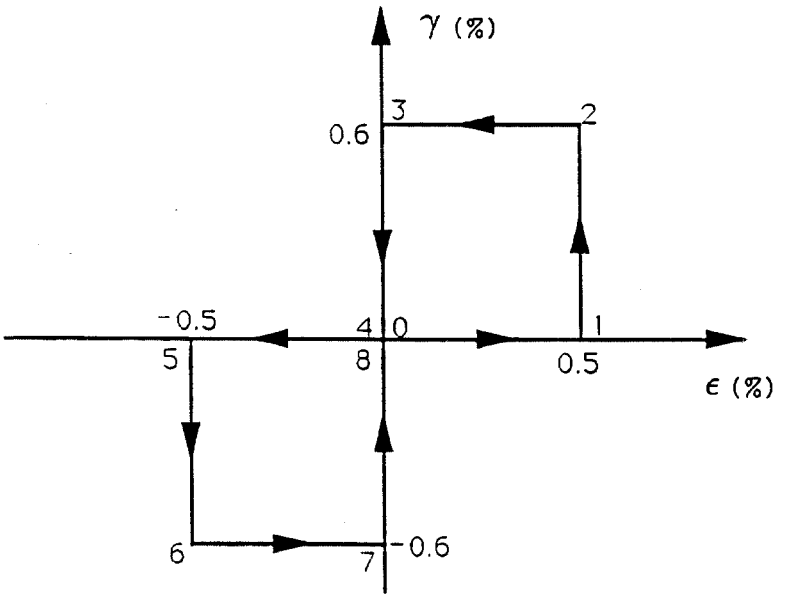

Figure 6.4 Prescribed strain path for response of initial loading

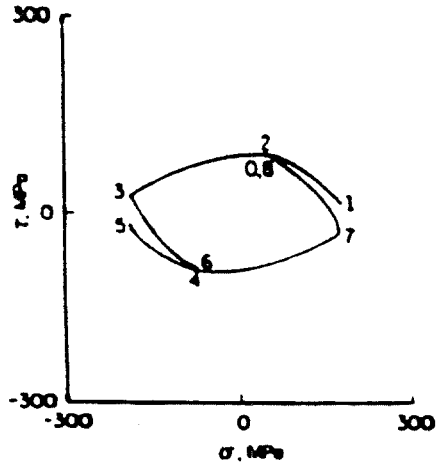

(a) biaxial stress space

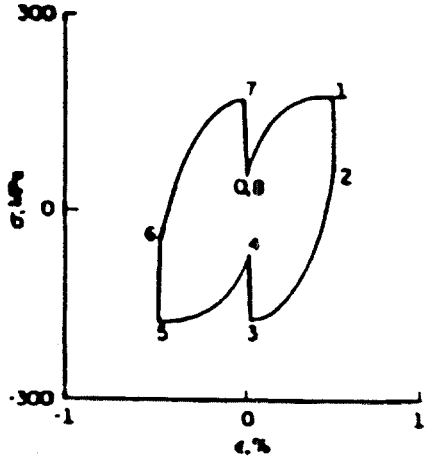

(b) axial stress-strain space

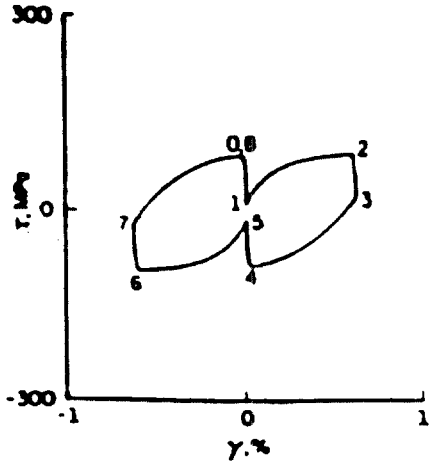

(c) shear stress-strain space

Figure 6.5 Experimentally-observed stress response of copper to the prescribed strain path given in Figure 6.4 (from [17])

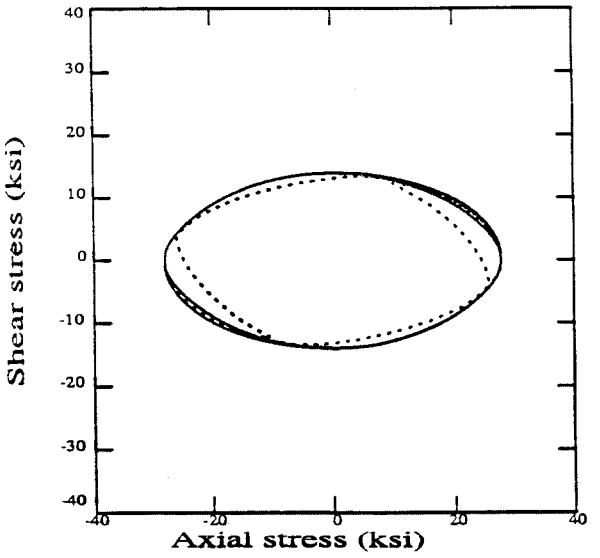

(a) biaxial stress space

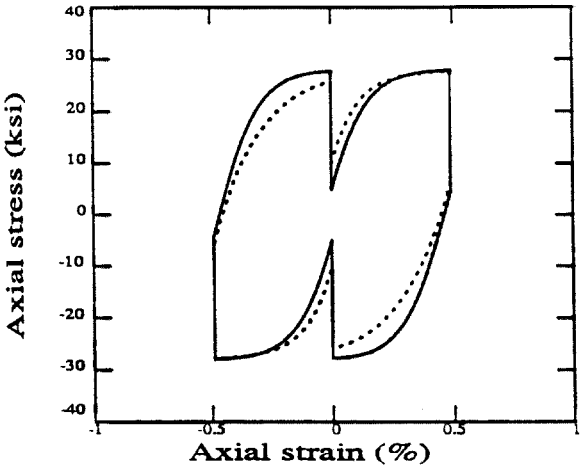

(b) axial stress-strain space

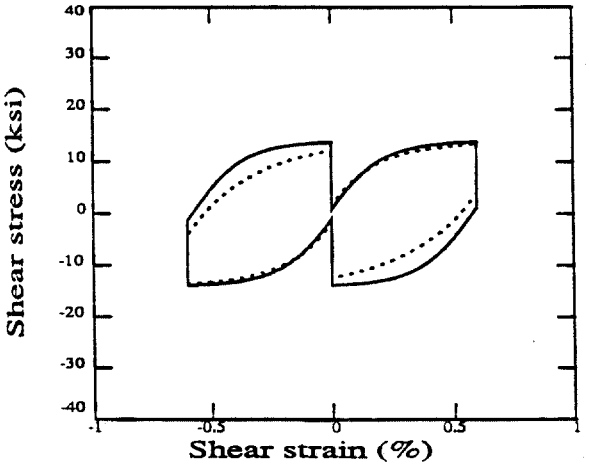

(c) shear stress-strain space

Figure 6.6 Stress response predicted by Eqn. (6.19) with the prescribed strain path given in Figure 6.4 (Eqn. (6.19) ——, DEM - - - -)

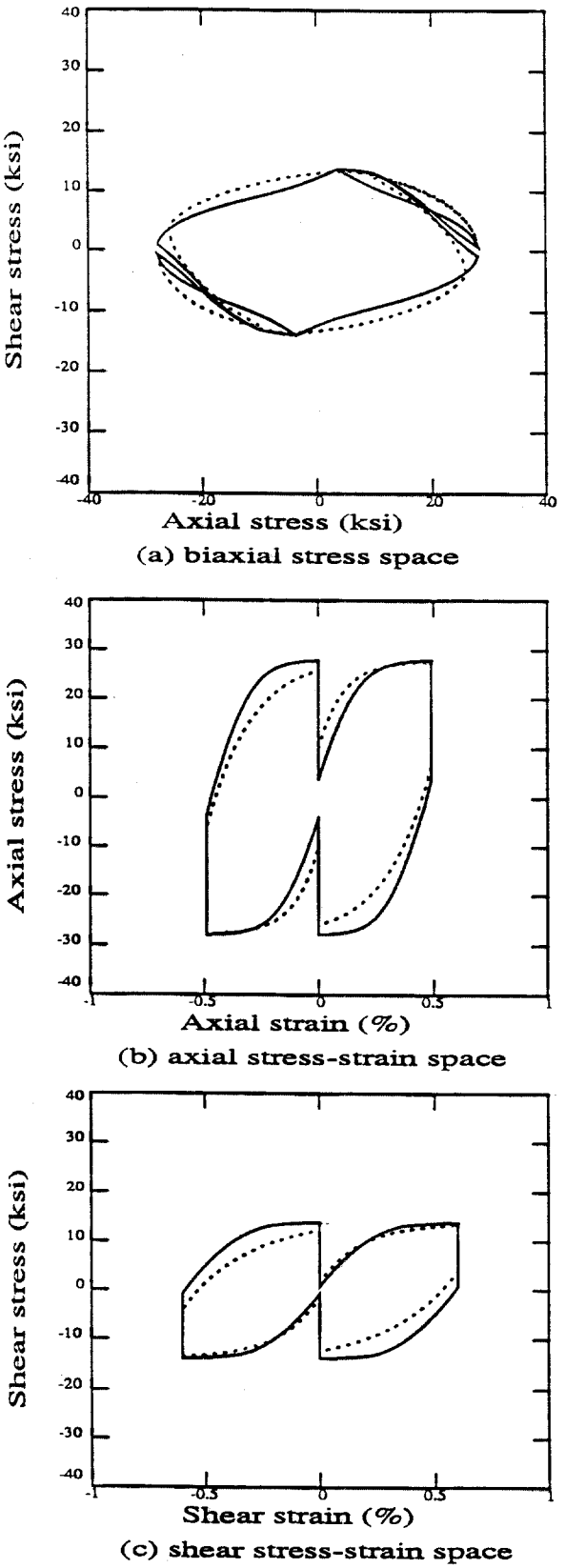

Figure 6.7 Stress response predicted by Eqn. (6.13) with the prescribed strain path given in Figure 6.4 (Eqn. (6.13) ——, DEM - - - -)

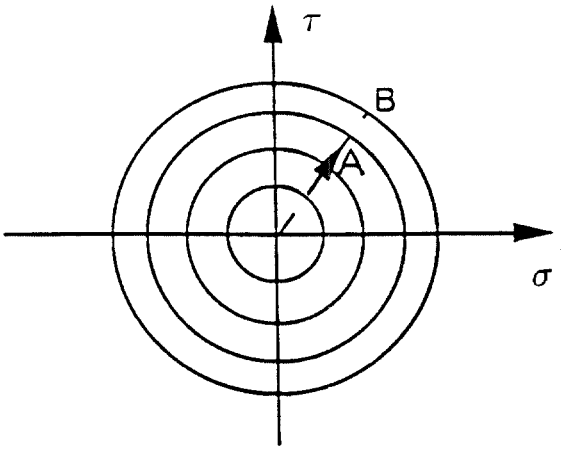

(a) initial configuration

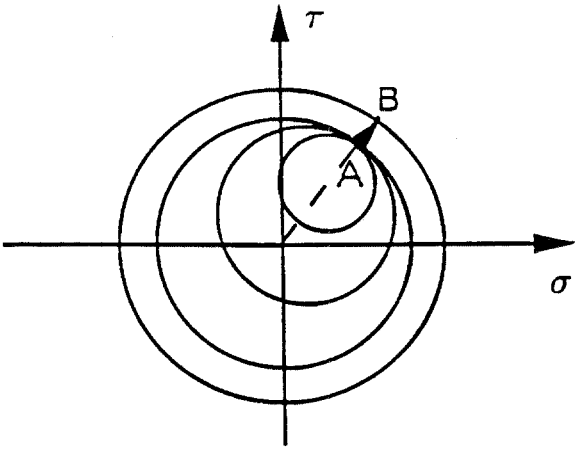

(b) current stress state A

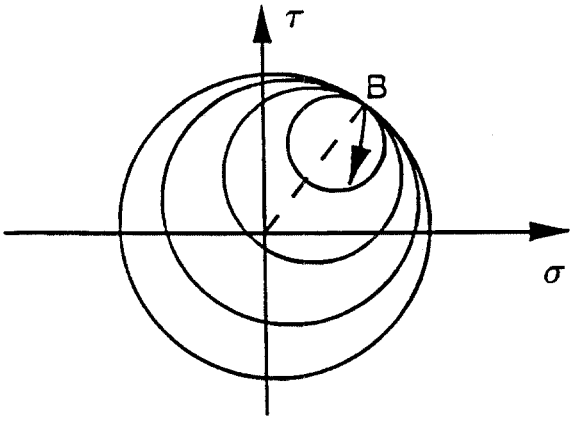

(c) current stress state B

Figure 6.8 Movement of yield surfaces with current stress state moving from A to B

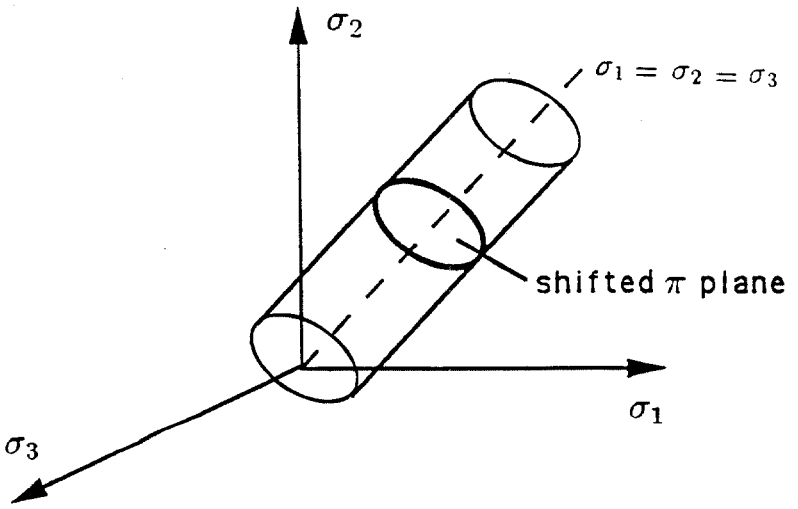

(a) von Mises yield condition

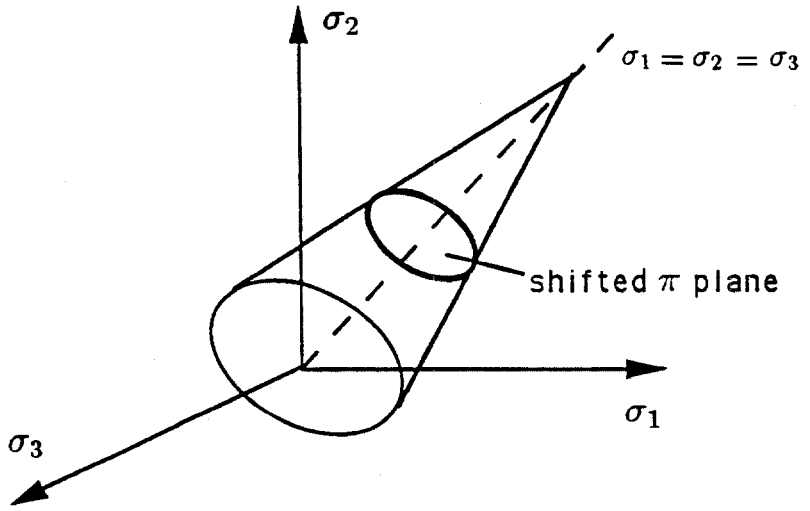

(b) Drucker-Prager yield condition

Figure 6.9 Different yield surfaces and shifted π planes in the principal stress space

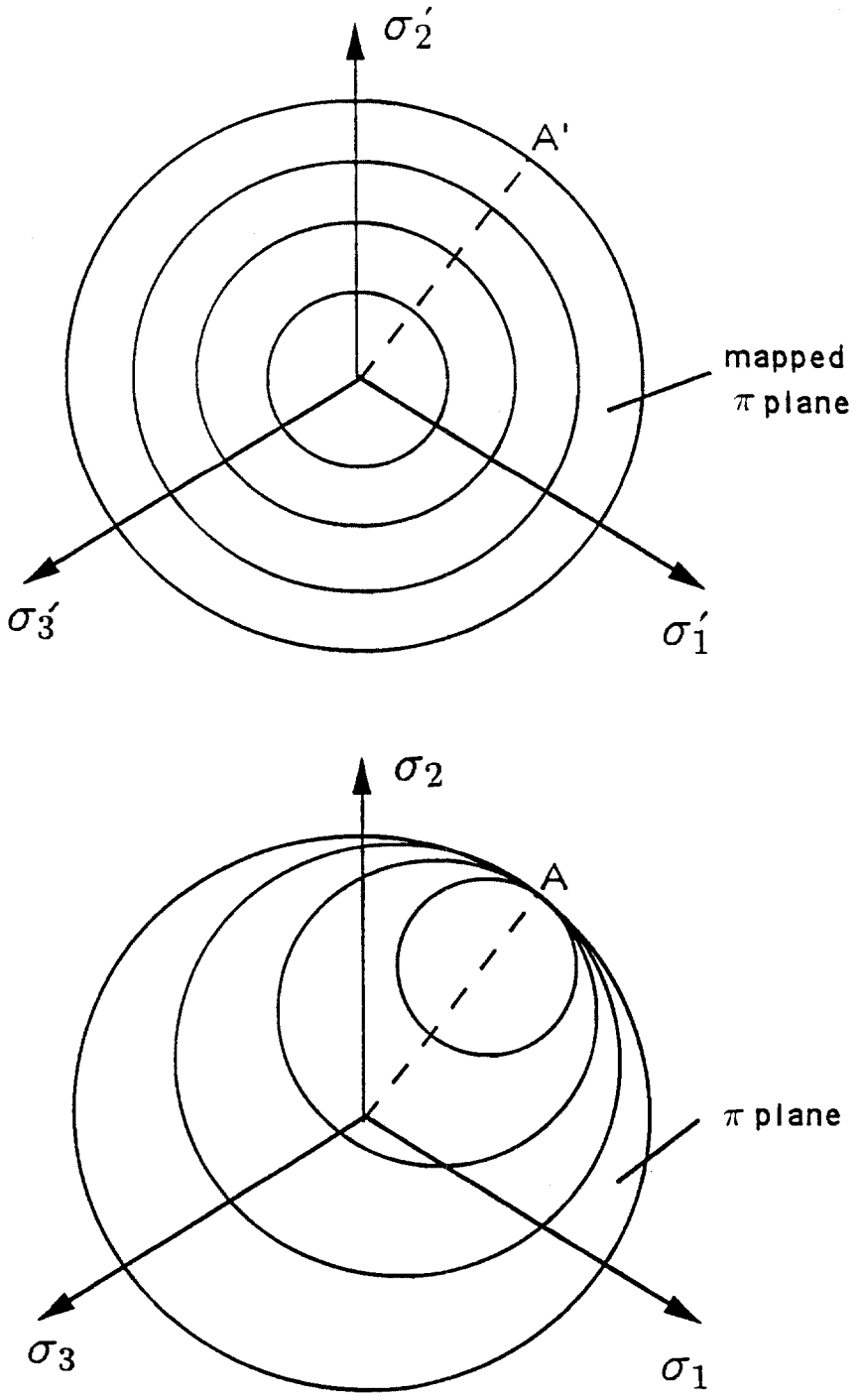

Figure 6.10 Transformation on the π plane where A' is image of A

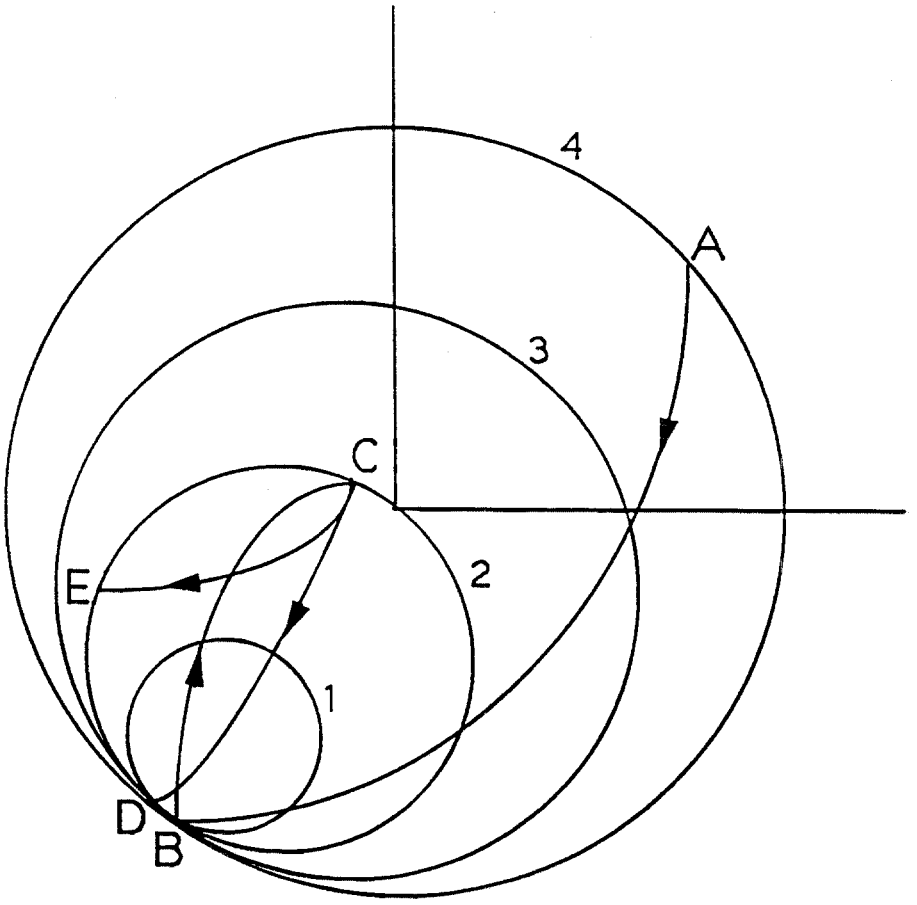

Figure 6.11 Illustration of completed loops and numerical difficulty associated with the transformation approach

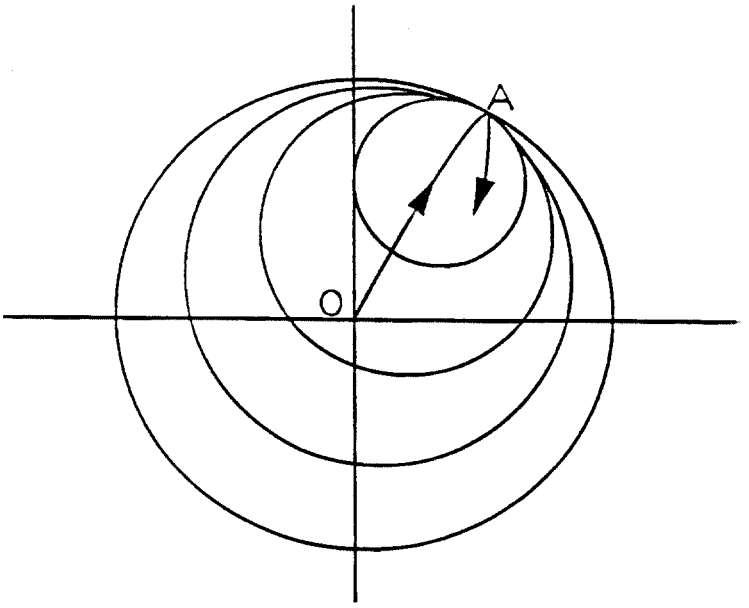

(a) unloading from point A

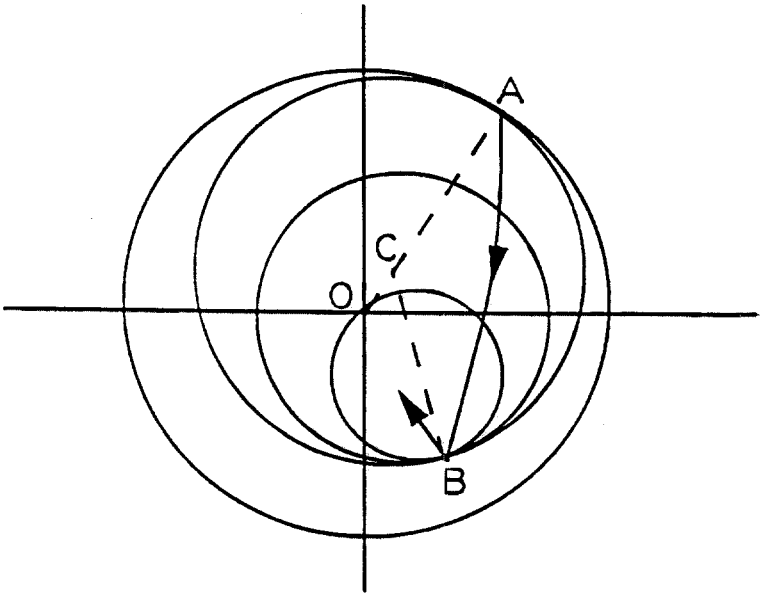

(b) unloading from point B with new center C

Figure 6.12 Geometrical consideration of transient response

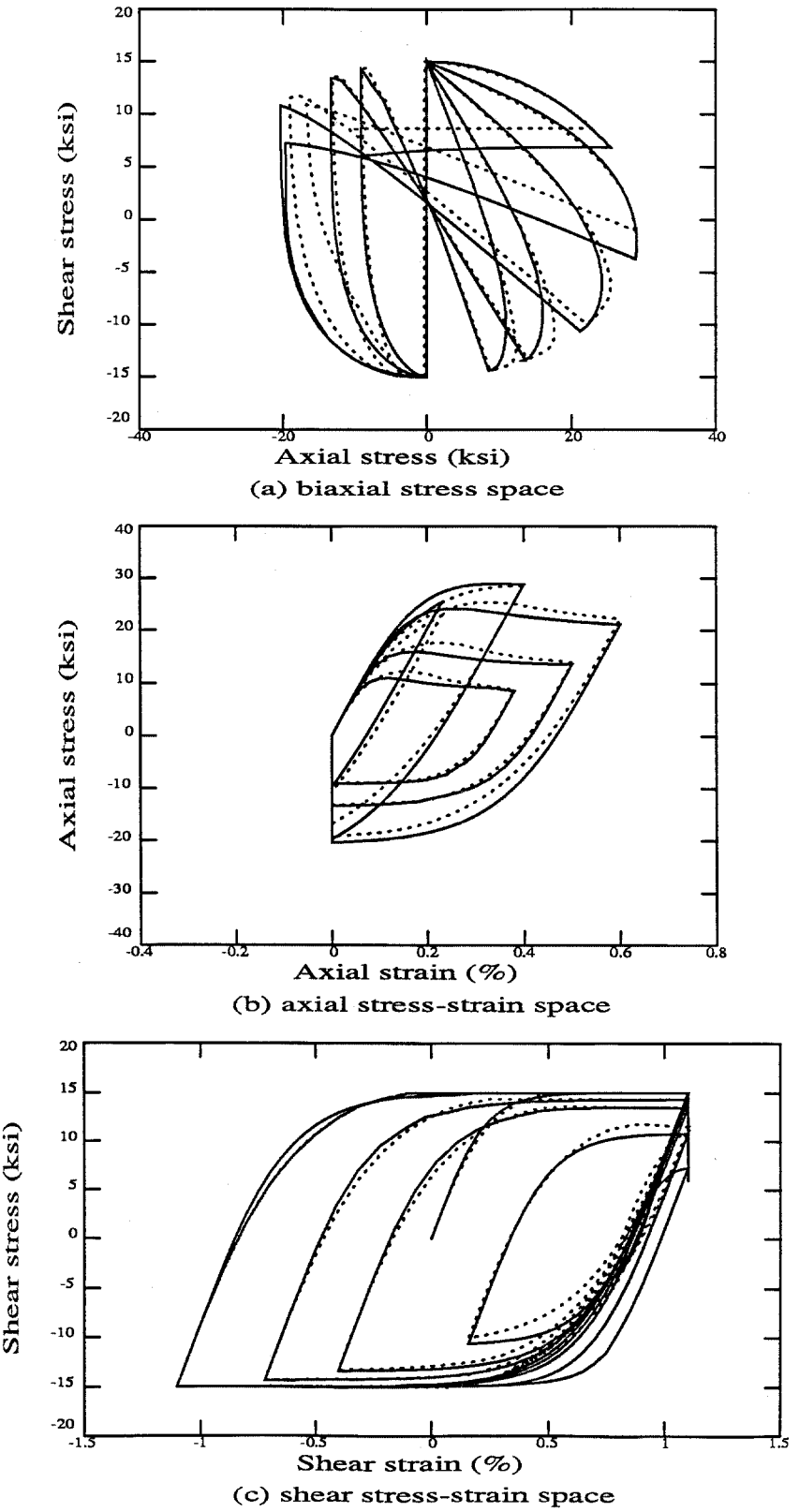

Figure 6.13 Stress response predicted by a generalized Masing model subject to the prescribed strain path given in Figure 5.6(a)
(Masing ——, DEM - - - -, both using Tresca's yield criterion)

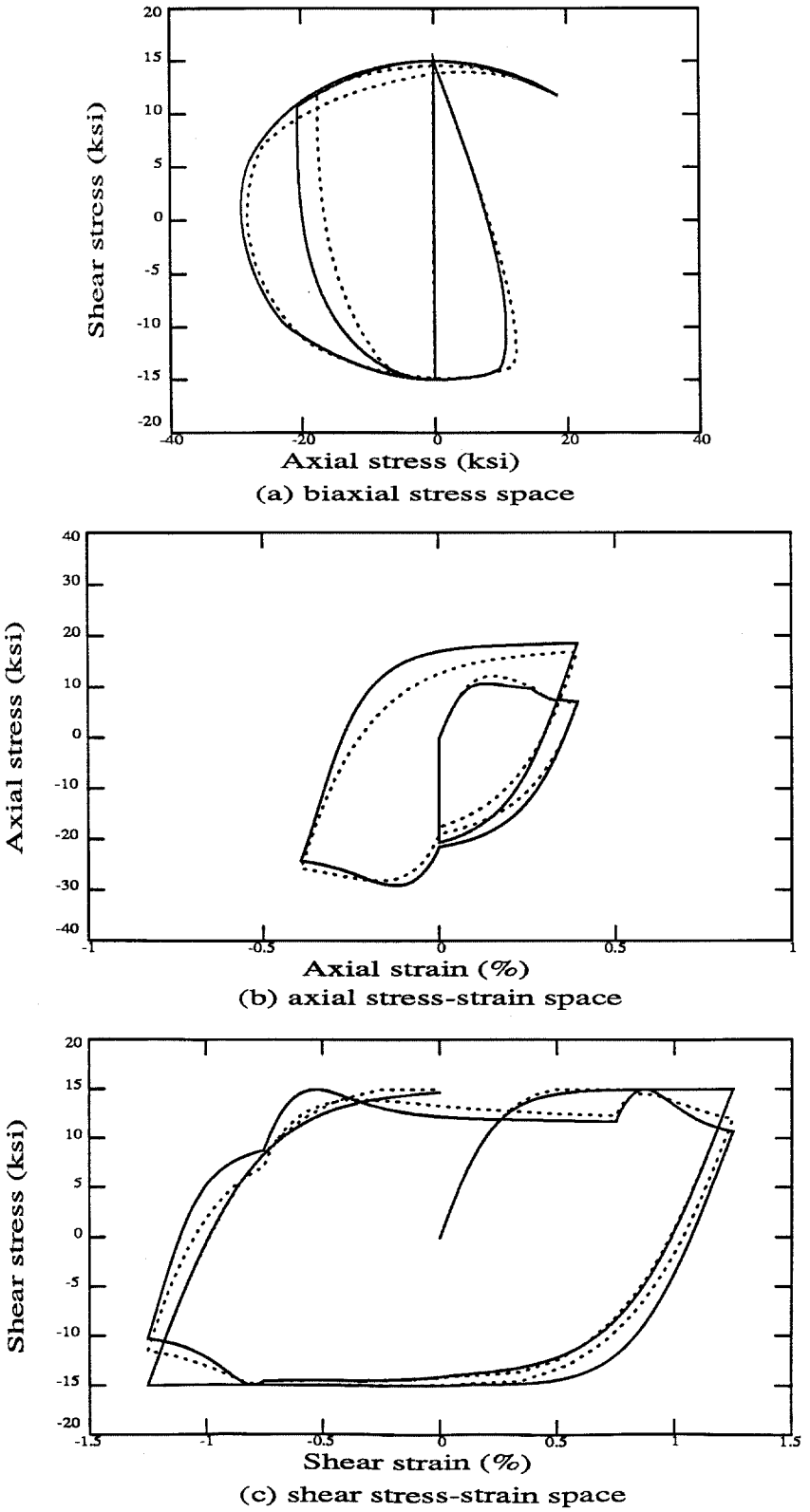

Figure 6.14 Stress response predicted by a generalized Masing model subject to the prescribed strain path given in Figure 5.6(b)
(Masing ——, DEM - - - -, both using Tresca's yield criterion)

CHAPTER 7
SUMMARY AND CONCLUSIONS

Analytical modeling of one-dimensional hysteresis and general multi-axial plasticity is studied in this research, with particular emphasis on the parsimony of model parameters and the physical consistency of model behavior. Based on the previous chapters of this thesis, a summary and some conclusions drawn from the results are presented as follows:

(1) Practical considerations of system identification and its implications for system modeling are studied, so that criteria of good models for mechanical systems can be used to provide guidelines for general modeling. A model which is good for forward (response) analysis is not necessarily good for identification studies, unless it is parsimonious in its parameters and robust to model error as well as measurement noise.

(2) Various one-dimensional hysteretic models are examined in detail, including both deteriorating and non-deteriorating models. Several models described solely by differential equations have been shown to exhibit unrealistic behavior which violates Drucker's postulates of stability. A general formulation for modeling of degrading systems is presented based on the formulation of the Distributed-Element Model (DEM) and the introduction of a damage index function. A new class of deteriorating Masing models, whose behavior can be completely described by a few simple mathematical rules and the extended Masing rules, is also proposed to substitute for a special class of maximum-displacement-controlled deteriorating DEMs. The modeling procedure and numerical implementation of this class of Masing models is much easier than that of the DEMs, so that its applicability to system identification studies is improved.

(3) The endochronic theory, which provides a unifying approach for plasticity without the need to introduce yield conditions, is studied and implemented for response simulation. A very efficient modeling technique based on the endochronic theory is proposed to make the model more suitable for identification applications. Besides, inspired from the study of cyclic hardening behavior, the extension of a DEM to account for cyclic hardening (or softening) behavior can be effectively done by simply making the ultimate strength of the model an appropriate function of plastic deformation.

(4) The one-dimensional DEMs are generalized so that they can be applied to the case where multi-dimensional loading conditions are considered. In the generalization, an invariant-yield-surface theory is proposed, in which no kinematic hardening rule is needed to account for the subsequent yielding and strain hardening behavior. The numerical implementation of the new DEMs is simple and efficient, and the model behavior is physically consistent, as justified by comparison of predictions with experimental results from the literature. An important advantage of this new DEM for plasticity is that for an isotropic material, if the yield condition has been appropriately chosen, then the general model needs only two parameters, in addition to Young's modulus and Poisson's ratio, which can be identified simply from a *uni-axial* virgin loading curve of the material. In addition, we may choose some constants involved in the yield condition as parameters to be identified, so that through system identification techniques, the "best" yield condition for a complex structural or material system can be found.

(5) Important properties of material behavior in cyclic plasticity are discussed, and a new theory is presented to elucidate the properties based on the behavior of the proposed multi-dimensional DEMs. The establishment of the theory provides us with instructive insight into the elastic-plastic response mechanisms of real materials under complicated loading conditions.

(6) Generalized Masing rules for cyclic plasticity are proposed based on a plane-geometry transformation method. When combined with a response formula valid for initial loading, they provide an alternative model for cyclic plasticity to the multi-dimensional DEMs, which require the introduction of a substantial number of elements in response calculation in order for sufficient accuracy. This new approach actually provides a highly efficient way of implementing the classical multi-yield-surface theory with Mroz' kinematic hardening rule, which is otherwise computationally impractical. The proposed transformation rules governing general multi-axial cyclic response again give better insight into the physical mechanisms of response in cyclic plasticity.

The original motivation of this research was to develop general classes of inelastic models that could be used in system identification of structural systems from their response data. However, the models proposed in this study are of interest themselves in that they are simple, parsimonious models which give remarkably good results of response predictions for copper and presumably for other materials or structural systems (some minor modification or extension may be needed though). Furthermore, the proposed models involve only a few physically-based parameters so that in general, no special identification technique is needed for determining appropriate parameter values for a particular system of interest, although better result might be obtained if system identification procedures were used.

In light of the above summary, a few suggestions for future exploration in related subjects may be made as follows:

(I) In the study of degrading hysteretic systems, new damage index functions, which should be physically consistent in nature and mathematically tractable, could be proposed to improve the modeling of various effects of degradation, such as the pinching behavior exhibited by reinforced-concrete structures.

(II) Further tests of the validity of the generalized multi-dimensional Masing models, which employ the proposed plane-geometry transformation method, could be

performed in multi-axial plasticity problems. This additional verification could be done by comparing with experimental observations obtained from higher-dimensional loading tests, when available, or by comparing with some other well-behaved models, such as the new multi-dimensional DEMs and the modified endochronic models.

(III) Further study could be made of the interactive effects of multi-dimensional loading on the response behavior of structural systems, such as their ductility, ultimate strength, and hysteretic energy dissipation, using the proposed physically-consistent models.

(IV) The multi-dimensional DEMs or Masing models could be applied to identification studies using response data from structural systems subject to multi-axial real or laboratory-simulated earthquake excitations. By treating some constants in the yield conditions required for the models as parameters to be identified, we may also find the "best" yield conditions for different complex structural systems.

(V) An investigation could be made of possible extensions of the proposed theory of multi-dimensional DEMs and Masing models for rate-dependent plasticity, creep, relaxation, deterioration and other such material behavior.

REFERENCES

[1] Bathe, K.J. (1982), Finite Element Procedures in Engineering Analysis, Prentice-Hall, New Jersey.

[2] Bazant, Z.P., and Bhat, P.D. (1976), "Endochronic theory of inelasticity and failure of concrete," *Journal of the Engineering Mechanics Division*, ASCE, Vol. 102, EM4, PP. 701-722.

[3] Beck, J.L. (1978), "Determining Models of Structures from Earthquake Records," *Report No. EERL 78-01*, California Institute of Technology, Pasadena.

[4] Beck, J.L. and Jayakumar, P. (1986), "Application of system identification to Pseudo-dynamic test data from a full-scale six-story steel structure," *Proc. Interational Conference on Vibration Problems in Engineering*, Xian, China.

[5] Beck, J.L. and Dowling, M.J. (1988), "Quick algorithms for computing either displacement, velocity or acceleration of an oscillator," *Int. J. Earthquake Eng. and Struct. Dynam.*, Vol. 16, pp. 245-253.

[6] Beck, J.L. (1990), " Statistical system identification of structures," *Structural Safety and Reliability*, ASCE, II, pp. 1395-1402.

[7] Beck, J.L. and Katafygiotis, L.S. (1991), "Updating of a model and its uncertainties utilizing dynamic test data," *Proc. 1st International Conference on Computational Stochastic Mechanics*, Greece, Computational Mechanics Publications, Southampton, pp. 125-136.

[8] Chaboche, J.L. (1986), "Time-independent constitutive theory for cyclic plasticity," *Int. J. Plasticity*, Vol. 2, pp. 149-188.

[9] Cifuentes, A.O. and Iwan, W.D. (1989), "Nonlinear system identification based on modelling of restoring force behavior," *Soil Dynamics and Earthquake Engineering*, Vol. 8, No. 1, pp. 2-8.

[10] Clough, R.W. (1966), "Effect of Stiffness Degradation on Earthquake Ductility Requirements", *Technical Report No. 66-16*, Department of Civil Engineering, University of California, Berkeley.

[11] Flügge, W. (1975), Viscoelasticity, 2nd ed., Springer-Verlag, New York.

[12] Franchi, A., Genna, F., and Paterlini F. (1990), "Research note on quasi-convexity of the yield function and its relation to Drucker's postulate," *Int. J. Plasticity*, Vol. 6, pp. 369-375.

[13] Gates, N.C. (1977), "The Earthquake Response of Deteriorating Systems," *Report No. EERL 77-03*, California Institute of Technology.

[14] Graesser E.J. and Cozzarelli, F.A. (1991), "A multi-dimensional hysteretic model for plastically deforming metals in energy absorbing devices," *Technical Report NCEER-91-0006*, State University of New York, Buffalo.

[15] Greenberg, M.D. (1978), Foundations of Applied Mathematics, Prentice-Hall, Inc., New Jersey.

[16] Hoshiya, M. and Maruyama, O. (1987), "Identification of nonlinear structural systems," *Proc. 5th International Conference on Applications of Statistics and Probability in Soil and Structural Engineering*, Vancouver, Canada, Vol. 1, pp. 182-189.

[17] Hsu, S.Y., Jain, S.K., and Griffin O.H. (1991), "Verification of endochronic theory for nonproportional loading paths," *Journal of Engineering Mechanics*, ASCE, Vol. 117, No. 1, pp. 110-131.

[18] Iemura, H. and Jennings, P.C. (1974), "Hysteretic response of a nine-story reinforced concrete building," *Int. J. Earthquake Eng. and Struct. Dynam.*, Vol. 13, pp. 183-201.

[19] Iwan, W.D. (1966), "A distributed element model for hysteresis and its steady-state dynamic response," *Journal of Applied Mechanics*, ASME, Vol. 33, No. 4, pp. 893-900.

[20] Iwan, W.D. (1967), "On a class of models for the yielding behavior of continuous and composite systems," *Journal of Applied Mechanics*, ASME, Vol. 34, No. 3, pp. 612-617.

[21] Iwan, W.D. (1973), "A model for the dynamic analysis of deteriorating structures," *Proc. 5th World Conference on Earthquake Engineering*, Rome, Italy, pp. 1782-1791.

[22] Iwan, W.D. and Cifuentes, A.O. (1986), "A model for system identification of degrading structures," *Int. J. Earthquake Eng. and Struct. Dynam.*, Vol. 14, pp. 877-890.

[23] Jayakumar, P. (1987), "Modeling and Identification in Structural Dynamics," *Report No. EERL 87-01*, California Institute of Technology.

[24] Jayakumar, P. and Beck, J.L. (1988), "System identification using nonlinear structural models," *Structural Safety Evaluation Based on System Identification Approaches, Proc. Workshop at Lambrecht/Pfalz*, pp. 82-102.

[25] Jazwinski, A.H. (1970), Stochastic Process and Filtering Theory, Academic Press.

[26] Kachanov, L.M. (1971), Foundations of the Theory of Plasticity, North-Holland Co., Amsterdam.

[27] Kadison, R.V. and Ringrose, J.R. (1983), Fundamentals of the Theory of Operator Algebras, Prentice-Hall.

[28] Kalman, R.E. (1960), "A new approach to linear filtering and prediction problems," *Journal of Basic Engineering*, ASME, Vol. 83, pp. 35-45.

[29] Katafygiotis, L.S. and Beck, J.L. (1991), "An efficient treatment of model uncertainties for the dynamic response of structures," *Proc. 1st International Conference on Computational Stochastic Mechanics*, Greece, Computational Mechanics Publications, Southampton.

[30] Lamba, H.S. and Sidebottom, O.M. (1978), " Cyclic plasticity for nonproportional paths: part I - cyclic hardening, erasure of memory, and subsequent strain hardening experiments; part II - comparison with predictions of three incremental Plasticity models," *Journal of Engineering Materials and Technology*, Vol. 100, pp. 96-111.

[31] Masing, G. (1926), "Eigenspannungen Und Verfestigung Beim Messing (Self Stretching and Hardening for Brass)," *Proc. 2nd International Congress for Applied Mechanics*, Zurich, Switzerland, pp. 332-335 (in German).

[32] McDowell, D.L. (1989), "Evaluation of intersection conditions for two-surface plasticity theory," *Int. J. Plasticity*, Vol. 5, pp. 29-50.

[33] McVerry, G.H. and Beck, J.L. (1983), "Structural Identification of JPL Building 180 Using Optimally Synchronized Earthquake Records," *Report No. EERL 83-01*, California Institute of Technology.

[34] Mendelson, A. (1968), Plasticity: Theory and Application, MacMillan, New York.

[35] Mroz, Z. (1967), "On the description of anisotropic workhardening," *Journal of the Mechanics and Physics of Solids*, Vol. 15, pp. 163-175.

[36] Ozdemir, H. (1976), "Nonlinear Transient Dynamic Analysis of Yielding Structures," *Ph.D. Dissertation*, Division of Structural Engineering and Structural Mechanics, Department of Civil Engineering, University of California, Berkeley.

[37] Park, Y.J., Wen, Y.K., and Ang, A.H-S. (1986), "Random vibration of hysteretic systems under bi-directional ground motions," *Int. J. Earthquake Eng. and Struct. Dynam.*, Vol. 14, pp. 543-557.

[38] Saiidi, M. and Sozen, M.A. (1979), "Simple and complex models for nonlinear seismic response of reinforced concrete structures," *Structural Research Series No. 465*, Civil Engineering Studies, University of Illinois, Urbana.

[39] Saiidi, M. (1982), "Hysteresis models for reinforced concrete," *Journal of the stuctural Division*, ASCE, Vol. 108, ST5, pp. 1077-1087.

[40] Sandler, I.S. (1978), "On the uniqueness and stability of endochronic theories of material behavior," *Journal of Applied Mechanics*, ASME, , Vol. 45, No. 2, pp. 263-266.

[41] Spiegel, M.R. (1964), Theory and Problems of Complex Variables, Schaum's Outline Series in Mathematics, McGraw-Hill.

[42] Sues, R.H., Mau, S.T. and Wen, Y-K. (1988), "Systems identification of degrading hysteretic restoring forces," *Journal of Engineering Mechanics*, ASCE, Vol. 114, No. 5, pp. 833-846.

[43] Sugiura, K., Lee, G.C. and Chang, K.C. (1987), "Endochronic theory for structural steel under nonproportional loading," *Journal of Engineering Mechanics*, ASCE, Vol. 113, No. 12, pp. 1901-1917.

[44] Takeda, T., Sozen,M.A., and Nielsen, N.N. (1970), "Reinforced concrete response to simulated earthquakes," *Journal of the stuctural Division*, ASCE , Vol. 96, ST12, pp. 2557-2573.

[45] Thyagarajan, R.S. (1989), "Modeling and Analysis of Hysteretic Structural Behavior," *Report No. EERL 89-03*, California Institute of Technology.

[46] Valanis, K.C. (1971), "A theory of viscoplasticity without a yield surface, part 1: general theory; part 2: application to mechanical behavior of metals," *Archive of Mechanics*, Vol. 23, No. 4, pp. 517-551.

[47] Valanis, K.C. (1980), "Fundamental consequences of a new intrinsic time measure : plasticity as a limit of the endochronic theory," *Archive of Mechanics*, Vol. 23, No. 2, pp. 171-191.

[48] Valanis, K.C. and Read, H. (1982), "New endochronic plasticity model for soils," *Soil Mechanics - Transient and Cyclic Loads*, Edited by Pande, G.N. and Zienkiewicz, O.C., Wiley, New York.

[49] Valanis, K.C. and Fan, J. (1984), "A numerical algorithm for endochronic plasticity and comparison with experiment," *Computers and Structures*, Vol. 19, No. 516, pp. 717-724.

[50] Watanbe, O., and Atluri, S.N. (1986), "Internal time, general internal variable, and multi-yield-surface theories of plasticity and creep: a unification of concepts," *Int. J. Plasticity*, Vol. 2, No. 1, pp. 37-57.

[51] Wen, Y.K. (1976), "Method for random vibration of hysteretic systems," *Journal of the Engineering Mechanics Division*, ASCE, Vol. 102, EM2, pp. 249-263.

[52] Wen, Y.K. (1980), "Equivalent linearization for hysteretic system under random excitations," *Journal of Applied Mechanics*, ASME, Vol. 47, No. 1, pp. 150-154.

[53] Wen, Y.K. and Ang, A. H-S. (1988), "Inelastic modeling and system identification," *Structural Safety Evaluation Based on System Identification Approaches, Proc. Workshop at Lambrecht/Pfalz*, pp. 142-160.

[54] Whiteman, I.R. (1959), "A mathematical model depicting the stress-strain diagram and the hysteresis loop," *Journal of Applied Mechanics*, ASME, pp. 95-100.

[55] Wylie, C.R. (1975), Advanced Engineering Mathematics, 4th ed., McGraw-Hill.

[56] Yoder, P.J. (1980), "A Strain-Space Plasticity Theory and Numerical Implementation," *Report No. EERL 80-07*, California Institute of Technology.

APPENDIX A

Operator Theory on Convex Sets

Some results from the operator theory on convex sets are summarized here to provide a theoretical basis for the derivation of important properties of the multi-dimensional Distributed-Element Models given in Chapter 5. A more complete presentation of operator theory can be found in Reference [27].

We define in the following some basic operations of point sets.

[Definition A1]: (Addition and Multiplication)

If $X \equiv \{x : x \in X\}$ and $Y \equiv \{y : y \in Y\}$, then

$$X + Y = \{x + y : x \in X, y \in Y\}, \quad aX = \{ax : x \in X\}. \tag{A.1}$$

[Definition A2]: (Convex Combination)

A vector $\underline{\sigma} \subset \Re^n$ is said to be a *convex combination* of N elements, $\underline{\sigma}_k, k = 1, 2, \ldots, N$, if

$$\underline{\sigma} = \sum_{k=1}^{N} a_k \underline{\sigma}_k, \qquad a_k > 0, \ \sum_{k=1}^{N} a_k = 1 \tag{A.2}$$

[Definition A3]: (Convex Set)

A set $\Omega \subset \Re^n$ is said to be *convex* if it contains *every* convex combination of *two* elements in Ω, i.e.,

$$\underline{\sigma}_1, \underline{\sigma}_2 \in \Omega \ \text{ and } \ \alpha \in [0, 1] \implies \alpha\underline{\sigma}_1 + (1 - \alpha)\underline{\sigma}_2 \in \Omega. \tag{A.3}$$

Based on the above definitions, we have the following important theorems regarding convex sets.

[Theorem A1]:

A convex set Ω contains *every* convex combination $\sum_{k=1}^{n} a_k \underline{\sigma}_k$ of elements $\underline{\sigma}_1, \underline{\sigma}_2, \ldots, \underline{\sigma}_n$ of Ω , for *all* positive integers n.

APPENDIX B

Derivation of Transformation Formulas for Generalized Masing Rules for Multi-Axial Cyclic Response Behavior

In the following, we will derive the transformation formulas (6.23), (6.24) based on the classical multi-yield-surface theory and the Mroz kinematic hardening rule. In the derivation, yield surfaces associated with a model are treated as circles in the two-dimensional $\sigma - \tau$ stress space. The validity of this simplification has been discussed in Sec. 6.3.2.

In order to employ the same response formula (e.g., Eqn. (6.19)) for all response branches in the multi-axial cyclic (strain) loading case, the stress state variables $\underline{\sigma}$ involved in the response formula should be modified by a suitable transformation, as suggested by Masing's hypothesis for cyclic hysteretic response in the one-dimensional case. The transformation must be able to characterize the change of situations among different response branches so as to appropriately reflect various behavior corresponding to different loading conditions. Recall that Masing's hypothesis for one-dimensional hysteresis implies that the response of an unloading or reloading branch corresponding to some particular response of initial loading can be obtained by introducing the transformation:

$$(x', r') = (\frac{x - x_0}{2}, \frac{r - r_0}{2}) \qquad (B.1)$$

to the state variables (x, r) involved, where x_0 and r_0 represent the displacement and the restoring force corresponding to a load reversal point for that particular response branch. Based on the ideas behind Masing's hypothesis, we want to find a transformation that can adequately reflect the difference between response of initial loading and that of subsequent load reversals. Consider the two response situations in Fig. B.1(a) and (b), in which the multi-axial yielding behavior is accounted for by the classical multi-yield-surface theory with Mroz' kinematic hardening rule. The

idea proposed here is that if we can find a transformation formula that maps the geometrical configuration in Fig. B.1(a) to that in B.1(b), then we can use a response formula, which is good for initial loading, to describe the response corresponding to subsequent unloading or reloading branches. To transform the geometrical configuration in Fig. B.1(a) to that in B.1(b), or vice versa, we introduce a series of mappings as follows:

(I) $w_1 = z - (\sigma_0 + i\tau_0)$: $\quad (w_1 \equiv \sigma_1 + i\tau_1, \quad z \equiv \sigma + i\tau)$

This mapping is a translation of $\sigma_0 + i\tau_0$, as defined in Fig. B.1(a), so that the unloading point A gets mapped to the origin in the w_1 plane.

(II) $w_2 = w_1\, e^{i(\frac{\pi}{2} - \theta_0)}$: $\quad (w_2 \equiv \sigma_2 + i\tau_2 \equiv r_2\, e^{i\theta_2})$

The second mapping is a counterclockwise rotation of $\frac{\pi}{2} - \theta_0$, where θ_0 is defined in Fig. B.1(a). After the two transformations w_1, w_2, the geometrical configuration in the z plane (Fig. B.1(a)) is mapped into that in the w_2 plane, as shown in Fig. B.2(a).

(III) $w_3 = \dfrac{2}{w_2}$: $\quad (w_3 \equiv \sigma_3 + i\tau_3 \equiv r_3\, e^{i\theta_3})$

This mapping maps the circles in the w_2 plane into horizontal lines in the w_3 plane, as shown in Fig. B.2(b).

(IV) $w_4 = (r_3 \sin\theta_3)\, e^{i(2\theta_3 - \theta_0)}$: $\quad (w_4 \equiv \sigma_4 + i\tau_4 \equiv r_4\, e^{i\theta_4})$

This mapping maps the horizontal lines in the w_3 plane into concentric circles in the w_4 plane, as shown in Fig. B.2(c). Note that there may be some other mappings that can do the same job as w_4 does for transforming the overall geometrical configurations, but care must be taken in choosing the mapping so that the direction of a plastic strain increment, which is determined using the normality principle, is preserved after transformation. To make the idea clearer, let us look at the two graphs in Fig. B.3(a) and (b), which show respectively the geometrical configurations after and before transformation. In order to meet the normality rule,

we need that the points A, B, C, and D in Fig. B.3(b) be mapped to A', B', C', and D' in Fig. B.3(a) so that they have exactly the same outward normal direction. Thus, by geometry we require that

$$\angle x = \frac{1}{2}\angle y, \qquad \angle y = \theta_0 - \theta. \tag{B.2}$$

It can be easily shown that the transformation formula w_4 given in (IV) satisfies the conditions required by (B.2).

(V) $w = \dfrac{1}{w_4}$: $\quad (w \equiv \sigma' + i\tau')$

The geometrical configuration after the transformation can be found to be just the one shown in Fig. B.1(b), in which the coordinates of the unloading point A' is the same as those of point A in Fig. B.1(a).

With the above transformations, the overall transformation which maps the configuration in Fig. B.1(a) to that in Fig. B.1(b) can be found by composition rule as

$$w = \frac{-r_1}{2\sin\theta_2}\, e^{-i\theta_4},$$

which is the formula given in Eqn. (6.23), and where

$$r_1 = \sqrt{(\sigma - \sigma_0)^2 + (\tau - \tau_0)^2}, \quad \theta_2 = \theta_1 - \theta_0 + \frac{\pi}{2},$$

$$\theta_1 = \tan^{-1}\left(\frac{\tau - \tau_0}{\sigma - \sigma_0}\right), \quad \theta_0 = \tan^{-1}\left(\frac{\tau_0}{\sigma_0}\right),$$

$$-\theta_4 = 2\theta_2 + \theta_0 = 2\theta_1 - \theta_0 + \pi,$$

as given in Eqn. (6.24).

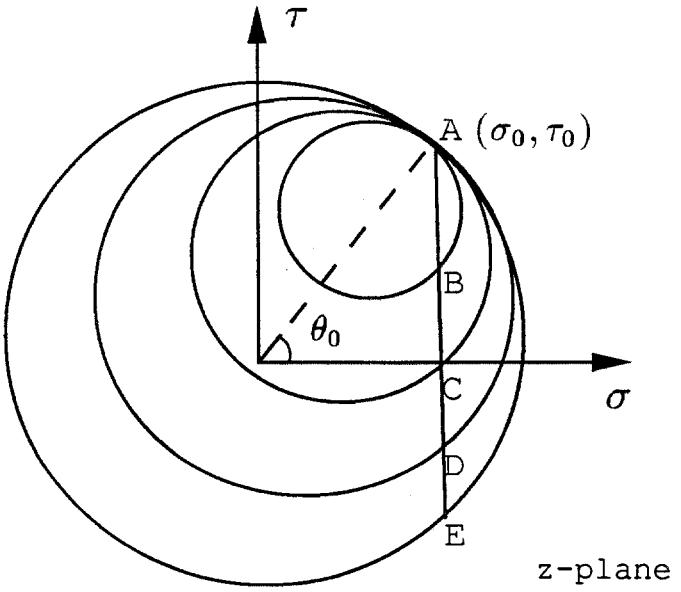

(a) configuration before transformation

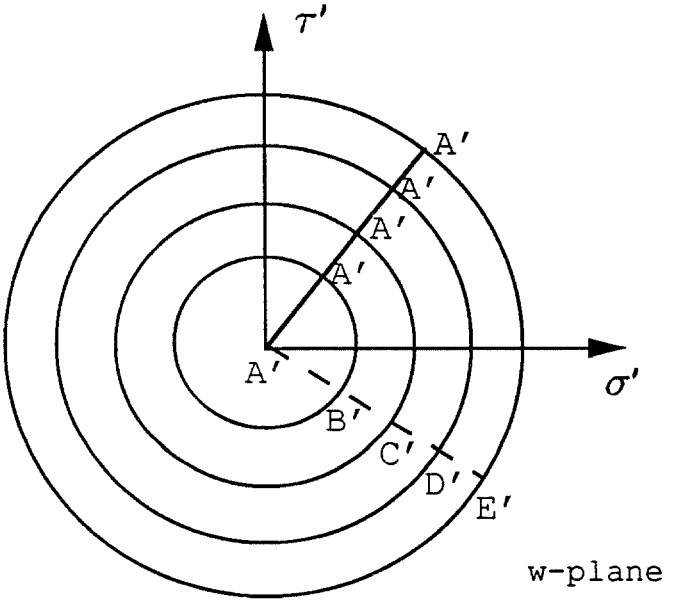

(b) configuration after transformation

Figure B.1 Geometrical configurations before and after transformation

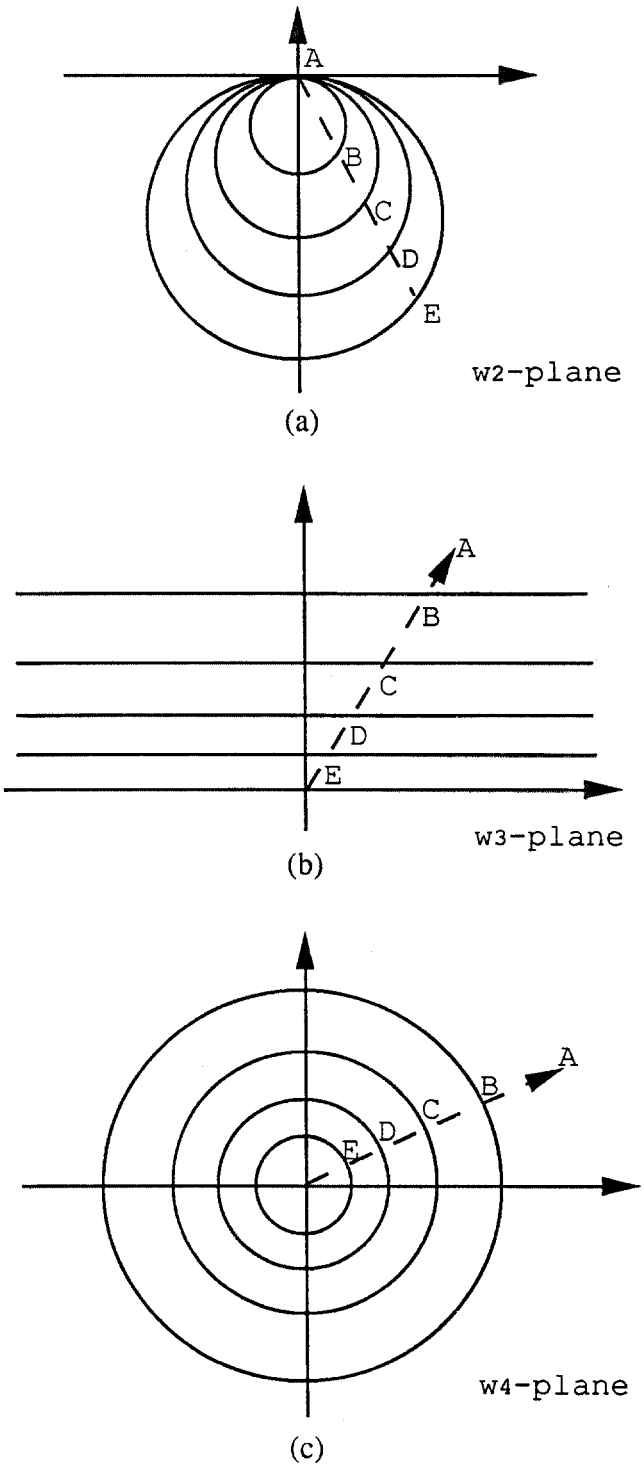

Figure B.2 Configurations at different transformation stages

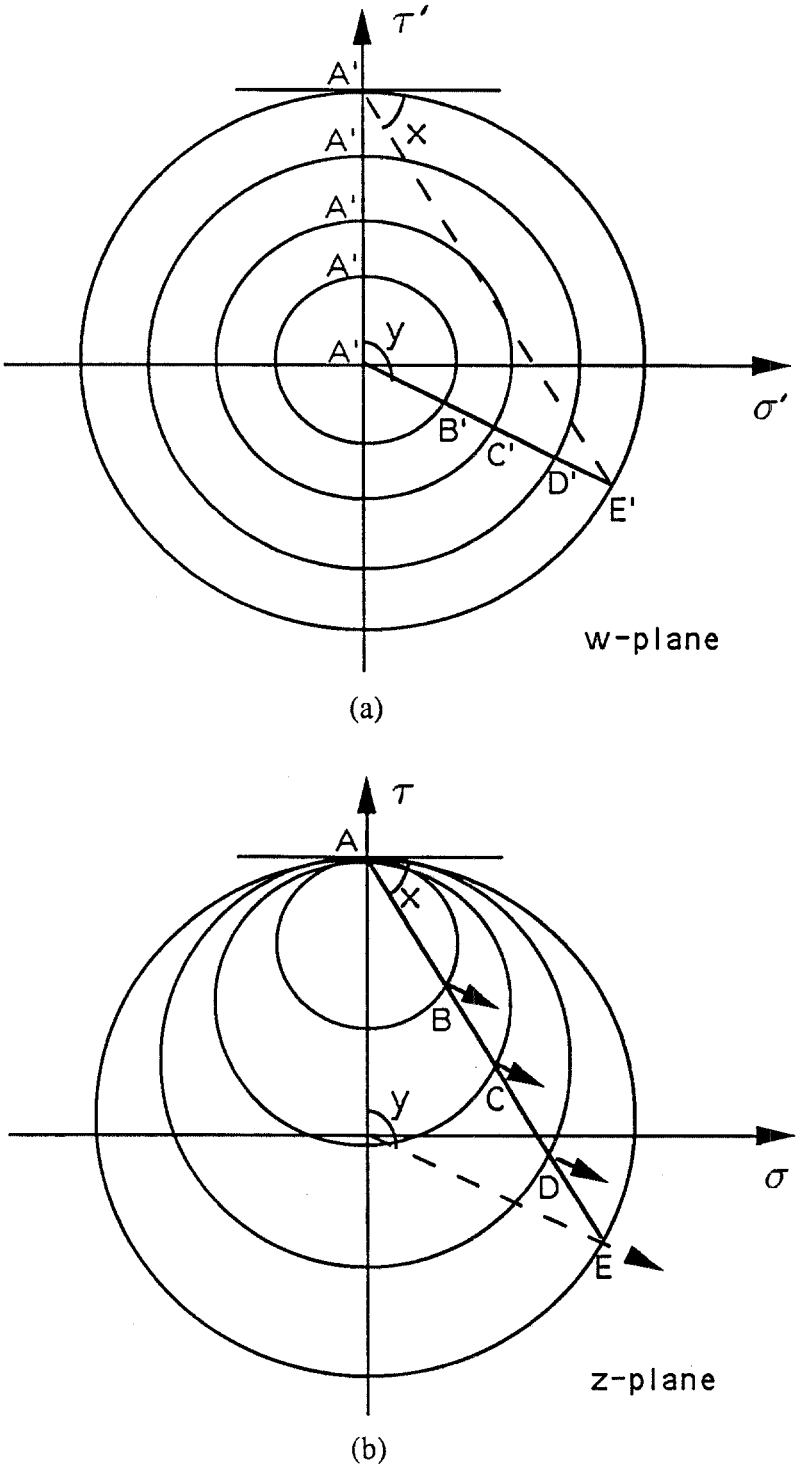

Figure B.3 Conditions of the principle of normality on the proposed transformation

CALIFORNIA INSTITUTE OF TECHNOLOGY

Reports Published by

Earthquake Engineering Research Laboratory (EERL)*
Dynamics Laboratory (DYNL)
Disaster Research Center (DRC)
Soil Mechanics Laboratory (SML)

Note: (PB ---) are Accession Numbers assigned by the National Technical Information Service (NTIS) and may be ordered through NTIS at 5285 Port Royal Road, Springfield, Virginia, 22161. (N/A) indicates that the report is no longer available at Caltech.

1. Alford, J.L., G.W. Housner and R.R. Martel, "Spectrum Analysis of Strong-Motion Earthquake," 1951. (Revised August 1964). (N/A)

2. Housner, G.W., "Intensity of Ground Motion During Strong Earthquakes," 1952. (N/A)

3. Hudson, D.E., J.L. Alford and G.W. Housner, "Response of a Structure to an Explosive Generated Ground Shock," 1952. (N/A)

4. Housner, G.W., "Analysis of the Taft Accelerogram of the Earthquake of 21 July 1952." N/A)

5. Housner, G.W., "A Dislocation Theory of Earthquakes," 1953. (N/A)

6. Caughey, T.K. and D.E. Hudson, "An Electric Analog Type Response Spectrum," 1954. (N/A)

7. Hudson, D.E. and G.W. Housner, "Vibration Tests of a Steel-Frame Building," 1954. (N/A)

8. Housner, G.W., "Earthquake Pressures on Fluid Containers," 1954. (N/A)

9. Hudson, D.E., "The Wilmot Survey Type Strong-Motion Earthquake Recorder," 1958. (N/A)

10. Hudson, D.E. and W.D. Iwan, "The Wilmot Survey Type Strong-Motion Earthquake Recorder, Part II," 1960. (N/A)

11. Caughey, T. K., D.E. Hudson and R.V. Powell, "The CIT Mark II Electric Analog Type Response Spectrum Analyzer for Earthquake Excitation Studies," 1960. (N/A)

---

* To order directly by phone: (703) 487-4650.

12. Keightley, W.O., G.W. Housner and D.E. Hudson, "Vibration Tests of the Encino Dam Intake Tower," 1961. (N/A)

13. Merchant, H.C., "Mode Superposition Methods Applied to Linear Mechanical Systems Under Earthquake Type Excitation," 1961. (N/A)

14. Iwan, W.D., "The Dynamic Response of Bilinear Hysteretic Systems," 1961. (N/A)

15. Hudson, D.E., "A New Vibration Exciter for Dynamic Test of Full-Scale Structures," 1961. (N/A)

16. Hudson, D.E., "Synchronized Vibration Generators for Dynamic Tests of Full-Scale Structures," 1962. (N/A)

17. Jennings, P.C., "Velocity Spectra of the Mexican Earthquakes of 11 May and 19 May 1962," 1962. (N/A)

18. Jennings, P.C., "Response of Simple Yielding Structures to Earthquake Excitation," 1963. (N/A)

19. Keightley, W.O., "Vibration Tests of Structures," 1963. (N/A)

20. Caughey, T.K. and M.E.J. O'Kelly, "General Theory of Vibration of Damped Linear Dynamic Systems," 1963. (N/A)

21. O'Kelly, M.E.J., "Vibration of Viscously Damped Linear Dynamic Systems," 1964. (N/A)

22. Nielsen, N.N., "Dynamic Response of Multistory Buildings," 1964. (N/A)

23. Tso, W.K., "Dynamics of Thin-Walled Beams of Open Section," 1964. (N/A)

24. Keightley, W.O., "A Dynamic Investigation of Bouquet Canyon Dam," 1964. (N/A)

25. Malhotra, R.K., "Free and Forced Oscillations of a Class of Self-Excited Oscillators," 1964.

26. Hanson, R.D., "Post-Elastic Response of Mild Steel Structures," 1965.

27. Masri, S.F., "Analytical and Experimental Studies of Impact Dampers," 1965.

28. Hanson, R.D., "Static and Dynamic Tests of a Full-Scale Steel-Frame Structures," 1965.

29. Cronin, D.L., "Response of Linear, Viscous Damped Systems to Excitations Having Time-Varying Frequency," 1965.

30. Hu, P.Y.-F., "Analytical and Experimental Studies of Random Vibration," 1965.

31. Crede, C.E., "Research on Failure of Equipment when Subject to Vibration," 1965.

32. Lutes, L.D., "Numerical Response Characteristics of a Uniform Beam Carrying One Discrete Load," 1965. (N/A)

33. Rocke, R.D., "Transmission Matrices and Lumped Parameter Models for Continuous Systems," 1966. (N/A)

34. Brady, A.G., "Studies of Response to Earthquake Ground Motion," 1966. (N/A)

35. Atkinson, J.D., "Spectral Density of First Order Piecewise Linear Systems Excited by White Noise," 1967. (N/A)

36. Dickerson, J.R., "Stability of Parametrically Excited Differential Equations," 1967. (N/A)

37. Giberson, M.F., "The Response of Nonlinear Multi-Story Structures Subjected to Earthquake Excitation," 1967. (N/A)

38. Hallanger, L.W., "The Dynamic Stability of an Unbalanced Mass Exciter," 1967.

39. Husid, R., "Gravity Effects on the Earthquake Response of Yielding Structures," 1967. (N/A)

40. Kuroiwa, J.H., "Vibration Test of a Multistory Building," 1967. (N/A)

41. Lutes, L.D., "Stationary Random Response of Bilinear Hysteretic Systems," 1967.

42. Nigam, N.C., "Inelastic Interactions in the Dynamic Response of Structures," 1967.

43. Nigam, N.C. and P.C. Jennings, "Digital Calculation of Response Spectra from Strong-Motion Earthquake Records," 1968.

44. Spencer, R.A., "The Nonlinear Response of Some Multistory Reinforced and Prestressed Concrete Structures Subjected to Earthquake Excitation," 1968. (N/A)

45. Jennings, P.C., G.W. Housner and N.C. Tsai, "Simulated Earthquake Motions," 1968.

46. "Strong-Motion Instrumental Data on the Borrego Mountain Earthquake of 9 April 1968," (USGS and EERL Joint Report), 1968.

47. Peters, R.B., "Strong Motion Accelerograph Evaluation," 1969.

48. Heitner, K.L., "A Mathematical Model for Calculation of the Run-Up of Tsunamis," 1969.

49. Trifunac, M.D., "Investigation of Strong Earthquake Ground Motion," 1969. (N/A)

50. Tsai, N.C., "Influence of Local Geology on Earthquake Ground Motion," 1969. (N/A)

51. Trifunac, M.D., "Wind and Microtremor Induced Vibrations of a Twenty-Two Steel Frame Building," EERL 70-01, 1970.

52. Yang, I-M., "Stationary Random Response of Multidegree-of-Freedom Systems," DYNL-100, June 1970. (N/A)

53. Patula, E.J., "Equivalent Differential Equations for Non-linear Dynamic Systems," DYNL-101, June 1970.

54. Prelewicz, D.A., "Range of Validity of the Method of Averaging," DYNL-102, 1970.

55. Trifunac, M.D., "On the Statistics and Possible Triggering Mechanism of Earthquakes in Southern California," EERL 70-03, July 1970.

56. Heitner, K.L., "Additional Investigations on a Mathematical Model for Calculation of Run-Up of Tsunamis," July 1970.

57. Trifunac, M.D., "Ambient Vibration Tests of a Thirty-Nine Story Steel Frame Building," EERL 70-02, July 1970.

58. Trifunac, M.D. and D.E. Hudson, "Laboratory Evaluations and Instrument Corrections of Strong-Motion Accelerographs," EERL 70-04, August 1970. (N/A)

59. Trifunac, M.D., "Response Envelope Spectrum and Interpretation of Strong Earthquake Ground Motion," EERL 70-06, August 1970.

60. Keightley, W.O., "A Strong-Motion Accelerograph Array with Telephone Line Interconnections," EERL 70-05, September 1970.

61. Trifunac, M.D., "Low Frequency Digitization Errors and a New Method for Zero Baseline Correction of Strong-Motion Accelerograms," EERL 70-07, September 1970.

62. Vijayaraghavan, A., "Free and Forced Oscillations in a Class of Piecewise-Linear Dynamic Systems," DYNL-103, January 1971.

63. Jennings, P.C., R.B. Mathiesen and J.B. Hoerner, "Forced Vibrations of a 22-Story Steel Frame Building," EERL 71-01, February 1971. (N/A) (PB 205 161)

64. Jennings, P.C., "Engineering Features of the San Fernando Earthquake of February 9, 1971," EERL 71-02, June 1971. (PB 202 550)

65. Bielak, J., "Earthquake Response of Building-Foundation Systems," EERL 71-04, June 1971. (N/A) (PB 205 305)

66. Adu, R.A., "Response and Failure of Structures Under Stationary Random Excitation," EERL 71-03, June 1971. (N/A) (PB 205 304)

67. Skattum, K.S., "Dynamic Analysis of Coupled Shear Walls and Sandwich Beams," EERL 71-06, June 1971. (N/A) (PB 205 267)

68. Hoerner, J.B., "Model Coupling and Earthquake Response of Tall Buildings," EERL 71-07, June 1971. (N/A) (PB 207 635)

69. Stahl, K.J., "Dynamic Response of Circular Plates Subjected to Moving Massive Loads," DYNL-104, June 1971. (N/A)

70. Trifunac, M.D., F.E. Udwadia and A.G. Brady, "High Frequency Errors and Instrument Corrections of Strong-Motion Accelerograms," EERL 71-05, 1971. (PB 205 369)

71. Furuike, D.M., "Dynamic Response of Hysteretic Systems With Application to a System Containing Limited Slip," DYNL-105, September 1971. (N/A)

72. Hudson, D.E. (Editor), "Strong-Motion Instrumental Data on the San Fernando Earthquake of February 9, 1971," (Seismological Field Survey, NOAA, C.I.T. Joint Report), September 1971. (PB 204 198)

73. Jennings, P.C. and J. Bielak, "Dynamics of Building-Soil Interaction," EERL 72-01, April 1972. (PB 209 666)

74. Kim, B.-K., "Piecewise Linear Dynamic Systems with Time Delays," DYNL-106, April 1972.

75. Viano, D.C., "Wave Propagation in a Symmetrically Layered Elastic Plate," DYNL-107, May 1972.

76. Whitney, A.W., "On Insurance Settlements Incident to the 1906 San Francisco Fire," DRC 72-01, August 1972. (PB 213 256)

77. Udwadia, F.E., "Investigation of Earthquake and Microtremor Ground Motions," EERL 72-02, September 1972. (PB 212 853)

78. Wood, J.H., "Analysis of the Earthquake Response of a Nine-Story Steel Frame Building During the San Fernando Earthquake," EERL 72-04, October 1972. (PB 215 823)

79. Jennings, P.C., "Rapid Calculation of Selected Fourier Spectrum Ordinates," EERL 72-05, November 1972.

80. "Research Papers Submitted to Fifth World Conference on Earthquake Engineering, Rome, Italy, 25-29 June 1973," EERL 73-02, March 1973. (PB 220 431)

81. Udwadia, F.E. and M.D. Trifunac, "The Fourier Transform, Response Spectra and Their Relationship Through the Statistics of Oscillator Response," EERL 73-01, April 1973. (PB 220 458)

82. Housner, G.W., "Earthquake-Resistant Design of High-Rise Buildings," DRC 73-01, July 1973. (N/A)

83. "Earthquake and Insurance," Earthquake Research Affiliates Conference, 2-3 April, 1973, DRC 73-02, July 1973. (PB 223 033)

84. Wood, J.H., "Earthquake-Induced Soil Pressures on Structures," EERL 73-05, August 1973. (N/A)

85. Crouse, C.B., "Engineering Studies of the San Fernando Earthquake," EERL 73-04, March 1973. (N/A)

86. Irvine, H.M., "The Veracruz Earthquake of 28 August 1973," EERL 73-06, October 1973.

87. Iemura, H. and P.C. Jennings, "Hysteretic Response of a Nine-Story Reinforced Concrete Building During the San Fernando Earthquake," EERL 73-07, October 1973.

88. Trifunac, M.D. and V. Lee, "Routine Computer Processing of Strong-Motion Accelerograms," EERL 73-03, October 1973. (N/A) (PB 226 047/AS)

89. Moeller, T.L., "The Dynamics of a Spinning Elastic Disk with Massive Load," DYNL 73-01, October 1973.

90. Blevins, R.D., "Flow Induced Vibration of Bluff Structures," DYNL 74-01, February 1974.

91. Irvine, H.M., "Studies in the Statics and Dynamics of Simple Cable Systems," DYNL-108, January 1974.

92. Jephcott, D.K. and D.E. Hudson, "The Performance of Public School Plants During the San Fernando Earthquake," EERL 74-01, September 1974. (PB 240 000/AS)

93. Wong, H.L., "Dynamic Soil-Structure Interaction," EERL 75-01, May 1975. (N/A) (PB 247 233/AS)

94. Foutch, D.A., G.W. Housner and P.C. Jennings, "Dynamic Responses of Six Multistory Buildings During the San Fernando Earthquake," EERL 75-02, October 1975. (PB 248 144/AS)

95. Miller, R.K., "The Steady-State Response of Multidegree-of-Freedom Systems with a Spatially Localized Nonlinearity," EERL 75-03, October 1975. (PB 252 459/AS)

96. Abdel-Ghaffar, A.M., "Dynamic Analyses of Suspension Bridge Structures," EERL 76-01, May 1976. (PB 258 744/AS)

97. Foutch, D.A., "A Study of the Vibrational Characteristics of Two Multistory Buildings," EERL 76-03, September 1976. (PB 260 874/AS)

98. "Strong Motion Earthquake Accelerograms Index Volume," Earthquake Engineering Research Laboratory, EERL 76-02, August 1976. (PB 260 929/AS)

99. Spanos, P-T.D., "Linearization Techniques for Non-Linear Dynamical Systems," EERL 76-04, September 1976. (PB 266 083/AS)

100. Edwards, D.B., "Time Domain Analysis of Switching Regulators," DYNL 77-01, March 1977.

101. Abdel-Ghaffar, A.M., "Studies of the Effect of Differential Motions of Two Foundations upon the Response of the Superstructure of a Bridge," EERL 77-02, January 1977. (PB 271 095/AS)

102. Gates, N.C., "The Earthquake Response of Deteriorating Systems," EERL 77-03, March 1977. (PB 271 090/AS)

103. Daly, W., W. Judd and R. Meade, "Evaluation of Seismicity at U.S. Reservoirs," USCOLD, Committee on Earthquakes, May 1. (PB 270 036/AS)

104. Abdel-Ghaffar, A.M. and G.W. Housner, "An Analysis of the Dynamic Characteristics of a Suspension Bridge by Ambient Vibration Measurements," EERL 77-01, January 1977. (PB 275 063/AS)

105. Housner, G.W. and P.C. Jennings, "Earthquake Design Criteria for Structures," EERL 77-06, November 1977 (PB 276 502/AS)

106. Morrison, P., R. Maley, G. Brady and R. Porcella, "Earthquake Recordings on or Near Dams," USCOLD, Committee on Earthquakes, November 1977. (PB 285 867/AS)

107. Abdel-Ghaffar, A.M., "Engineering Data and Analyses of the Whittier, California Earthquake of January 1, 1976," EERL 77-05, November 1977. (PB 283 750/AS)

108. Beck, J.L., "Determining Models of Structures from Earthquake Records," EERL 78-01, June 1978 (PB 288 806/AS)

109. Psycharis, I., "The Salonica (Thessaloniki) Earthquake of June 20, 1978," EERL 78-03, October 1978. (PB 290 120/AS)

110. Abdel-Ghaffar, A.M. and R.F. Scott, "An Investigation of the Dynamic Characteristics of an Earth Dam," EERL 78-02, August 1978. (PB 288 878/AS)

111. Mason, A.B., Jr., "Some Observations on the Random Response of Linear and Nonlinear Dynamical Systems," EERL 79-01, January 1979. (PB 290 808/AS)

112. Helmberger, D.V. and P.C. Jennings (Organizers), "Strong Ground Motion: N.S.F. Seminar-Workshop," SL-EERL 79-02, February 1978.

113. Lee, D.M., P.C. Jennings and G.W. Housner, "A Selection of Important Strong Motion Earthquake Records," EERL 80-01, January 1980. (PB 80 169196)

114. McVerry, G.H., "Frequency Domain Identification of Structural Models from Earthquake Records," EERL 79-02, October 1979. (PB-80-194301)

115. Abdel-Ghaffar A.M., R.F. Scott and M.J. Craig, "Full-Scale Experimental Investigation of a Modern Earth Dam," EERL 80-02, February 1980. (PB-81-123788)

116. Rutenberg, A., P.C. Jennings and G.W. Housner, "The Response of Veterans Hospital Building 41 in the San Fernando Earthquake," EERL 80-03, May 1980. (PB-82-201377)

117. Haroun, M.A., "Dynamic Analyses of Liquid Storage Tanks," EERL 80-04, February 1980. (PB-81-123275)

118. Liu, W.K., "Development of Finite Element Procedures for Fluid-Structure Interaction," EERL 80-06, August 1980. (PB 184078)

119. Yoder, P.J., "A Strain-Space Plasticity Theory and Numerical Implementation," EERL 80-07, August 1980. (PB-82-201682)

120. Krousgrill, C.M., Jr., "A Linearization Technique for the Dynamic Response of Nonlinear Continua," EERL 80-08, September 1980. (PB-82-201823)

121. Cohen, M., "Silent Boundary Methods for Transient Wave Analysis," EERL 80-09, September 1980. (PB-82-201831)

122. Hall, S.A., "Vortex-Induced Vibrations of Structures," EERL 81-01, January 1981. (PB-82-201849)

123. Psycharis, I.N., "Dynamic Behavior of Rocking Structures Allowed to Uplift," EERL 81-02, August 1981. (PB-82-212945)

124. Shih, C.-F., "Failure of Liquid Storage Tanks Due to Earthquake Excitation," EERL 81-04, May 1981. (PB-82-215013)

125. Lin, A.N., "Experimental Observations of the Effect of Foundation Embedment on Structural Response," EERL 82-01, May 1982. (PB-84-163252)

126. Botelho, D.L.R., "An Empirical Model for Vortex-Induced Vibrations," EERL 82-02, August 1982. (PB-84-161157)

127. Ortiz, L.A., "Dynamic Centrifuge Testing of Cantilever Retaining Walls," SML 82-02, August 1982. (PB-84-162312)

128. Iwan, W.D. (Editor) "Proceedings of the U.S. National Workshop on Strong-Motion Earthquake Instrumentation, April 12-14, 1981, Santa Barbara, California," California Institute of Technology, Pasadena, California, 1981.

129. Rashed, A., "Dynamic Analysis of Fluid-Structure Systems, " EERL 82-03, July 1982. (PB-84-162916)

130. National Academy Press, "Earthquake Engineering Research--1982."

131. National Academy Press, "Earthquake Engineering Research--1982, Overview and Recommendations."

132. Jain, S.K., "Analytical Models for the Dynamics of Buildings," EERL 83-02, May 1983. (PB-84-161009)

133. Huang, M.-J., "Investigation of Local Geology Effects on Strong Earthquake Ground Motions," EERL 83-03, July 1983. (PB-84-161488)

134. McVerry, G.H. and J.L. Beck, "Structural Identification of JPL Building 180 Using Optimally Synchronized Earthquake Records." EERL 83-01, August 1983. (PB-84-162833)

135. Bardet, J.P., "Application of Plasticity Theory to Soil Behavior: A New Sand Model," SML 83-01, September 1983. (PB-84-162304)

136. Wilson, J.C., "Analysis of the Observed Earthquake Response of a Multiple Span Bridge," EERL 84-01, May 1984. (PB-85-240505/AS)

137. Hushmand, B., "Experimental Studies of Dynamic Response of Foundations," SML 83-02, November 1983. (PB-86-115383/A)

138. Cifuentes, A.O., "System Identification of Hysteretic Structures," EERL 84-04, 1984. (PB-240489/AS14)

139. Smith, K.S., "Stochastic Analysis of the Seismic Response of Secondary Systems," EERL 85-01, November 1984. (PB-85-240497/AS)

140. Maragakis, E., "A Model for the Rigid Body Motions of Skew Bridges," EERL 85-02, December 1984. (PB-85-248433/AS)

141. Jeong, G.D., "Cumulative Damage of Structures Subjected to Response Spectrum Consistent Random Process," EERL 85-03, January 1985. (PB-86-100807)

142. Chelvakumar, K., "A Simple Strain-Space Plasticity Model for Clays," EERL 85-05, 1985. (PB-87-234308/CC)

143. Pak, R.Y.S., "Dynamic Response of a Partially Embedded Bar Under Transverse Excitations," EERL 85-04, May 1985. (PB-87-232856/A06)

144. Tan, T.-S., "Two Phase Soil Study: A. Finite Strain Consolidation, B. Centrifuge Scaling Considerations," SML 85-01, August 1985. (PB-87-232864/CC)

145. Iwan, W.D., M.A. Moser and C.-Y. Peng, "Strong-Motion Earthquake Measurement Using a Digital Accelerograph," EERL 84-02, April 1984. (PB-91-170191/AS)

146. Beck, R.T. and J.L. Beck, "Comparison Between Transfer Function and Modal Minimization Methods for System Identification," EERL 85-06, November 1985. (PB-87-234688/A04)

147. Jones, N.P., "Flow-Induced Vibration of Long Structures," DYNL 86-01, May 1986. (PB-88-106646/A08)

148. Peek, R., "Analysis of Unanchored Liquid Storage Tanks Under Seismic Loads," EERL 86-01, April 1986. (PB-87-232872/A12)

149. Paparizos, L.G., "Some Observations on the Random Response of Hysteretic Systems," EERL 86-02. 1986. (PB-88235668/CC)

150. Moser, M.A., "The Response of Stick-Slip Systems to Random Seismic Excitation," EERL 86-03, September 1986. (PB-89-194427/AS)

151. Burridge, P.B., "Failure of Slopes," SML 87-01, March 1987. (PB-89-194401/AS)

152. Jayakumar, P., "Modeling and Identification in Structural Dynamics," EERL 87-01, May 1987. (PB-89-194146/AS)

153. Dowling, M.J., "Nonlinear Seismic Analysis of Arch Dams," EERL 87-03, September 1987. (PB-89-194443/AS)

154. Duron, Z.H., "Experimental and Finite Element Studies of a Large Arch Dam," EERL 87-02, September 1987. (PB-89-194435/AS)

155. Whirley, R.G., "Random Response of Nonlinear Continuous Systems," EERL 87-04, September 1987. (PB-89-194153/AS)

156. Peng, C.-Y., "Generalized Model Identification of Linear and Nonlinear Dynamic Systems," EERL 87-05, September 1987. (PB-89-194419/AS)

157. Levine, M.B., J.L. Beck, W.D. Iwan, P.C. Jennings and R. Relles, "Accelerograms Recorded at Caltech During the Whittier Narrows Earthquakes of October 1 and 4, 1987: A Preliminary Report," EERL 88-01, August 1988. (PB-91-170100)

158. Nowak, P.S., "Effect of Nonuniform Seismic Input on Arch Dams," EERL 88-03, September 1988. (PB-89-194450/AS)

159. El-Aidi, B., "Nonlinear Earthquake Response of Concrete Gravity Dam Systems," EERL 88-02, August 1988. (PB-89-193124/AS)

160. Smith, P.W., Jr., "Considerations for the Design of Gas-Lubricated Slider Bearings," DYNL 89-01, January 1988. (PB-91-170126)

161. Donlon, W.P., Jr., "Experimental Investigation of the Nonlinear Seismic Response of Concrete Gravity Dams," EERL 89-01, January 1989. (PB-91-170118)

162. Jensen, H.A., "Dynamic Response of Structures with Uncertain Parameters," EERL 89-02, September 1989. (PB-91-154187/AS)

163. Thyagarajan, R.S., "Modeling and Analysis of Hysteretic Structural Behavior," EERL 89-03, October 1989. (PB-91-154195)

164. US-China Joint Project on Strong Ground Motion Measurements, "Digital Near Source Accelerograms Recorded by Instrumental Arrays in Tangshan, China," EERL 89-04. (PB-91-154112)

165. Tan, P., "Numerical Simulations of Two-Dimensional Saturated Granular Media," SML 90-02, October 1989. (PB-91-170255/AS)

166. Allard, M.A., "Soil Stress Field Around Driven Piles," SML 90-01, October 1989. (PB-91-170084)

167. Hou, Z., "Nonstationary Response of Structures and Its Application to Earthquake Engineering," EERL 90-01, April 1990. (PB-91-170092)

168. Levine, M., "Accelerogram Processing Using Reliability Bounds and Optimal Corrections Methods," EERL 90-02, June 1990. (PB-91-170209/AS)

169. Papadimitriou, K., "Stochastic Characterization of Strong Ground Motion and Applications to Structural Response," EERL 90-03, October 1990. (PB-91-170217/AS)

170. Beck, Robert T., "Fundamental Problems in the Application of Structural Identification Procedures to Damage Detection," EERL 91-03, May 1991. (PB-

171. Katafygiotis, Lambros S., "Treatment of Model Uncertainties in Structural Dynamics," EERL 91-01, May 1991. (PB-

172. Hall, John F., Michael J. Dowling and Bahaa El-Aidi, "Defensive Design of Concrete Gravity Dams," EERL 91-02, October 1991.

173. Yan, Liping, "Seismic Deformation Analysis of Earth Dams: A Simplified Method," SML 91-01, November 1991. (PB-

174. Challa, M.V.R., "Nonlinear Seismic Behaviour of Steel Planar Moment-Resisting Frames," EERL 92-01, April 10, 1992. (PB-